# DEVELOPMENT AND PERFORMANCE EVALUATION OF TUNGSTEN CARBIDE BASED SELF LUBRICATING CUTTING TOOL

*A THESIS*

*Submitted by*

**A.MUTHURAJA**

*For the award of the degree*

*of*

**DOCTOR OF PHILOSOPHY**

**DEPARTMENT OF MECHANICAL ENGINEERING**

**INDIAN INSTITUTE OF TECHNOLOGY GUWAHATI**

**MARCH 2016**

# CERTIFICATE

It is certified that the work contained in this thesis entitled **Development and Performance Evaluation of Tungsten Carbide based Self Lubricating Cutting Tool** by **A.Muthuraja,** a student in Department of Mechanical Engineering, Indian Institute of Technology Guwahati, India, for the award of the degree of **Doctor of Philosophy** has been carried out under my supervision and this work has not been submitted elsewhere for the degree.

**Dr. S. Senthilvelan**
Associate Professor
Department of Mechanical Engineering
Indian Institute of Technology Guwahati
Guwahati - 781039, Assam, India.

# Acknowledgements

I am deeply indebted to my thesis supervisor, **Dr. S. Senthilvelan**, for his valuable guidance and steady encouragement throughout my Ph.D program. His constant encouragement, enormous goodwill and unruffled patience made me work at ease and kept me highly motivated throughout my stay with him. Starting from formulating the problems to the final experimental results and their physical interpretations, he remained profoundly involved in my thesis work. He provided me with innovative ideas, helpful books and journals that were very helpful in successfully completing the present thesis. I have immensely benefited from each and every moment of my association with him. I would like to thank **Prof. P. S. Robi, Prof. A. Srinivasan** and **Dr.Sukhomay Pal** members of my Doctoral Committee who had steered me into the right path by providing comments, ideas and sharing their expertise throughout my tenure.

I thank the Head, Department of Mechanical Engineering, IIT Guwahati for providing me all the necessary facilities and funding to carry out this research work.

I would like to express my sincere thanks to **Dr. S. Kanagaraj, Dr. G. Pugazhenthi, Dr. Sidananda Sarma,** and **Dr. Senapathi** for having valuable discussions and suggestions during my experimental work.

I would like to thank **Mr. Kaustubh Acharyya**, and **Dr. Deba Kr. Sarma, Mr. N.K. Das, Mr. Chandan Banikya, Mr. Upen Gohain, Mr. Dilip Chetri, Mr. Dhaneswar Khaklary, Mr. Minesh Ch. Maedhi, Mr. Dipak Kr. Deka, Mr. Bijoy Kr. Choudhury, Mr. Nidul Saikia, Mr. Mrinal Sarma** and their teammates for helping me a lot during the fabrication process in the workshop. I express my wholehearted gratitude to the technical staff of Mechanical Engineering Department, **Mr. Rituraj Saikia, Mr. Sanjib Sarma, Mr. Jiten**

**Basumatary, Mr. Pranjol Paul** and **Mr. Dhruba Jyoti Bordoloi, Mr. Saiffuddin Ahmed** for their contribution and tireless help rendered throughout my research work.

I am sincerely thankful to **Dr. Satheeshkumar Veeraswamy, Dr. Subramanian, Mr. Kodeeswaran** and **Mr. Kalidasan** for their kind help and valuable suggestion during the research work. **Dr. Shanmuga Priya and Mr. Someshwaran** needs a special mention for providing valuable and timely help rendered during the research work. My heartfelt thanks to my research colleagues, **Arun, Sivaramakrishnan, Dr. Anilkumar Deepati, Dr. Biswajid Parida, Mr. Gajanan Shelke, Mr. Sridar, Ravikanth, Avinesh Varma, Vignesh Babu, Manish Kumar Kamal, Woldetinsay, Dr. A. Ghatak. Purnendu Mandel, Vinoth, Mahesh, Anil Kumar, Vaibav, Johnney Mertens, Rashmi Ranjan, Prakashkumar Sahu, Kishor Kumar, Aravind, Sandeep Kumar, Anurag Mishra, Arnika** and my heartfelt thanks to all my friends who helped me directly and indirectly and for their remarkable moral support.

I would like to express my gratitude to my parents **A. Padma** and **M. Ayyankalai** for their patience, wishes and the enormous trust they repose in my abilities at all times. I appreciate the warmth and motivation extended by Sister **A. Anitha** and my brother **A. Venkateswaran**. I thank my aunty **Mrs. Kanagavalli Chinnaiya** and her family for encouraging me to reach higher studies. Above all I thank the Almighty who bestowed me this opportunity for acquiring a research qualification.

**A.Muthuraja**

# ABSTRACT

**KEYWORDS***:* Tungsten carbide; Cutting tool; Solid lubricant; Friction; Wear; Temperature.

In manufacturing industries, major attention has been given to the dry machining due to the harmful effect and difficult handling of cutting fluids. This thesis intends to develop a solid lubricant cutting tool for carrying out dry machining. Tungsten carbide (WC) is considered for cutting tool material and calcium fluoride ($CaF_2$) is considered for solid lubricant and powder metallurgy as a method for developing cutting tool material. The various amount of $CaF_2$ (0-10 wt.%) were milled with tungsten carbide along with 10 wt.% of cobalt binder. Superior relative density (94 %) is achieved at 40 h of milling time and 400 MPa pressure. Compacted materials were subsequently sintered up to 1450 °C under nitrogen atmosphere in a tube furnace. The fractured surface of the considered materials confirmed that material with 5 and 7 wt.% of $CaF_2$ exhibited superior bonding between carbide particles. Considered material with 5 wt.% $CaF_2$ exhibited superior hardness (85 HRA) and transverse rupture strength (1500 MPa) while compressed at 400 MPa. Developed materials were made to slide over the silicon carbon abrasive sheet and sintered disc with various normal loads and at a sliding speed. Under both abrasive and adhesive conditions, material with 5 wt.% $CaF_2$ exhibited superior wear resistance and the lowest friction coefficient. The measured net surface temperature of the test specimen also confirmed this fact. The worn out test surface and the counter material surface revealed, traces of calcium and fluoride. Plain WC and WC with 5 wt.% $CaF_2$ materials were considered to understand the cutting tool performance. WC-Co-5 wt.% $CaF_2$ cutting tool generated 20-40 % lesser cutting force and 15-18 % lesser flank wear. Curlier and the smaller saw tooth of chip generated from WC-Co-5 wt. % $CaF_2$ cutting tool confirmed the lesser heat generation in cutting and improved surface finish of the machined surface.

# TABLE OF CONTENTS

# LIST OF FIGURES

# LIST OF TABLES

# NOMENCLATURE

## Symbols

| | |
|---|---|
| $TRS$ | Transverse rupture strength in MPa |
| $P$ | Applied force to fracture in N |
| $b$ | Width of the samples in mm |
| $H$ | Height of the samples in mm |
| $L$ | Distance between two parallel supports of three point bending fixture in mm |
| $K_{IC}$ | Fracture toughness in $MNm^{-3/2}$ |
| $P$ | Indentation load in N |
| $HV$ | Hardness in MPa |
| $A$ | Constant factor |
| $Z$ | Wear rate in $mm^3/nm$ |
| $V$ | Volume loss due to wear in $mm^3$ |
| $X$ | Sliding Distance in m |
| $F_N$ | Normal Load in N |
| $v$ | Velocity in m/sec |
| $wt$ | Weight in g or mg |

## Greek Symbols

| | |
|---|---|
| $\mu$ | Coefficient of friction |
| $\lambda$ | Wavelength of X-ray Beam |
| Å | Armstrong |
| $\beta_{hkl}$ | Full width at Half Maxima |

| | |
|---|---|
| ε | Microstrain |
| % | Percentage |
| θ | Incident Angle |

## Units

| | |
|---|---|
| *s* | Second |
| *h* | hour |
| °C | Centigrade (or) Celsius |

# CHAPTER 1

# INTRODUCTION AND LITERATURE SURVEY

## 1.1 INTRODUCTION

In the last one decade, the significant amount of research and development are being carried out in the domain of cutting tool materials. Present work attempted to identify the scope of using solid lubricant in the cutting tool application. In the present work, tungsten carbide was considered as base material; cobalt as binding material and calcium fluoride as solid lubricant material for the development of cutting tool material. This chapter covers required introduction about cutting tool materials and relevant literature review pertaining to the material development, mechanical characterization, friction, wear performance and cutting tool performance evaluation.

### 1.1.1 Cutting Tool

The demands of the manufacturing industry led to the development of improved machine tools, cutting tools and production process. The cutting tool plays a major role in achieving the full potential of any metal cutting operation. The performance of cutting tool material in a given machining application is mainly determined by following properties (HMT, 1980)

- Higher hardness than that of the workpiece material being machined, so that it can penetrate into the work material.
- Hot hardness, necessary to enable the cutting tool to retain its cutting ability and hardness at the high temperatures developed at the tool-chip interface.
- Wear resistance-The chip tool and chip work interface are exposed to severe conditions, adhesive and abrasion wear is very common. The cutting tool material

should therefore have high adhesive and abrasion resistance to improve the effective life of the tool.

- Low friction- The coefficient of friction between the chip and tool should be low which would allow lower wear rates and better chip flow.
- Toughness, necessary to enable the tool withstand the forces, to absorb shocks associated with interrupted cuts and to prevent the chipping of the fine cutting edge.

Among the cutting tool materials, plain carbide steels (0.6-1.5 % of carbon) with very small alloy additions such as Manganese, Silicon, Tungsten, Molybdenum, Chromium and Vanadium are the earlier tool materials used. However, beyond 200°C, these materials lose their hardness and cease to cut. Later, Taylor and White developed High Speed Steel and its cutting speed was 3-5 times more than that of carbon tool steel. These tool materials have significant quantities of tungsten, molybdenum, chromium and vanadium. In the recent years, HSS tool steels are also being produced through the powder metallurgy route. Around 1926, cemented carbides were invented by Germany. Cemented carbides are produced by the cold compaction of tungsten carbide powder in a binder such as cobalt followed by liquid phase sintering. Up to now, cemented carbides are the largest percentage of cutting tools used in metal cutting production (Rao, 2009).

### 1.1.2 Tungsten Carbide Cutting Tool

Tungsten carbide was developed during the First World War to replace the costly diamond wire drawing dies for tungsten filaments (Upadhyaya, 1998). Later utilisation of tungsten carbide was extended for cutting tool application and wear resistant machine parts. Tungsten gained major industrial importance at the beginning of the 20$^{th}$ century due to its technical application as alloying element in high-speed

steel and as filament wire in incandescent lamps (Yih and Wang, 1979). For both applications, pure tungsten was produced in powder form. Even after 90 years, the significance of tungsten carbide remains undiminished in industry applications due to the combination of very high hardness and good fracture toughness with high wear resistance. After the Second World War, the growth of powder metallurgy expanded rapidly due to economical processing and unique properties (Upadhyaya and Upadhyaya, 2011). Tungsten carbide is generally synthesized by the powder metallurgy route (Sarin, 1981). Tungsten carbide materials have been widely used for manufacturing of cutting tools, drilling bits, mining, and high wear resistant parts. Cutting tools should be able to withstand high temperature, fatigue, abrasion, attrition, and chemical induced wear (Edwards, 1993; Trent, 1984). In the past one decade, there was a significant advance achieved in powder manufacturing techniques. Initially straight tungsten carbide with cobalt as the bonding material formed the basic constituent of the tool material. Later, the addition of carbides with titanium, tantalum, niobium, etc extended their range of application. Currently there are more than 400 varieties of carbides marketed by various manufacturers (HMT, 1980). Manufacturing of tungsten carbide based cutting tool consists of the following

- Binding of the individual carbide and cobalt in proper proportion after thorough mixing.
- Addition of process control agent followed by drying, pressing, granulating or pelletizing and screening.
- Pressing of blanks to the desired shape and size with shrinkage allowance.
- Pre-sintering to remove the lubricant and to give sufficient strength for carrying out operations before the final sintering.
- High temperature sintering in nitrogen or vacuum atmosphere.

- Grinding or lapping depending on the requirements.

Most commercial grades of tungsten carbide-cobalt tool materials meant for metal cutting operations contain cobalt in the range of 3-12 %. With the increasing of cobalt content, the apparent hardness of the tool material drops. The grain size also affects the hardness of the carbides, the larger the grain size the lower the hardness.

### 1.1.3 Solid Lubricants

Solid lubricants are solid materials that exhibit very low friction and moderately low wear in sliding in the absence of external supply of lubricant (Bhushan, 2002). Solid lubricants are used whenever conventional lubricants are not suitable. Solid lubricants are thin films composed of a single solid, or a combination of solids introduced between two rubbing surfaces for the purpose of reducing friction and wear (Sliney, 1992). Direct microscopic observations of the dynamics of solid lubrication show that sliding is accompanied by severe ductile shear of the solid lubricant film (Sliney, 1978). This implies that to provide a low friction coefficient, the solid lubricant must have low shear strength.The most commonly solid lubricants are graphite molybdenum disulfide and PTFE. Graphite and $MoS_2$ have lamellar structure or hexagonal layer lattice structure. These layers are separated by relatively large distance and held together by weak van der Waals type bonding. Conventional solid lubricants such as graphite, $MoS_2$ and graphite fluoride get oxidized or dissociated on or above 500°C. Several inorganic salts with low shear strength and film forming ability are used as solid lubricants. $CaF_2$ and $CaF_2$-$BaF_2$ are non layered inorganic compounds. These solid lubricants exhibit low shear strength and form a surface film of low shear strength at high ambient temperatures (Bhushan, 2002). Oxidatively stable fluorides, such as $CaF_2$ and $BaF_2$, are lubricious from about 400 to 900 °C

(Sliney *et al.* 1965). Solid lubricant materials are used in the form of bulk solids or films as well as dry powders, soilds impregnated with solid lubricants and dispersions.

## 1.2 LITERATURE REVIEW

### 1.2.1 Milling Characteristics in Powder Metallurgy Process

In cemented carbide industry, ball milling is one of the well accepted methods for mixing and grinding of carbide materials (Suryanarayana, 2001; Lameck, 2005; Upadhyaya, 1998). The prime objective of ball milling, apart from particle size reduction, is to make sure that every carbide particle is coated with cobalt. In addition, it creates new active surfaces as well it increases defective structure of both carbides and metal binder. Various researchers (Bafrooei *et al.* 2014; Mandel *et al.* 2014) have carried out the milling process to study the effect of ball milling speed, ball to charge ratio, environment, amount of process control agent, amount of bonding and base material over particle morphology, size, contamination, density, hardness and strength.

Senthilvelan and Robi (2008) used $MoS_2$ with tungsten carbide to develop self-lubricating cutting tool material through ball milling and sintering. From the preliminary investigation, milling speed, ball and charge ratio were fixed in addition to the arrival of the optimum percentage of solid lubricant $MoS_2$. Reid *et al.* (2008) studied milling of alumina powder, where different milling media under identical conditions were used. It was found that zirconia media exhibited lowest contamination by 3-4% and the addition of zirconia found to increase toughness.

Duman *et al*. (2012) investigated the effect of stearic acid in milling. With the increase in stearic acid, relative density of the sintered material found to be decreased. Shin *et al.* (2013) investigated the effect of ball size on the particle size at the varying

milling speed. It was observed that optimum ball diameter decreased with increased speed and particle size increases with powder loading. Canakci *et al.* (2013) investigated milling parameters on particle size. Process control agent was found to play a significant role over particle size and morphology and consequently influencing cold welding and fracturing mechanisms. Dvornik and Zaytsev (2013) investigated energy storage at particle surfaces and interfaces during ball milling. A specific interface area of WC-Co was found to increase with milling time. The process control agent in ball milling was found to prevent excessive cold welding. Among the various process control agent, stearic acid is the most commonly used agent due to its higher melting temperature and existence of solid state in room temperature.

Zhang *et al.* (2008) optimized planetary ball milling parameters of tungsten carbide/cobalt powder. The volume of ball milling medium and milling speed found to be most significant and the weight ratio of the ball to powder was found to be least significant. Beyond a critical speed, milling balls was found to damage the inner walls of the bowl. Gheisari *et al.* (2009) investigated milling speed on powder morphology and particle size. At higher speed, the cold welding rate predominates over fracturing mechanism. Mahmoodan *et al*. (2009) milled WC based material and investigated the effect of the ball-powder ratio. It is observed that particle size decrease with the increase in ball-powder ratio for the chosen condition.

Avettand *et al*. (2003) investigated the milling parameters of tungsten carbide based materials, wherein contamination after prolonged milling time was observed. Hewitt and Kibble (2009) utilized high energy ball milling and reported the effect of ball milling time on nanostructure of WC-Co composites. Particle size was reduced with the increase in milling time, however beyond particular time, contamination

found to increase. With the decrease in particle size, the onset of WC-Co eutectic was found to decrease which aids the sintering process. Hedayati *et al.* (2011) produced the PEEK/$SiO_2$ nanocomposite using high energy ball milling. Milling deteriorated the crystallinity of PEEK and $SiO_2$ nanoparticles dispersed homogeneously with PEEK matrix, after 15 h of ball milling.

Liu *et al.* (2012) reported the effect of milling time on CNT reinforced Al matrix composites. Composite strength found to improve up to particular milling time and decrease beyond. Meng *et al.* (2013) processed WC nanoparticles using ball milling. The particle size reduction rate found to decrease gradually with the increase in milling time due to agglomeration. Cemented carbide was processed using planetary type mill (Mandel *et al.* 2014). Investigation confirmed that tungsten carbide particles were covered by cobalt and absence of particle growth. Refined particles produced with increasing milling time, but further increase in milling time caused agglomeration. Babu *et al.* (2014) synthesized copper nano powder using ball milling. Oxygen content in powders was found to be increased with milling time at atmospheric condition and low level contamination at argon atmosphere. Wang *et al.* (1997) prepared tungsten carbide by ball milling. A reduction of the average particle size of material upto 45 h was observed and beyond this time, the morphology of the particles remains unchanged. The EDS analysis revealed iron contamination from the steel mill and balls on longer milling. At the higher milling, $CaF_2$ exhibited extreme plastic deformation and contribute agglomeration (Sliney, 1982).

As the energy of milling is significantly high, it is necessary to carry out the milling process in the protective atmosphere to reduce heat generation and prevent oxidation (Upadhyaya, 1998). Hewitt and Kibble (2009) investigated the effect of

milling temperature on WC-10 Co powders. It was found that powder milled at -30° C exhibited high relative density compared to milled powder at room temperature.

It is observed that, not many investigations have been carried out to understand the milling characteristics of solid lubricant cutting tool material. Hence, it is also observed that there is a need to understand comprehensively to achieve maximum strength and lubrication characteristics of the proposed tungsten carbide based solid lubricant material.

### 1.2.2 Compaction Characteristics in Power Metallurgy Process

Mechanical properties of the materials prepared though powder metallurgy route are strongly influenced by the compaction. Compaction induces high stresses in the powders. Type of lubrication, pressing and compaction rate strongly influences the compaction process. The pressure increases with increase in the contact area between the grains, and particles experience extensive plastic deformation (Moon and Choi, 1985). In general, lubricants are added to the powder systems to reduce die-wall friction. The effects of using zinc stearate on the green and sintered density of a Ti-6A1-4V hydride-dehydride powder were examined at different compaction pressures (Ederer, 1999). Addition of the lubricant increases the green and sintered density by increasing compatibility. Briscoe and Rough (1998) investigated the effects of the die-wall friction in powder compaction of ceramic powders. The overall green density decreases with increase in compact aspect ratio. Green density of powder compacts increased with compaction pressure. Good wetting between WC and Co gives superior mechanical properties (Stojanovic *et al*. 1999).

The presence of liquid phase during sintering increases the sintering rate and the sintering temperature depends on cobalt binder in the WC-Co system (German, 1996;

Uhrenius *et al*. 1976; Upadhyaya, 1998). Taha *et al.* (1995) investigated the compaction behaviour of zirconia powders. The plastic behavior of the finer particle was observed during compaction which improved the green strength. Cha *et al*. (2001) investigated the effect of grain size on mechanical properties of WC-10Co cemented carbides. It was found that the hardness of WC-10Co increased with decrease in the grain size. Poquillon *et al.* (2002) studied the effect of morphology on compaction behavior of iron powders. A linear variation of density with compaction pressure was observed. The green strength was found to be increased with the compaction pressure. Showaiter and Youseffi (2008) investigated compaction, sintering and mechanical properties of 6061Al powder, higher porosity was observed at the low compaction pressure. Hewitt and Kibble (2009) investigated the consolidation of WC-Co nano composites. It was found that densification and hardness increased with compaction pressure and decreased with the milling time. The investigation on compaction behaviour revealed the presence of soft agglomerates in the calcined powder (Koley *et al*. 2011). Huang *et al*. (2009) studied the influence of solid lubricants, $BaF_2$,$CaF_2$ (5-20%). With the increase in $BaF_2$, hardness found to reduces due to the poor interparticle adhesion.

The effect of compaction pressure on densification of Mo powder was investigated (Garg *et al*. 2007). It was observed that the relative density was found to increase with increase in compaction pressure. Wang (2007) investigated the effect of powder type and compaction pressure on density and hardness of the sintered steels. The hardness of steel was found to increase with the increasing compaction pressure.

Yamaguchi *et al*. (1997) carried out compaction and sintering characteristics of the AI-Cu composite. Sinter density found to be less than that of the green compact, but the sintered hardness of composite increases. Jia *et al.* (1998) investigated

microstructure, hardness and toughness of the nanostructured and conventional WC-Co composites. Nanostructured composite with smaller grains promotes solubility and the finer grade exhibits superior fracture strength. Zhang *et al.* (2010) studied the microcrack number density during plastic deformation of WC–Co composite. It was found that high microcrack number density led to low hardness and high toughness. Khan *et al.* (2008) reported the effect of grain refinement on aluminium powder, hardness found to increase due to the grain refinement. Poussard *et al.* (2008) investigated the compaction characteristics of iron and phosphated iron powders. Relative density of iron with and without phosphate powder increases with compaction pressure. Mahmoodan *et al*. (2009) investigated WC–Co-TaC nano powders, hardness found to decrease with the increase in ball powder ratio and TaC content. Saha *et al*. (2012) investigated the compaction behaviour of nanostructured alumina powder. Green strength was strongly influenced by the particle size and distribution. From the prior research works, it is revealed that milling time and compaction pressure are major influencing process parameters in the material development via powder metallurgy. Hence, there is a need to investigate compaction characteristics of the proposed cutting tool material.

### 1.2.3 Mechanical Strength of Materials Developed via Powder Metallurgy Process

Tungsten carbide based metals have been used for cutting tools and other wear-resistant components due to its high hardness, good strength, excellent wear and erosion resistance. Transverse rupture strength (TRS) is used as an index for strength for cutting tool materials. Various investigations have been conducted to improve this strength and tribological performance with fine size particles, reinforcements, surface coating and material addition. Upadhyaya and Bhaumik (1988) sintered a WC-Co

material and evaluated hardness and transverse rupture strength. Nickel was considered as a binder material; however cobalt exhibited a superior binding behavior. Goudarzi and Akhlaghi (2013) studied the effect of nanosize silicon carbide (2.5-7%) with pure aluminium. With the increase in silicon carbide amount, milled particle size found to reduce. Fine size particles contribute to increase in density and micro hardness. Similar behaviour was also observed with aluminium magnesium matrix. Sharifi *et al*. (2011) developed and evaluated the mechanical properties of aluminium reinforced with boron carbide (5-15%). With the increase in boron carbide, hardness found to increase due to the presence of extremely harder phase. Tousi *et al.* (2011) studied the effect of alumina (1-7 %) on aluminium; with the increase in alumina, hardness of the composite found to increase.

Lin *et al.* (2012) studied the effect of molybdenum on mechanical properties of WC-TiC-Ni cemented carbides. Density and transverse rupture strength were found to decrease, due to the presence of pores. Liu *et al.* (2006) studied the effect of TiC and TiN (0-10 %) on the mechanical properties of titanium carbo nitride based cermets. With the addition of TiC, TRS found to increase upto 10 % due to its ceramic phase. TRS found to increase with the addition of TiN upto 5 %, and decreased beyond 5 % due to the release of nitrogen and formation of pores. Liu *et al.* (2003) studied the effect of Mo (4-12 %) on the mechanical properties of TiC based cermets with nano TiN. Due to the coarser ceramic phase of Mo, flexural strength of the cermet found to reduce. Fractography of the test specimen revealed trans-granular and inter-granular fractures. Wang *et al.* (2010) studied the influence of Mo (1-7%) on the microstructure and mechanical properties of TiC-based cermets. Mo found to improve the wettability and refine the grains of the hard phase. Transverse rupture strength found to increase with the increase in Mo.

Momozawa *et al.* (2012) investigated the effect of manganese (1-5%) over $TiC/TiB_2$ base cermets. Hardness and TRS found to increase upto 1 %. Beyond this amount, manganese evaporates and form residual pores resulted in the reduction of TRS. Song *et al.* (2014) reported the effect of titanium carbide (10-30 %) on ternary titanium boride. The higher amount of titanium carbide lowered the pores; increased density thereby increased micro hardness and flexural strength. Suzuki and Hayashi (1966) studied the effect of TiC (6-17 %) in the tungsten carbide material. 6 % TiC alloy exhibited higher strength than that of 11 and 17 %. Beyond this amount, TRS found to decrease due to the poor wettability. Martin *et al.* (2007) investigated the uniaxial compaction of bismuth-tantalum composites. Tantalum is considerably harder and stiffer than Bi. Yield strength of the composite was found to increase upto 0.3 % of Ta and decrease beyond. Deng *et al.* (2005) studied the effect of solid lubricants, $CaF_2$, $MoS_2$ and BN (5-15 %) content on flexural and hardness of $Al_2O_3/TiC$ composites. With the addition of these solid lubricants, hardness and flexural strength was found to decrease due to the formation of micro crack in the sintered materials. The characteristics of cracks formation on WC-Co cemented carbide materials by Vickers indentation technique was investigated (Zhang *et al.*, 2008; Dobrzanski and Dolzanska, 2010; Schubert *et al.*, 1998).

From the literature, it is observed that reinforcement and solid lubricant has the considerable effect on mechanical strength. Hence, there is a need to understand the effect of the solid lubricant amount on the mechanical strength of the proposed tungsten carbide based solid lubricant materials.

### 1.2.4 Abrasive Wear Performance

Importance of dry machining has been increased in recent years, as conventional cutting fluids are hazardous to the people and environment. However, limited tool

life, higher production times are some of the major limitations associated with the dry machining. Hence, solid lubricant is identified as the potential solution for the above problem. Abrasive wear is the material loss due to the passage of hard material over the soft surface. The abrasive wear process involves dissipation of frictional work and its resultant damage is relatively larger than adhesive wear (Briscoe, 1981).

Deng *et al.* (2007) developed $Al_2O_3$/TiC/$CaF_2$ composites and evaluated the performance of the sliding wear. It was found that material without $CaF_2$ exhibited significant surface damage and abrasive wear was identified as a dominant wear mechanism. Dhanasekaran and Gnanamoorthy (2007) developed sintered steel (Fe-C-Cu) with solid lubricant, $MoS_2$ and abrasive wear performance was investigated. Kagnaya *et al.* (2009) investigated the wear performance of WC-Co cutting tool material in the pin on disc configuration and measured surface temperature. Bonny *et al.* (2010) evaluated the friction and wear behavior of WC-Co carbide with different (6-12 wt.%) cobalt concentration with the aid of the reciprocating sliding wear tribometer. With the increase in load, a decrease in friction coefficient was observed due to the reduction of surface roughness.

Deng and Cao (2007) developed $Al_2O_3$/TiC with various amounts of $CaF_2$ solid lubricant and evaluated the tribological performance with the block on ring configuration. Li and Xiong (2008) developed nickel based composite with solid lubricants, graphite and molybdenum disulfide and evaluated its tribological performance. At room temperature, graphite contributed for the reduction of friction and $MoS_2$ contributed for the reduction of friction at higher temperature. Mixture of graphite and molybdenum sulphide contribute to the superior wear resistance and reduced friction at a wide range of temperature. With the increase in quantity of $MoS_2$, coefficient of friction and wear rate was found to be decreased. Pazhanivel *et*

*al*. (2015) investigated the scratch resistance and wear resistance of carbon coated tungsten carbide inserts. Carbon coated WC insert exhibited the lower coefficient of friction than uncoated WC insert. Machined workpiece also exhibited superior surface finish when machined with carbon coated WC insert as compared to that of commercial WC insert.

From the prior works, it was observed that various solid lubricants, including calcium fluoride, molybdenum di-sulphide, titanium di-boride, tungsten di-sulphide, and graphite were used to reduce friction and wear. It is also observed that very few works have been carried out on the development of solid lubricant cutting tool material and there is a need to understand the abrasive wear behavior of such solid lubricant cutting tool material.

### 1.2.5 Adhesive Wear Performance

Tungsten carbide based materials are preferred for cutting tool applications due to its superior hardness and transverse rupture strength. Many attempts were made to understand the wear performance under adhesive sliding condition of these classes of materials, since cutting tool interaction with the workpiece is analogous to the adhesive wear. A significant amount of works has been carried out in the past to understand the effect of carbide content, cobalt content over friction and wear behavior. Klaasen *et al.,* (2010) evaluated the adhesive wear performance of the tungsten carbide and titanium carbide materials by turning mild steel at low speed and sliding wear tests. With the increase in carbide content, wear resistance was found to increase. The increase in proof stress and hardness were identified as possible contributions. During sliding, cobalt binder was formed as tribofilms on the surface due to the extrusion of binder material. Okonkwo *et al*., (2012) evaluated the sliding

wear performance of low carbon steel against hardened tool steel at various temperatures. Profilometer measurement and scanning electron micrograph confirmed the material removal and deposition during adhesive wear. At lower temperature, material was found to be deposited, whereas at higher temperature material found to be removed.

Kagnaya *et al*., (2009) evaluated the sliding wear performance of WC-Co pins against AISI 1045 steel discs to understand the relationship between heat generation and wear. Friction coefficient and the measured surface temperature of the pin exhibited similar behavior with respect to the time. Bonny *et al*., (2010) investigated the tribological performance of WC-10 wt. % Co and WC-12 wt.% Co against WC- 6 wt.% Co in the reciprocating test rig. The worn-out surface revealed various mechanism including polishing of grains, adhesion of wear debris, surface binder removal, grain cracking, grain fragmenting and grain pull out under various loads and speeds. Removal of binder has been identified as the major failure mechanism while investigating the wear performance to understand the effect of the load and sliding speed.

Pirso *et al*. (2004) investigated the friction and wear performance of tungsten carbide with various amounts (6-20 wt.%) of cobalt against the steel disc in the block on disc test configuration. With the increase in binding material, wear resistance found to be decreased due to the reduction of the bulk hardness. Removal of binder phase was predominantly observed as the primary failure mechanism. Cemented carbide with lower binder content generated more frictional heat due to its less thermal conductivity. Pirso *et al*. (2006) evaluated the sliding wear performance of tungsten, titanium and chromium carbides against the steel disc. With the increase in binder contents (10-32%), frictional resistance of the tungsten carbide cermets found

to increase. Tungsten carbide cermets with higher binder content generated less temperature due to its high thermal conductivity. Surface damage of the tungsten carbide cermets confirmed the boundary between carbide grains as the weakest link. Engqvist *et al*. (2000) investigated the wear of tungsten carbide with different binders (0, 6 and 11 wt.%) against the same material under air and nitrogen environments. At severe loads (350 N, 3000 rpm), thinner tribofilms were developed when compared to those of mild tests (150 N and 1500 rpm). Test under nitrogen environment tribofilm formed slightly better than atmospheric environment. Binderless carbide formed thinner tribofilms which primarily consist of $WO_3$. Mild sliding in the air produced tribofilm which primarily consist of WC, whereas severe sliding in the air consists of $WO_3$. Barium and calcium fluorides were plasma sprayed over mild steel substrates (Yuan, 2010) and evaluated for the friction wear performance. Stainless steel balls were slid against $CaF_2$ coated substrate discs at dry condition. Discontinuous tribo-reaction layers were observed on the worn out surface of the coating. The worn-out surface of the coating revealed the abrasive wear as the primary failure.

Bolton and Gant (1998) added solid lubricants, manganese sulfide, to high speed steels to reduce friction and improve wear resistance. Developed materials were evaluated for three point bend strength and fracture toughness.

From the above literature, it is observed that few works have been carried to understand the effect of carbide and cobalt contents over the tribological performance. Few works have been carried out by adding solid lubricant as coating as well as fillers and evaluated them for the friction and wear performance. No work has been attempted to understand the adhesive wear performance of tungsten carbide based solid lubricant material.

### 1.2.6 Diffusive wear

Diffusive wear is a process of atomic transfer at the contacting asperities. The tool matrix or the constituents of the work material may be dissolved into the work or chip surfaces as chip passes. Deng et al. (2008) studied the diffusive wear of titanium alloy with WC/Co cutting tool. There was no evidence of diffusion of titanium alloys on the rake surface of WC/Co carbide tool at cutting speed of 20 m/min. When cutting speed increased from 20 to 120 m/min, diffusive wear increased rapidly. Due to high diffusion rate, tool tip broken completely after 10 minutes of machining. Lin et al. (2008) investigated wear behaviour of CBN tool material. With the increase in cutting speed, thin layer was formed due to diffusion on the tool-chip interface. Later this thin layer reduced wear rate and enhanced tool life. Wang and Liu (2016) used ceramic tool to machine AISI H13 steel. It was found that combination of adhesive and diffusive wear with micro chipping and Fe from work piece diffused on the tool faces. Astakhov (2006) studied the effect of cutting feed, depth of cut on tool wear rate. When temperature at the tool-chip and tool-workpiece interfaces increases, tool became softened and it promoted diffusive and oxidation wears.

### 1.2.7 Performance Evaluation of Cutting Tool

In recent years, manufacturing industries are shifting their focus towards green manufacturing (machining without coolants) to protect the environment from the harmful effect of coolants. However, dry machining generates more heat between cutting tool and work-piece which in turn reduces cutting tool life and increases production time. Research and developments are being carried out to develop cutting tool material to improve wear resistant by texturing, coating as well as with the addition of solid lubricants (Xing[1,2] *et al*. 2014; Deng *et al*. 2006).

Xing[1] *et al*. (2014) developed various textured $Al_2O_3$/TiC cutting tools and burnished with solid lubricant, $MoS_2$. Developed cutting tool with wavy micro scale textures on the rake face exhibited superior wear resistance. Xing[2] *et al*. (2014) developed $WS_2$/Zr coated $Al_2O_3$/TiC ceramic cutting tools with and without textures. A textured tool was found to be effective while machining hardened steel and it reduced the cutting force, cutting temperature, and friction between tool-chip interfaces compared with others. Deng *et al*. (2005) prepared $Al_2O_3/TiB_2$ cutting tool material with different $TiB_2$ content through hot pressing and sintering. Cutting tool materials were developed and evaluated for its performance under high speed machining. The oxidation products of $TiB_2$ grains acted as lubricant and increase wear resistance and reduce the coefficient of friction. Deng *et al*. (2006) developed $Al_2O_3$/TiC with $CaF_2$ though milling, compacting and sintering route. Hardened steel and cast iron was machined by developed materials. The friction coefficient with $Al_2O_3/TiC/CaF_2$ ceramic cutting tools was reduced compared with other investigated materials due to the formation of a self-lubricating film on the tool-chip interface.

Deng *et al*. (2009) drilled micro-holes and filled with molybdenum disulfide on the rake and flank surface of WC/Co tools. The cutting forces and friction coefficient with self-lubricated tools were significantly reduced compared to that of the conventional tool. Micro holes at the rake surface exhibited less force than that of cutting tool having holes at the flank surface. Lei *et al*. (2009) drilled micro holes on the rake surface of the tungsten carbide cutting insert. Oil and tungsten disulphide were used to fill up these micro holes. Both liquid as well as solid lubricants were found to be equally effective in reducing the contact length and coefficient of friction at the chip–tool interface. Brandt (1986) investigated flank and crater wear mechanisms of alumina-based tools when machining steel. It was found that crater

wear occurred due to superficial plastic deformation of the thin layer of alumina as a ductile or brittle fracture. Addition of TiC and TiN increased the wear rate due to the diffusion.

Dixit *et al*. (2012) investigated environmentally friendly machining; wherein mild steel was machined by coated carbide tool under dry and air-cooled machining with cutting parameter of 150-300 m/min, feed of 0.1 mm/rev, and depth of cut of 1 mm. It was found that the surface roughness and cutting forces increases with air-cooled turning. Yigit *et al*. (2008) investigated the effect of cutting speed in turning nodular cast iron with coated and uncoated cutting tools. Cutting forces found to decrease with the increase in cutting speed.

From the literature survey, it is found that research works are being carried out to improve the wear resistance of cutting tool through texturing, coating with the addition of solid lubricants. From the above literature, it is inferred that commonly used cutting tools, tungsten carbide and thermally stable calcium fluoride were not attempted to develop cutting tool materials. This work attempts to understand the performance of tungsten carbide based calcium fluoride material as cutting tool.

## 1.3 MOTIVATION

Dry machining is well recognized method to achieve clean manufacturing technology. From the literature review, it is observed that there is a scope of developing tungsten carbide based solid lubricant material for cutting tool application. It is also observed that there is a need to understand milling and compaction characteristics of the proposed cutting tool material for the effective material development. A proposed cutting tool material necessitates the evaluation of properties including transverse

rupture strength, abrasive wear performance, and adhesive wear performance before the cutting tool performance.

## 1.4 OBJECTIVE AND METHODOLOGY

The main objective of this thesis is to develop the tungsten carbide based self-lubricating cutting tool material and to understand its performance. In the current investigation, tungsten carbide, cobalt and calcium fluoride material were considered as the base, binding and solid lubricant materials, respectively for the proposed cutting tool materials

The major activities involved in the main objectives are;

- Milling and compaction characteristics of WC-10 % wt. Co-$CaF_2$ composites.
- Evaluation of Transverse ruptures strength and fracture toughness.
- Evaluating the friction and wear performance of the sintered specimen under abrasive and adhesive conditions.
- Development of cutting tool with the proposed material and cutting tool and performance evaluation under machining.

## 1.5 ORGANIZATION OF THE THESIS

First chapter presented the brief introduction on cutting tool materials, literature review on parameters of the powder metallurgy process, strength evaluation, friction, wear and performance of solid lubricant cutting tool materials. From the literature review, motivation and objective of the present work along with the methodology adopted are outlined in this chapter.

The second chapter reported various stages of material development which includes milling and compaction characterization of the tungsten carbide with various amount of calcium fluoride. In this chapter, evaluation of transverse rupture strength along with the detailed fractography to understand the bonding mechanism of considered materials is reported in this chapter.

The third chapter reported abrasive wear performance of developed materials. Developed sintered materials were slide against abrasive sheet. Continuous measurement of coefficient of friction, wear and temperature is reported in this chapter. In addition, worn out surface observed under scanning electron microscope and non contact 3D profile meter is reported in this chapter.

Sintered materials were slide against commercial WC-Co disc to evaluate the adhesive performance and reported in the fourth chapter. Both test and counter materials were examined to understand the adhesive wear mechanism and reported in this chapter. In this chapter, scratch resistance of the considered test material is also reported.

Sintered materials were developed into single point cutting tool and turning investigation was reported in fifth chapter. Continuous measurement of cutting forces and temperature is reported along with the chip morphology inspection.

Major conclusions drawn from this thesis is reported in sixth chapter.

# CHAPTER 2

# DEVELOPMENT OF TUNGSTEN CARBIDE BASED SELF-LUBRICATING CUTTING TOOL MATERIAL

## 2.1 INTRODUCTION

Ball milling is one of the most well accepted methods for mixing and grinding of carbide materials (Suryanarayana, 2001; Lameck, 2005). Suryanarayana (2001, 2004) has reported a paper on wet and dry milling process. The contamination in the powder mixture can be reduced by using dry milling than wet milling process. Therefore, dry milling has been found to be more efficient method.

Dvornik and Zaytsev (2013) studied the milling process of nanosized WC–Co powders and the power requirement and the energy transfer are considered. It was observed that increase in milling time induced agglomerates. Shiau *et al.* (1998) reported effect of milling and particle size distribution with microstructure of alumina powders. It was observed that the large contamination due to milling medium influences the densification rate powder milled.

From the prior investigations, it is observed that not much investigation have been carried out to understand the milling characteristics of solid lubricant cutting tool material. Senthilvelan and Robi (2008) also investigated and concluded that there is a need to understand ball milling characteristics to achieve superior strength as well as lubrication characteristics of the proposed new material. Aim of the present chapter is to develop tungsten carbide based solid lubricant material by investigating the effect of ball milling time and solid lubricant material on particle size.

## 2.2 MATERIALS AND PROCESSING

Commercially available tungsten carbide (WC) of 15-18 µm size with 99.8% purity (Rapicut carbides) is used as a basic cutting tool material due to its high hardness, good strength, and excellent wear resistance. Cobalt (Co) of 20-30 µm size with 99.5% purity (Loba Chemie) is used as a binder and 10 wt.% of Co is commonly used for the development of the WC based composite (Hewitt and Kibble, 2009; Cha *et al.,* 2001). Among solid lubricants, calcium fluoride ($CaF_2$) of 170-180 µm size with 98% of purity (Loba Chemie) is considered for cutting tool application due to the fact that it offers lubrication even at higher temperature (Sliney, 1982). Figure 2.1 shows the chosen initial powders, where stearic acid is used as process controlling agent to avoid cold welding.

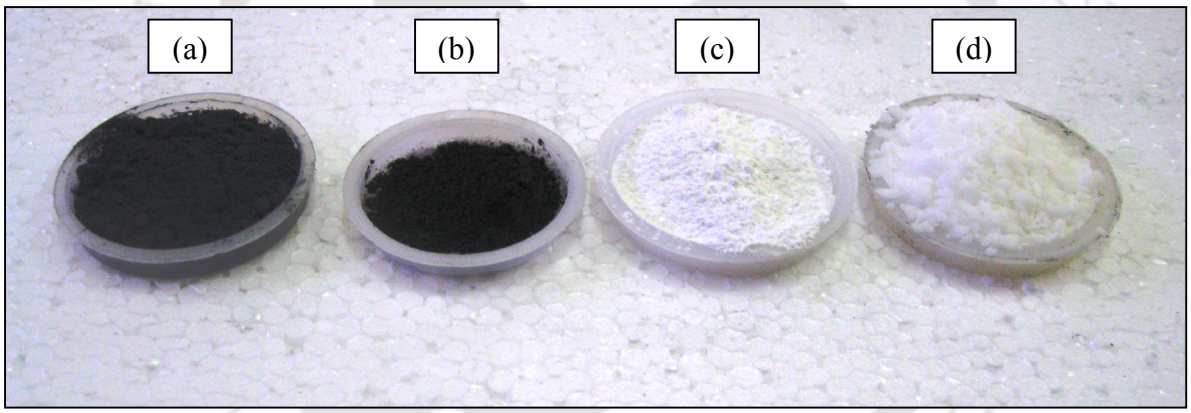


*Fig. 2.1 Initial powders: (a) Tungsten carbide (b) Cobalt (c) Calcium fluoride (d) Stearic acid.*

Stearic acid of 1-5 wt.% is commonly being used (Zhang *et al.,* 1999) and 4 wt.% is considered for the present investigation. Considered materials were milled in the planetary ball mill (Insmart system, PBM07) under a nitrogen (0.5 kg/cm²) atmosphere. Figure 2.2 (a-c) shows the planetary ball milling, close up view of bowl with gas line, and bowls with balls powder mixture. Plate speed and bowl speed are 90 and 207 rpm and the powder to ball ratio was taken as 1:5.

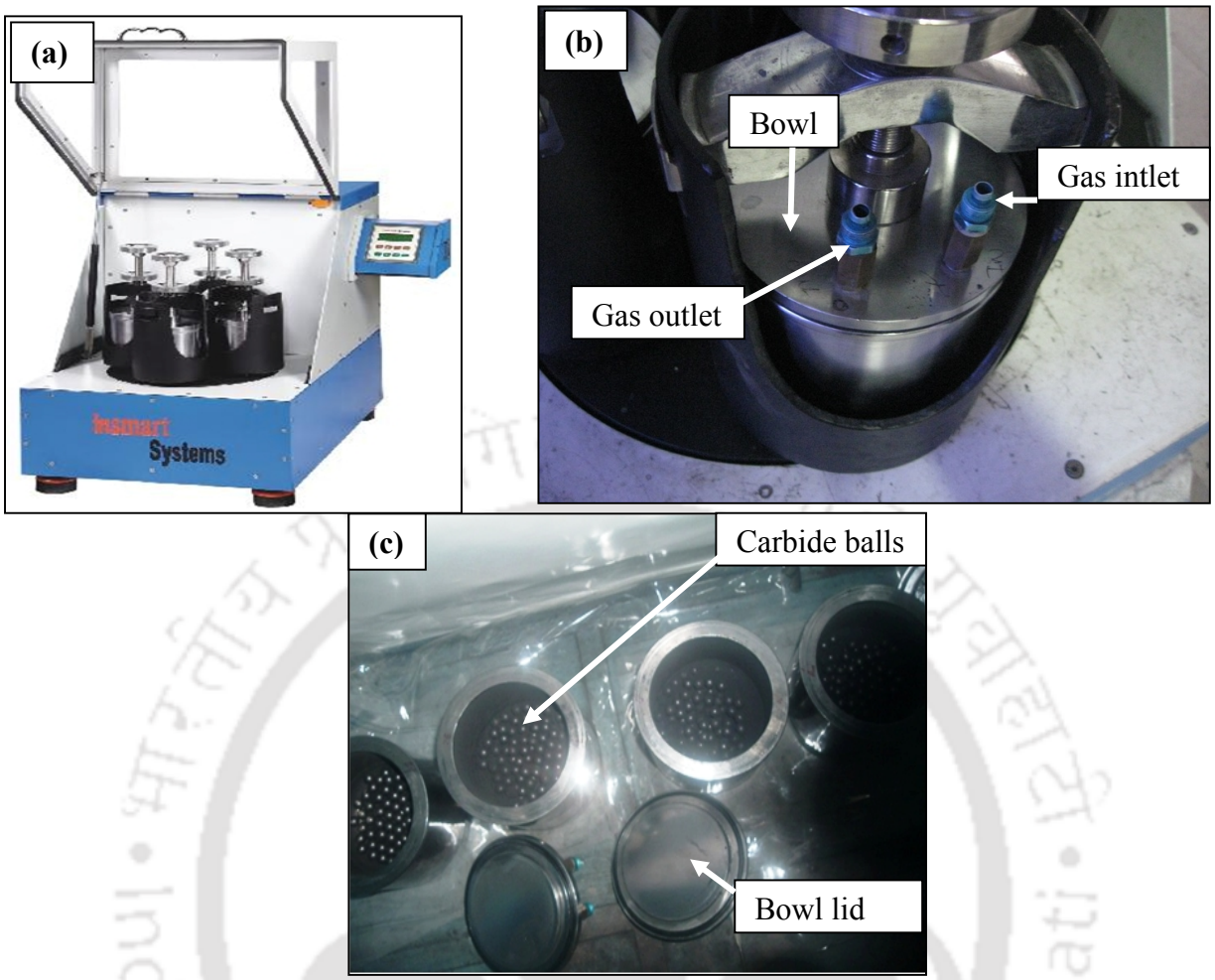


*Fig. 2.2 (a) Planetary ball milling (b) Close up view of bowl (c) Bowls filled with ball-powder mixture.*

Plate speed and powder ball ratio was decided to avoid contamination. WC was milled with 10 wt.% of Co and 5 wt.% of $CaF_2$ at 20, 40, 60, 80 and 100 h for the milling characterization. After the completion of every milling process, the milled powders were opened and kept for 1 to 2 hours inside the glove box to avoid oxidation effect. Figure 2.3 shows the glove box which is used to protect milled powders from oxidation.

To understand the effect of solid lubricant on transverse rupture strength (TRS), various weight percentages (0, 3, 5, 7 and 10) of $CaF_2$ was considered and milled upto 40 h. Milled

particles were characterized with the aid of a scanning electron microscope (SEM), laser particle size analyser (LPSA) and an X-ray diffraction (XRD).

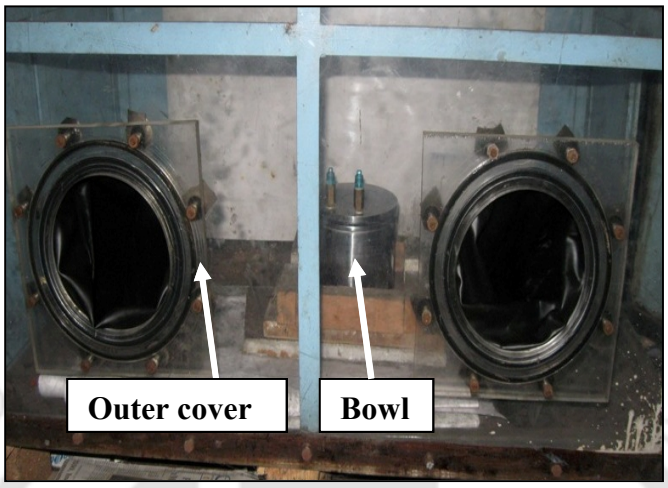


*Fig. 2.3 View of glove box*

Green compacted test specimens (40 X 16 X 5 mm) were compacted uniaxially in the pressure 200-400 MPa as per the ASTM B331-95 with the aid of universal testing machine (UTE 20). Figure 2.4(a-b) shows the developed dies and punches. The die and punches are cleaned by acetone and polished using fine abrasive sheet of 1000-1200 grit size after every compaction. For uniaxial compaction, 1000 kN capacity universal testing machine (UTE 20) is used to obtain green compacted specimen (Fig. 2.5). Hewitt *et al.* (2009) and Hewitt and Kibble (2009) also developed tungsten carbide based material by compacting milled powder in the range of 100-400 MPa. Subsequently test specimens were sintered in a tube furnace (Bysakh, Okay 70T7) under nitrogen atmosphere (0.5 kg/cm$^2$) to avoid oxidation (Fig. 2.6a). Fig. 2.6b shows the sintering cycle adopted. During sintering, initially specimens were heated upto 400° C at the rate of 2° C/min to prevent crack formation and stearic acid was removed by maintaining at 400° C for 60 min.

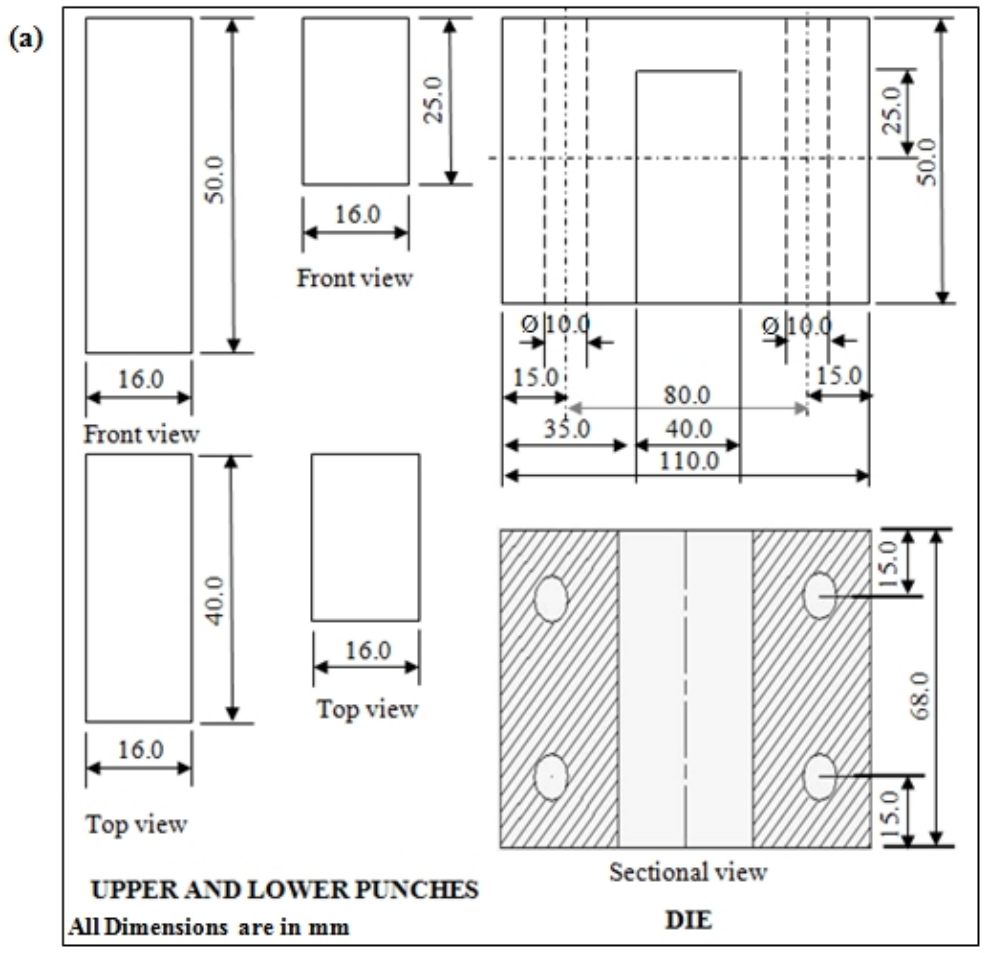


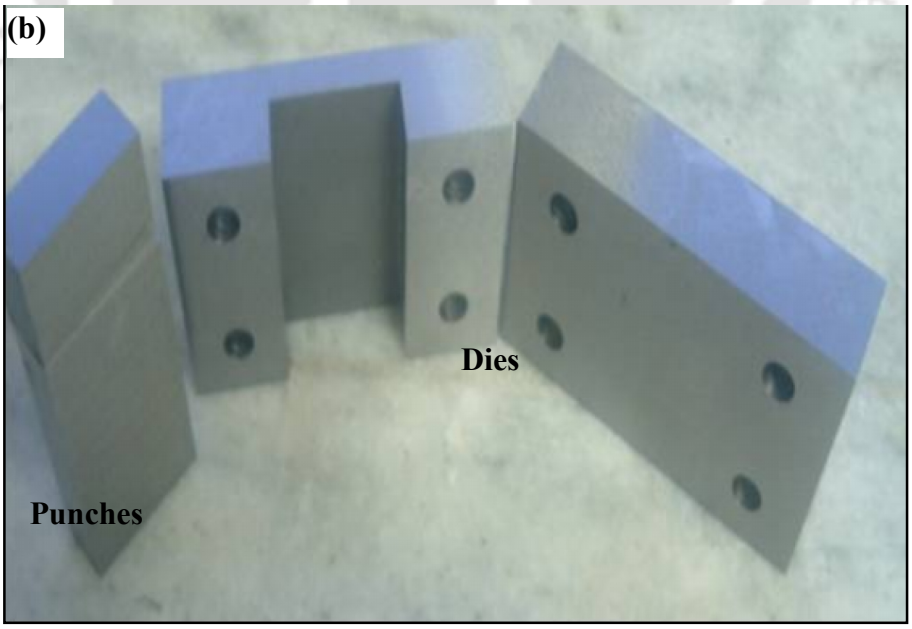


*Fig. 2.4 Die for transverse rupture strength specimen: (a) Die and punch drawing (b) View of the manufactured die*

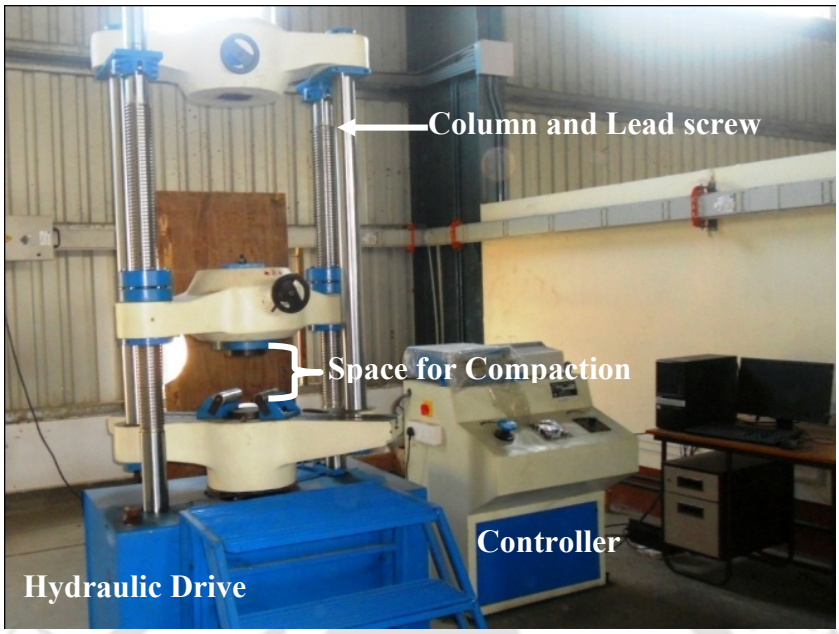


*Fig. 2.5 Universal testing machine used for compaction*

Later specimens were heated up to 1200° C at the rate of 5° C/min and then to 1450° C at the rate of 3° C/min. After reaching 1450° C, specimens were maintained for 60 min then cooled up to the ambient temperature at the rate of 3°C/min. Subsequently, density of the sintered specimens was measured by the Archimedes method (ASTM B962-08).

Test specimens were weighed in air, then subsequently submerged in the oil to seal the surface connected porosity again specimen was weighed. In the vacuum oven, the pressure was maintained at 7 kPa with atmospheric temperature for 30 minutes then maintained the atmosphere pressure kept the specimens in submerged condition for 30 minutes. Excess oil was removed with an absorbent, subsequently specimen was weighed. The Water container was supported over the pan of the weighing balance using a suitable bridge so that bridge does not restricted the free movement of the balance pan. Then the specimen was weighed under water and its density was calculated based on Archimedes' principle. Same procedure was followed to determine green and sintered density.

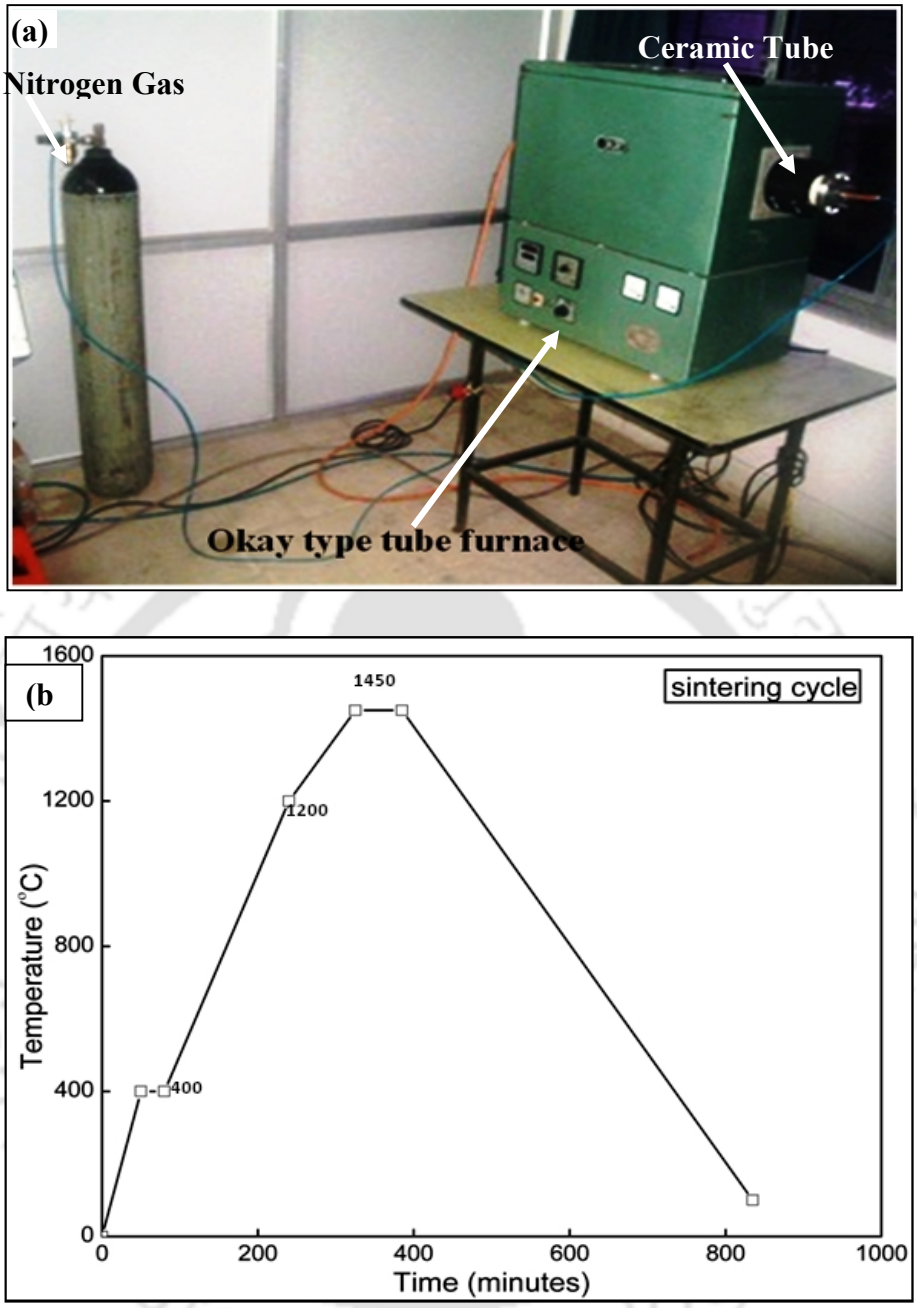


*Fig. 2.6 (a) View of the tube furnace (b) Selected sintering cycle*

Sintered sample surfaces were ground and polished for the investigation of morphology and element distributions with the aid of SEM and EDS. Servo hydraulic dynamic testing machine (Instron 8801 J) shown in figure (2.7a) is used to evaluate transverse rupture strength (TRS) of the developed material as per ASTM B 925-08. Loading rate was fixed as 0.25 mm/min. TRS was evaluated using the following equation.

$$TRS = 3PL/2bh^2 \quad (2.1)$$

Where

TRS : Transverse rupture strength, MPa

P : Applied force to fracture, N

L : Distance between two parallel supports, mm

b and h : Width and Height of the samples respectively, mm.

Figure 2.7(b) shows the developed fixture for three point bending test to determine transverse rupture strength of sintered specimen.

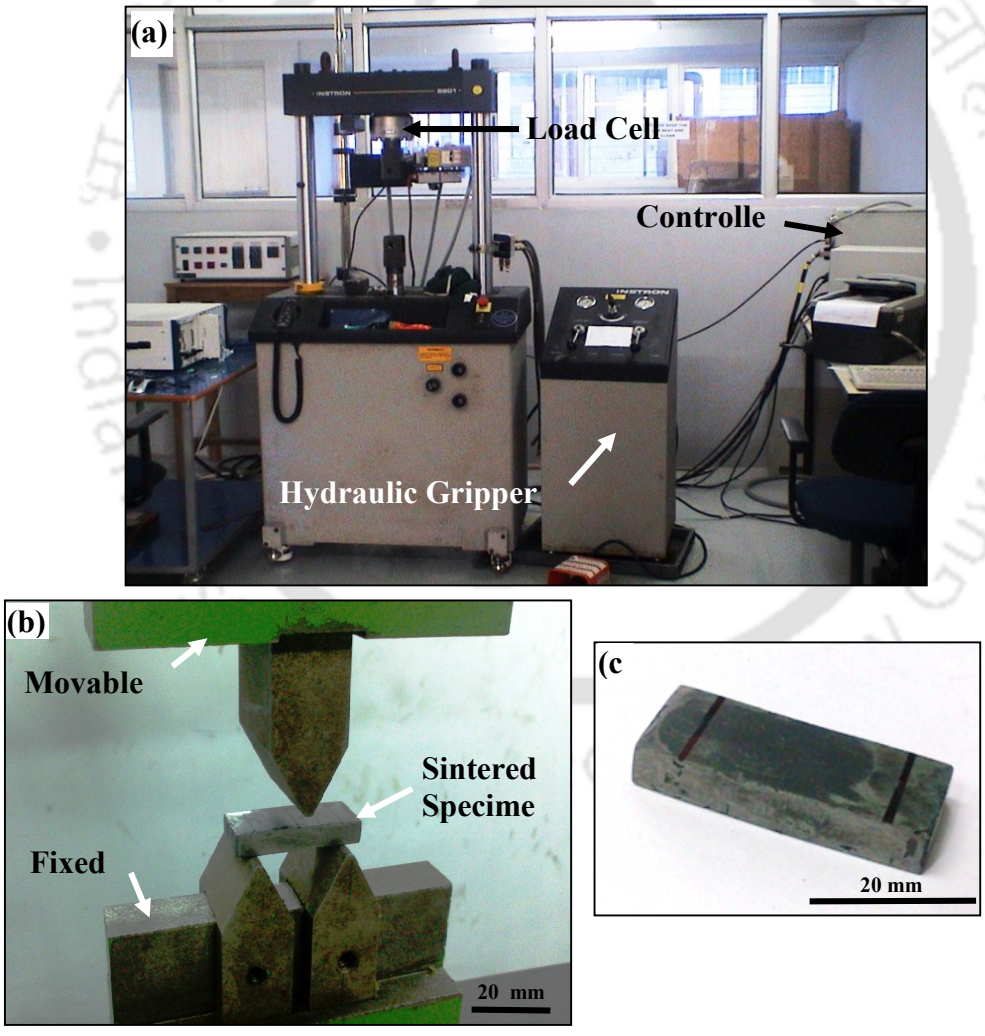


*Fig. 2.7 (a) Servo hydraulic testing machine (b) Developed fixture for TRS evaluation (c) Sintered specimen*

The sintered specimens were positioned on the supports and tests were carried out as per ASTM B406-96. The bending fixture used for test was made up of hardened steel. Figure 2.7(c) shows the sintered specimen. The sintered specimen was polished and made to required dimension for acquiring transverse rupture strength of all materials of WC-Co with different percentage of calcium fluoride. Fractured surfaces of the TRS specimens were investigated with the aid of scanning electron microscope to understand the failure morphology. Hardness of the sintered samples was evaluated with the aid of Rockwell hardness tester.

Diamond Brale indenter of scale A with 60 kgf load was used to measure the hardness of the sintered specimens. Vickers diamond indentation were made on the test specimens after polishing with indenting load of about 50 kgf (Fig. 2.8(a-b)) to evaluate fracture toughness. Total crack length produced at opposite corners of indent was measured with the help of optical microscope (Carl Zeiss Axiotech model upright optical microscope) as in figure 2.9(a-b). With the crack length and measured hardness,

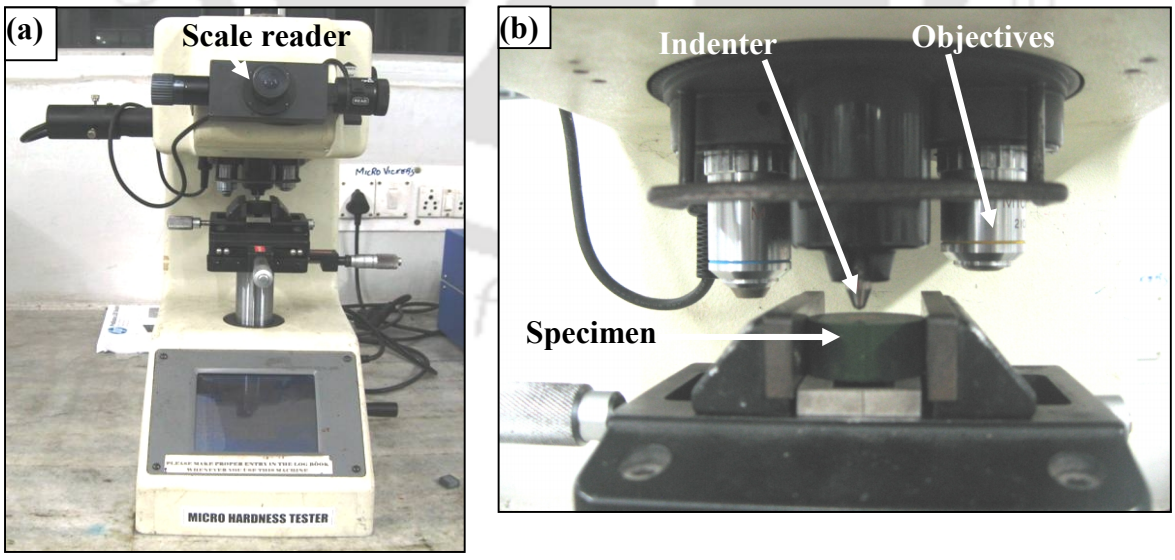


*Fig. 2.8(a) Vicker hardness tester with mounted specimen (b) Close up view*

Palmqvist fracture toughness was computed using following relation (Shatov, et al, 2006, Shetty, et at., 1985)

$$K_{IC} = A\sqrt{HV}\sqrt{P/\sum L} \qquad (2.2)$$

Where

$K_{IC}$ : Fracture toughness, $MNm^{-3/2}$

$P$: Indentation load, N

A: constant factor 0.0028

HV: Hardness, MPa

$\sum L$ : Sum of crack length, mm

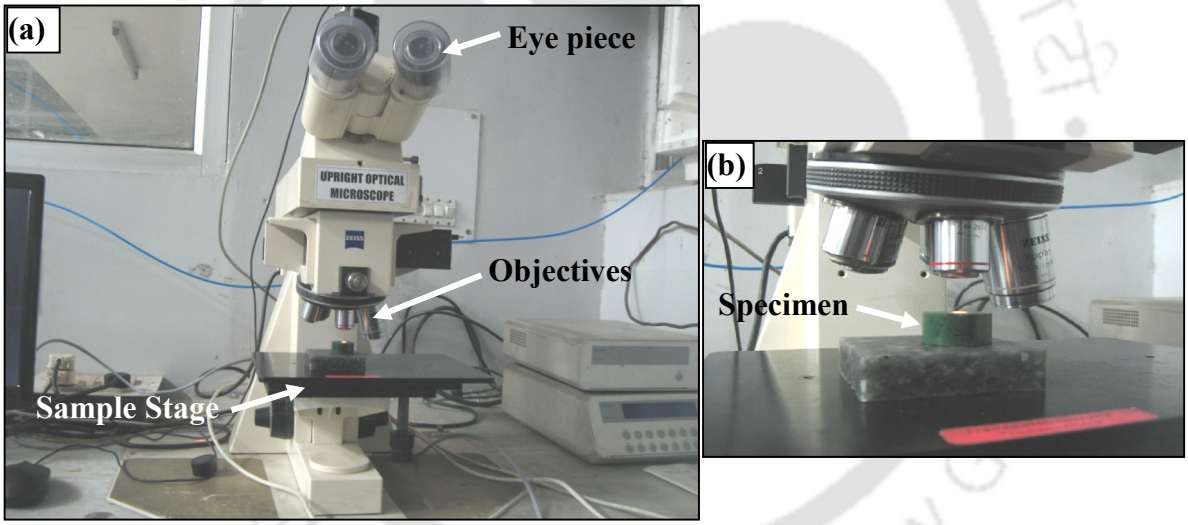


Fig.2.9 (a) Optical microscope used to observe indentation (b) Close up view

## 2.3 MILLING CHARACTERISTICS OF DEVELOPED MATERIALS

In the processing of powder materials, small grain sizes generally increase with the surface to volume ratio of the mixer, and promote sintering. Due to that, diffusion rate increases and this may lead to decrease in the sintering temperature. So, it is essential to reduce grain size and mechanical milling is chosen to decrease particle size of tungsten carbide based cutting tool

material. Milled powders were observed under a scanning electron microscope (LEO, 1430 vp) to study the morphology.

Figure 2.10(a-c) shows the morphology of procured WC, Co and $CaF_2$ particles. It is observed that the particle size of the cobalt and calcium fluoride is bigger than that of tungsten carbide. Cobalt particle shape is nearly spherical which can improve the packing density.

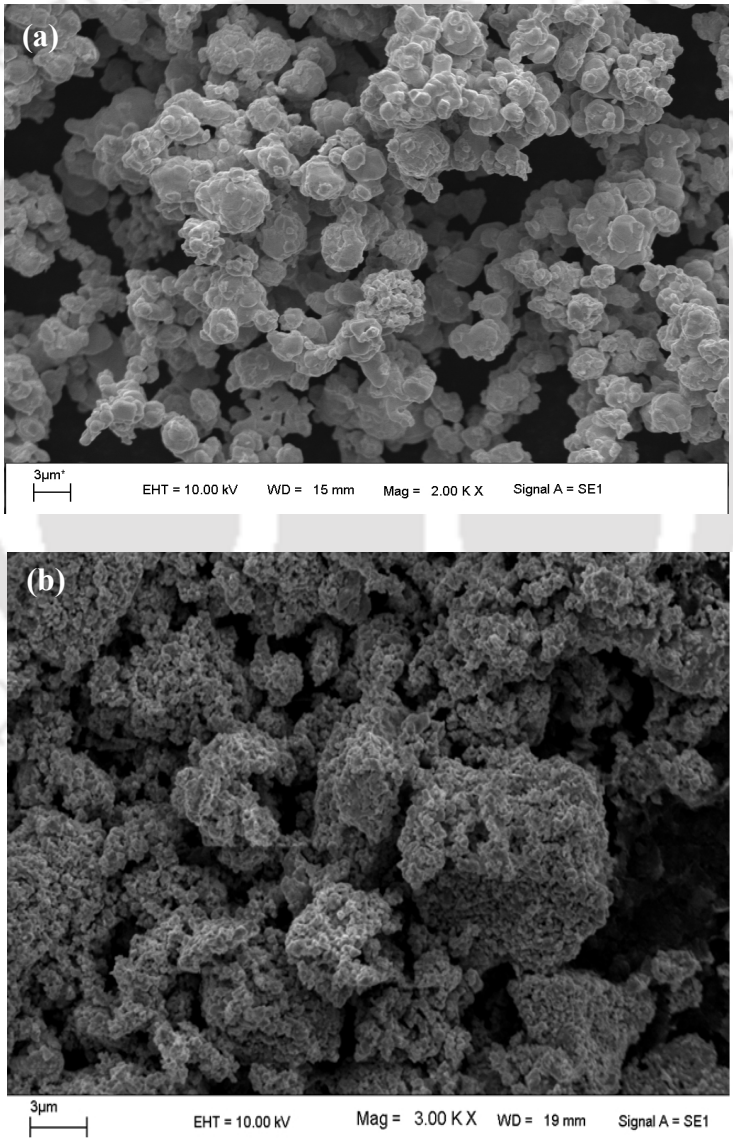

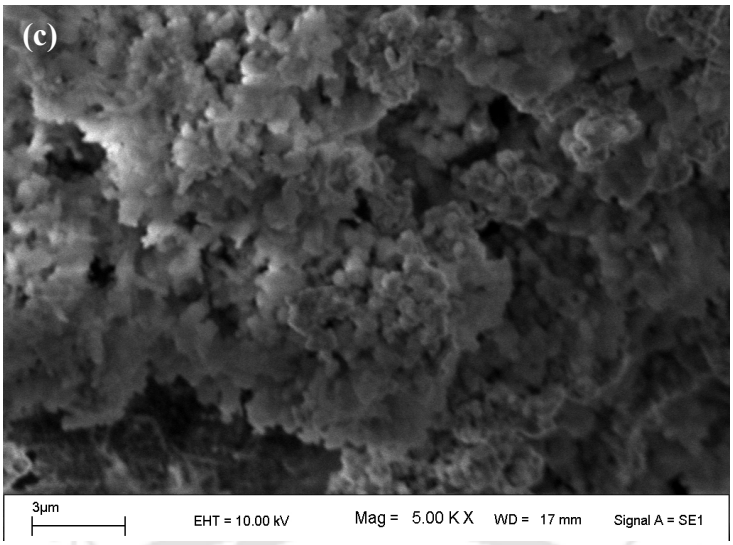


*Fig. 2.10 Morphology of as received material: (a) A tungsten carbide (b) A cobalt (c) A calcium fluoride.*

Figure 2.11(a-c) shows the morphology of WC-Co-5 wt.% $CaF_2$ powder after 20, 40 and 100 h of ball milling. Most particles exhibit a reduced size and rounded like morphology after 40 h of milling. However, a significant difference was not observed from the morphology of milled powders at different hours of milling.

The sizes of the milled powders were analysed at various milling period with the aid of Laser Particle Size Analyser (Malvern, Master size APA 2000). This unit can measure particles in the range 0.02 to 2000 µm. Milled powders were sonicated for an hour in millipore water for uniform dispersion (Hewitt and Kibble, 2009). Dispersed particles were then computed for average particle size distribution, D50. For different milling duration, D50 was obtained by plotting the particle size in µm over the volume frequency in % of the particles.

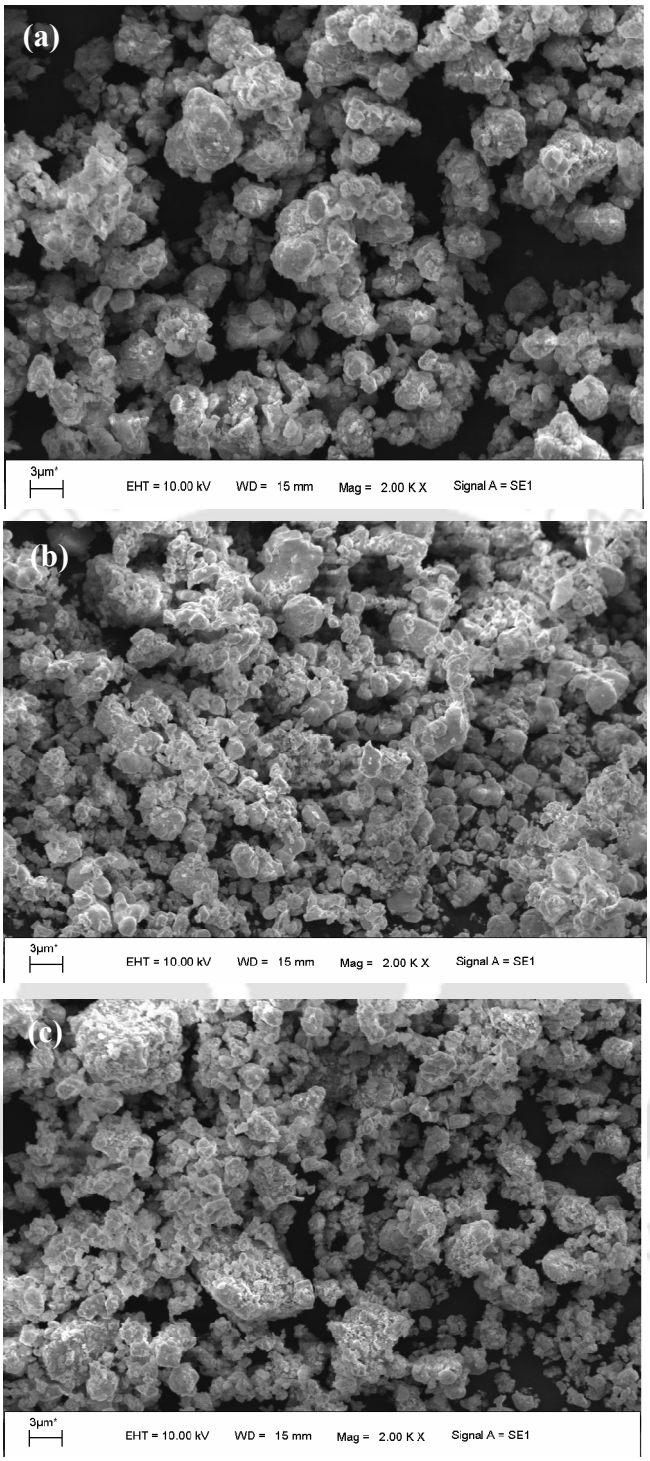


*Fig. 2.11(a) Morphology of WC-Co-5 wt.% $CaF_2$ after 20 h (b) Morphology of WC-Co-5 wt.% $CaF_2$ after 40 h (c) Morphology of WC-Co-5 wt.% $CaF_2$ after 100 h.*

Figure 2.12 shows the average particle size distribution of WC-Co-5 wt.% $CaF_2$ powders after various hours of milling. After 20 and 40 h of milling, the average particle size has reduced to 4.8 and 0.4 μm respectively.

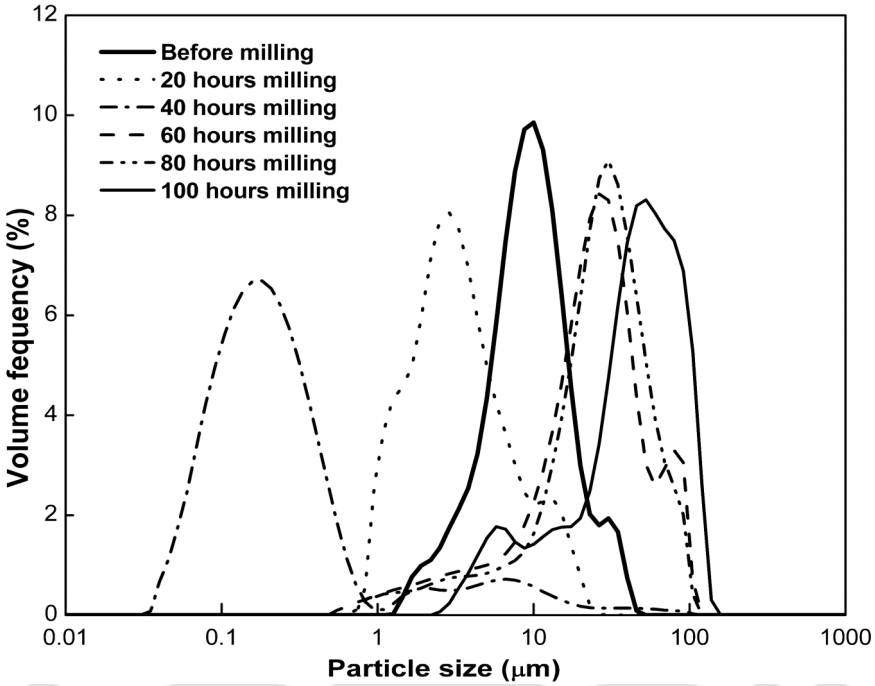


*Fig. 2.12 Particle size distribution of powders prepared with different ball milling time*

Beyond 40 h of milling, particles begin to embed with each other due to the strong cohesion between particles which result in increased resistance to the fracture. The average particle size at 80 and 100 h of milling shows 33 and 53 μm respectively. Gordo *et al*., (2005) milled the Fe-TiCN composite for 4-12 h and observed the particle size. The particle size reduced to 1.5 μm after 10 h of milling and increased to 15μm after 12 h of milling due to the cold welding.

Raghu *et al.,* (2001) prepared copper tungsten by mechanical alloys and observed the particle size increase after 10 h of milling. Figure 2.13 shows the particle distribution of milled powders for different percentage of solid lubricant, calcium fluoride. Results revealed

the effect of $CaF_2$ amount over particle size is insignificant and lies between 1-5 μm except for 10 wt.% of $CaF_2$. At higher amount, due to extreme ductility, $CaF_2$ exhibits extreme plastic deformation and contribute agglomeration (Sliney, 1982). Han *et al.,* (2012) observed the effect of different percentage of Ni with W powder and uniform distribution of particle size was observed at 5% Ni.

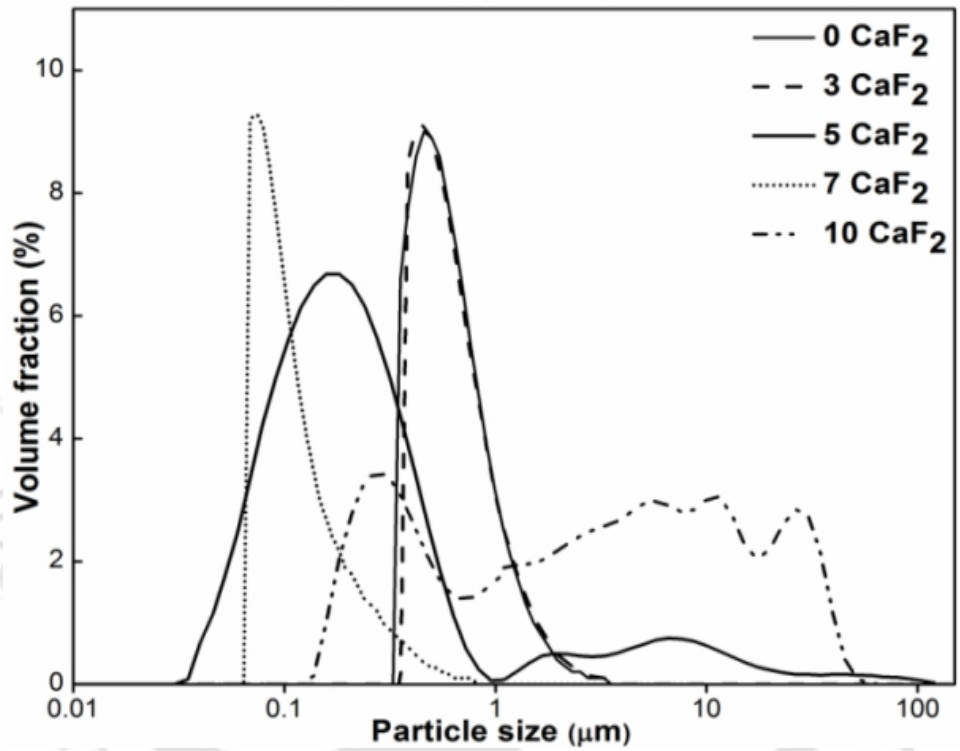


*Fig. 2.13 Particle size distributions of powders prepared with different percentage of calcium fluoride at 40 hours milling.*

### 2.3.1 Powder Crystallinity

Crystallinity of developed materials was evaluated with the aid of an X-ray diffractometer (Bruker D8 Advance). XRD patterns were obtained with Cu Kα radiation (λ = 0.1504 Å) in $10° \leq 2\theta \leq 75°$ in steps 0.05°. Full width at half maximum (FWHM) is denoted by $\beta_{hkl}$ and this is obtained with the aid of Powder X, diffraction data analysis software. Microstrain (ε) values for milled powders were obtained by computing the ratio between d-spacing of milled

and raw pattern. Peak broadening due to microstrain was determined by the Wilson formula. Borah *et al.,* (2007) utilized the Wilson formula for the material characterization. Crystallite sizes of milled powders were obtained using the Scherrer's equation (Langford and Wilson, 1978) XRD patterns of the milled mixture at various milling hours are shown in figure 2.14. The results revealed the broadening of diffraction peaks with an increase in milling hours.

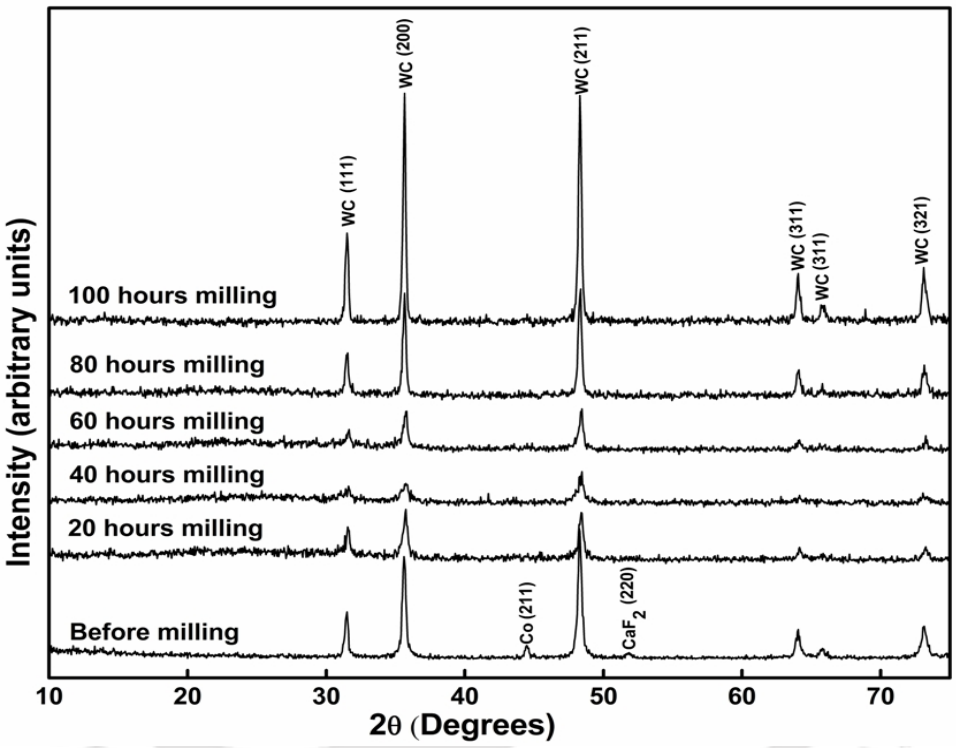


*Fig. 2.14 XRD patterns of milled powders with different ball milling time*

Crystallite size of the investigated material is in the range of 16-26 nm. From figure 2.15, it is observed that the average crystallite size of the milled powder reduces considerably up to 60 h of milling. Brittle characteristics of the tungsten carbide contribute to the rapid fragmentation of the particle and hence the crystallite size is also reduced. Beyond 60 h of milling, increase in crystallite size was observed due to the particle agglomeration. Lu *et al.,* (2005) also utilized XRD to identify the effect of milling time on the crystallite size of Mg–Ti and Mg-Al composites. Crystallite size is rapidly decreased after 20 h of milling and small

reduction of crystallite size at 40 h of milling. Enayati *et al.,* (2005) prepared the WC–Co powder by ball milling up to 40 h and observed a 15–20 nm crystallite size.

Figure 2.15 shows microstrain in the range of 0.5-0.6% of considered powders at various milling periods. Microstrain is directionally proportional to the energy required to fracture the particles. From the microstrain analysis, it is revealed that beyond 60 h of milling, energy required to fracture the particles increases due to the increased particle and crystallite size.

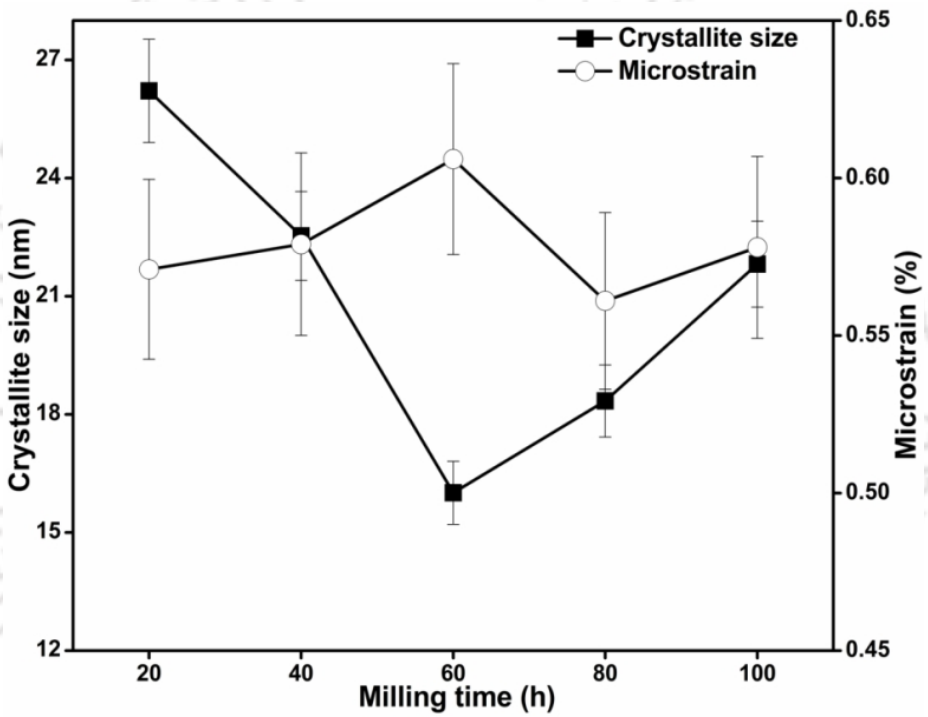


*Fig. 2.15 Crystallite size and microstrain of material at various milling hours*

Borah et *al.,* (2007) investigated the effect of milling time on microstrain while milling RuAl and observed a similar behavior; microstrain increased up to 0.45% then decreases to 0.35% after 30 h. Avettand *et al.,* (2003) investigated the milling parameters of tungsten carbide based materials and observed a crystallite size of 5 nm and 0.25% strain after 30 h.

## 2.4 MECHANICAL PROPERTIES OF DEVELOPED MATERIAL

### 2.4.1 Compaction Characterization

Compaction characteristics of the powder at various milling hours were investigated. Camphor was applied on the die and punch surfaces to reduce friction and prevent micro cracks on the green compacted specimens. Milled powders were compacted at various pressures, 200, 250, 300, 350 and 400 MPa. Figure 2.16 shows two major stage of compaction and slope of the curve indicate densification. In the first stage (upto 50 kN) densification was found to increase rapidly due to inter particle sliding and rearrangement.

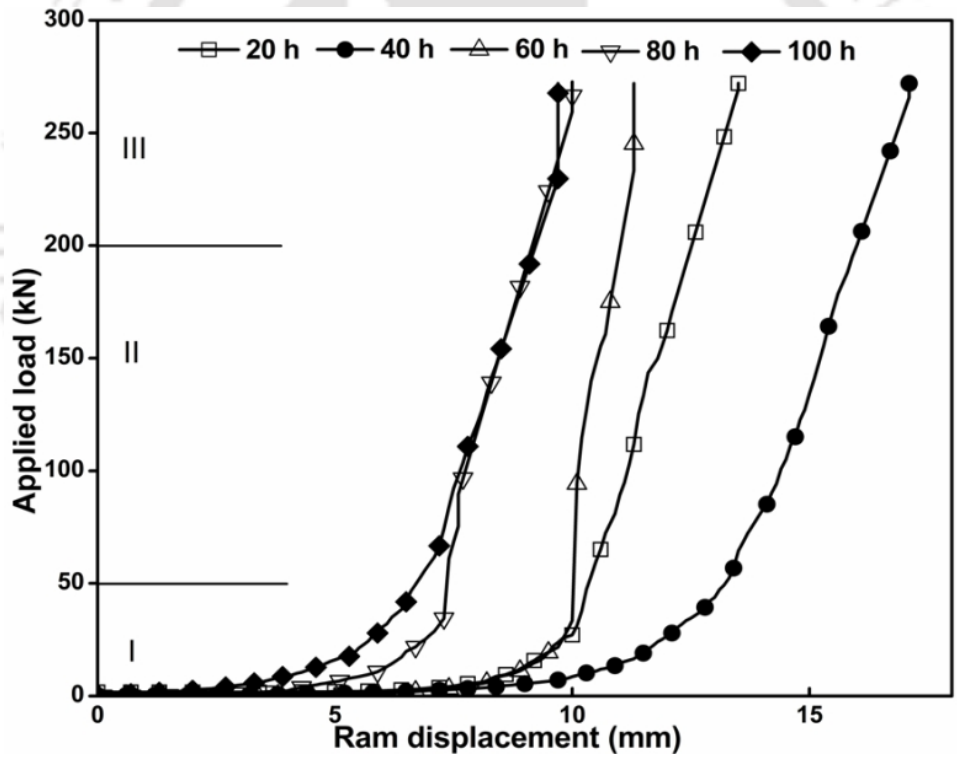


*Fig. 2.16 Compaction curve of test material at various milling hours*

In the second stage, densification increases gradually due to the elastic deformation of particles (Poquillon *et al*., 2000). Though last stage is distinctly not visible in the present investigation, plastic deformation occurs in this stage. Figure 2.17 shows the effect of milling

period and compaction pressure on sintered density. Results confirmed that relative density of the sintered sample increases with the compaction pressure and with milling time upto 40 h. Superior relative density, 94% (14.634 g/cm$^3$) is achieved at 400 MPa pressure and 40 h of milling time. Sintered specimen density has infinitesimal effect of compact pressure unlike green density.

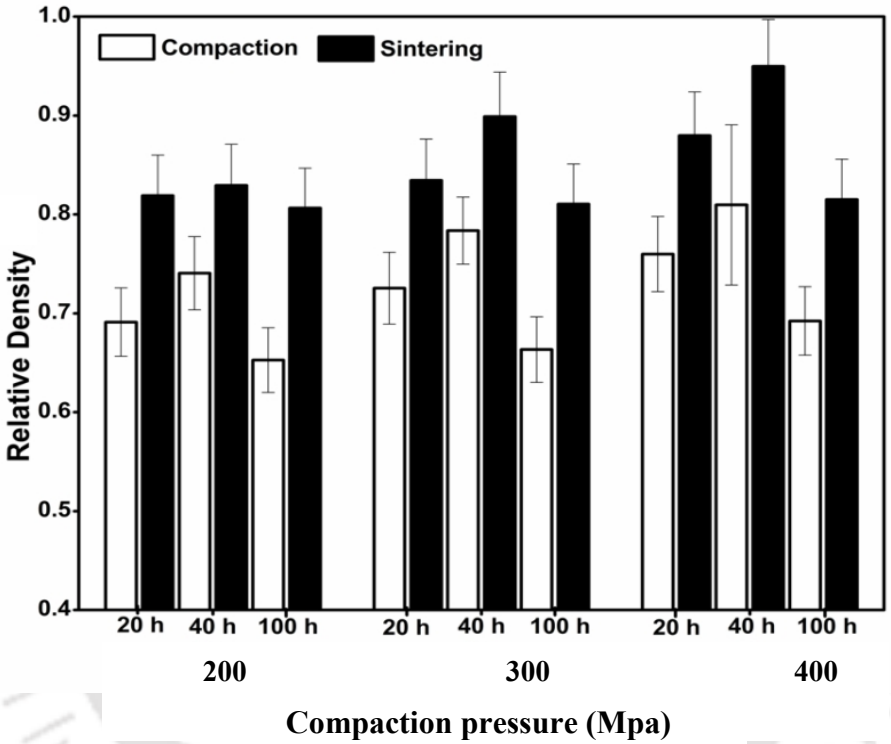


*Fig. 2.17 Effect of compaction pressure and milling hours on relative density of material*

Hewitt and Kibble (2009) investigated the effect of milling time on WC-Co composite and obtained 14.34 g/cm$^3$ after 60 h of milling in the pressure less sintering, beyond 60 h density found to reduce. Jia et al., (1998) developed WC-10 % Co composite at sintering temperature of 1350˚C and achieved theoretical density of 14.93 g/cm$^3$.

Figure 2.18 shows the effect of milling period and compaction pressure over sintered hardness. Test specimen exhibited superior densification and hardness at 40 h of milling for the considered compacted pressures of 200-400 MPa. The superior hardness 85 HRA (900 HV) was obtained at 40 h of milled composite.

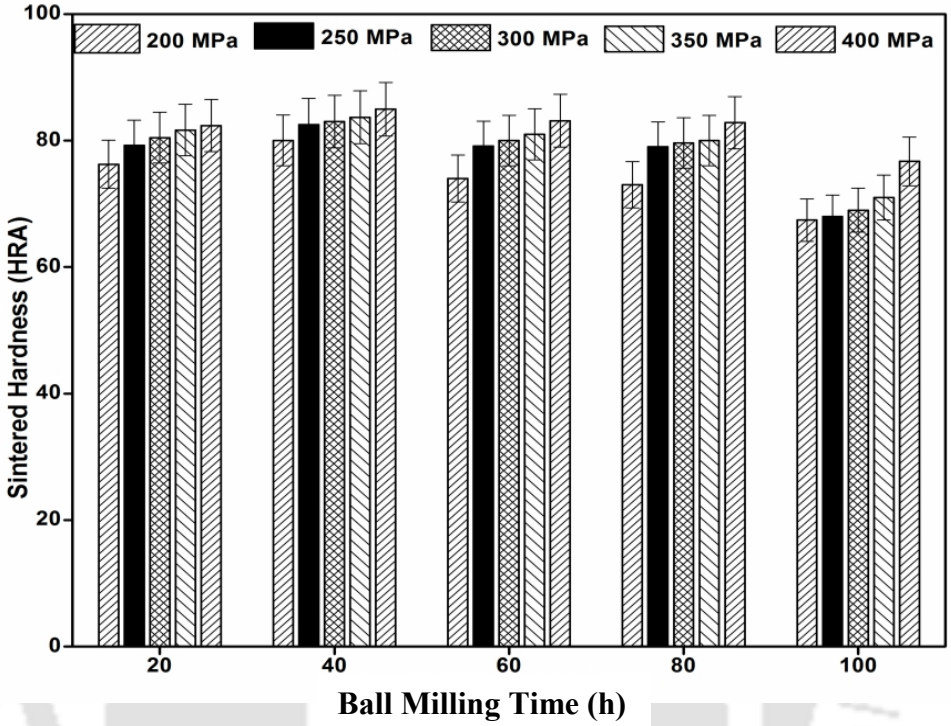


*Fig. 2.18 Effect of compaction pressure and milling hours on hardness of test material*

Reduced particle size contributes to this superior density and hardness. Similar to particle size and density, hardness also reduces beyond 40 h of milling. Hewitt and Kibble (2009) obtained 1300 HV hardness after 60 h of milling in the pressure less sintering, beyond 60 h hardness found to reduce. Peng *et al*., (2013) also obtained the maximum hardness of 86 HRA of WC-Co particle reinforced iron matrix.

### 2.4.2 Sintering Characterization

To understand the effect of milling hours on sintered surface, microstructures of sintered specimens are investigated using scanning electron microscope. Sintered specimens were

sectioned, polished by 220-800 grit emery sheets followed by diamond polish, cleaned with Murakami's etchant to observe sintering quality.

Figure 2.19(a-b) shows etched WC-Co material without $CaF_2$ showing more porosity with poor bonding between individual particles. Figure 2.19(c-d) shows etched WC-Co material with 5 wt.% $CaF_2$ showing few porosity with good bonding between individual particles. The Co is known for the excellent binder for WC.

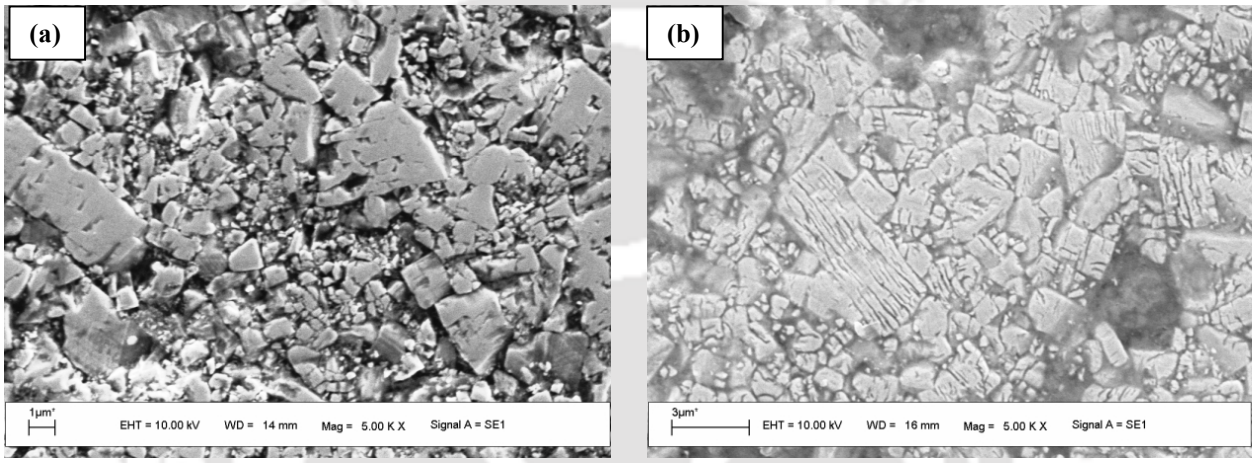


*Fig. 2.19 (a-b) Scanning electron micrograph of sintered specimen without calcium fluoride*

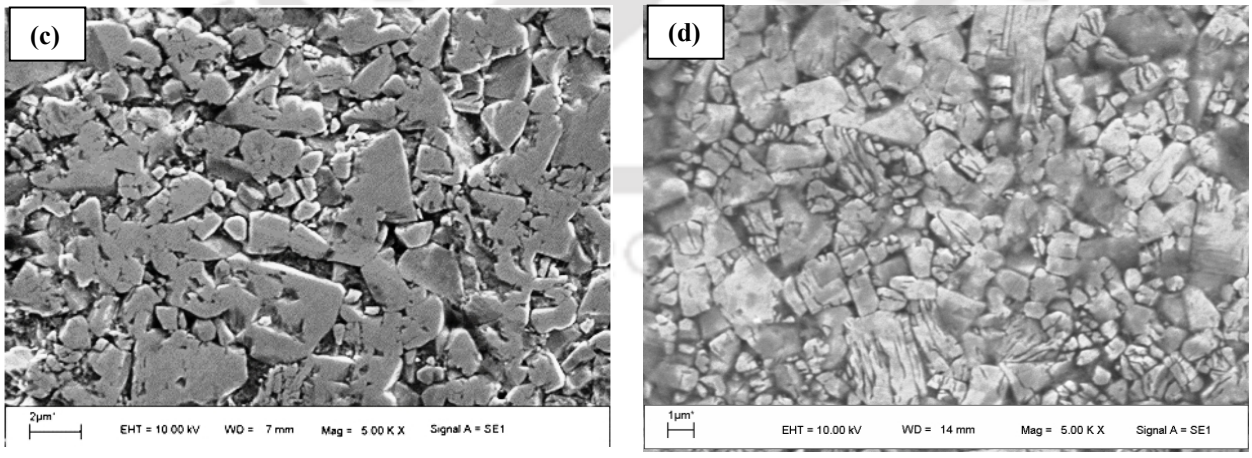


*Fig. 2.19 (c-d) Scanning electron micrograph of sintered specimen with 5 wt.% calcium fluoride*

Density of the straight WC-Co material under considered milling, compaction and sintering conditions exhibited 12.30 ± 0.73 g/cc density. However, with the addition of $CaF_2$, bonding between the WC-Co particles is getting altered during compaction. WC-Co with 3 wt.% $CaF_2$ (insufficient lubricant) exhibited poor density (11.42 ± 0.65 g/cc) than straight WC-Co. Similarly, WC-Co with 10 wt.% $CaF_2$ (excess lubricant) exhibited poor density (10.91 ± 0.22 g/cc) than straight WC-Co. WC-Co with 7 wt.% $CaF_2$ exhibited almost same density (12.99 ± 0.88 g/cc) when compared to that of straight WC-Co material. WC-Co with 5 wt.% $CaF_2$ exhibited superior density (14.64 ± 0.14 g/cc) than that of straight WC-Co material. Figure 2.20 (a-g) shows EDS of sintered specimens, where presence of all the constituent materials is confirmed.

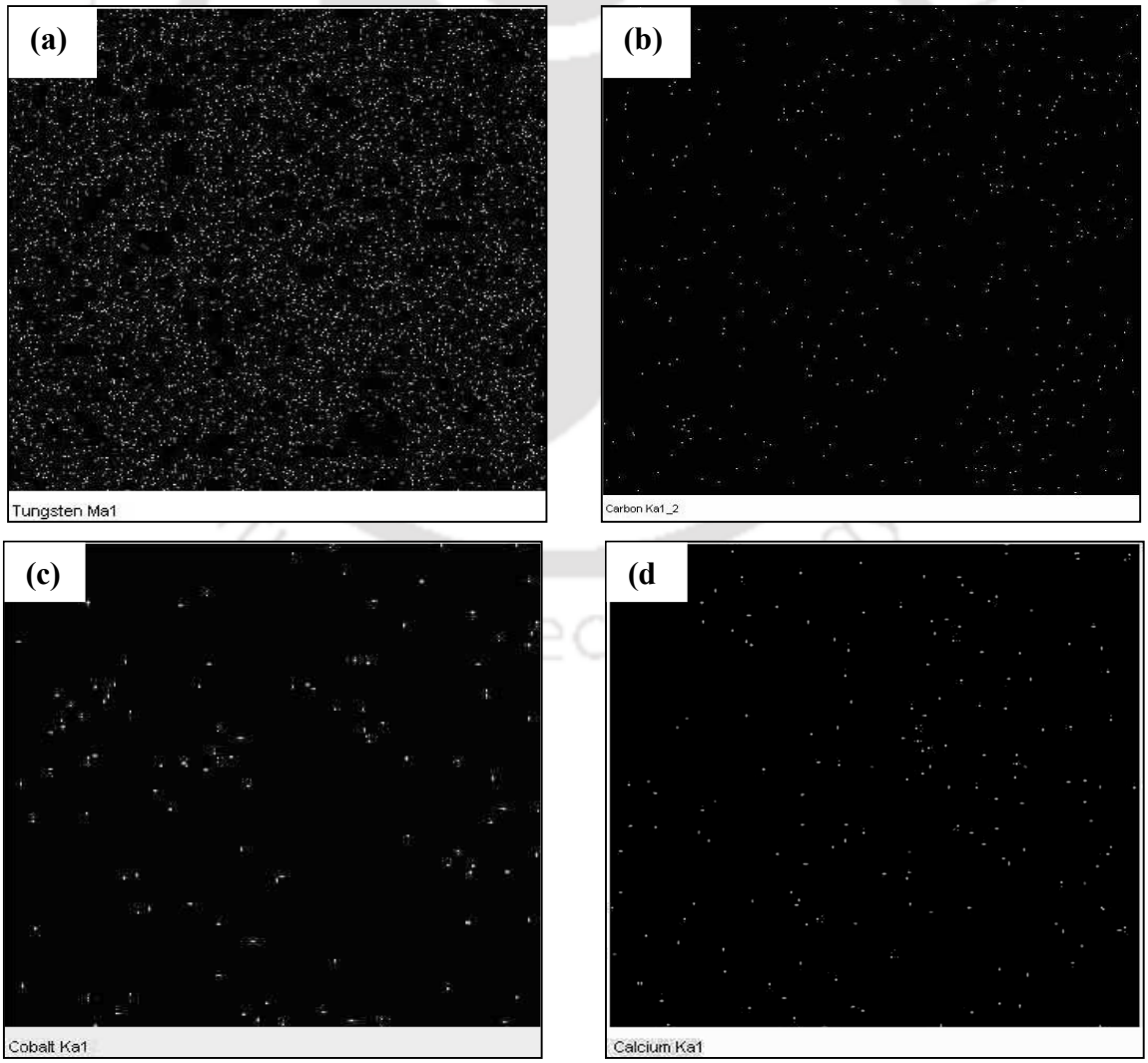

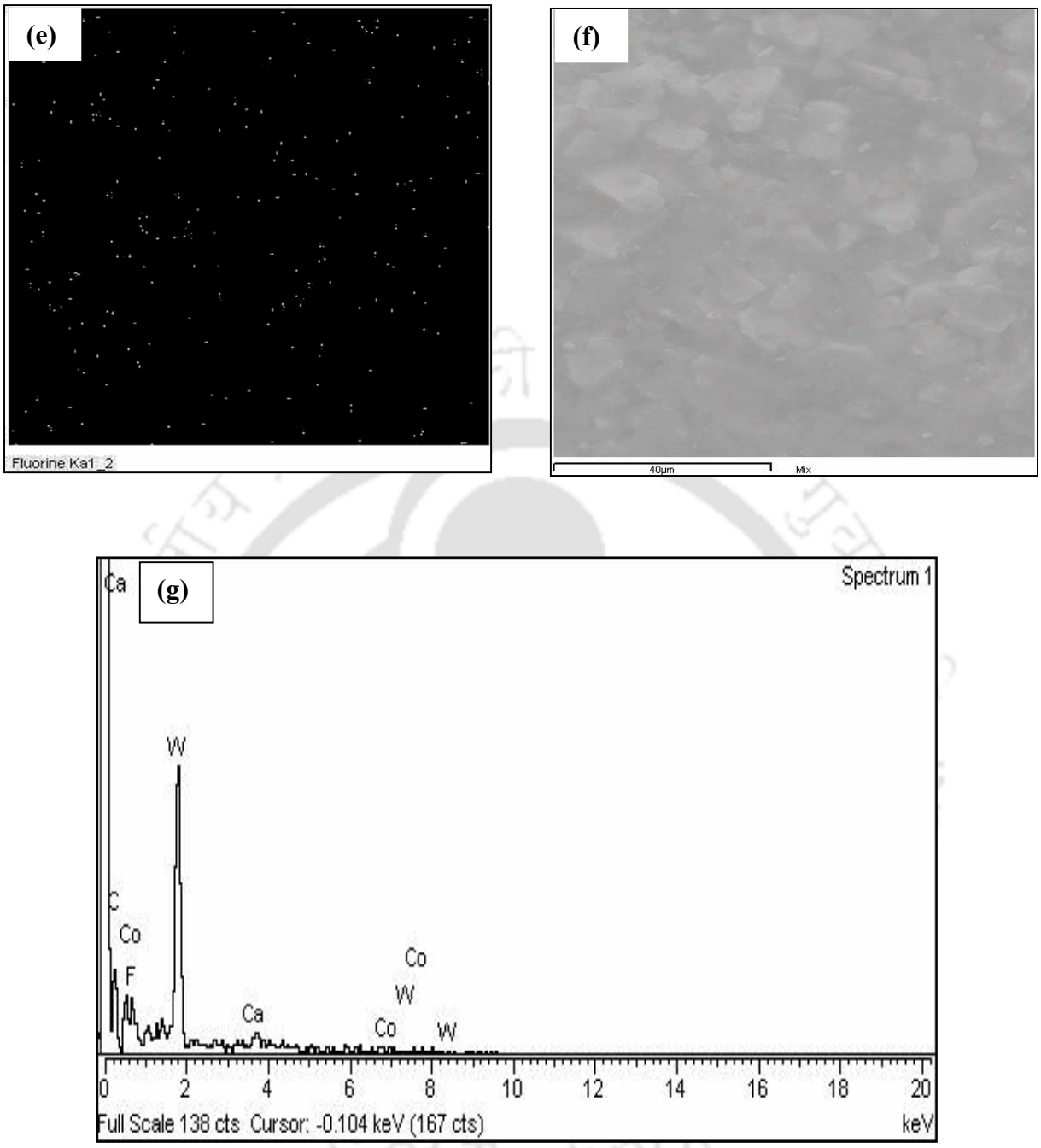


*Fig. 2.20 EDS Mapping of; (a) Tungsten (b) A carbon (c) A cobalt (d) A calcium (e) A fluoride (f) EDS area of sintered tungsten carbide with 5 wt.% $CaF_2$ (g) EDS plot showing presence of constituents*

### 2.4.3 Transverse Rupture Strength

Transverse rupture strength of the sintered specimen was evaluated by conducting 3-point bend test with the aid of servo hydraulic testing machine. Figure 2.21(a-b) shows the presence of spherical agglomerates at the fractured surface of WC-Co without $CaF_2$. Presence of spherical agglomerates confirms the sintering defects. Similar features were also observed at the fractured surface of WC-Co with 10 wt.% $CaF_2$ (Figure 2.21(g-h)). However no such spherical shape agglomerates were observed at fractured surface of the WC-Co with 5 wt.% $CaF_2$ and 7 wt.% $CaF_2$ with good bonding between grain boundaries were observed.

Figures 2.21(c-d) and 2.21(e-f) shows the fractured specimen of WC-Co with 5 and 7% $CaF_2$, where individual particles were observed to be closed packed and bonded with cobalt. Fracture surface of all the investigated materials showed intergranular fracture, which is confirmed by the clear separation around the grains (German, 1996). Shatov *et al.,* (2008) investigated the fractured surface of WC-Ni cemented carbide where mostly inter-crystalline fracture along the carbide interface was observed.

Gu and Shen (2007) observed similar spherical agglomerates called balling phenomenon while laser sintering copper based metal powder. During sintering, excessive melting reduces the surface energy and melt break up into agglomerates of spherical shape. Li *et al*. (2012) also observed balling behavior while laser sintering stainless steel and nickel powder due to the poor wetting. In sufficient and excess amount of $CaF_2$ deteriorates wetting as well as contributes to the excess melting.

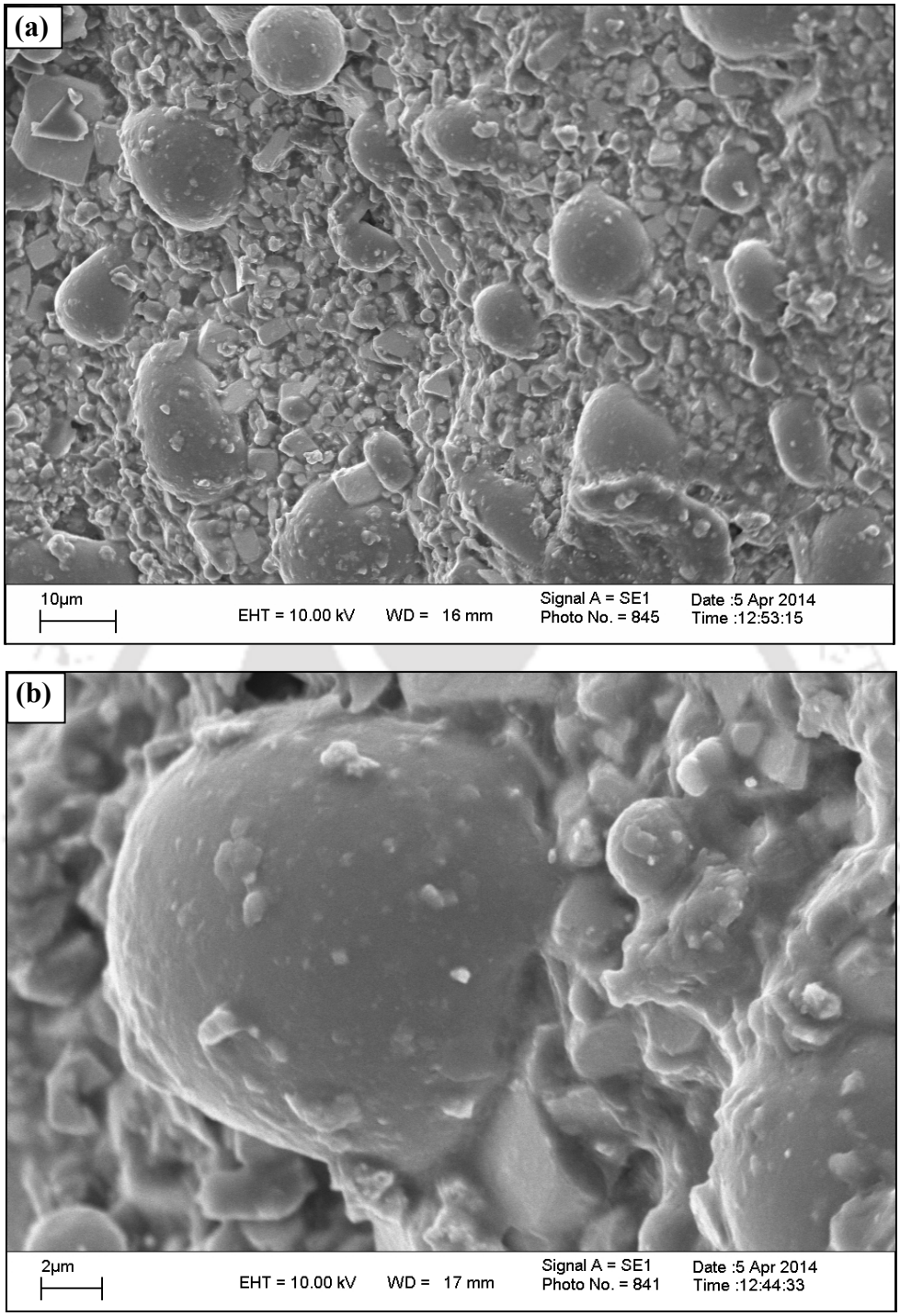


*Fig. 2.21(a) Fractured surface of sintered tungsten carbide with 0 wt.% $CaF_2$ showing a balling effect (b) Close up view of the fractured surface of sintered tungsten carbide with 0 wt.% $CaF_2$*

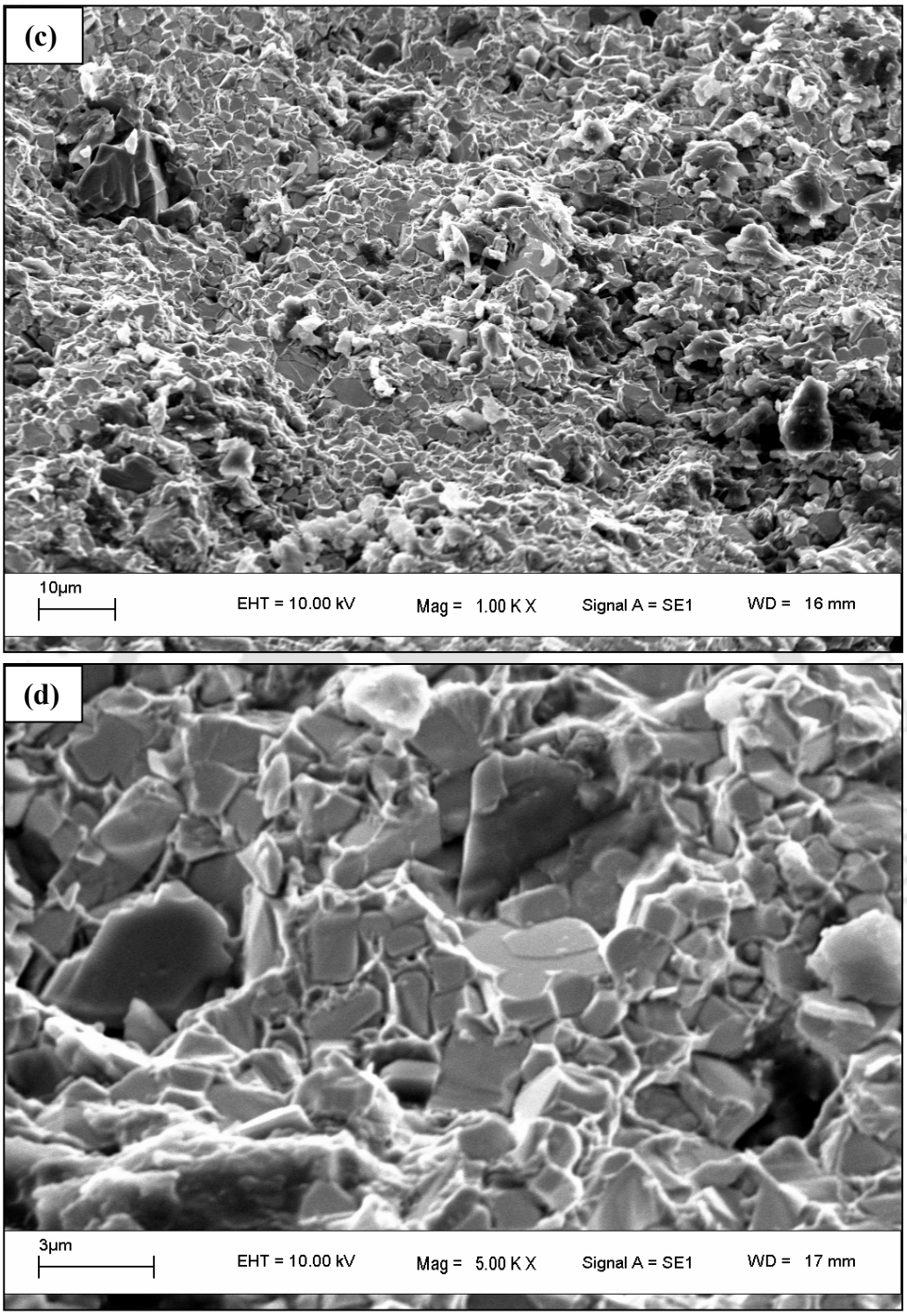


*Fig. 2.21(c) Fractured surface of sintered tungsten carbide with 5 wt.% $CaF_2$ showing no balling effect (d) Close up view of the fractured surface of sintered tungsten carbide with 5 wt.% $CaF_2$*

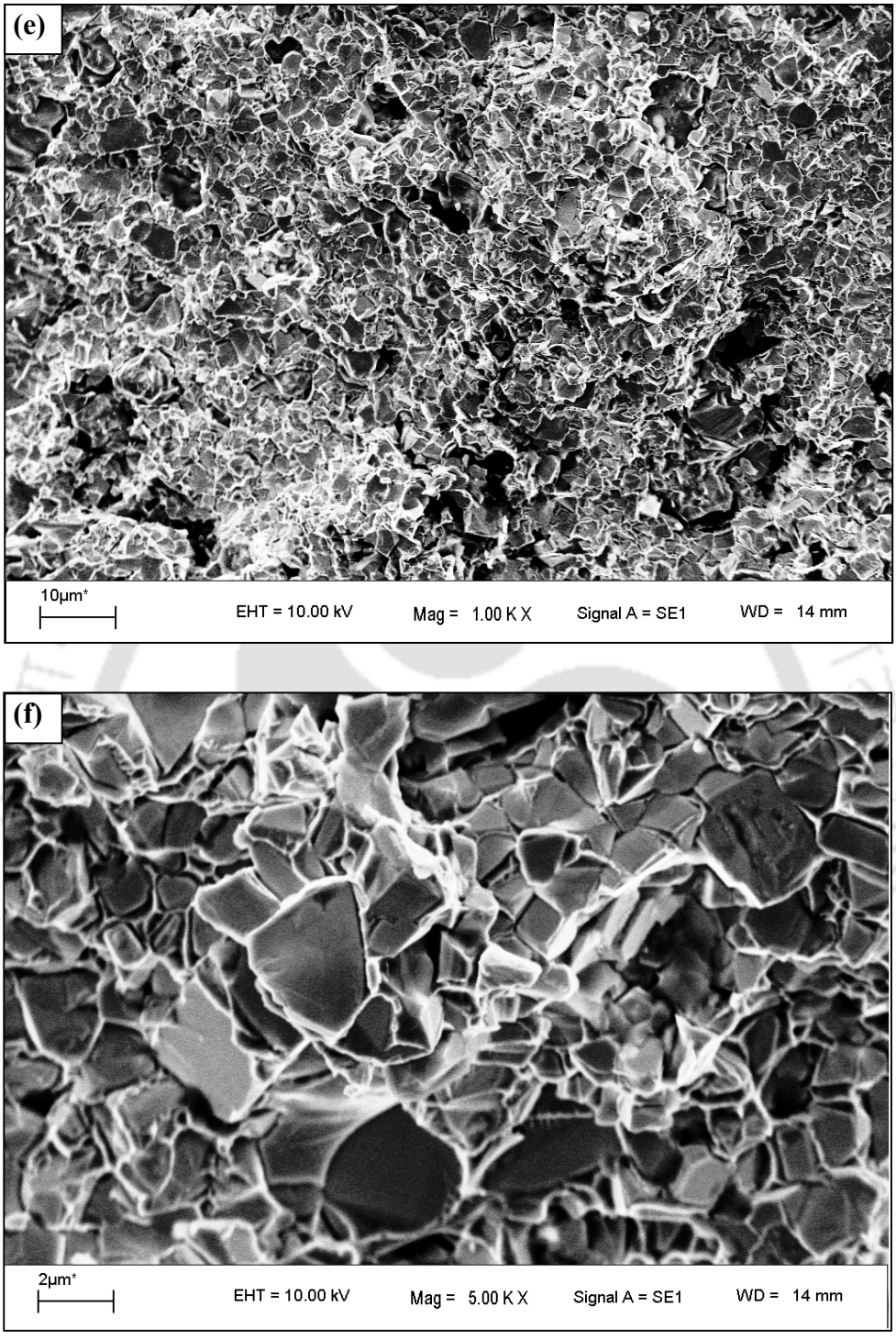


*Fig. 2.21 (e) Fractured surface of sintered tungsten carbide with 7 wt.% $CaF_2$ showing no balling effect (f) Close up view of the fractured surface of sintered tungsten carbide with 7 wt.% $CaF_2$*

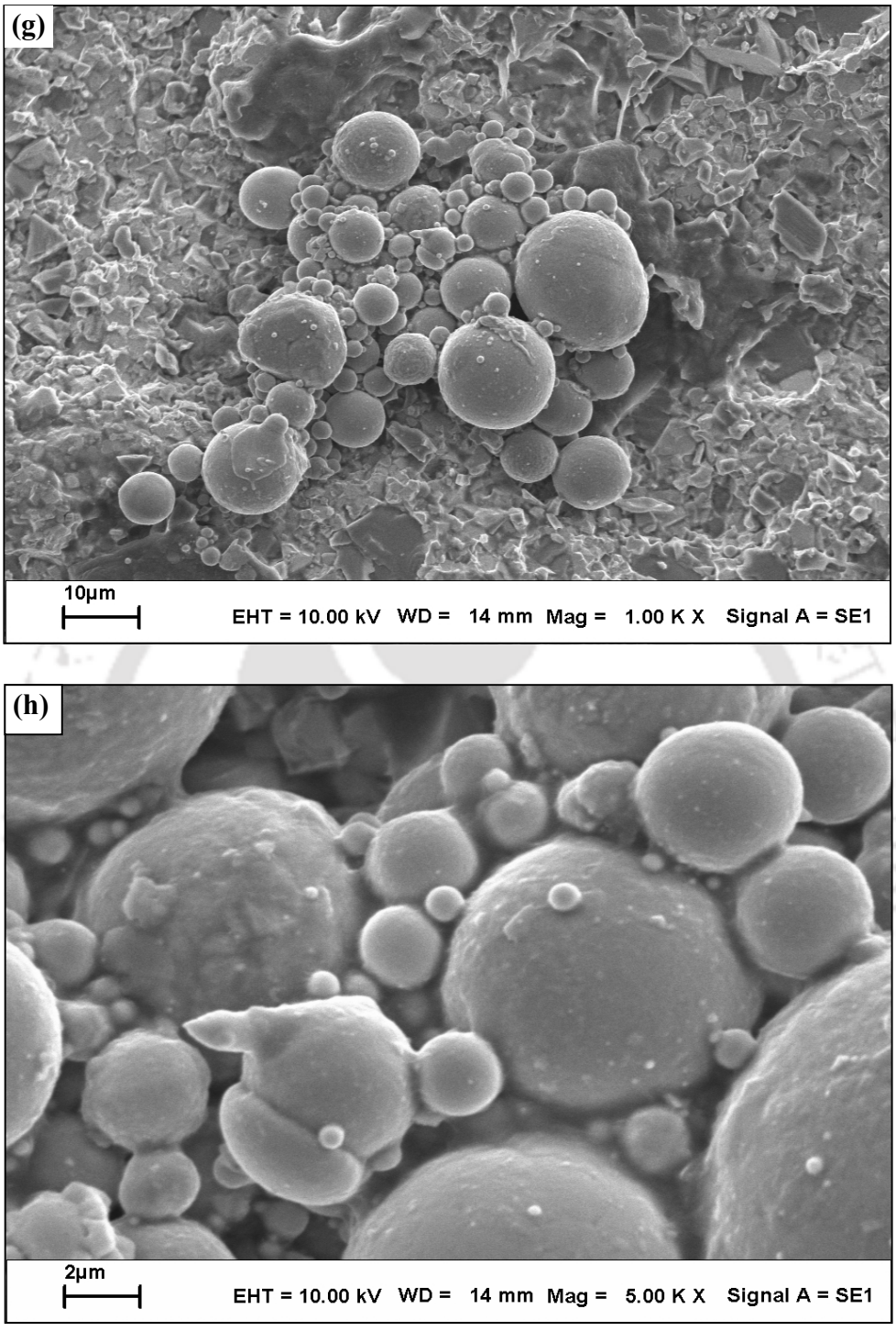


*Fig. 2.21(g) Fractured surface of sintered tungsten carbide with 10 wt.% $CaF_2$ showing balling effect (h) Close up view*

Figure 2.22 shows the transverse rupture strength of investigated sintered materials. Among the investigated material, WC-Co with 5 wt.% $CaF_2$ exhibited superior transverse rupture strength (1500 MPa) than that of other materials. Beyond 5 wt.% $CaF_2$, transverse rupture strength of tungsten carbide material reduces. Poor bonding was observed at material having more than 7 wt.% of $CaF_2$ , this is due to the presence of excessive soft materials in the boundaries of WC.

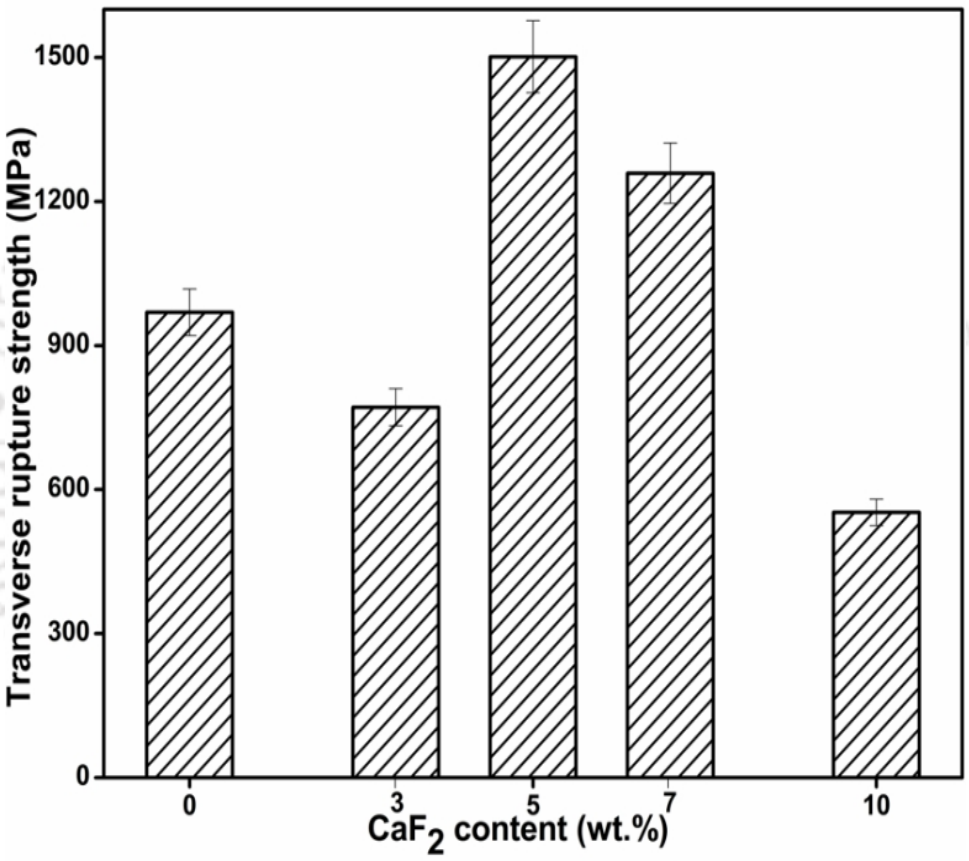


*Fig. 2.22 Effect of calcium fluoride on transverse rupture strength of sintered material*

Kato *et al*. (2003) and Lu *et al.* (2001) also observed similar strength behavior with graphite. Kato *et al*., (2003) reported the effect of graphite (5-40 %) on the bending strength of copper-tin composites. Superior bending strength of 350 MPa was achieved at 5% of graphite with copper-tin composites. With the increase in graphite upto 5%, an increase in bending strength

is observed then drops down due to the presence of pores. Cha *et al.,* (2001) also obtained transverse rupture strength in the range of 1600-1800 MPa, while developing nanocrystalline WC-10 Co cemented carbides. Upadhaya and Bhaumik (1988) also obtained transverse rupture strength in the range of 1000-2000 MPa while developing WC-Co with Nickel and Iron. Shaji and Radhakrishnan (2003) investigated the wear performance of grinding wheel bonded with various amount of calcium fluoride (5, 10 and 15 %). Results confirmed that fusion bonding nature of calcium fluoride helps to improve bonding strength and beyond saturation (in this case 10 wt.%) calcium fluoride weakens the bond.

Fractured surfaces of test materials were further observed under scanning electron microscope to confirm the bonding between tungsten carbide particles. Figure 2.23 (a-b) showed the intergranular fracture showing crack around the tungsten carbide particles for the straight WC-Co material for the considered milling, compaction and sintering conditions. Figure 2.23(c-d) showed superior bonding between tungsten carbide particles at WC-Co-5 % $CaF_2$ material. Figure 2.23(e-f) showed the intergranular fracture showing crack around the tungsten carbide particles for the WC-Co-10 wt.% $CaF_2$ material.

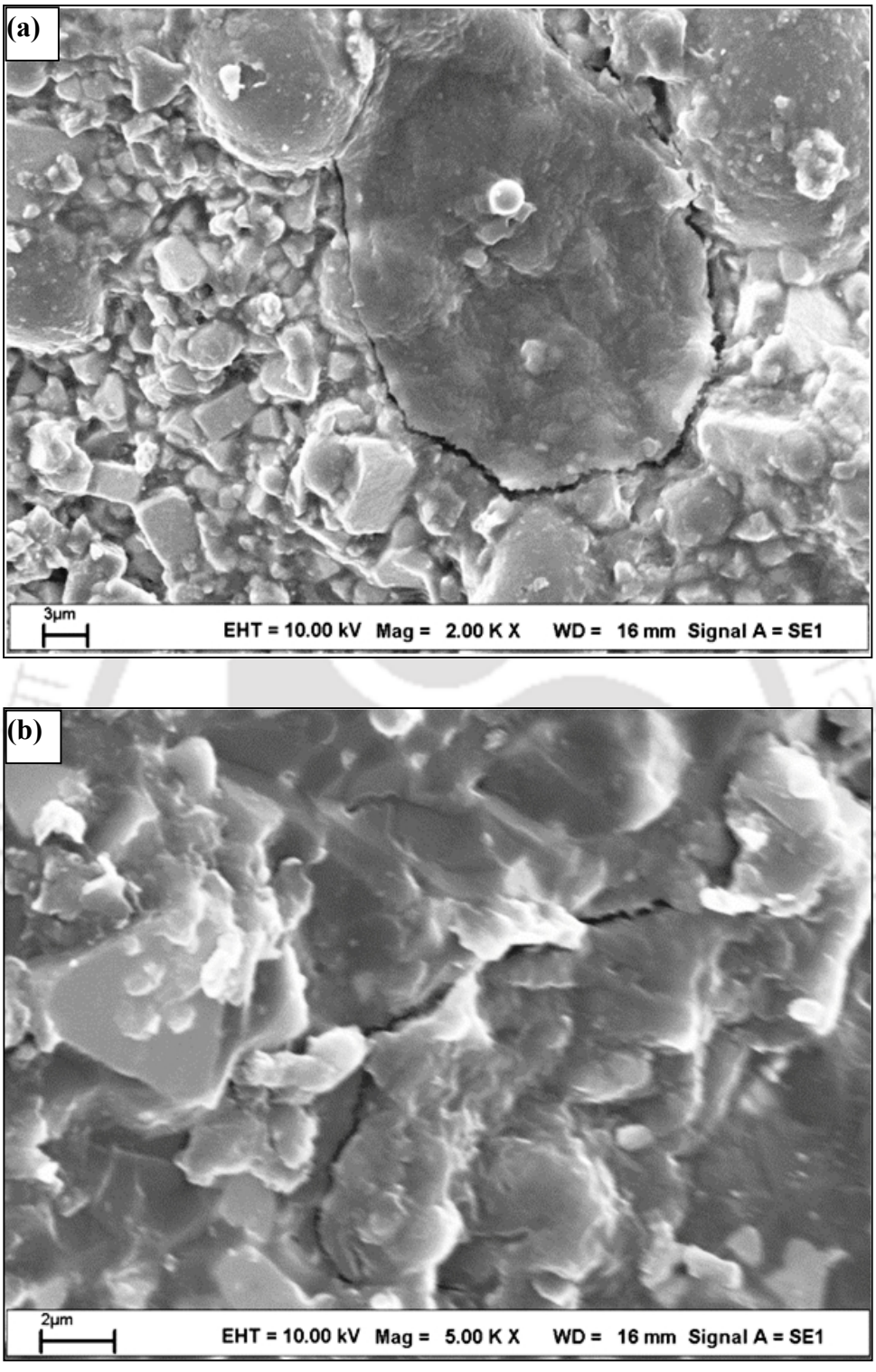


*Fig. 2.23(a) Intergranular fracture observed at fractured surface of straight WC-Co material (b) Close up view of the crack around tungsten carbide particles at the fracture surface of straight WC-Co material*

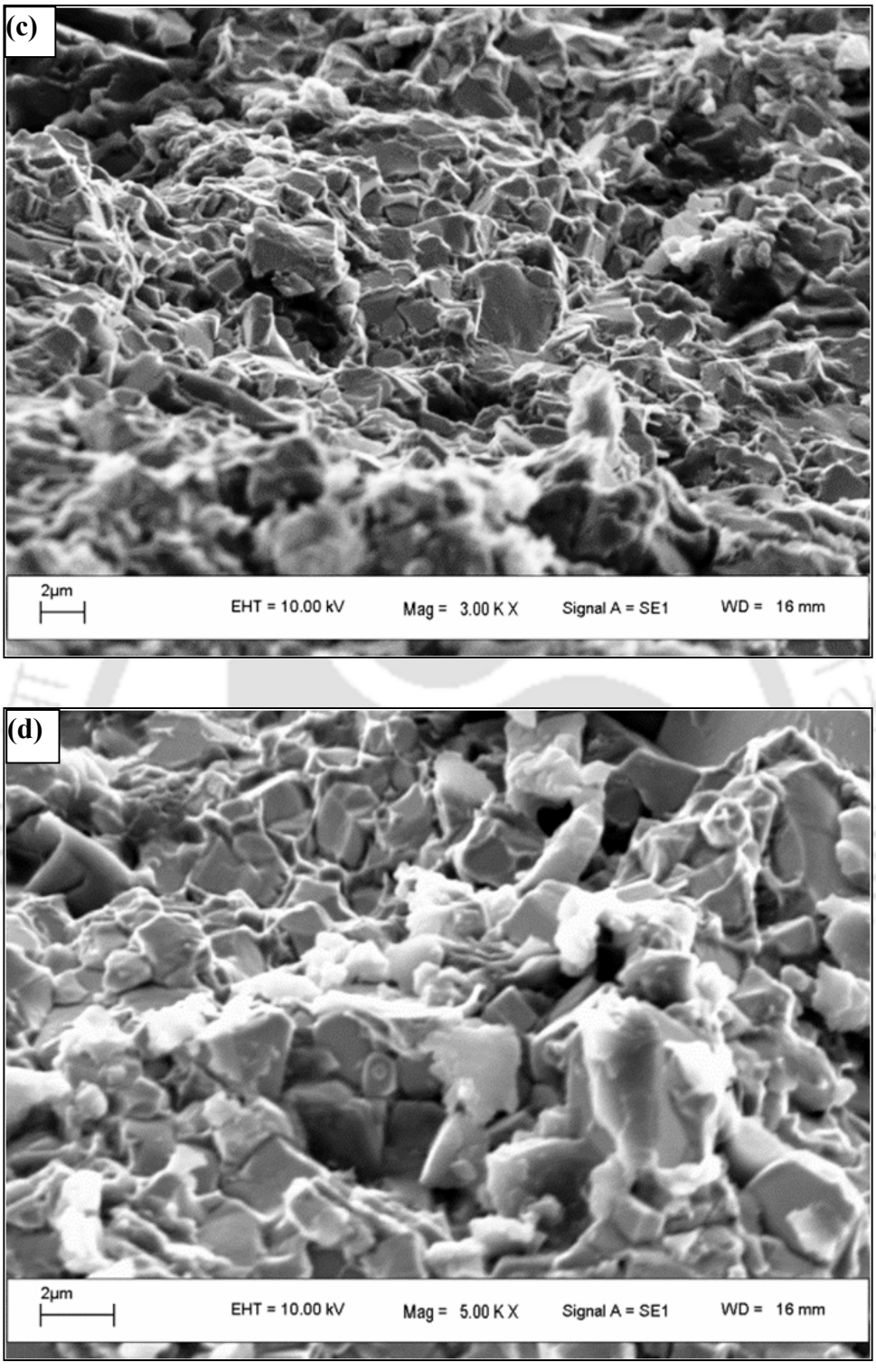


*Fig. 2.23(c) Superior bonding between tungsten carbide particles observed at fractured surface of WC-Co-5 wt.% $CaF_2$ material (d) Close view of superior bonding between tungsten carbide particles observed at fractured surface of WC-Co-5 wt.% $CaF_2$ material*

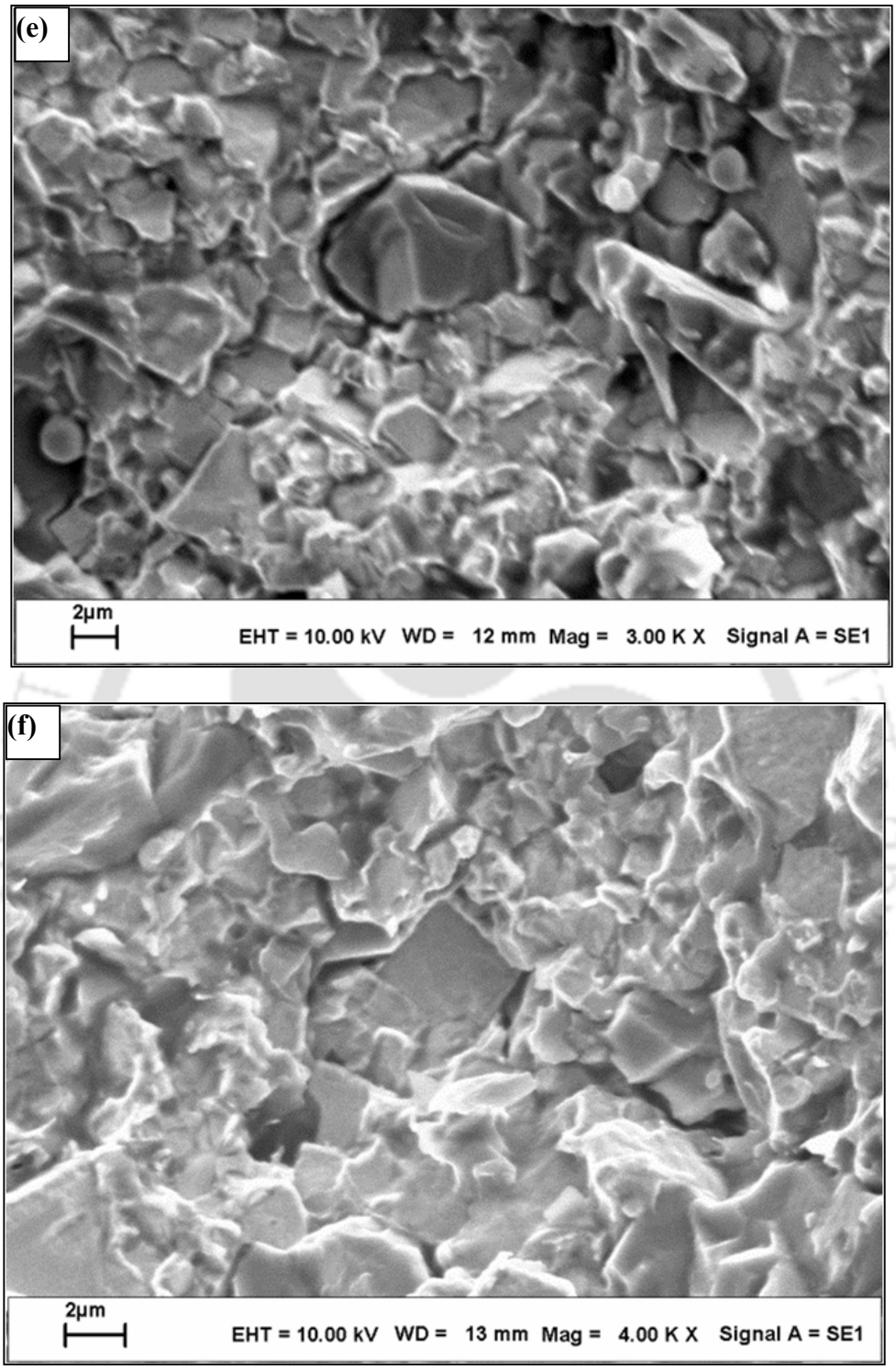


*Fig. 2.23(e) Intergranular fracture observed at fractured surface of WC-Co-10 wt.% $CaF_2$ material (f) Close up view of the crack around a tungsten carbide particles at the fracture surface of straight WC-Co-10 wt.% $CaF_2$ material*

Poor bonding among the tungsten carbide particles in the straight WC-Co as well as at WC-Co-3 wt.% $CaF_2$ and WC-Co-10 wt.% $CaF_2$ is due to the presence of spherical agglomerates which is called balling, a sintering defect. In spite of good compatibility between WC and Co, this sintering defect is exhibited in the straight WC-Co material. This could be due to the chosen milling, compaction and sintering conditions. However, no such spherical shape agglomerates were observed at the fractured surface of the WC–Co with 5 wt.% $CaF_2$.

### 2.4.4 Fracture Toughness of specimen

Figure 2.24(a-e) shows the image of the indented tungsten carbide without calcium fluoride and Figure 2.25(a-e) shows the indented tungsten carbide with 5 wt.% calcium fluoride specimens. From the measured crack length and hardness, fracture of the WC-Co and WC-Co-5 wt.% $CaF_2$ found out to be 13.2 and 12.8 $MNm^{-3/2}$ respectively. As anticipated, fracture toughness of the test specimen decreases with increase in hardness. Hardness HV50 of WC-Co and WC-Co-5 wt.% $CaF_2$ was 1076 and 1325 kg $mm^{-2}$.

Schubert *et al*., (1998) investigated sixty five commercial and lab sintered WC-Co materials having Vickers hardness 1440-2200 HV30 exhibits fracture toughness of 8-12 $MNm^{-3/2}$. Zhang *et al.,* (2008) investigated fracture toughness of functionally graded WC-Co materials and found fracture toughness about 15.3 $MNm^{-3/2}$.

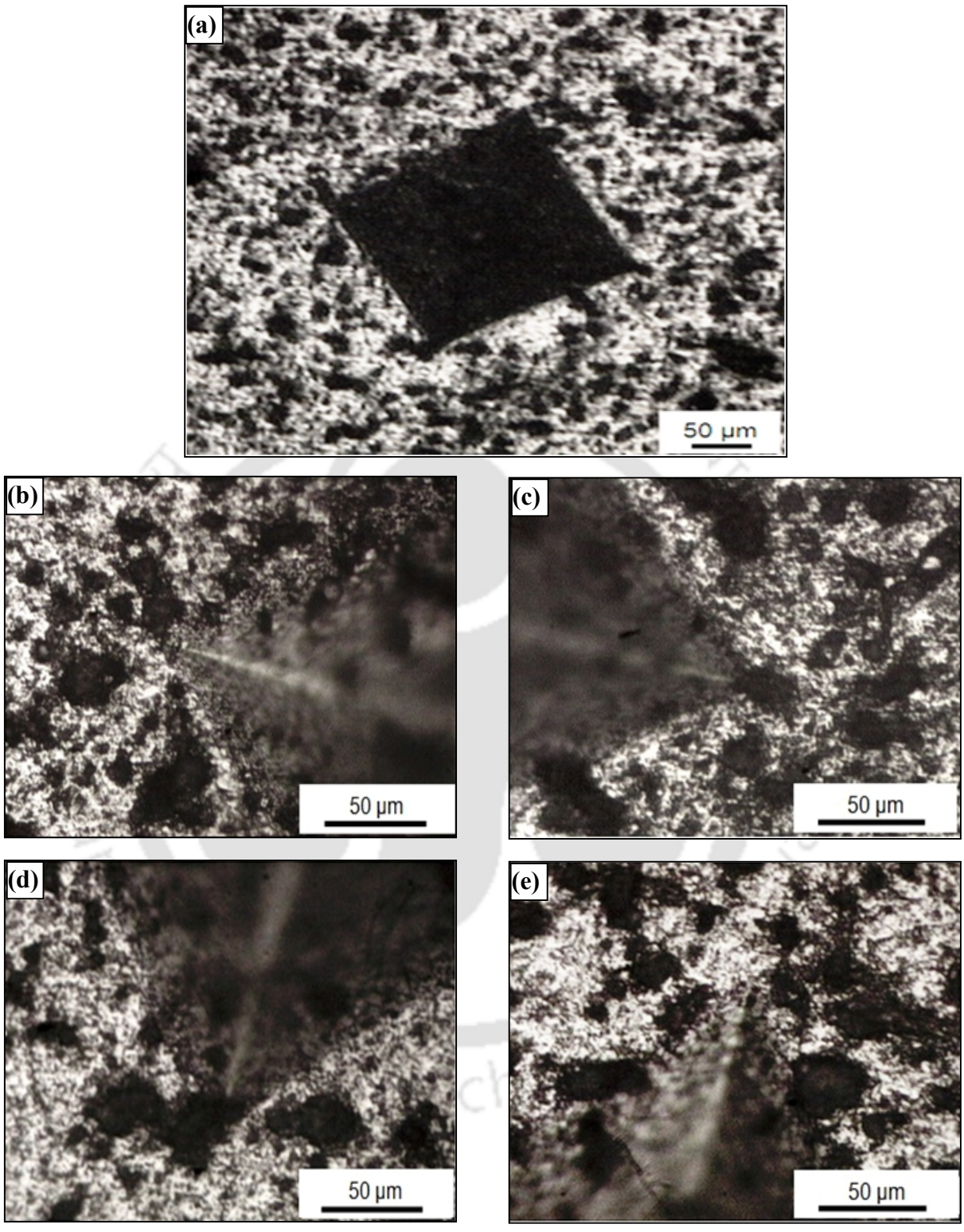


*Fig. 2.24(a) Indented image of developed material without calcium fluoride: (b) Left side (c) Right side (d) Bottom side (e) Top side*

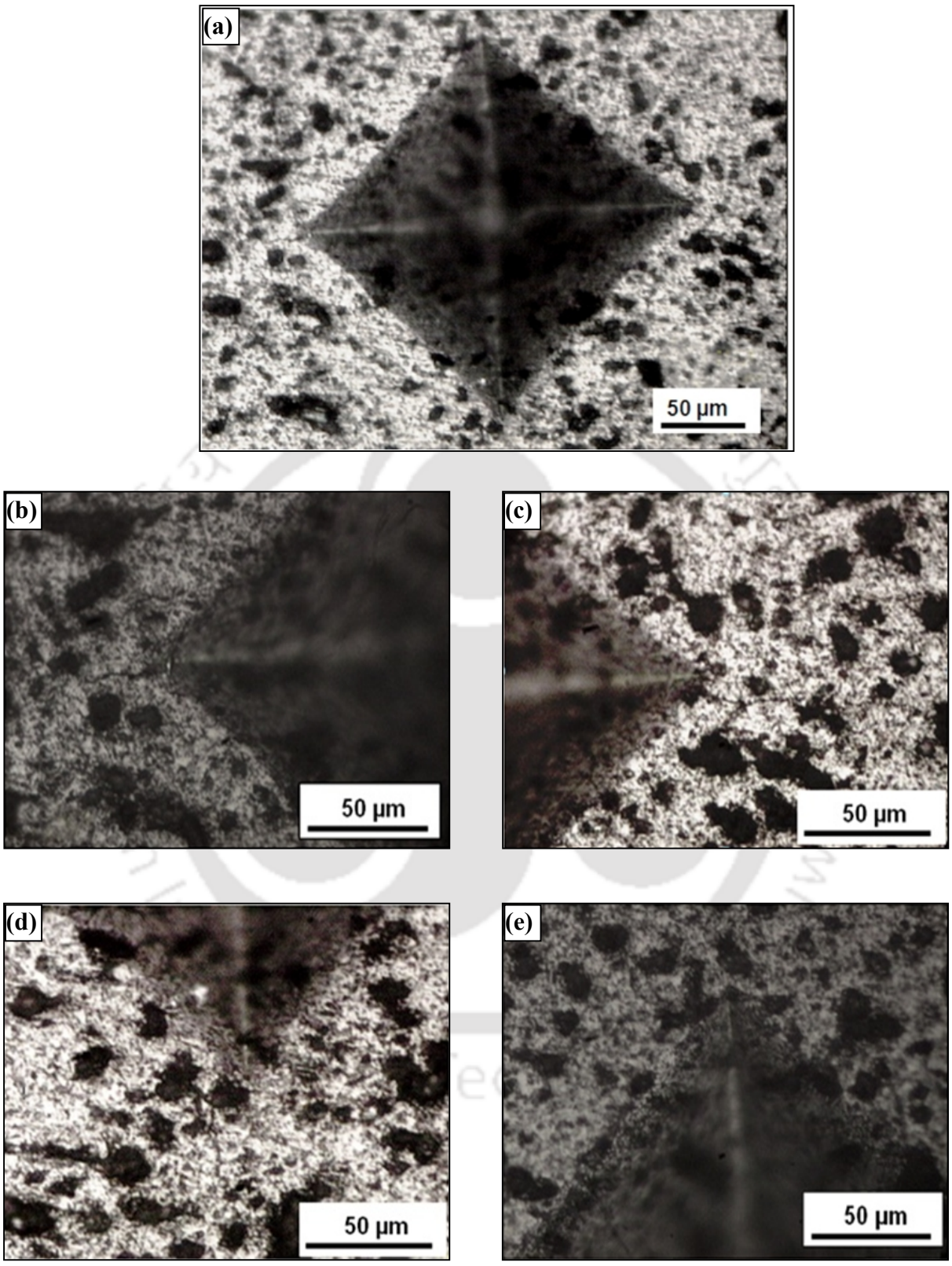


*Fig. 2.25(a) Indented image of developed material with 5 wt.% calcium fluoride; (b) Left side (c) Right side (d) Bottom side (e) Top side*

## 2.5 SUMMARY

This chapter shows the significant effect of milling time on density and hardness of the developed solid lubricant cutting tool materials. Amount of solid lubricant in the cutting tool material affects the transverse rupture strength significantly. Following major conclusions were arrived from the present work

- 40 hours of milling period was found to be most suitable for the chosen materials and this milling condition offers superior density and hardness.
- In sufficient and excess amount of $CaF_2$ reduces wetting and excess melting which results in sintering defect.
- Transverse rupture strength of various considered metals confirmed that the WC-Co with 5 wt.% of $CaF_2$ is suitable for the solid lubricant material.

# CHAPTER 3

# ABRASIVE WEAR PERFORMANCE OF TUNGSTEN CARBIDE BASED SELF LUBRICATING CUTTING TOOL MATERIAL

## 3.1 INTRODUCTION

Cutting tool experiences adhesion, abrasion and diffusion wear during its service. Abrasive wear most commonly occurred in metal cutting when the material being cut contains many hard particles (carbide, nitrides, oxides and non-metallic inclusions). Hence, the cutting tool material must be reasonably wear resistant against the work piece material under adhesive and abrasive wear mechanism (Abdel and El-Hofy, 2014; Grzesik *et al*., 2006). Therefore, it is necessity to understand the friction and wear performance of the developed tungsten carbide based solid lubricant material. Many attempts (Shipway *et al*., 2005; Rajinikanth and Venkateswarlu, 2011; Jia and Fischer, 1998) have been made in the past to understand the friction and wear performance of tungsten carbide based materials. However, investigations on the influence of solid lubricant material on friction and wear characteristics of WC-Co system are limited (Deng *et al*., 2011; Deng *et al*., 2012). Addition of solid lubricant affect the friction and wear properties of WC-Co material and the inclusion of varying solid lubricant percentage need to be understood for the better utilization.

Few works have been carried by adding calcium fluoride with tungsten to improve friction wear performance. Yuan *et al*. (2010) used composite coating with WC, Co, Cu, $BaF_2$, and $CaF_2$ for the plasma spray to enhance the wear resistance. 10 wt.% Cu and 10 wt.% $BaF_2$ /$CaF_2$ in a WC–Co matrix exhibited excellent frictional and wear performance. Qiao *et al*., (2013) developed the tungsten, aluminum, and cobalt and calcium fluoride composite and

evaluated the mechanical and tribological performance. Coefficient of friction was found to be reduced due to the presence of solid lubricants. Bolton and Gant (1996) investigated the addition of $CaF_2$ and MnS solid lubricant with high speed steel to develop a composite to improve wear properties. From the investigation (microstructure and XRD analysis) it is found that only slight wetting between the high speed steel and solid lubricant particle was found to have occurred. In this chapter, abrasive wear behavior of tungsten carbide based solid lubricant materials were examined with the aid of pin on disc test set up. The effect of fiber solid lubricants on tribological properties of friction and wear under multi pass abrasive wear condition were investigated.

## 3.2 TEST MATERIALS FOR ABRASIVE WEAR STUDY

In this work, the friction and wear performance of sintered cutting tool material (0-10 wt.% $CaF_2$) were carried out with the aid of the pin on disc tribometer (Ducom, TR-201) in accordance with ASTM G 99. Detailed methodology was adopted for material development; evaluation of density, hardness, fracture toughness and transverse rupture strength of the cutting tool material with the various amount of solid lubricants have been reported in chapter 2. Table 3.1 listed out evaluated mechanical properties of developed cutting tool materials.

*Table 3.1 Properties of developed cutting tool materials.*

| Test material | Hardness (HRA) | Density (kg/mm$^3$) | TRS (MPa) |
|---|---|---|---|
| WC-Co-0$CaF_2$ | 82.34 ± 3 | 12.3 ± 0.7 | 969 ± 48 |
| WC-Co-3$CaF_2$ | 82.2 ± 2 | 11.4 ± 0.7 | 772 ± 39 |
| WC-Co-5$CaF_2$ | 84.95 ± 2 | 14.6 ± 0.1 | 1502 ± 75 |
| WC-Co-7$CaF_2$ | 84.15 ± 2 | 12.9 ± 0.9 | 1259 ± 63 |
| WC-Co-10$CaF_2$ | 82.25 ± 2 | 10.9 ± 0.2 | 553 ± 28 |

To check whether oxidation product ($WO_3$) is present or not, XRD was carried out on both straight WC–Co and WC–Co–5 wt.% $CaF_2$ sintered material. Figure 3.1 show the XRD of test materials, where in no peaks (22°, 35°) corresponds to $WO_3$ was observed. Thus absence

of $WO_3$ is confirmed. Developed solid lubricant materials were cut into specimens of 6 X 6 X 15 mm having initial surface roughness (Ra) of 0.65 μm. For the abrasive test, the silicon carbide abrasive sheet of 220 grit size was fixed on the steel disc. As such, there is no correlation of cutting tool application with this particular grade (220 grit) of abrasive sheet. The initial and final weight and roughness of the test specimen were measured using weighing balance (0.1 mg accuracy).

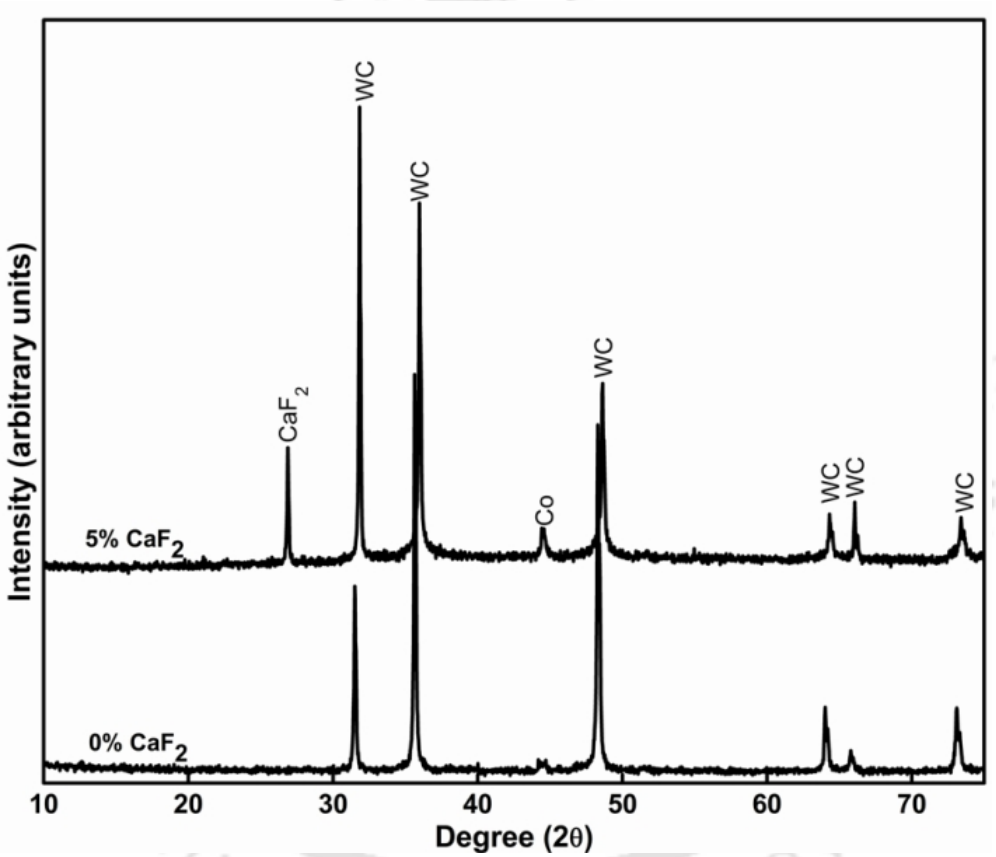


*Fig. 3.1 X-ray diffraction of straight WC-Co and WC-Co-5 wt.% $CaF_2$ material.*

The portable surface roughness tester (Mitutoyo, Surf test SJ-400) was used to measure the initial and final roughness of the test specimens. Continuous measurement of frictional force and wear during testing was carried out with the aid of strain gauge based load cell (0.1 N accuracy) and LVDT (0.1 μm accuracy) respectively. During testing, the surface temperature of test specimen is continuously measured with the thermal imaging camera (InfraTec hr

Head Vario CAM 480SL). Figures 3.2 (a-b) shows the pin on disc tribometer and a view of the test specimen, counter abrasive surface along with the thermal imaging camera. The worn-out surface of the test specimens was observed under the scanning electron microscope (LEO, 1430vp), as well as non-contact surface profilometer (Taylor Hobson, CCI MP).

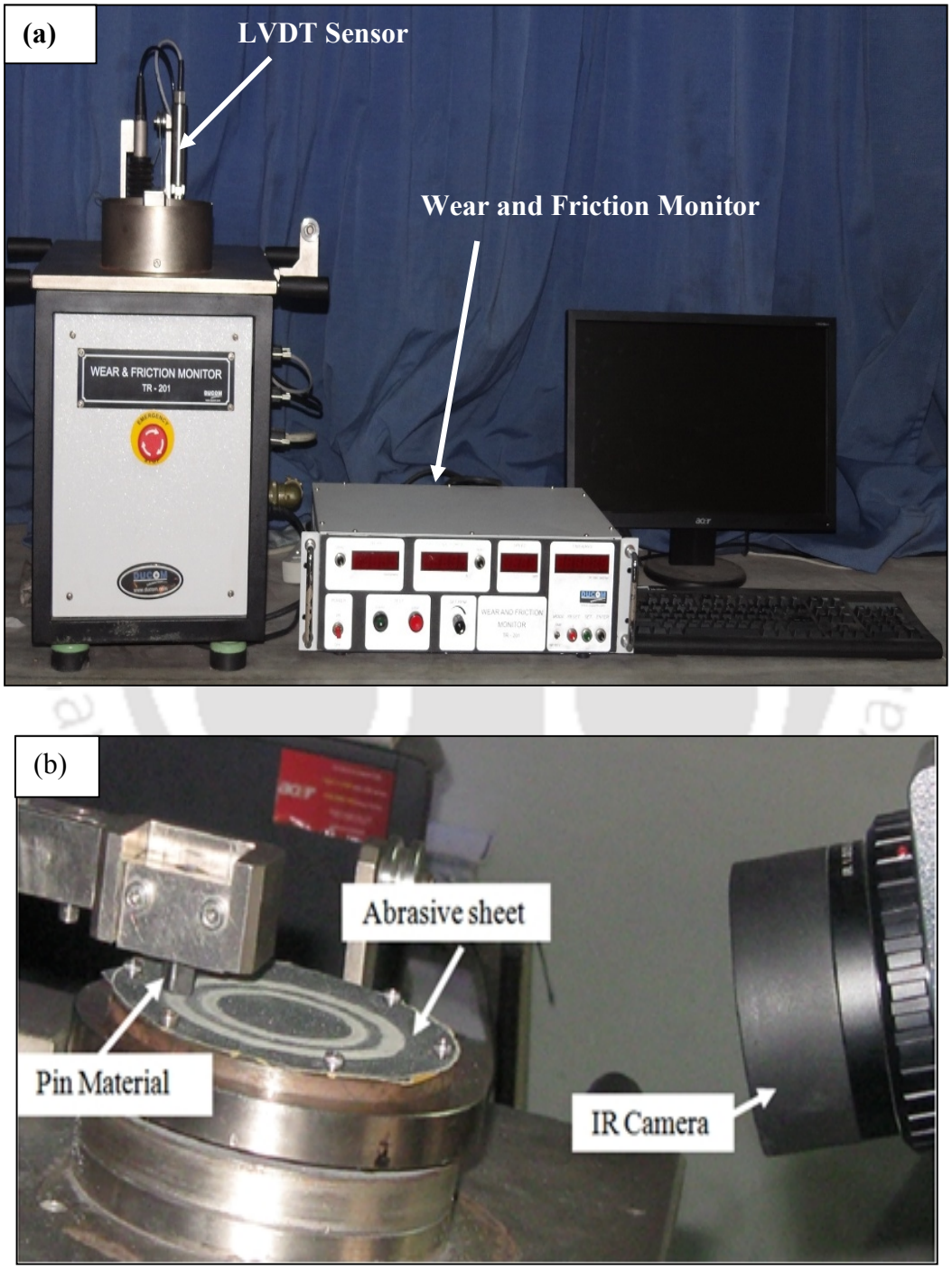


*Fig. 3.2 Abrasive wear performance evaluation: (a) Pin-on disc tribometer (b) A close up view of the test specimen, counter surface with thermal imaging camera.*

Figure 3.3 shows the non-contact surface profilometer and surface roughness tester. Friction and wear performance of the test specimens were carried out at a normal load of 19.6 N with 0.5 m/s surface velocity. Tests were carried out at dry and room temperature condition for 30-min duration.

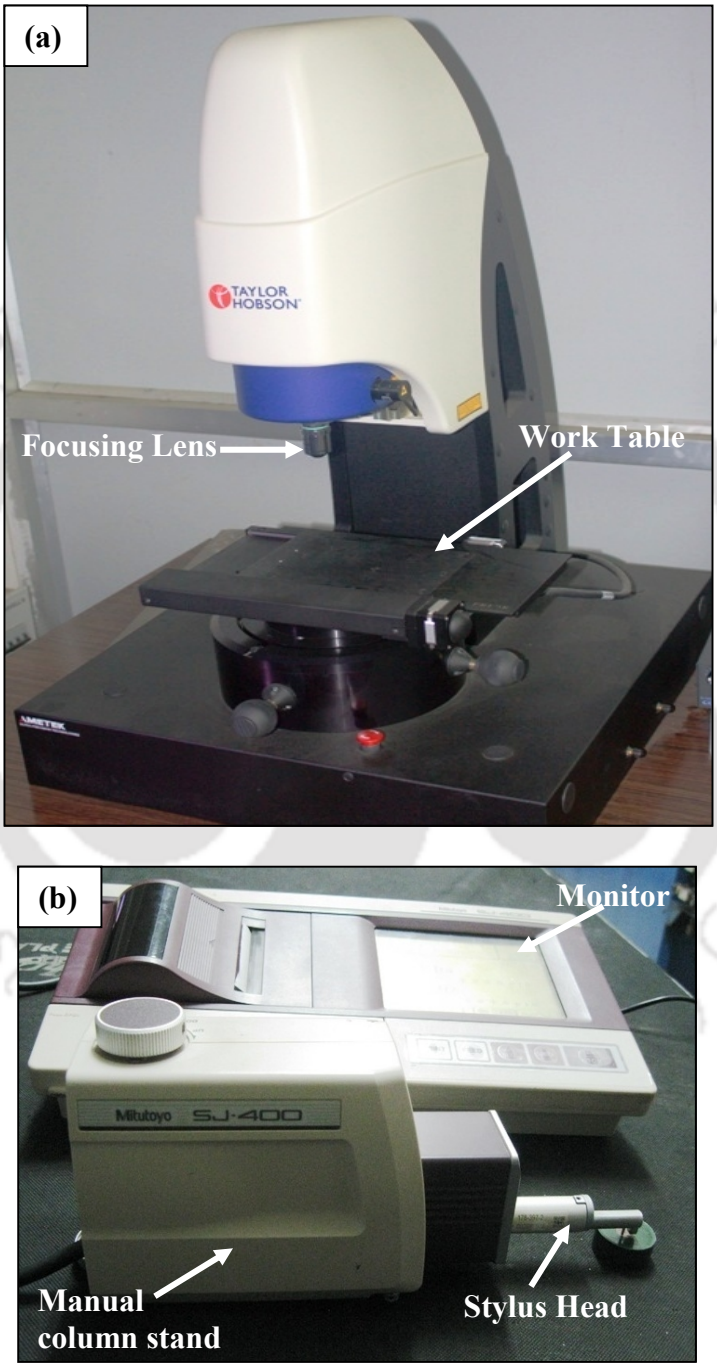


*Fig. 3.3 Equipments used for surface analysis: (a) Non-contact surface profilometer (b) Surface roughness tester*

Tests were also carried out at various normal loads (9.8, 19.6, 29.4 N) and wear rate, Z of test materials was computed using the following relation.

$$Z = \frac{V_m}{W \times X} \quad (3.1)$$

Where, Z: wear rate in $mm^3/nm$, $V_m$: Volume loss due to wear in $mm^3$, W: normal load in N, and X: sliding distance in m. These loads correspond to 1, 2 and 3 kg of normal loads. Friction wear of the developed materials was evaluated at various loads to simulate the various cutting speeds so that cutting tool experiences various forces at different cutting conditions. As such, there is no correlation between these loads and desired cutting speeds in cutting tool applications.

## 3.3 RESULTS AND DISCUSSION

### 3.3.1 Friction and Wear of the Test Materials

Specimens were made to slide against the new abrasive surface for every test. Figure 3.4(a) shows the coefficient of friction exhibited by the test materials. Tests were repeated for at least three times and the average value was considered for further analysis. It was observed that coefficient of friction gradually increases and the steady state reached after certain period. This behavior is due to the increase in contact area till surface asperities are worn-out. Measured coefficient of friction from 500 to 2000 s has been used for discussion, since there is a gradual rise in coefficient of friction. Sintered material without any amount of $CaF_2$ exhibited 0.40-0.44 coefficient of friction; however sintered material with 5 wt.% $CaF_2$ exhibited 0.25-0.28, which is least among all the investigated materials. The presence of $CaF_2$ reduces friction and lubricating behavior of $CaF_2$ is due to the lamella structure having less shear strength. All the considered test materials (3, 5, 7 and 10 wt.%) with $CaF_2$ exhibited less friction than straight WC-Co due to its lubrication effect. Material with 3 and 10 wt.% $CaF_2$ exhibited 0.35-0.39 coefficient of friction; however, material with 5 and 7 wt.% $CaF_2$

exhibited only 0.25-0.30 coefficient of friction. This minor difference could be due to the slightly higher hardness. Surface hardness of material with 3 and 10 wt.% shows 80-84 HRA, whereas for the 5 and 10 wt.% it is 82-87 HRA. Figure 3.4(b) shows the online wear of the test specimen during the test. During testing, test specimen wears increases with the time and the position of the specimen is indicated by the position of the linear variable differential transformer sensor. This particular figure indicates one of the five trails conducted.

Figure 3.4(c) shows the weight loss after testing. Weights of the specimens were measured before and after test and the average value of the specimen with deviation is shown in figure. Except materials with 3 and 10 wt. % $CaF_2$, all other remaining material's behavior is the same in figures 3.4(b-c). Test material without $CaF_2$ exhibited 62 µm wears after 30 min; however, test material with 5 wt.% $CaF_2$ exhibited only 13 µm wear.

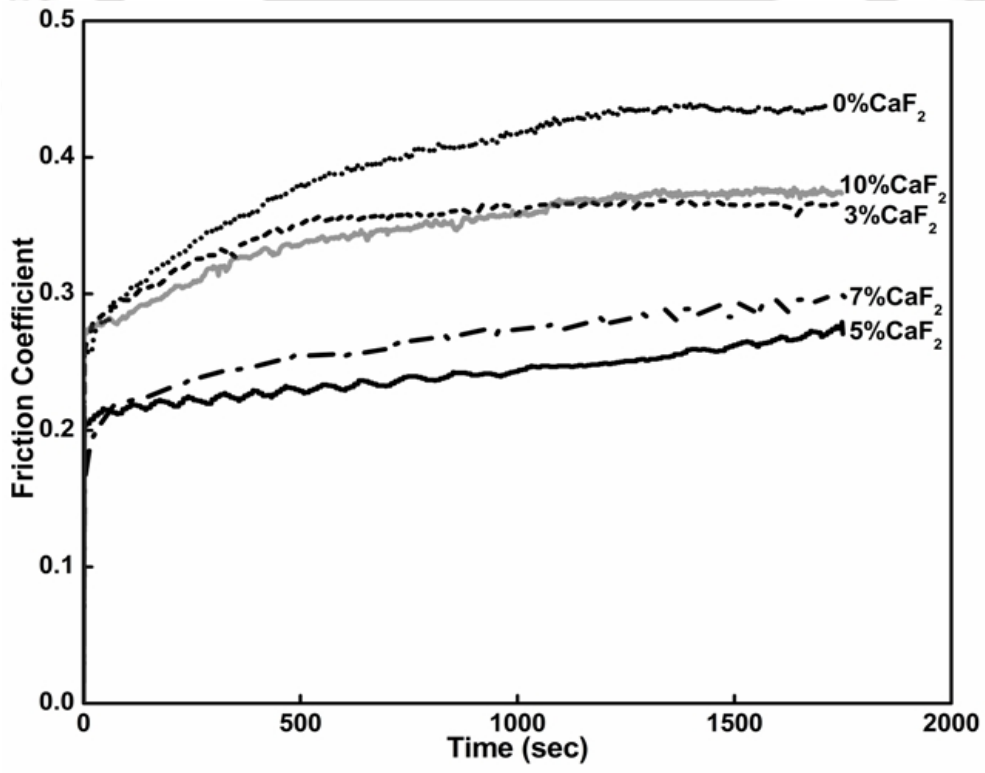


*Fig. 3.4 (a) Friction performance of the test material (v =0.5 m/s, $F_N$=19.62 N)*

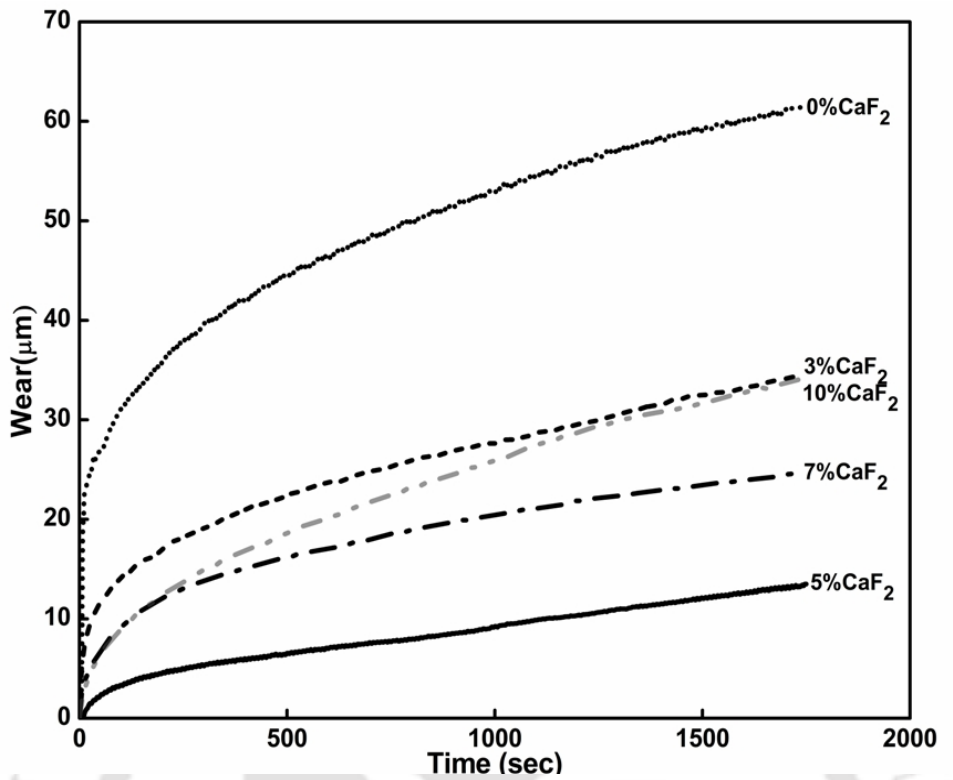


*Fig. 3.4 (b) Wear performance of the test material (v =0.5 m/s, $F_N$=19.62 N)*

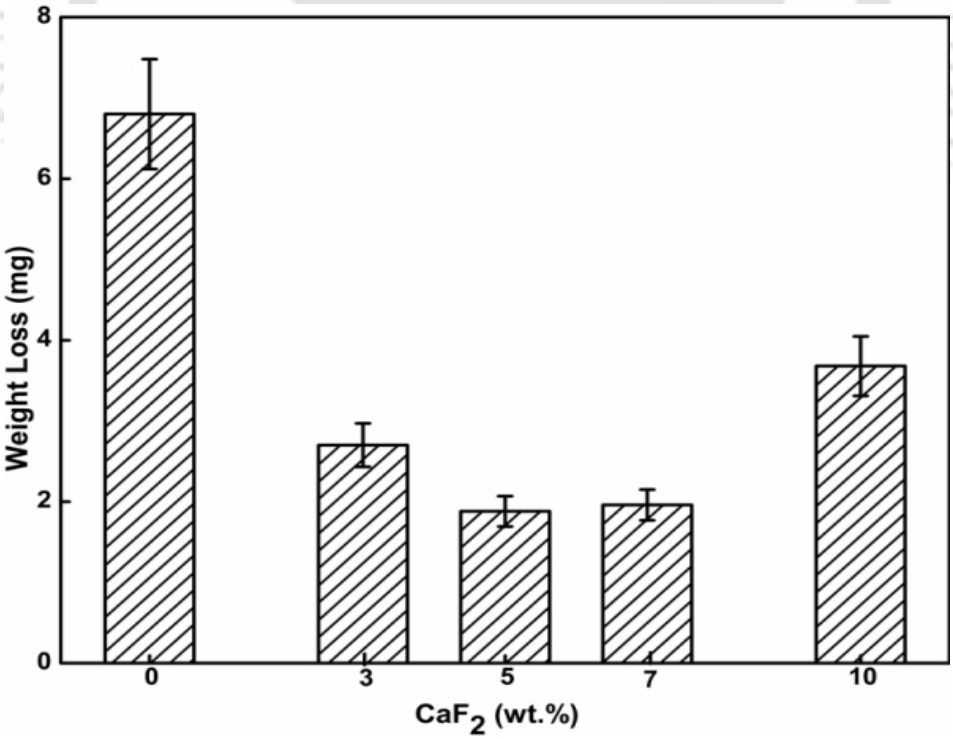


*Fig. 3.4 (c)* Weight loss of the test material (v =0.5 m/s, $F_N$= 19.62 N)

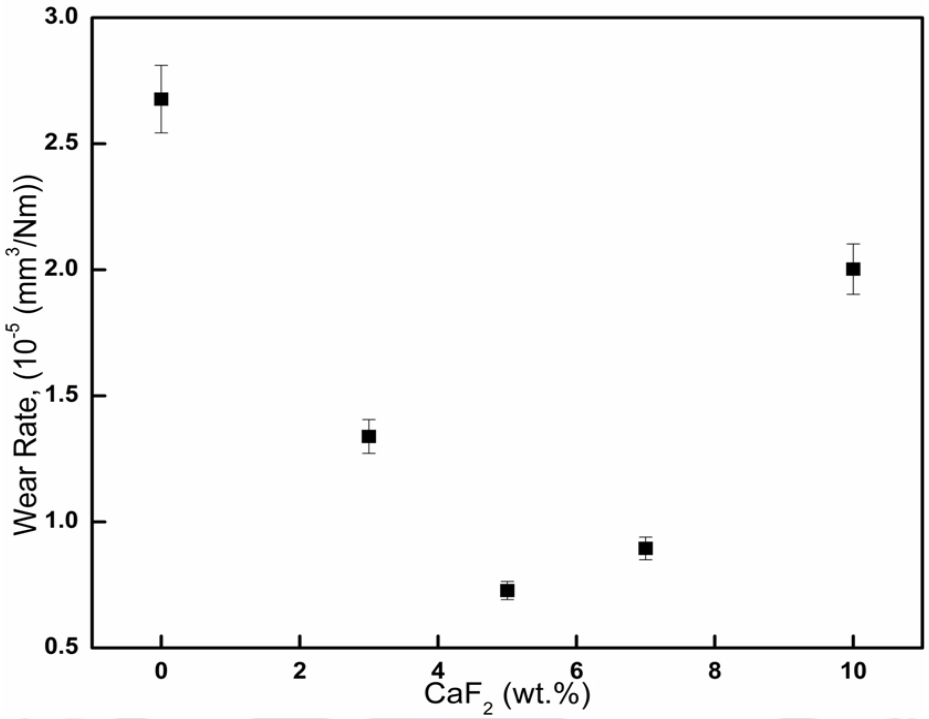


*Fig. 3.4 (d) Wear rate of the test material (v = 0.5 m/s, $F_N$= 19.62 N).*

Figure 3.4(c) shows the weight loss (the difference between the initial and final weight) of the investigated test material which also confirmed the same trend as that of wear. Due to its high hardness and presence of lubricant in the interacting sliding surface, 5 wt.% $CaF_2$ exhibited less wear loss. Similar to frictional behaviour, the addition of $CaF_2$ up to 5 wt.% helps to improve the wear resistance, beyond 5 wt.%, wear resistance was found to decrease as in figure 3.4(d). This behaviour is due to the hardness reduction (in spite of very minimal) beyond 5 wt.% $CaF_2$. The excess amount of $CaF_2$ reduces material strength as well as material hardness. Tests were carried at various normal loads and wear rate was computed (Table 3.2) which also confirmed the superior wear resistance of 5 wt.% $CaF_2$.

*Table 3.2 Wear test of test materials at various loads*

| Material | Wear rate($10^{-5}$ X $mm^3$/Nm) | | |
|---|---|---|---|
| | $F_n$=1kg | $F_n$=2kg | $F_n$=3kg |
| WC-Co-0$CaF_2$ | 0.9 ± 0.1 | 2.7 ± 0.3 | 3.9 ± 0.3 |
| WC-Co-3$CaF_2$ | 0.8 ± 0.1 | 1.3 ± 0.3 | 3.6 ± 0.2 |
| WC-Co-5$CaF_2$ | 0.2 ± 0.1 | 0.7 ± 0.2 | 1.4 ± 0.2 |
| WC-Co-7$CaF_2$ | 0.5 ± 0.1 | 0.9 ± 0.2 | 2.3 ± 0.3 |
| WC-Co-10$CaF_2$ | 0.9 ± 0.1 | 1.9 ± 0.4 | 3.6 ± 0.3 |

Similar behavior was also observed at $Al_2O_3$ /TiC with various amounts of $CaF_2$ solid lubricant by Deng and Cao (2007). Up to 10 wt.% $CaF_2$, an increase in wear resistance and decrease in coefficient of friction were observed and beyond this value, a decrease in wear resistance and an increase in coefficient of friction were observed. Hua *et al.,* (2012) investigated the tribological performance of laser cladding Ni–Cr/$TiB_2$ composite coatings with the addition of $CaF_2$. It was found that composite with $CaF_2$ exhibited higher wear resistance and lower friction coefficient.

Dhanasekaran and Gnanamoorthy (2007) evaluated the abrasive wear performance of Fe-C-Cu with $MoS_2$ against silicon carbide abrasive sheet. Material with 3 wt.% and 5 wt.% $MoS_2$ exhibited less friction and more wear resistance compared to that of Fe-C-Cu at various loads. Increased hardness and formation of lubrication film contributed to this behaviour.

### 3.3.2 Surface Temperature of the Test Materials

During surface interaction, asperities of silicon carbide particle slide over the test material and surface temperature due to the friction that increases rapidly. Figure 3.5(a) show the thermal image obtained during wear testing. Figure 3.5(b) show the measured surface temperature of test materials under 0.5 m/**s** sliding velocity and 19.6 N normal load. The maximum surface temperatures exhibited by 0, 3, 10, 7 and 5 wt.% $CaF_2$ are 80, 70, 55, 45 and 30 °C, respectively. Among the investigated material, 5 wt.% $CaF_2$ materials generated the least frictional temperature due to its less friction against silicon carbide particles. In addition, a gradual rise in surface temperature was not observed at WC-Co-5 wt.% $CaF_2$ material like other investigated materials. This behavior is due to the presence of lubricant material on the silicon carbide particles. Kagnaya *et al.,* (2009) also observed steady state temperature after the short term period (200 s) while investigating the tribological performance of WC–Co in the pin-on-disc tribometer. Wu *et al*., (2012) also observed lower

surface temperature by WC–Co with solid lubricant than that by WC–Co while investigating tribological behavior in dry sliding condition.

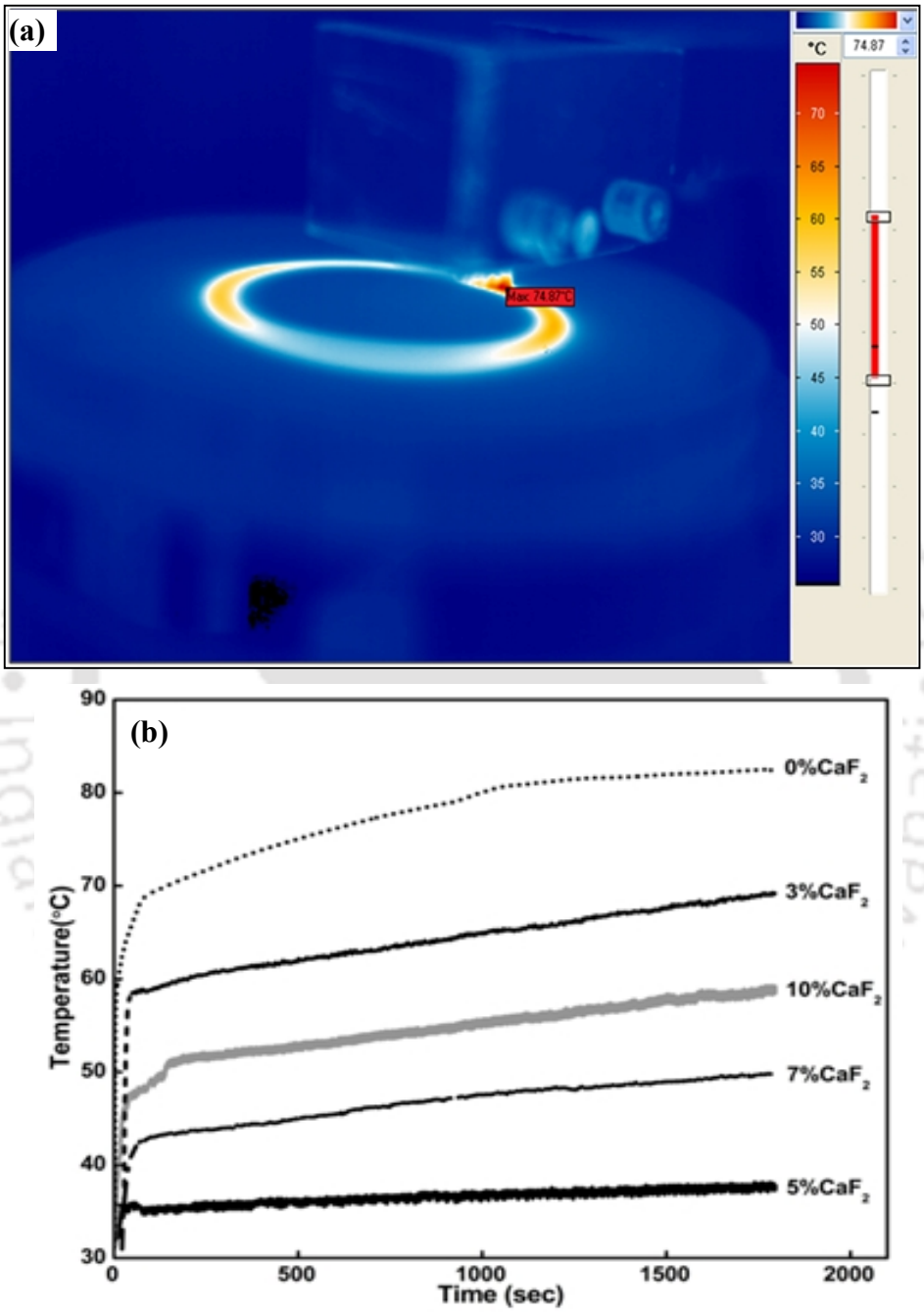


*Fig. 3.5 (a) Thermal image during test (v = 0.5 m/s, $F_N$=19.62 N) (b) Measured surface temperature of tested material during abrasive wear (v = 0.5 m/s, $F_N$=19.62 N).*

### 3.3.3 Wear Morphology of the Test Materials

To understand the wear morphology and confirm the presence of lubricant in the developed material, test materials were also observed under the scanning electron microscope. Figures 3.6 (a-b) shows the wear morphology of test material without $CaF_2$ .Wear morphology was confirmed with the domination of plowing over asperity deformation and adhesive interaction. The presence of hard abrasive grits (silicon carbide) on the counter surface caused plowing wear on the test surfaces due to the high friction and less hardness of the test material. Sliding of the hard silicon carbide particle over the test surface removed the binder and crack propagation along grains of tungsten carbide was distinctly observed. Due to the removal of bonding material, carbides are found to dislodge at the ridge of the tracks. Fragmentation of brittle tungsten carbide grains was distinctly revealed on the worn-out surface due to the absence of binder.

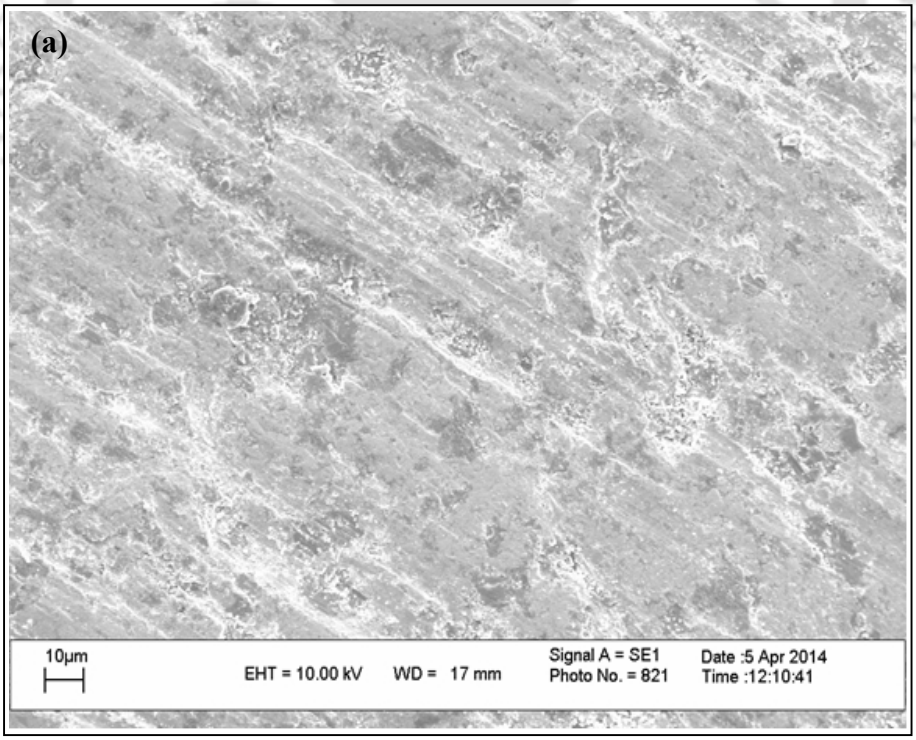

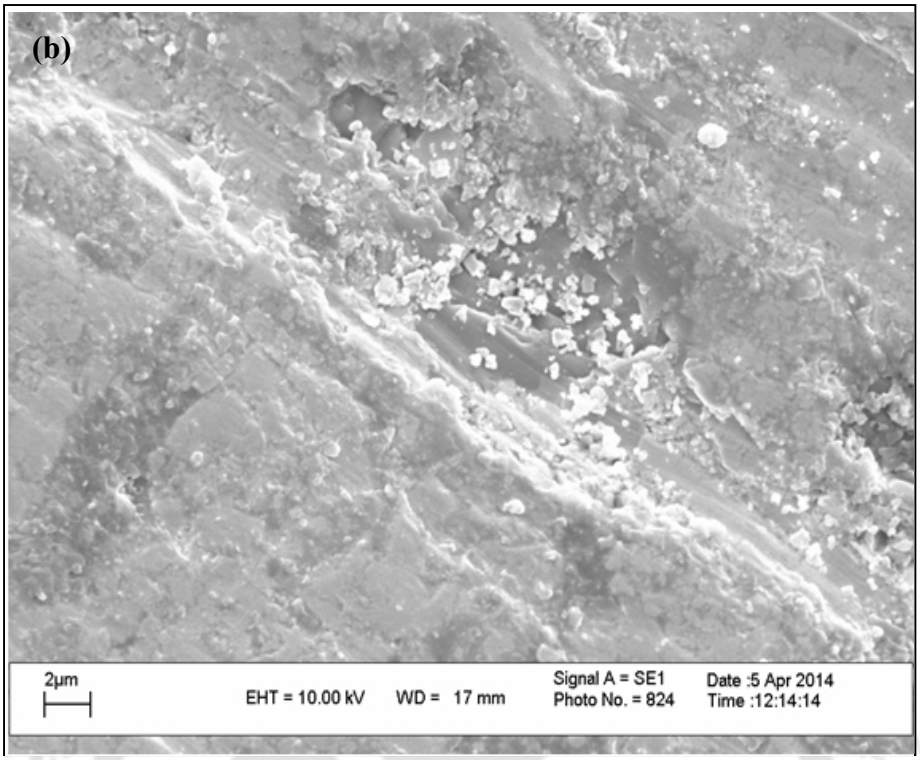


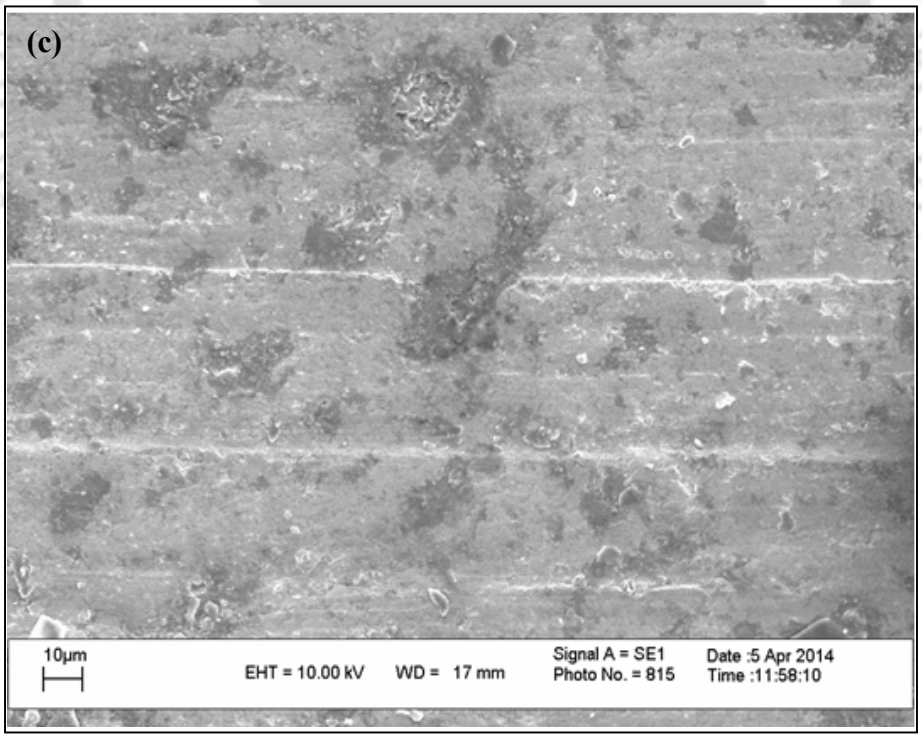

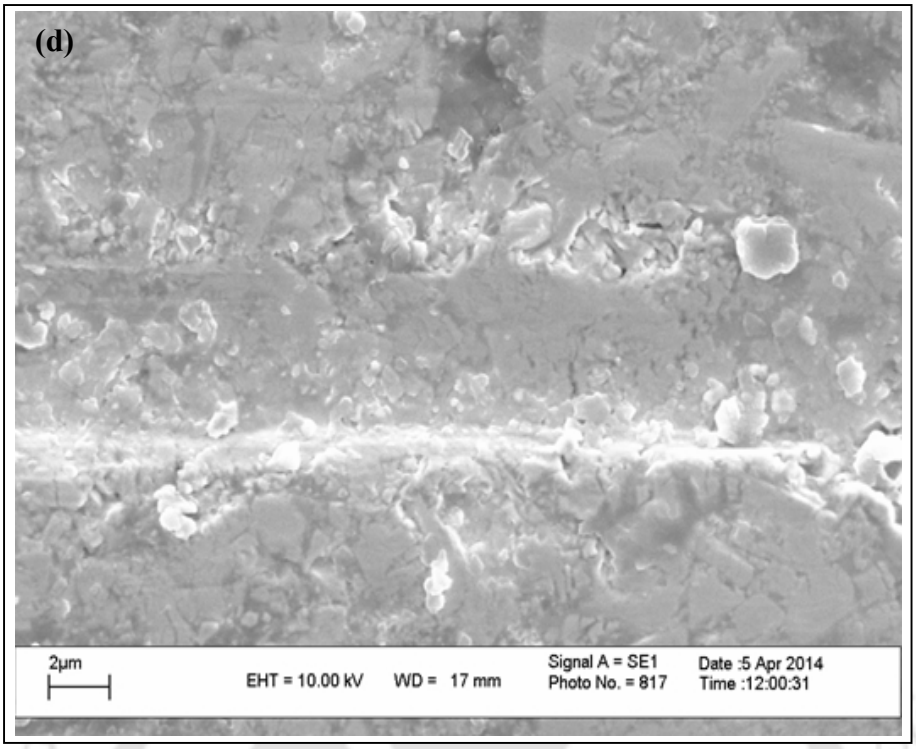


*Fig. 3.6 (a) Worn-out surface of WC-Co (v =0.5 m/s, $F_N$=19.62 N) (lower magnification) (b) Worn-out surface of WC-Co (v =0.5 m/s, $F_N$=19.62 N) (c) Worn-out surface of WC-Co-5 wt. % $CaF_2$ (lower magnification) and (d) Worn-out surface of WC-Co 5 wt.% $CaF_2$.*

Mosbah *et al.*, (2005) also observed similar wear morphology while investigating the abrasive wear of tungsten carbide iron-aluminide composites. Particle debonding and micro fracturing of carbide grains were observed at the wear morphology of WC-FeAl composites. With the reduction of tungsten carbide grain size, the wear resistance was found to be improved. Blombery *et al.*, (1974) investigated the abrasive wear mechanism of tungsten carbide cobalt composites and identified cobalt removal as the first stage with the consequent formation of surface pits with intergranular facets. Figures 3.6(c–d) show the wear morphology of test material with 5 wt.% $CaF_2$. The presence of $CaF_2$ is not only reduces friction but also improved material hardness. The increase in hardness improved wear resistance significantly; wear morphology as well as the final roughness of the test material confirmed this fact. In this material, only rubbing marks y the abrasive grits were observed

and plowing marks were very mild when compared to the material without $CaF_2$. Wear morphology of tested material with $CaF_2$ exhibited less surface damages, due to the reduction of surface friction. Ahmadian *et al*., (2005) also quantified surface damage of test material after abrasion from the wear morphology. WC-40 vol.% (FeAl-500 ppm B) exhibited better wear resistance than WC-40 vol.% (Ni Al-500 ppm B). Abrasive wear resistance was found to increase with boron up to 500 ppm; beyond this, no effect was observed. Figure 3.7 show the cross section of these test surfaces, which also confirmed the wear resistance of these materials. The average size of the silicon carbide abrasive particle used in this testing is in the range of 60-100 µm, figures 3.10(a-c) confirmed this fact. WC–10Co showed almost similar size (60-100 µm) crater formation, however worn-out surface of WC-10Co-5wt.% $CaF_2$ (figures 3.7(b), 3.7(d) and 3.7(f)) showed only 10–20 µm width and depth of wedge marks. However, worn-out surface of both straight WC-Co material and WC-Co-5 wt.% $CaF_2$ material did not show any ridge formation which confirmed the brittle fracture. This brittle fracture also confirmed the bonding failure between tungsten carbide particles.

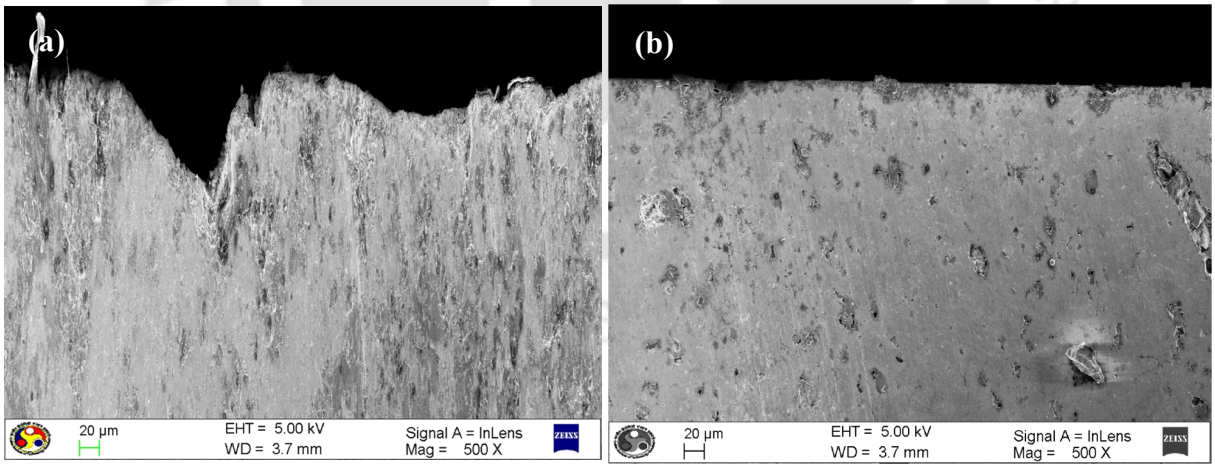

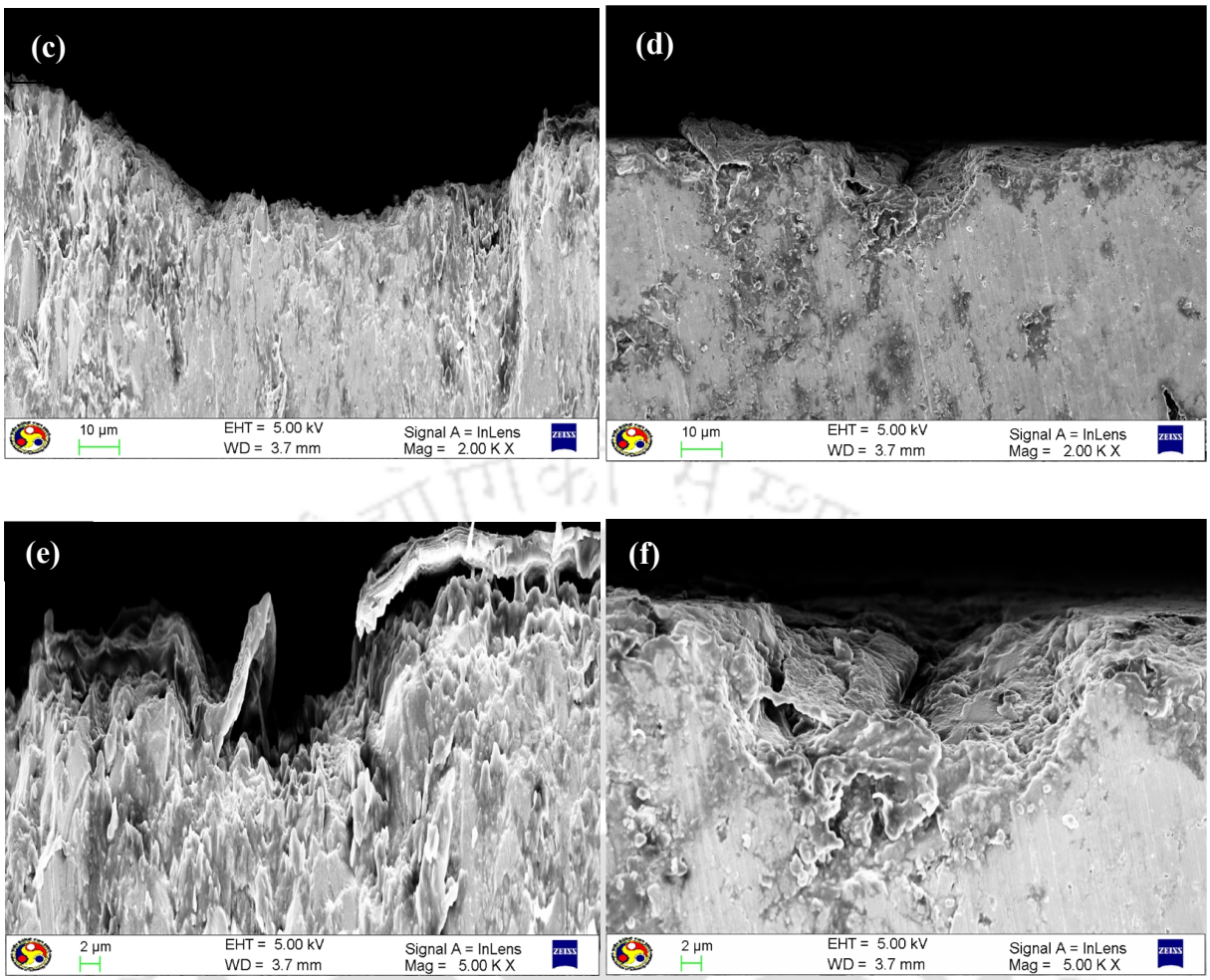


*Fig. 3.7 (a) Cross section of straight WC-Co material (b) Cross section of WC-Co-5 wt.% $CaF_2$ material (c) Brittle failure observed at cross section of straight WC–Co material (d) Wedge groove observed at cross section of WC-Co-5 wt.% $CaF_2$ material (e) Crater and hillocks observed at cross section of straight WC–Co material and (f) Close up view of wedge groove at cross section of WC-Co–5 wt.% $CaF_2$ material.*

From figures 3.7(d) and 3.7(f), it is clear that due to the load acting normal to the surface, the wedge groove with sufficient depth was formed, where very litter damage is observed adjacent to this groove. However, due to the more friction as well as a relatively weaker bond between tungsten carbide particles, adjacent materials around the craters have been significantly altered. From figures 3.7(c) and 3.7(e) crater and hillock features were observed on the worn-out surface of straight WC-Co material due to the dislodging of WC particles.

EDS analysis was carried out on the worn out surface of the test specimens.SEM and EDS mapping of WC-Co-5 wt.% $CaF_2$ worn-out surface after abrasive test are shown in figures 3.8(b-f). Figure 3.8(a) showed the considered worn-out surface for the EDS analysis. EDS spectrum of worn-out surface is shown in figure 3.8(g) which confirmed the presence of tungsten, carbon, cobalt, calcium and fluoride on the test surface.

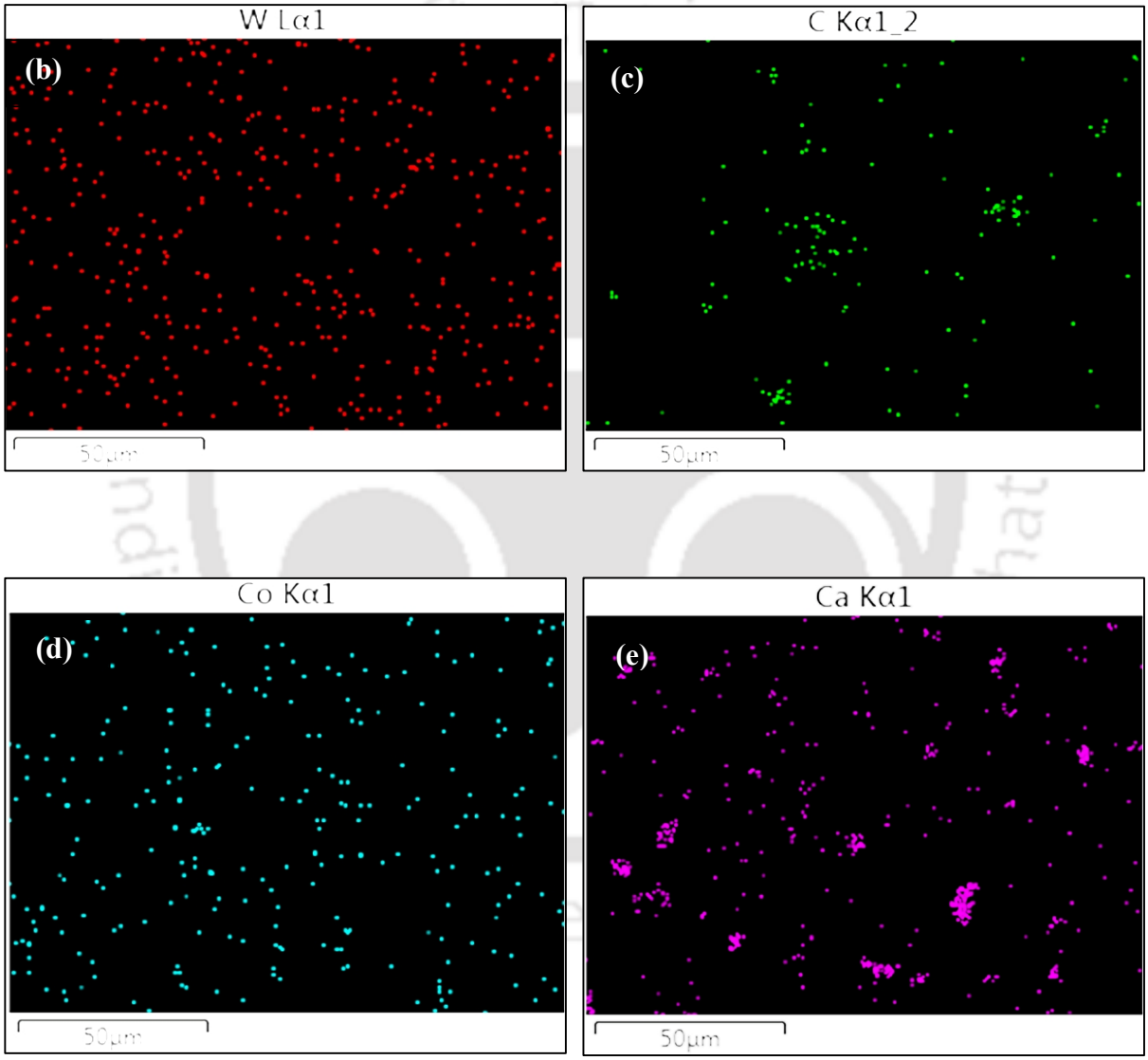

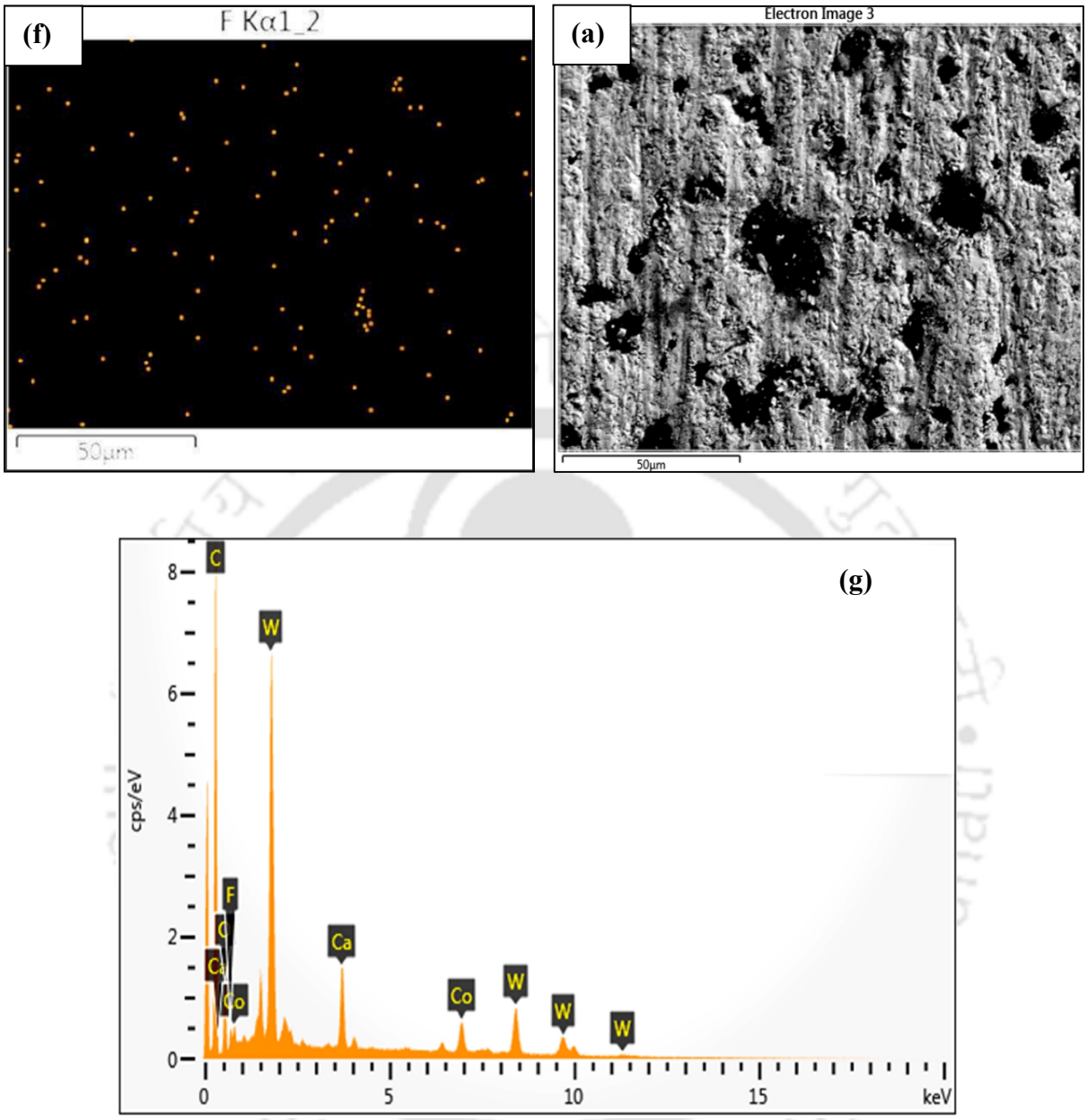


*Fig. 3.8 SEM for EDS mapping of worn-out surface of; (a) WC-Co-5 wt.% $CaF_2$; EDS mapping showing: (b) Tungsten distribution (c) Carbon distribution (d) Cobalt distribution (e) Calcium distribution (f) Fluoride distribution and (g) EDS spectrum plot of worn-out surface WC-Co-5 wt. % $CaF_2$.*

In addition, line scanning of the worn-out surface (WC-Co-5 wt.% $CaF_2$) was carried out to confirm the presence of all the included constituents. Figure 3.9(a) showed the SEM of the considered material and Figure 3.9(b) showed the line scan of the considered material.

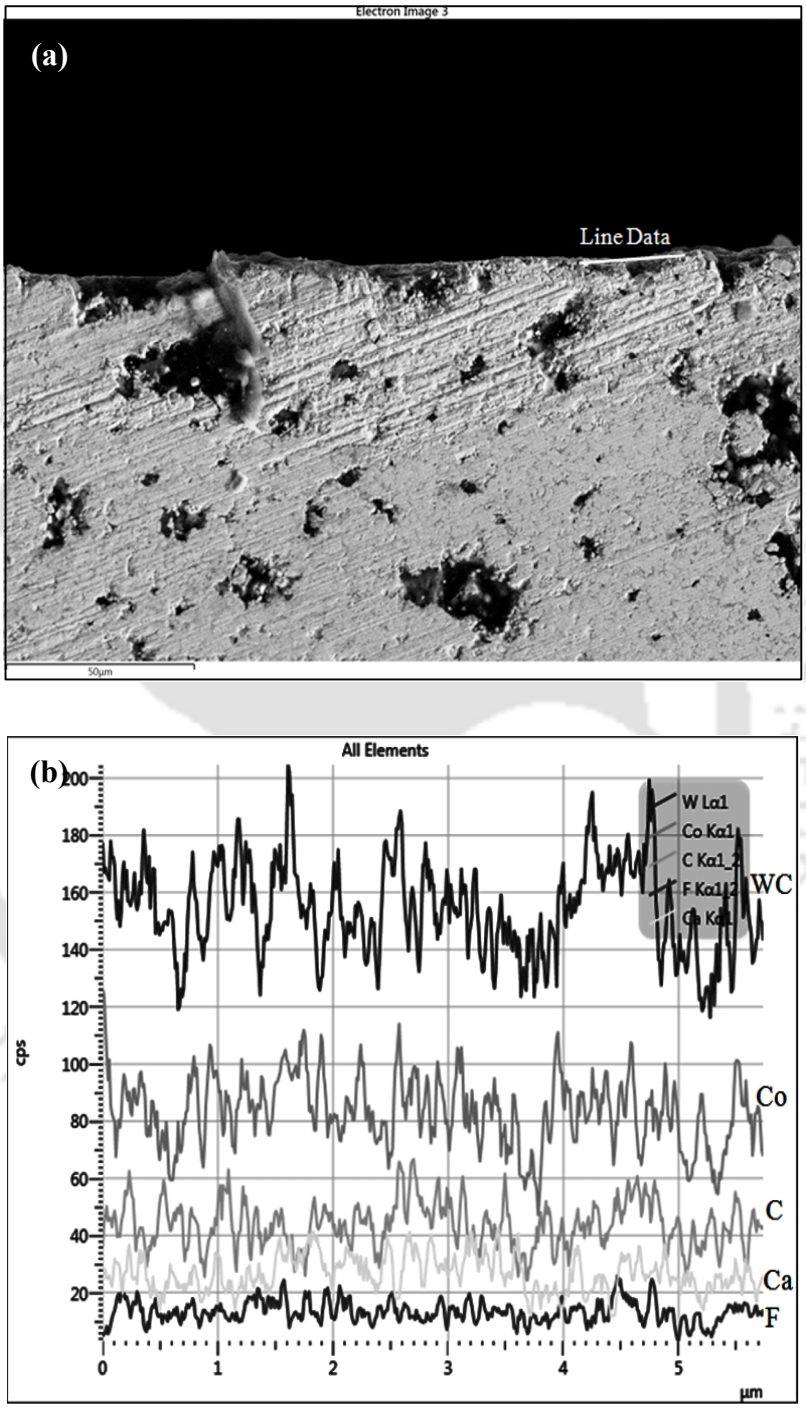


*Fig. 3.9 (a) SEM corresponding to chosen sintered surface WC–Co–5 wt.% $CaF_2$ and (b) Line scan data of WC-Co-5 wt.% $CaF_2$*

### 3.3.4 Wear Morphology of the Counter Materials

After wear test, mating abrasive sheets were examined under the scanning electron microscope to investigate the breakage of abrasive as well as microchips of test materials. Figure 3.10 (a) shows new abrasive sheet and figure 3.10 (b-c) shows the wear morphology of SiC abrasive sheets after testing against WC-Co and WC-Co-5 wt.% $CaF_2$ respectively. This morphology also confirmed binder failure as the primary and consequently carbide particles cracked and dislodged from the network. In both the sheet, wear debris was found to embed on the surface, and pullout, fracture and attrition of abrasive particles were also seen. However, the amount of wear debris covered abrasive particles is higher when slid against WC–Co compared to WC-Co-5 wt.% $CaF_2$.This behavior is due to the insufficient bonding between WC and Co particles as well as the absence of $CaF_2$ in the material.

Figures 3.10(d-e) shows the EDS spectrum of the abrasive sheet after testing against WC–Co–5 wt.% $CaF_2$. Traces of calcium and fluoride were seen on the abrasive particles (spectrum A in figure 3.10(c)) as well as wear debris (Spectrum B in figure 3.10(c)).

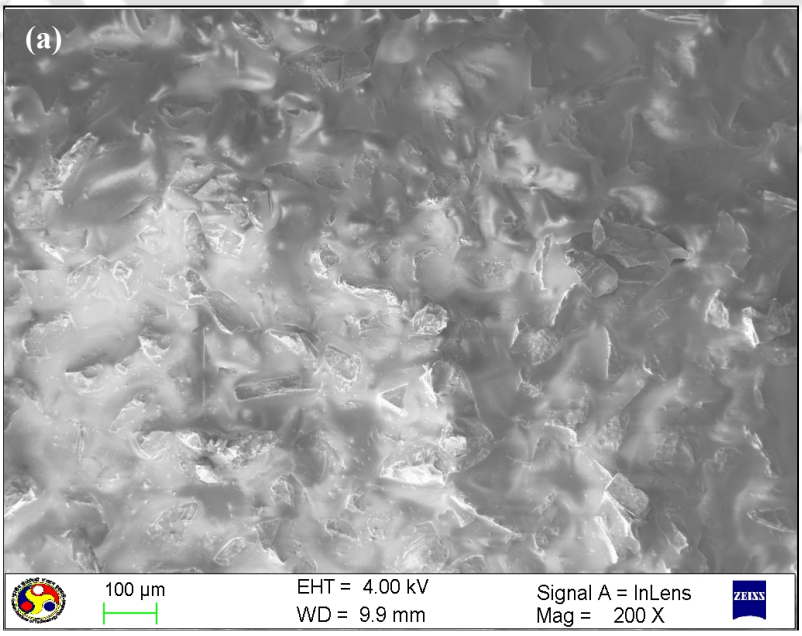

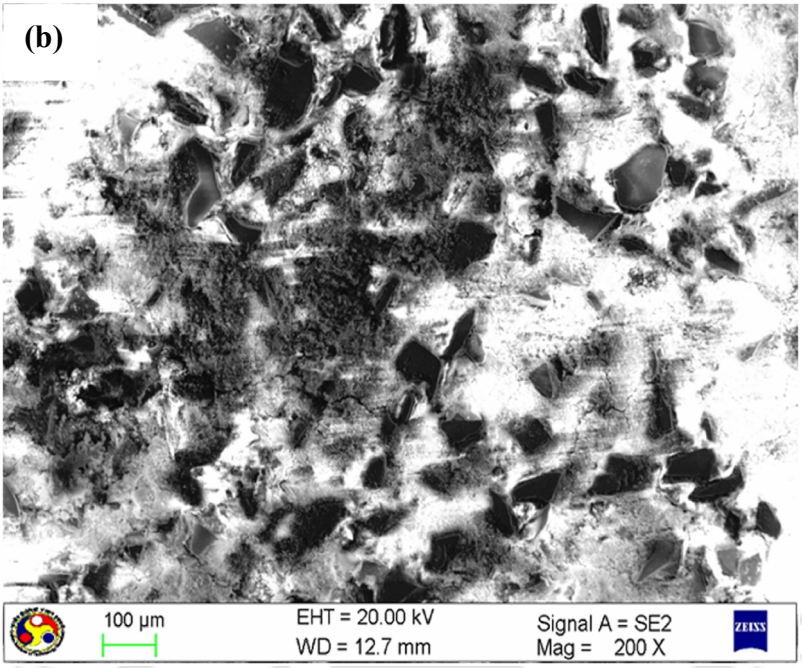


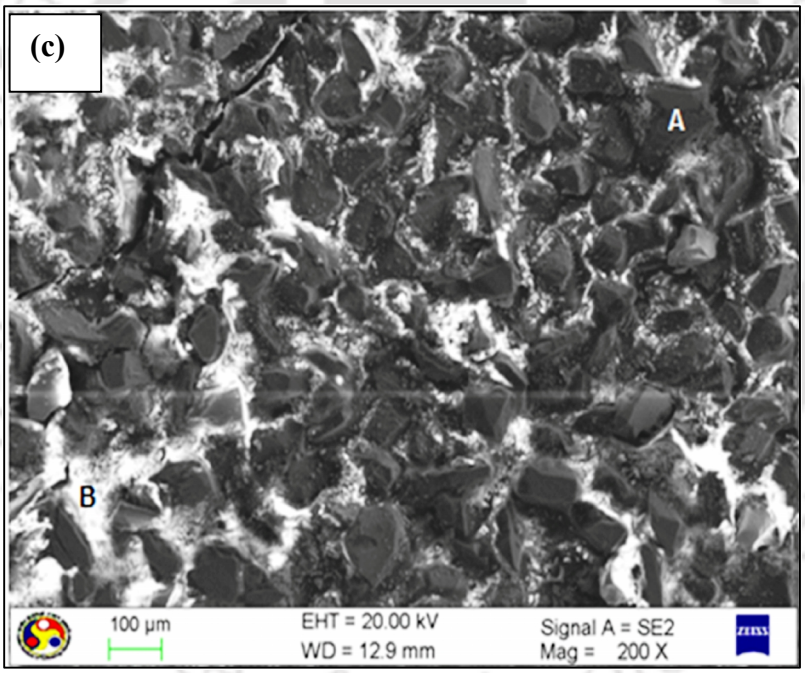


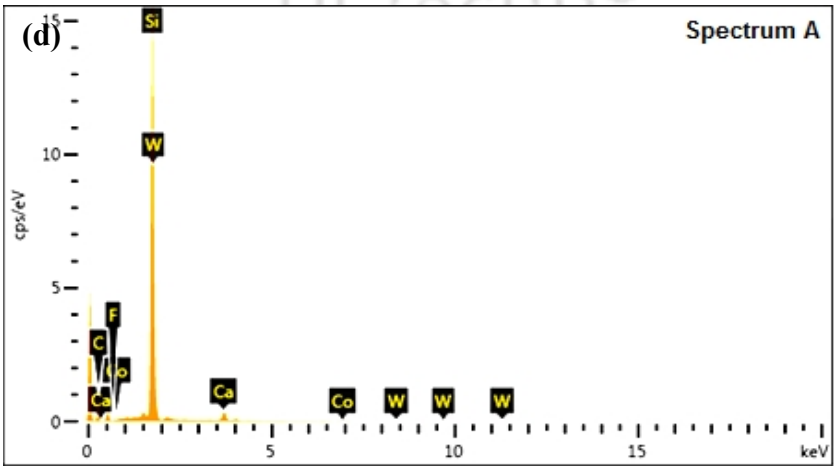

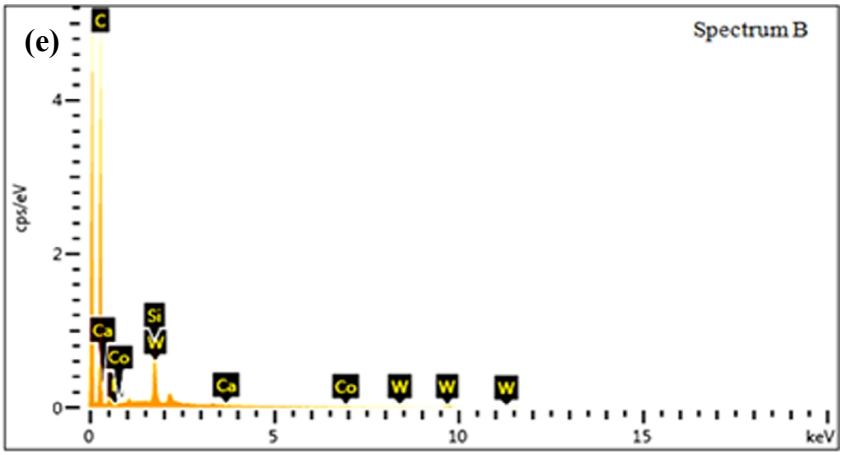


*Fig. 3.10 (a) SEM of new abrasive sheet (b) SEM of abrasive sheet after testing against WC-Co (v =0.5 m/s, $F_N$=19.62 N) (c) SEM of abrasive sheet after testing against WC-Co-5 wt.% $CaF_2$, (v =0.5 m/s, $F_N$=19.62 N) (d) EDS spectrum plot of black patches and (e) EDS spectrum plot of white patches.*

Jayashree *et al*., (2000) observed similar coherent thin film of PTFE while investigating the abrasive wear performance of polyethersulfone composite with solid lubricants (PTFE and $MoS_2$). The wear debris of the composite was observed in surfaces of the SiC sheet in addition to the transfer of PES over counter surface.

### 3.3.5 Surface Damage and Surface Roughness of the Test Materials

Surface damage after the abrasive wear test was investigated with the aid of non-contact 3D profiler and shown in figures 3.11(a-e). Wornout surface (0.8 × 0.8 mm) was observed and the direction of sliding was clearly visible in all the test materials. Micro cutting caused by the abrasive grit on the counter disc created scratches on the test surface and adhesive or asperity deformation traces were not observed. WC-Co-5 wt.% $CaF_2$ showed the smooth surface when compared to the other investigated materials. This behavior is due to the presence of $CaF_2$ in the developed material during surface interaction whereas, material with excess lubricants (WC-Co-7 wt.% $CaF_2$, WC-Co-10 wt.% $CaF_2$) and material with inadequate lubricants (WC-Co, WC-Co-3 wt.% $CaF_2$) exhibited severe plowing marks.

(a)

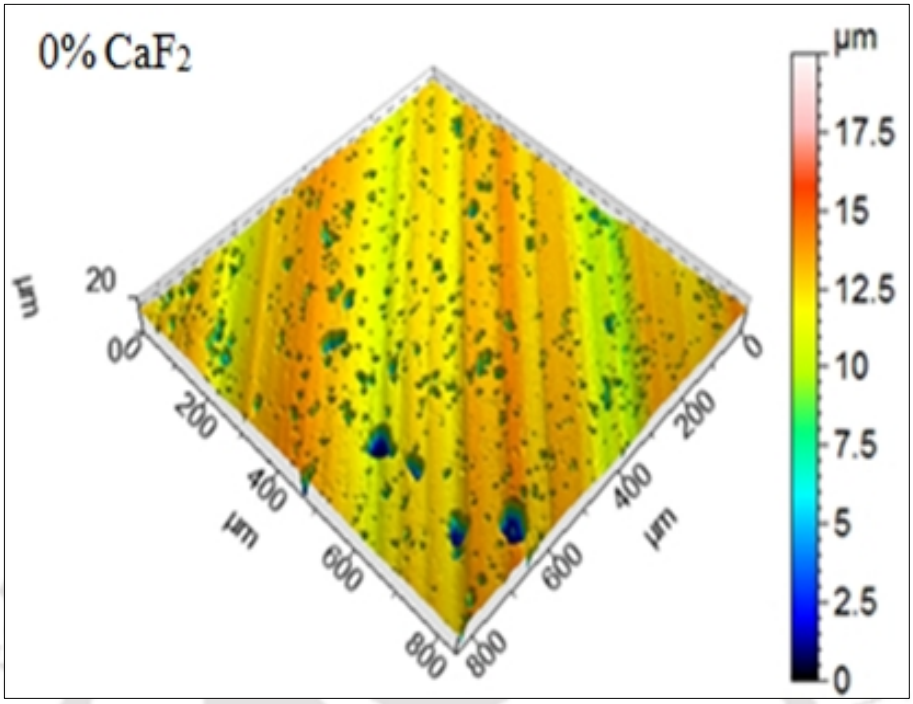


(b)

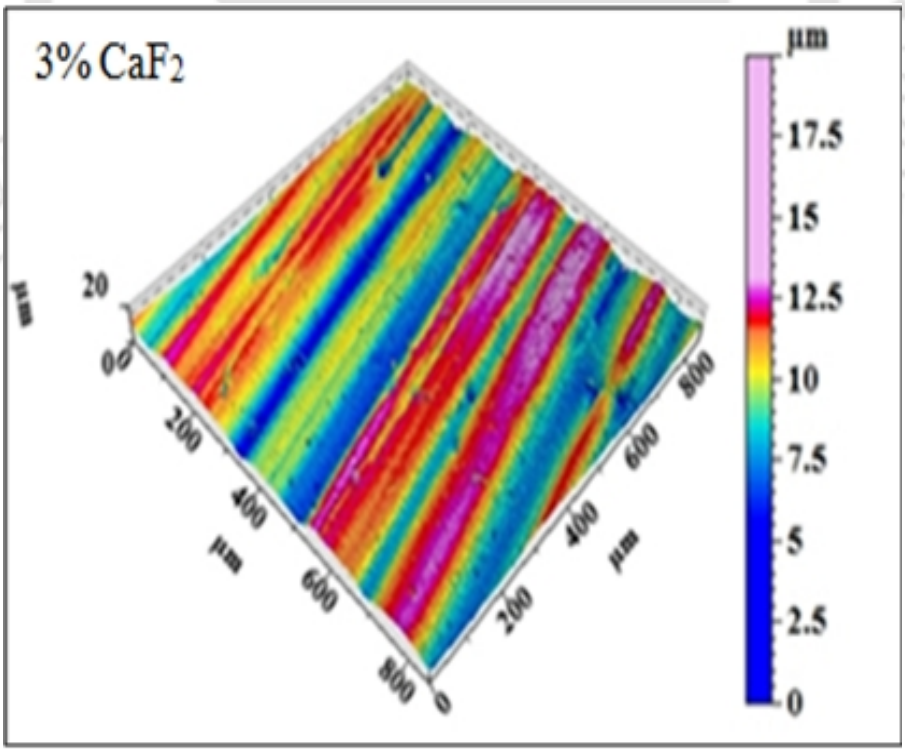

(c)

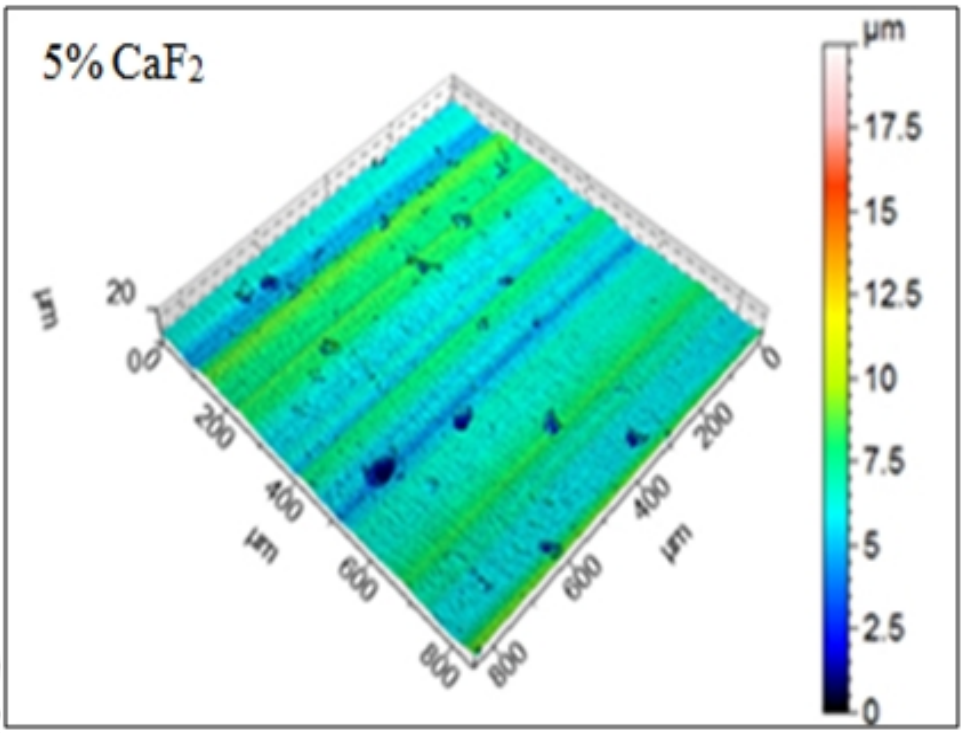


(d)

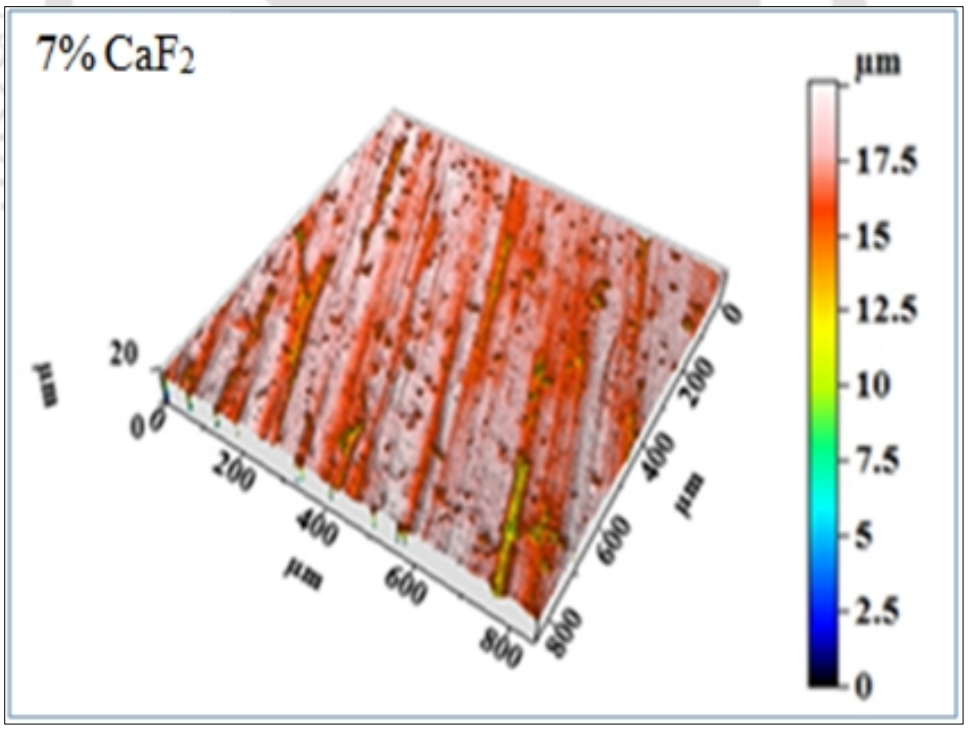

(e)

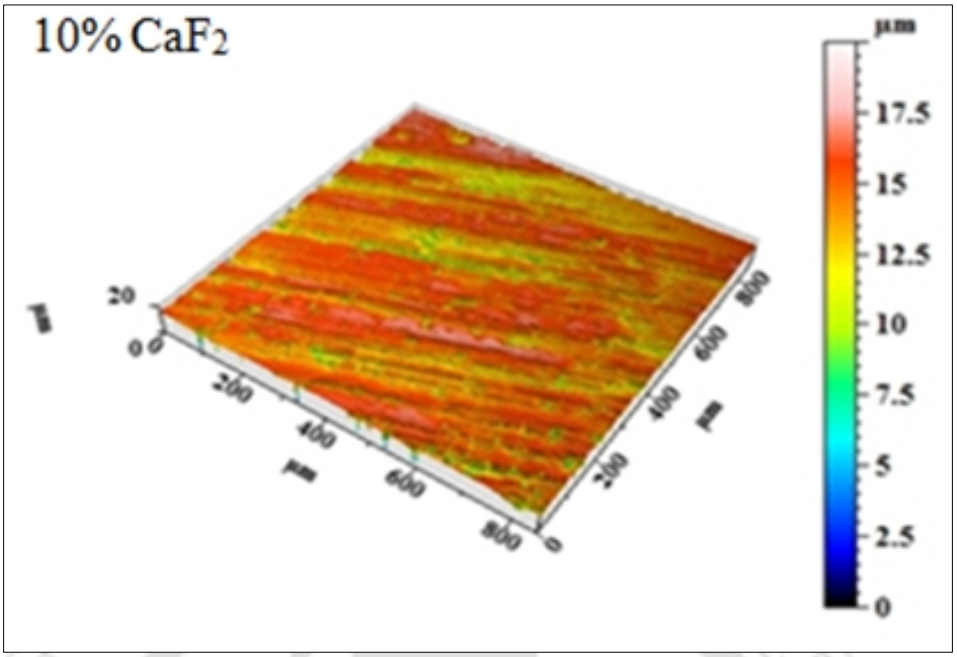


*Fig. 3.11(a) 3D non-contact surface image of the WC-Co (v =0.5 m/s, $F_N$=19.62 N) (b) 3D non-contact surface image of the WC-Co-3wt.% $CaF_2$ (c) 3D non contact surface image of the WC-Co-5 wt.% $CaF_2$ (d) 3D non-contact surface image of the WC-Co-7 wt.% $CaF_2$ and (e) 3D non-contact surface image of the WC-Co-10 wt.% $CaF_2$ (v = 0.5 m/s, $F_N$= 19.62 N).*

In addition, roughness of the worn-out surface was also measured by the contact stylus type roughness tester and figure 3.12 shows the roughness profile of the surface after the abrasive wear test. Test materials were prepared to have the same roughness (Ra = 0.65-0.68 µm) and the final surface roughness of the test material indicates its wear resistance. Test material with high surface roughness after testing indicates poor wear resistance of the material. The final surface roughness of the WC-Co-5 wt.% $CaF_2$ (Ra 0.53-0.62 µm) confirmed less frictional resistance/ coefficient of friction and polishing. During the testing, the presence of $CaF_2$ helps to reduce its surface roughness in spite of sliding against silicon carbide abrasive particles. Similarly, surface roughness of the WC-Co-7 wt.% $CaF_2$ (Ra 0.66–0.69 µm) confirmed its less resistance to friction and less wear resistance.

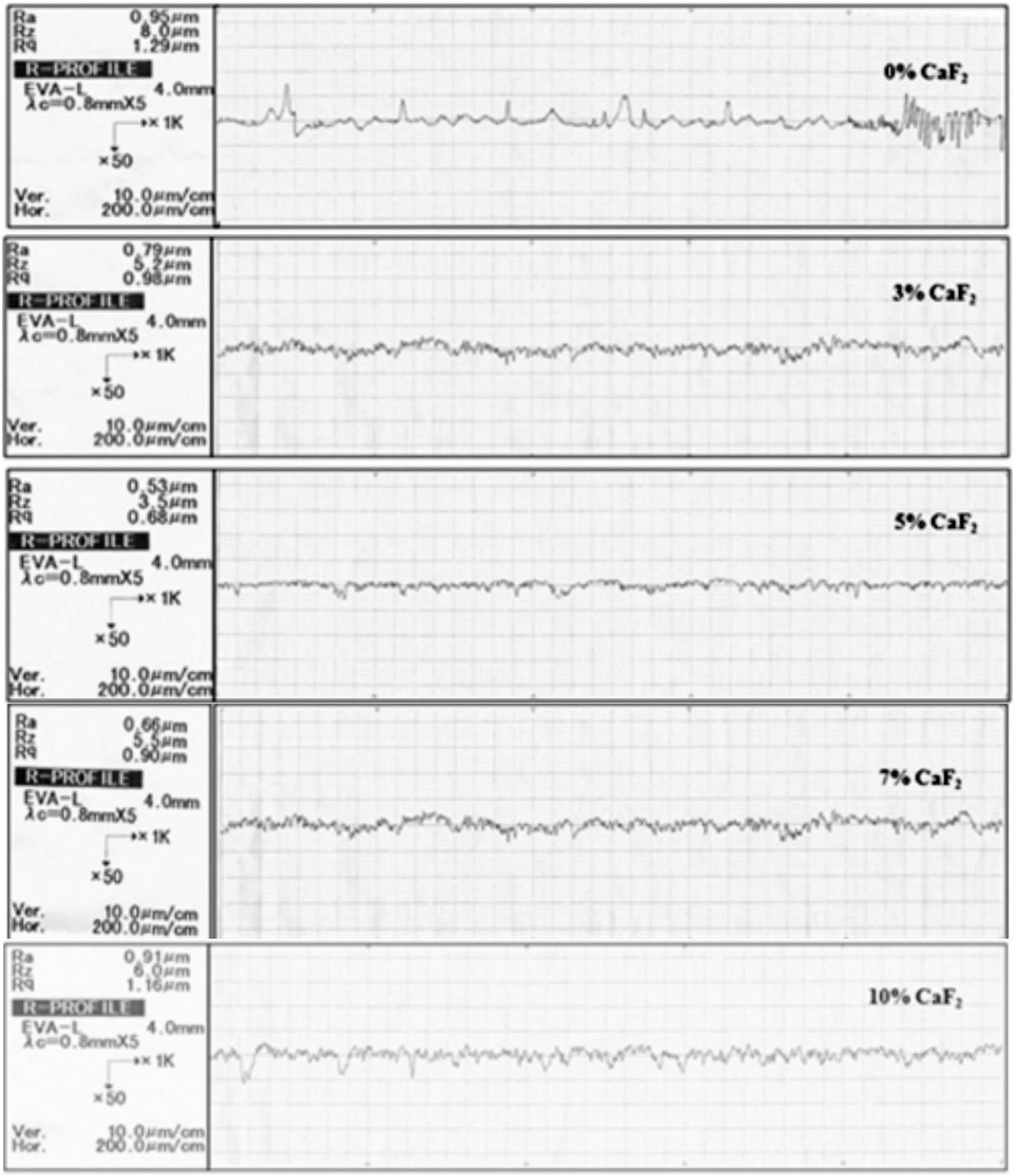


*Fig. 3.12 Final surface roughness of the test specimens after abrasive wear test (v = 0.5 m/s, $F_N$= 19.62 N)*

In spite of sliding against hard silicon carbide abrasive particles, surface roughness of the test material did not change from its initial condition due to the presence of calcium fluoride material. However, WC-Co-3 wt.% $CaF_2$ (Ra 0.76-0.82 µm) as well as WC-Co-10 wt.% $CaF_2$

(0.91-0.98 μm) exhibited poor surface roughness. In these materials, in spite of the presence of $CaF_2$ particles, poor hardness of these materials exhibited poor wear resistance. Though frictional resistances of these materials are lesser than those of straight WC-Co material, but it exhibited higher frictional resistance when compared to WC–Co with 5 wt.% and 7 wt.% $CaF_2$ material.

Final surface roughness of the test specimens after abrasive wear test (v = 0.5 m/s, F materials showed very high surface roughness (Ra 0.95-1.06 μm). Straight WC–Co material exhibited very poor wear resistance due to the absence of $CaF_2$ particles as well as lesser hardness when compared to WC-Co-5, 7 and 10 wt.% $CaF_2$ materials.

### 3.4 SCRATCH RESISTANCE OF TEST MATERIALS

In this work, to confirm the superior adhesive wear performance of WC-Co-5 wt.% $CaF_2$ material over straight WC-Co, a scratch test was carried out at with the aid of the scratch tester (Ducom, TR-101). Figures 3.13 (a-b) shows the scratch test equipment and close up view of the specimen with indentor. Diamond Brale indentor (scale C diameter 200 μm) was used with a normal load of 20 N and sliding speed of 0.3 mm/s. Figures (3.14 (a-b)) show the indented scratch marks observed on the straight WC-Co. Straight WC-Co material exhibited narrow and deep scratch, whereas WC-Co-5 wt.% $CaF_2$ material exhibited wide and shallow scratch (figures 3.15 (a-b)) for the same normal load and velocity of sliding. This behavior difference is due to the bond strength between adjoining carbide particles. In the WC-Co-5 wt.% $CaF_2$ material, strong bond exist between carbide particles. Due to which, indenter not able to plow in to the depth and applied load was transferred to the adjacent particles in the transverse direction. Hence adjoining carbide particles in the transverse direction also subjected to load.

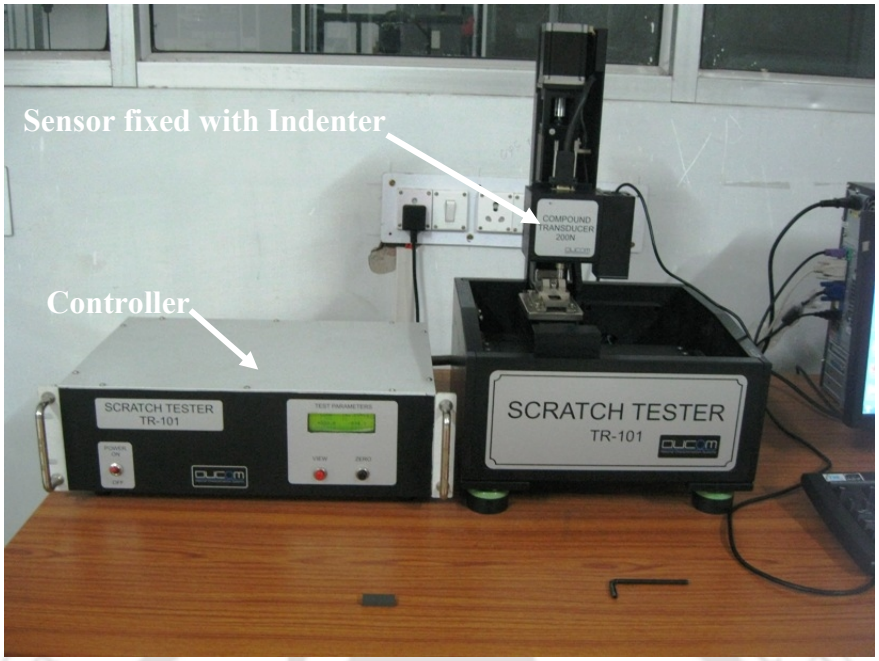


*Fig. 3.13 (a) View of the scratch tester*

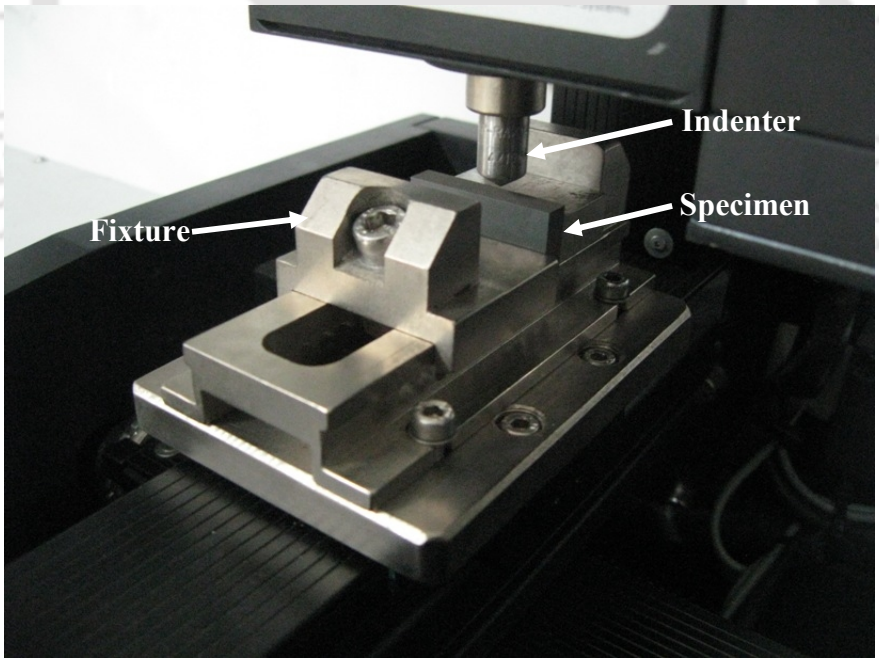


*Fig. 3.13 (b) Close up view showing indenter and specimen*

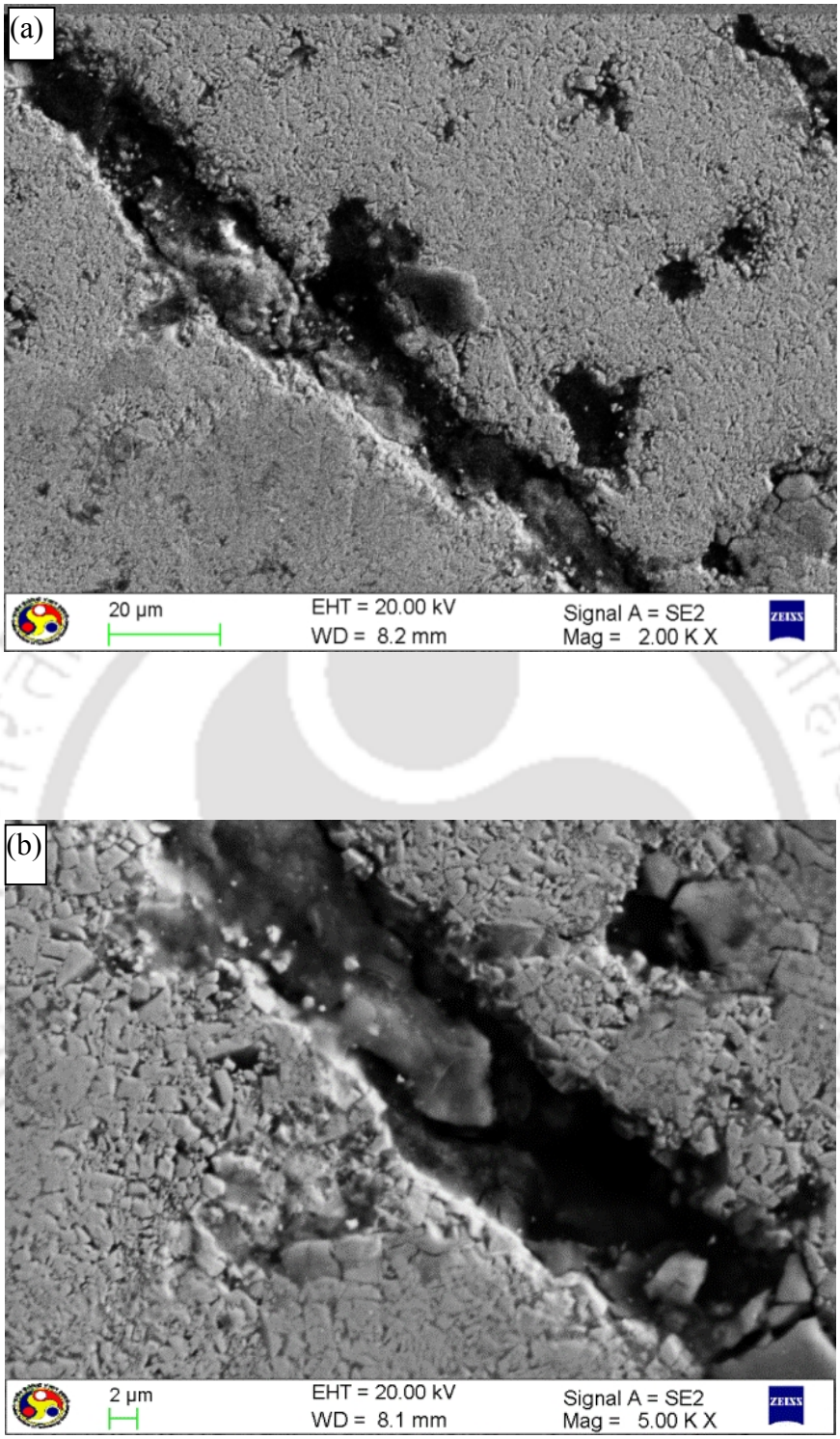


*Fig. 3.14 (a) Deep and narrow scratch at WC-Co material and (b) No disturbance of adjoining of carbide particles observed near the scratch at WC-Co material*

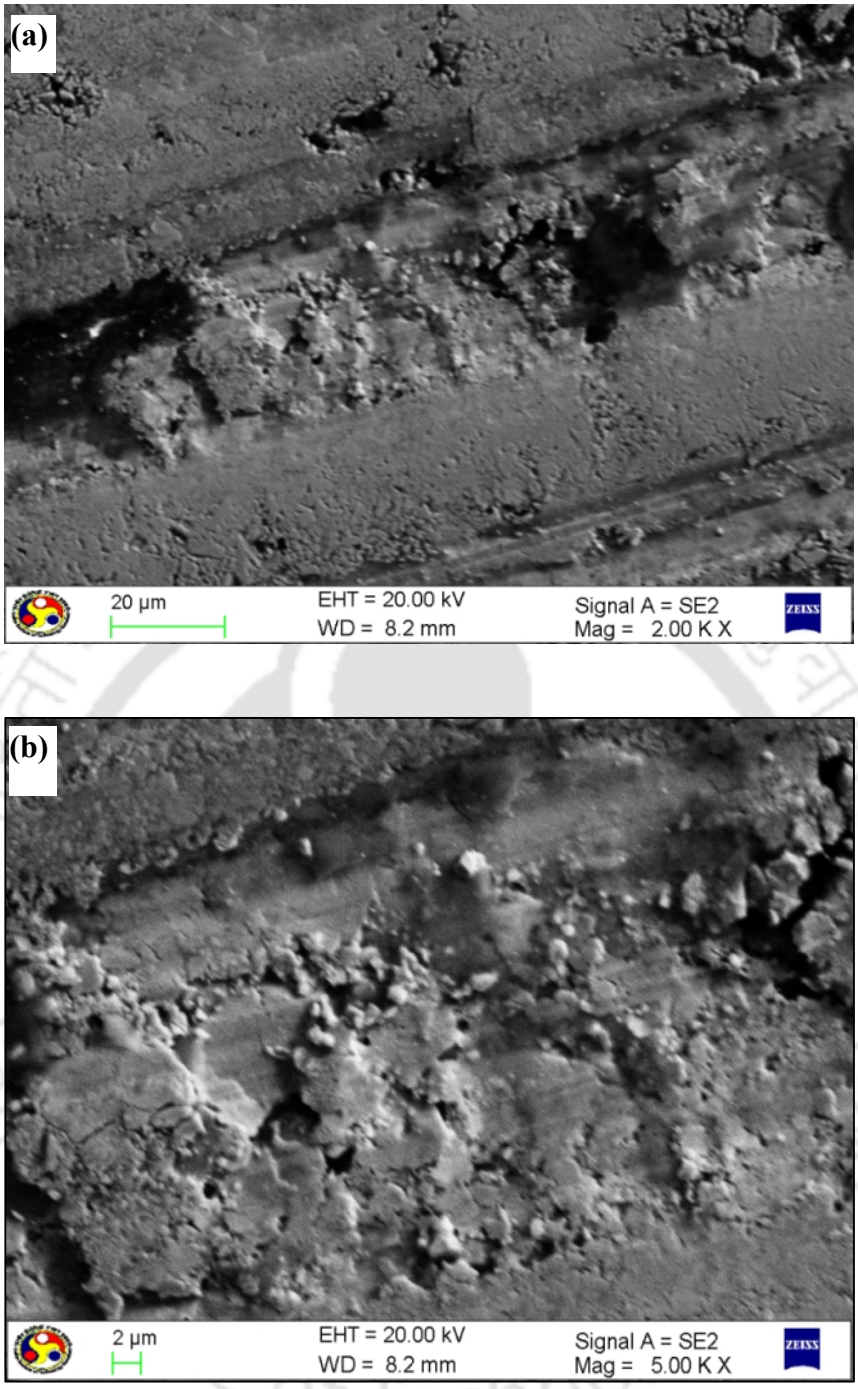


*Fig. 3.15 (a) Wide and shallow scratches at WC-Co-5 wt.% $CaF_2$ and (b) Deformed carbide particles observed at WC-Co-5 wt.% $CaF_2$*

Closely packed carbide particles and rubbing marks adjacent to the indentation marks confirmed this fact. In the case of straight WC-Co material, poor bonding among carbide

particles exits. Due to which indentor load transferred in the normal direction and formed plowing marks. Due to which, deep and narrow scratch marks were observed.

### 3.4 SUMMARY

Present study revealed the effect of solid lubricant over the abrasive wear performance of developed solid lubricant cutting tool material. The following major conclusions were arrived from the present work

- Among the investigated test material, WC-Co-5 wt.% $CaF_2$ exhibited superior wear resistance and the lowest friction coefficient (0.25-0.28) due to its combination of superior hardness and lubricating behavior at the test condition.
- Presence of $CaF_2$ in the developed material is confirmed through XRD. $CaF_2$ presence is confirmed on the worn-out test surface through, SEM-EDS, elemental mapping and line scanning plot.
- WC-Co-5 wt.% $CaF_2$ exhibited wedge groove feature whereas, the straight WC-Co material exhibited brittle fracture with crater and hillocks features.
- The measured temperature of test material confirmed that frictional heat is generated due to the surface interaction between test material and abrasive sheet. WC-Co-5 wt.% $CaF_2$ exhibited only 30 °C, whereas straight WC-Co exhibited up to 80° C under considered test conditions.
- The final surface roughness of the test material confirmed that WC-Co-5 wt.% (0.53-0.62 μm) and well as 3D surface profile confirmed superior wear resistance when compared to all other considered materials.
    - Shallow and wide scratch marks with the sign of closely packed carbide grains on the scratch edges revealed strong bonding between the adjoining carbide particles of WC-Co-5 wt.% $CaF_2$ material.

# CHAPTER 4

# ADHESIVE WEAR CHARACTERISTICS OF TUNGSTEN CARBIDE BASED SELF LUBRICATING CUTTING TOOL MATERIAL

## 4.1 INTRODUCTION

In machining, cutting tool interaction with the work piece is analogous to the adhesive sliding. Thus, many investigations on the adhesive wear performances of carbide materials were carried out to understand the effect of carbide content, cobalt content over friction and wear behavior. Bonny *et al*. (2010) performed sliding wear test to understand the effect of the load and sliding speed on tribological performance of tungsten carbide cobalt (10-12 wt.%) against WC-6 wt.% Co. Qiao *et al*. (2013) included calcium and barium fluoride with tungsten and aluminum to develop a composite for the cutting tool application. Developed materials were evaluated for friction and wear by reciprocating it against commercial silicon carbide ball. Calcium fluoride composites exhibited less friction. The worn-out surface of the fluoride composite revealed the adhesion wear as the predominant wear.

Bolton and Gant (1993) added solid lubricants, calcium fluoride, to high speed steels to improve wear properties and evaluated the phase reactions and chemical stability of the composites. Deng et *al*., (2007) included calcium fluoride fillers to the aluminum oxide and evaluated sliding wear performance. Developed materials were made into block and slide against the tungsten carbide disc. The worn-out surface of the developed materials without calcium fluoride revealed abrasive as the primary wear mechanism. Material with calcium fluoride revealed the thin tribo film on the worn out surface.

From the above literature, it is observed that considerable amount of work has been done to understand the friction wear behavior of cutting tool materials under adhesive condition. Few works have been carried to understand the effect of carbide and cobalt content over the tribological performance. Few works have been carried out by adding solid lubricant as coating as well as fillers and evaluated for the friction and wear performance. No work has been attempted to understand the adhesive wear performance of tungsten carbide based solid lubricant material and this chapter attempted the same for the comprehensive understanding.

## 4.2 TESTED MATERIALS FOR ADHESIVE WEAR STUDY

In this work, in-house developed tungsten carbide materials with the various amount of (0-10 wt.%) $CaF_2$ were made to slide against commercial WC-6 % Co (Rapicut carbides) in the pin on disc tribometer (Ducom, TR-201) in accordance with ASTM G 99. Considered, commercial disc material has higher hardness compared to that of developed material hardness (85 HRA). To avoid compound wear (both test and counter disc would loss material) counter disc with higher hardness was selected to evaluate the adhesive wear performance of the developed cutting tool materials. Mild steel was not considered for adhesive wear performance as the hardness (140 HB) is lesser than developed materials. Figure 4.1(a) shows the close up view the used sintered counter disc. Hardness of the disc material is 89-91 HRA and the initial surface roughness of the disc is 0.1-0.2 μm. Developed solid lubricant materials were cut into specimens of 6 × 6 × 15 mm having the initial surface roughness (Ra) of 0.07-0.12 μm. Weighing balance (0.1 mg accuracy) was used to measure the initial and final weight of the test specimen. Figures 4.1 (b-c) shows the surface of the counter disc (WC-6 wt. % Co) and WC-10 wt. % Co-5 % $CaF_2$). The initial and final roughnesses of the test specimen were measured by the portable surface roughness tester (Mitutoyo, Surf test SJ-400). Thermal imaging camera (InfraTec hr Head Vario CAM 480SL)

was used to measure the surface temperature of the test specimen continuously. Scanning electron microscope (LEO, 1430vp), as well as non-contact surface profilometer (Taylor Hobson, CCI MP) was used to investigate the worn-out surface of the test specimens.

Friction and wear performance of the test specimens were carried out at a normal load of 19.6 N with 0.5 m/s surface velocity. Tests were carried out at dry and room temperature condition for 30-min duration. Tests were also carried out at various normal loads (9.8, 19.6, 29.4 N) in abrasive wear study (Chapter 3). Out of these three loads one load (19.62 N) was considered to understand and correlate adhesive wear performance of the developed cutting tool materials and wear rate, $Z$ of test material was computed using the relation (Equation 3.1).

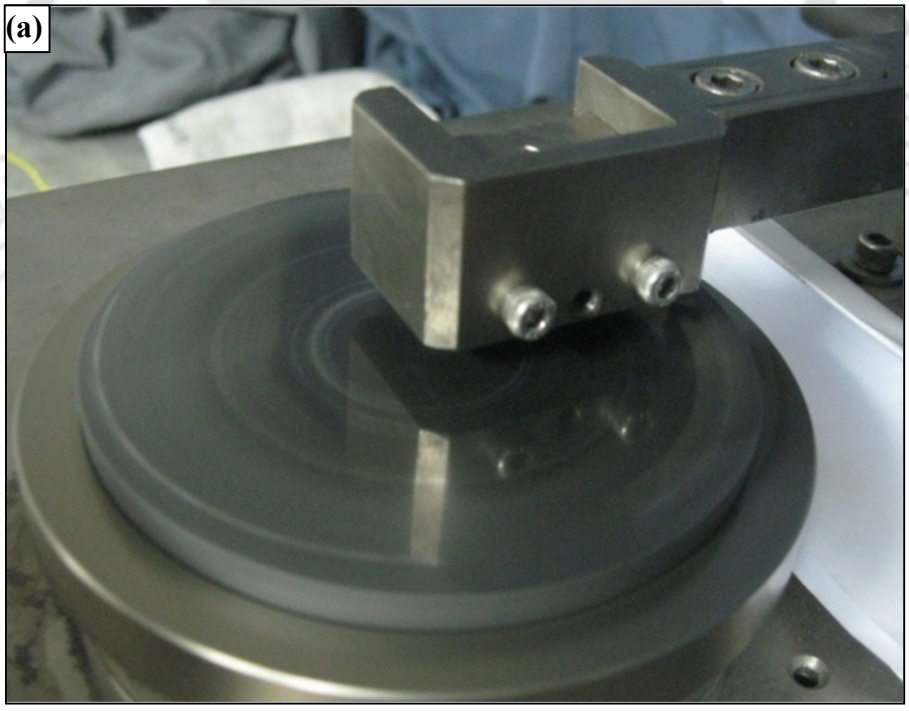

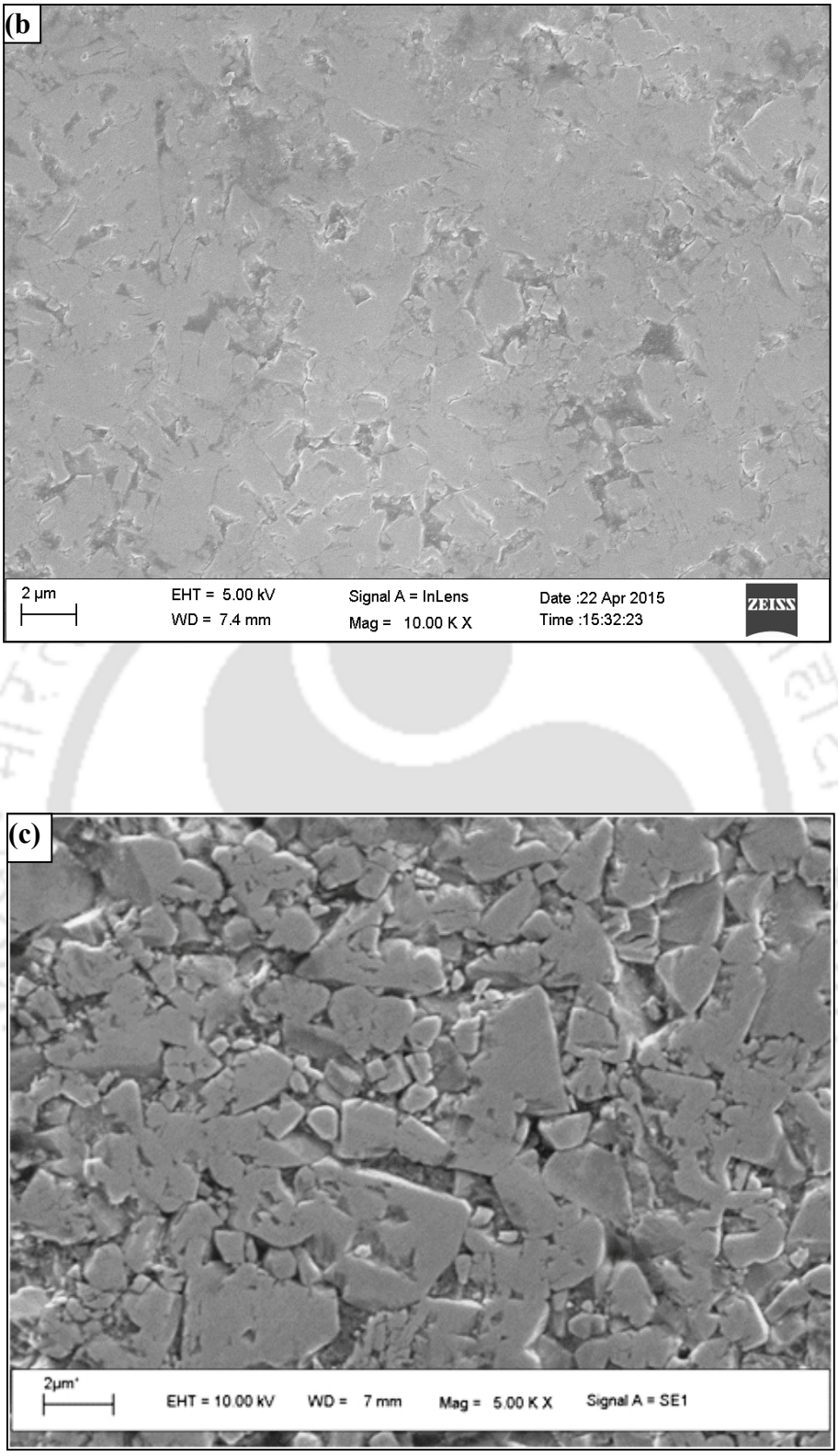


*Fig. 4.1 (a) Close up view of the counter disc used; (b Surface of the commercial WC-Co counter disc before testing; and (c) Surface of the WC-Co-5 wt.% $CaF_2$ test material before testing.*

## 4.3 RESULT AND DISCUSSION

### 4.3.1 Friction and wear of tested materials

Test specimens were made to slide against the commercial sintered disc (WC-6% Co) for the evaluation of adhesive wear performance. Figure 4.2 shows the friction of test materials, tests were repeated for at least three times and the average value was considered for further analysis. All the test material exhibited an increase in the initial stage and the steady state reached after certain period. Presence of asperities on the surface contributes to this behavior, after a certain period of interaction, contact area increases and reaches steady due to the worn out of these asperities. Many prior researchers (Okonkwo *et al*., 2012; Kagnaya *et al*., 2009; Bonny *et al*., 2010) also observed similar behavior i.e., a gradual increase in the beginning and reached the steady stage after certain time.

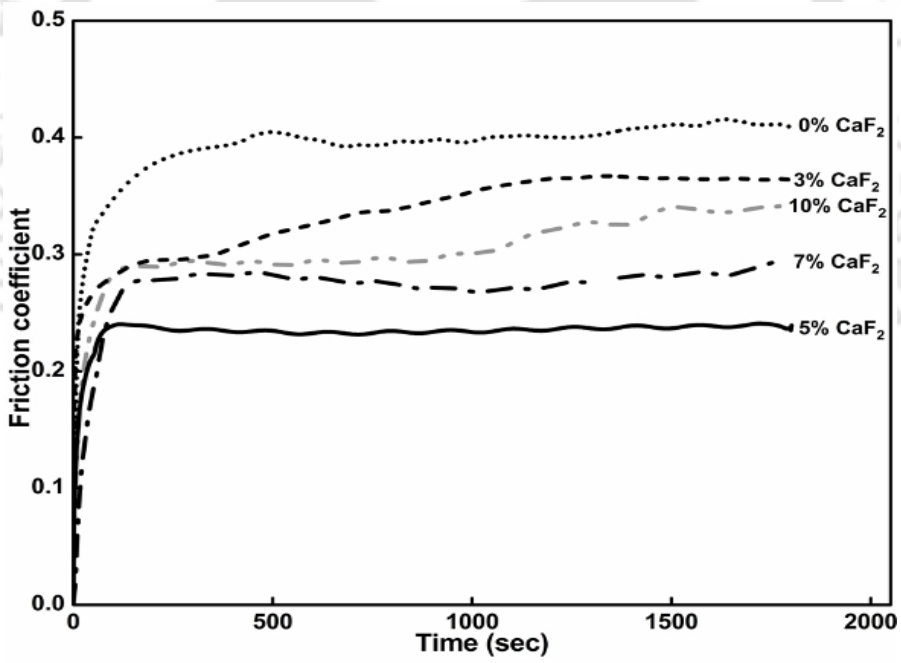


*Fig. 4.2 Friction performance of the test material (v =0.5 m/s, $F_N$=19.62 N)*

Measured coefficient of friction in the range of 500 to 2000 s was considered for discussion since there was a gradual rise in coefficient of friction. Sintered material without $CaF_2$ exhibited 0.39-0.41 coefficient of friction; however sintered material with 5 wt.% $CaF_2$

exhibited 0.23-0.24, which is least among all the investigated materials. The lamella structure of $CaF_2$ and less shear strength contributed to this lubricating behavior. All the considered test materials (3, 5, 7 and 10 wt.%) with $CaF_2$ exhibited lesser friction than straight WC-Co due to its lubrication effect. Material with 3 and 10 wt.% $CaF_2$ exhibited 0.29-0.34 coefficient of friction; however, material with 5 and 7 wt.% $CaF_2$ exhibited only 0.23-0.28 coefficient of friction, slightly high hardness of the material contributed to this behavior. Surface hardness of the material with 3 and 10 wt.% exhibited 80-84 HRA, whereas 5 and 10 wt. % exhibited 82-87 HRA. Deng *et al.*, (2007) also observed a reduction of coefficient of friction due to the addition of $CaF_2$ to the $Al_2O_3$ /TiC composites. Straight $Al_2O_3$ /TiC exhibited coefficient of friction 0.45-0.50, whereas addition of $CaF_2$ (5-15 %) reduced the coefficient of friction 0.26-0.32.

Figure 4.3 shows the online wear of the considered test material during the test and the position of the specimen is indicated by the position of the linear variable differential transformer sensor. Test material exhibited similar wear behavior as that of friction behavior (figure 4.2).

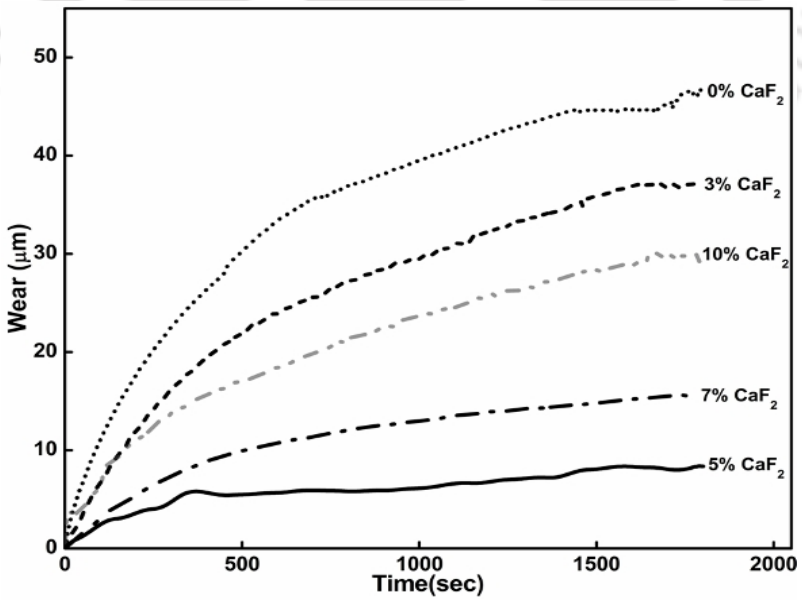


*Fig. 4.3 Wear performance of the test material (v =0.5 m/s; $F_N$=19.62 N)*

The material without $CaF_2$ exhibited the largest wear loss, whereas test material with 5wt.% $CaF_2$ exhibited least wear loss among considered materials. Material with 3 and 7wt.% $CaF_2$ exhibited more wear loss than that of 5 and 7 wt.% $CaF_2$, but less wear loss than that of straight WC. Weight loss exhibited by the considered test materials is shown in figure 4.4. Weights of the specimens were measured before and after test and the average value of the specimen with deviation is shown in figure. All the tests were repeated for three times, and the amount of deviation from the mean value is shown as error bars. The test material without $CaF_2$ exhibited 1.6 mg weight loss; however, test material with 5 wt.% $CaF_2$ exhibited only 0.45 mg weight loss. Test material with 5 wt. % $CaF_2$ exhibited least wear loss due to its high hardness and presence of lubricant in the interacting sliding surface. Tests were carried at various normal loads and wear rate was computed. Similar to frictional behavior, the addition of $CaF_2$ up to 5 wt.% helps to improve the wear resistance, beyond 5 wt.%, wear resistance found to decrease as shown in figure 4.5.

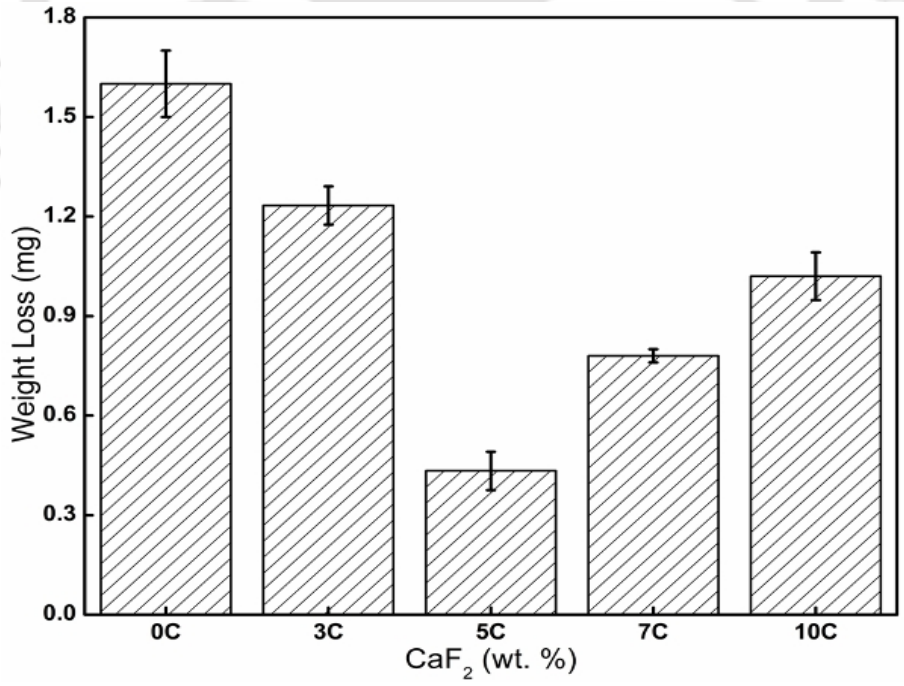


*Fig. 4. 4 Weight loss of the test material*

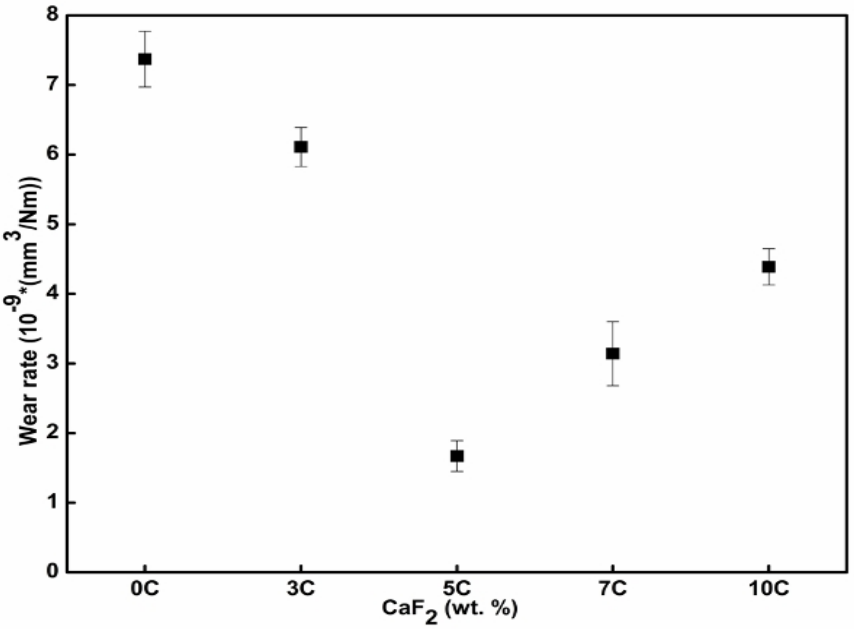


*Fig. 4. 5 Wear rate of the test material. (v = 0.5 m/s, $F_N$= 19.62 N).*

The addition of $CaF_2$ up to 5 wt.% helps to improve the wear resistance, beyond 5 wt.%, wear resistance decreased similar to friction behavior. The excess and insufficient amount of $CaF_2$ reduced material strength and material hardness (2.4.2 section). Deng and Cao (2007) observed similar behavior with $Al_2O_3$/TiC, up to 10 wt.% $CaF_2$, an increase in wear resistance and decrease in coefficient of friction were observed. Beyond this value, a decrease in wear resistance and an increase in coefficient of friction were observed.

### 4.3.2 Surface temperature of the test materials

Developed tungsten carbide test material was made to slide against commercial WC counter material; since the hardness difference between test materials (82-85 HRA) and counter material (89-91 HRA) is not significant. Both the test and counter materials were made out of tungsten carbide hence adhesion would be the primary wear mechanism due to the strong molecular attraction. During surface interaction, asperities of test and counter surface material slide past each other and frictional heat is generated. Figure 4.6 shows the measured surface temperature of test materials under 0.5 m/s sliding velocity and 19.6 N normal load.

The maximum surface temperatures exhibited by 0, 3, 10, 7 and 5 wt. % $CaF_2$ are 46, 40, 38, 34 and 31 °C, respectively.

The same test materials were made to slide against the silicon carbide abrasive sheet at the same normal load and sliding speed and reported in chapter 3 The maximum surface temperatures exhibited by 0, 3, 10, 7 and 5 wt.% $CaF_2$ when slid against silicon carbide abrasive sheets were 80, 70, 55, 45 and 30 °C, respectively (The amount of energy dissipated due to adhesive wear is significantly less when compared to that of abrasive wear.

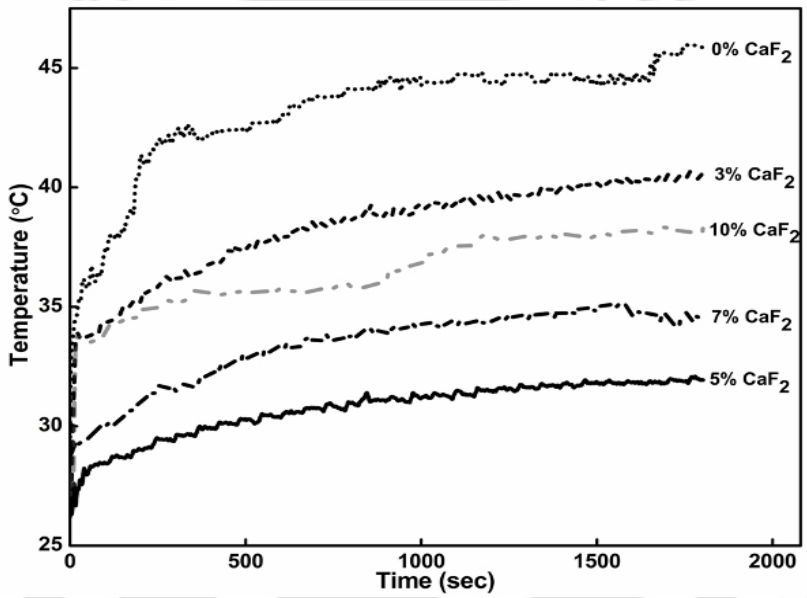


Fig. 4. 6 *Measured surface temperature of test material ($F_N$=19.6 N, V=0.5 m/s)*

Energy dissipated for the macro deformation (plowing) is significantly larger than that of micro deformation (asperity deformation). Higher surface temperature and at abrasive condition confirmed this fact.

### 4.3.3 Wear morphology

Worn-out test surface of the considered materials was observed under the scanning electron microscope to understand the wear morphology as well to confirm the presence of lubricant material. Figures 4.7 (a-b) shows the wear morphology of test material without $CaF_2$. Wear morphology confirmed primary failure as binder removal with no traces of plowing marks.

Due to the binder removal, closely packed tungsten carbide grains were dislodged and adjacent carbide grains were removed from the network leaving cavities on the surface.

Cracks were also observed on these surfaces (figure 4.7(b)) and poor bonding between the carbide particles contributed to this behavior. Poor bonding in the straight WC was also confirmed from the failure morphology while evaluating transverse rupture strength (section 2.4.2).

EDS was carried out on the worn out surface of straight WC-Co material and no new element was observed. Spectrum 1 corresponds to the white spot, spectrum 2 corresponds to grey spot and spectrum 3 corresponds to region with both white and grey spot. All these three regions (figures 4.7(c-e)) indicated the presence of tungsten, carbide and cobalt and no new element was identified. Pirso *et al*. (2004) also observed these types of surface failure when tungsten carbide slide against steel disc and binder was identified as the primary failure mechanism. Klaasen *et al*. (2010) also observed similar failure morphology, when titanium carbide with nickel binder was made to slide against the mild steel. Due to the weak nickel binder, dislodge of carbide grains in the network was observed.

(a)

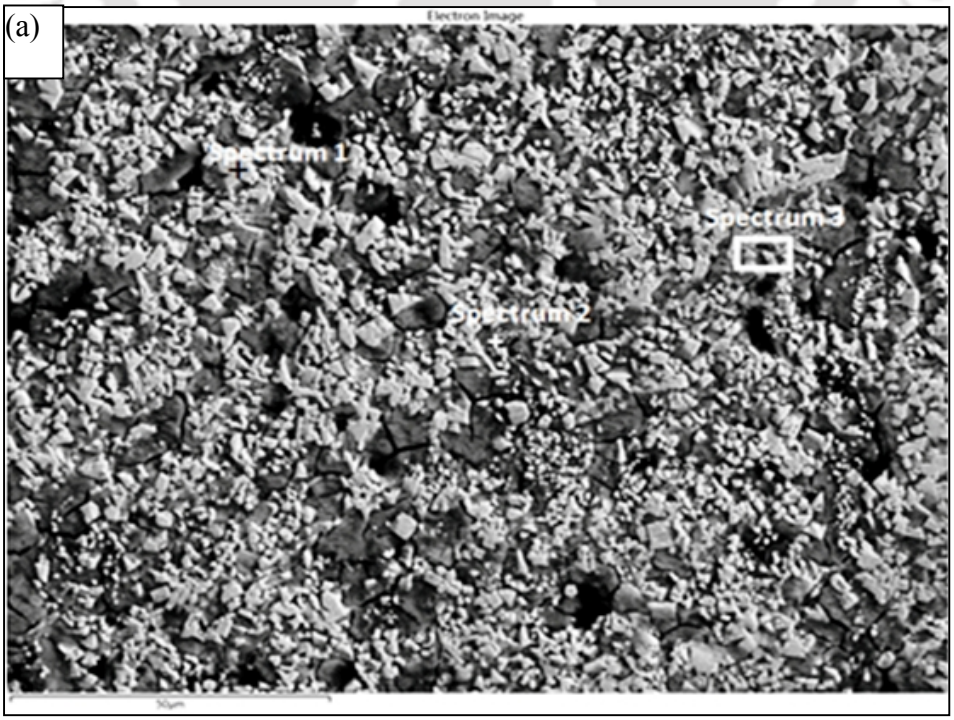

(b)

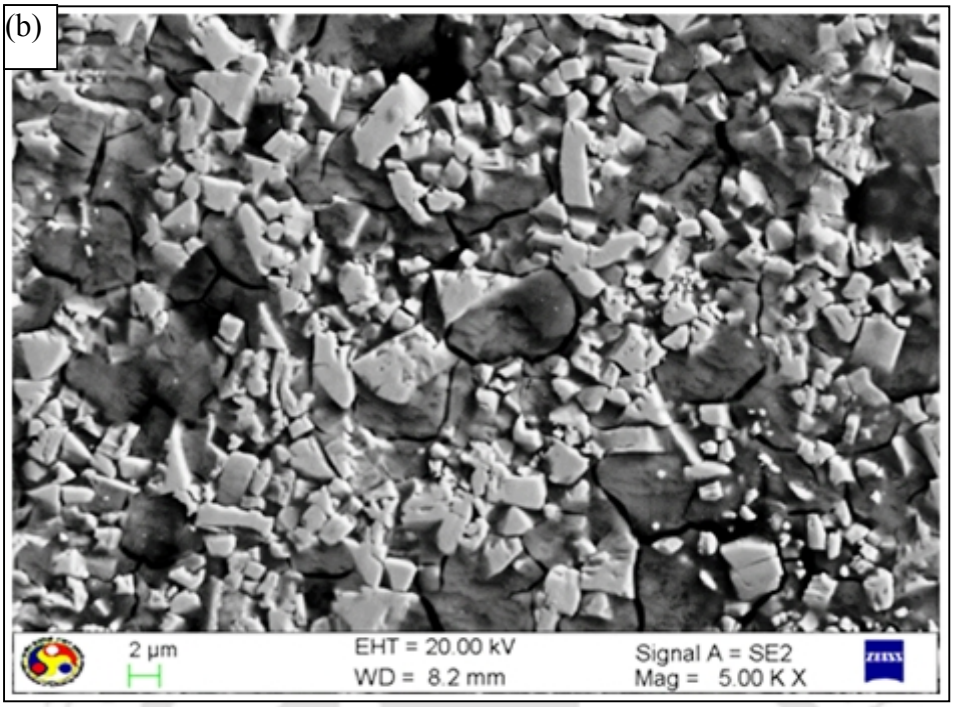


(c)

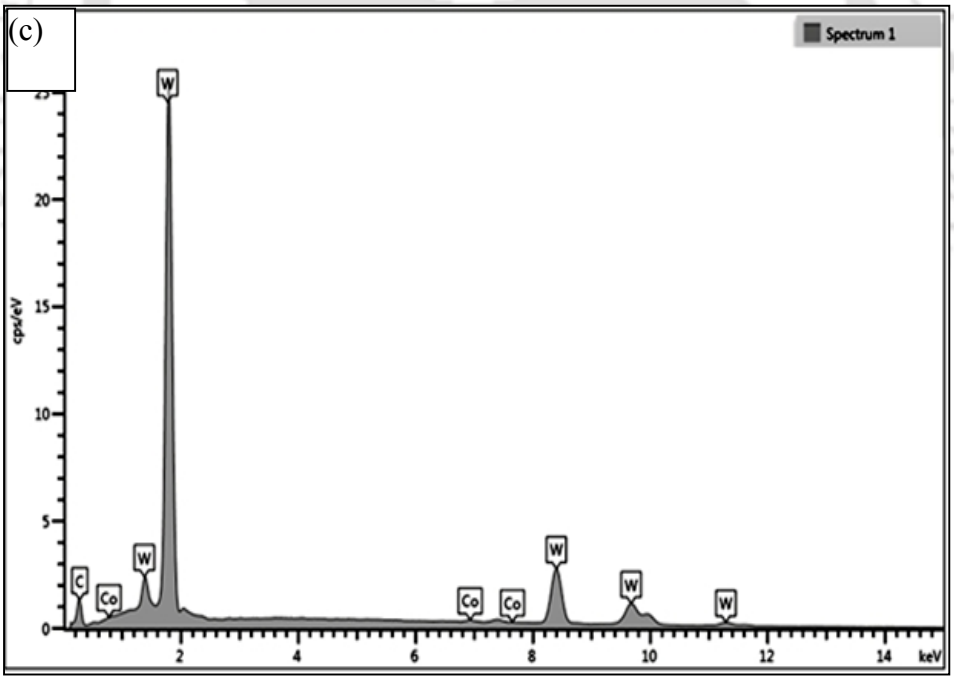

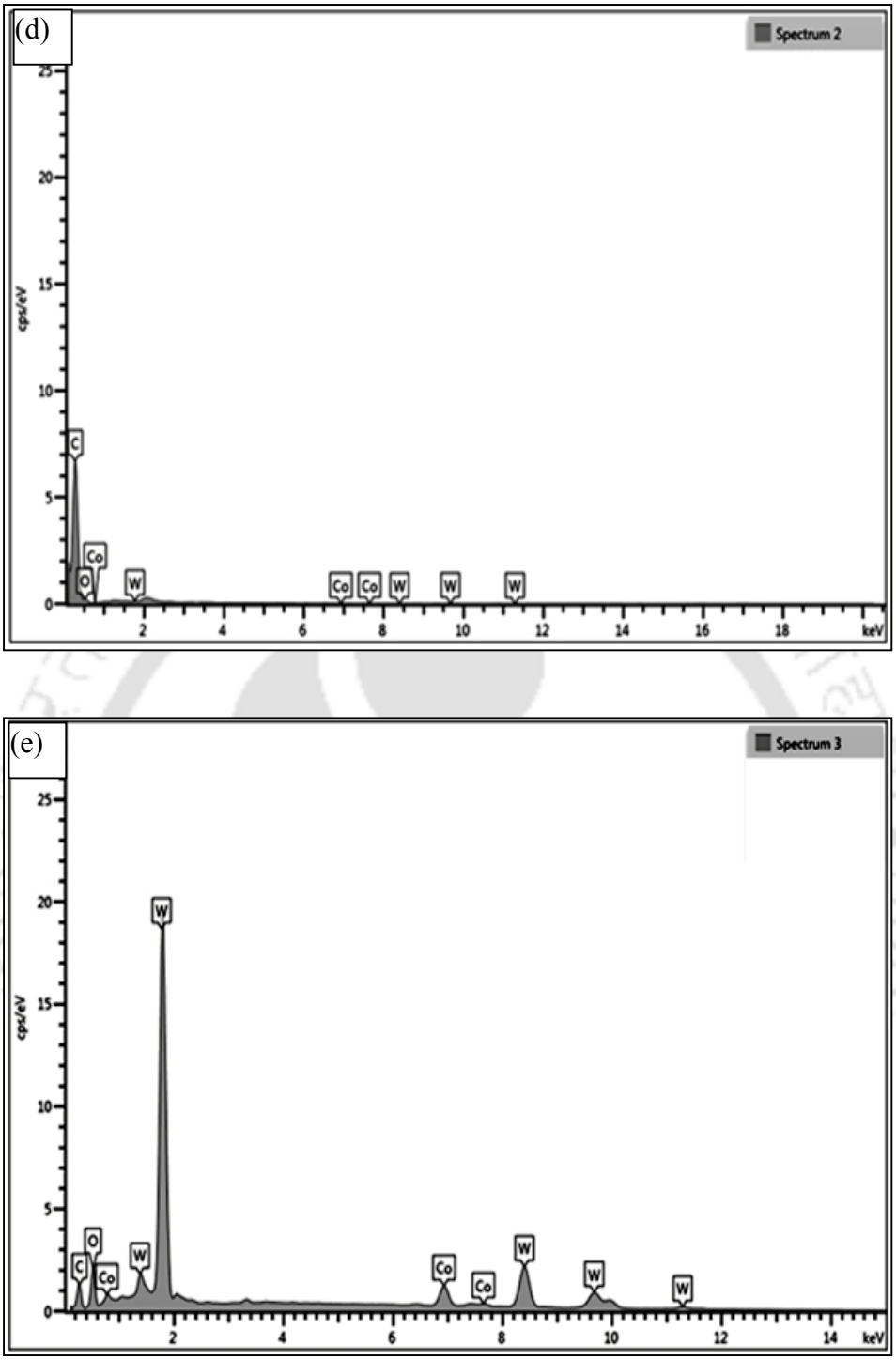


*Fig. 4.7 (a) Worn-out surface of the straight WC–Co material (b) Worn-out surface of the straight WC–Co, showing cracks around carbide particles (c) EDS of spectrum1: Worn-out surface of straight WC–Co material (d) EDS of spectrum 2: Worn-out surface of straight WC–Co material (e) EDS of spectrum 3: Worn-out surface of straight WC–Co material*

Gant *et al*. (2004) investigated the effect of corrosive media on the wear mechanism of tungsten carbide material. Failure surface indicated significant amount of cobalt binder removal as well as fracture of carbide grains. Gant and Gee (2011) carried out extensive review on micro scale abrasion testing. It is found that micro scale abrasion of WC hard metals not exhibit any fracture of WC grains. In the early stages, removal of binder phase was clearly seen followed by the progressive removal of WC grains as wear proceeds. Figures 4.8(a-b) shows the wear morphology of WC+ 5 wt.% $CaF_2$ material, where carbide grains were tightly intact and no trace of grain dislodgements was observed. Presence of $CaF_2$ has improved bonding between carbide grains, hence no binding failure was observed. EDS was carried out on the worn out surface of the WC-Co-5 wt.% $CaF_2$ to confirm the lubricant material, $CaF_2$ on the surface after testing. Figure 4.9(a) shows the considered micrograph of the worn-out surface with a shown line on which EDS spectrum was obtained and plotted in Figure 4.9(b).

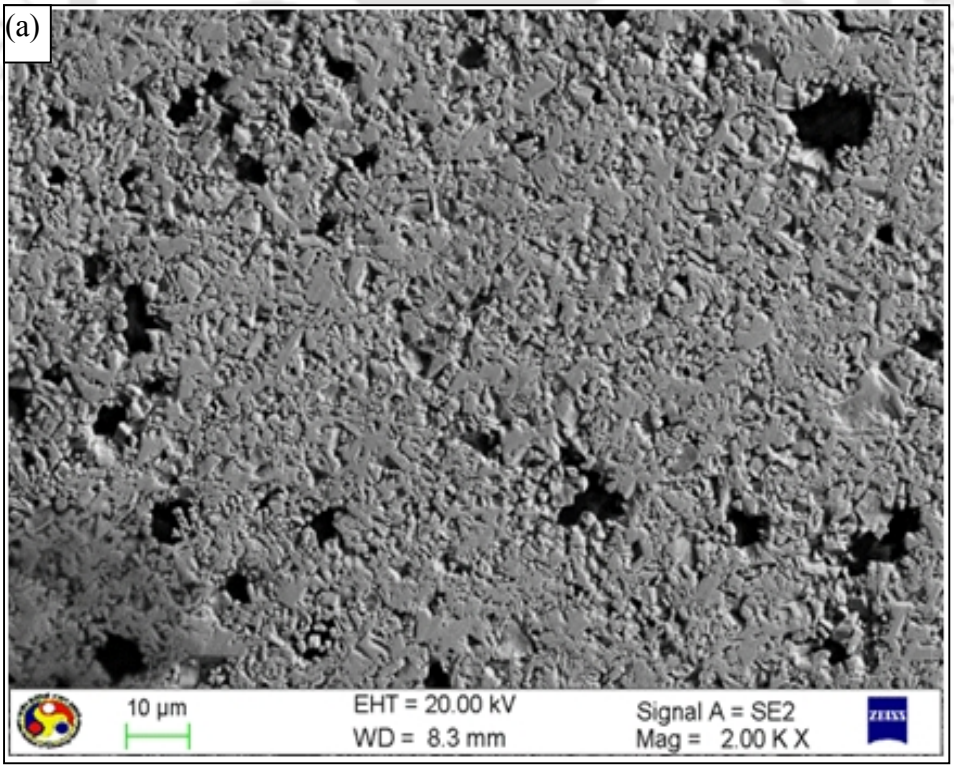

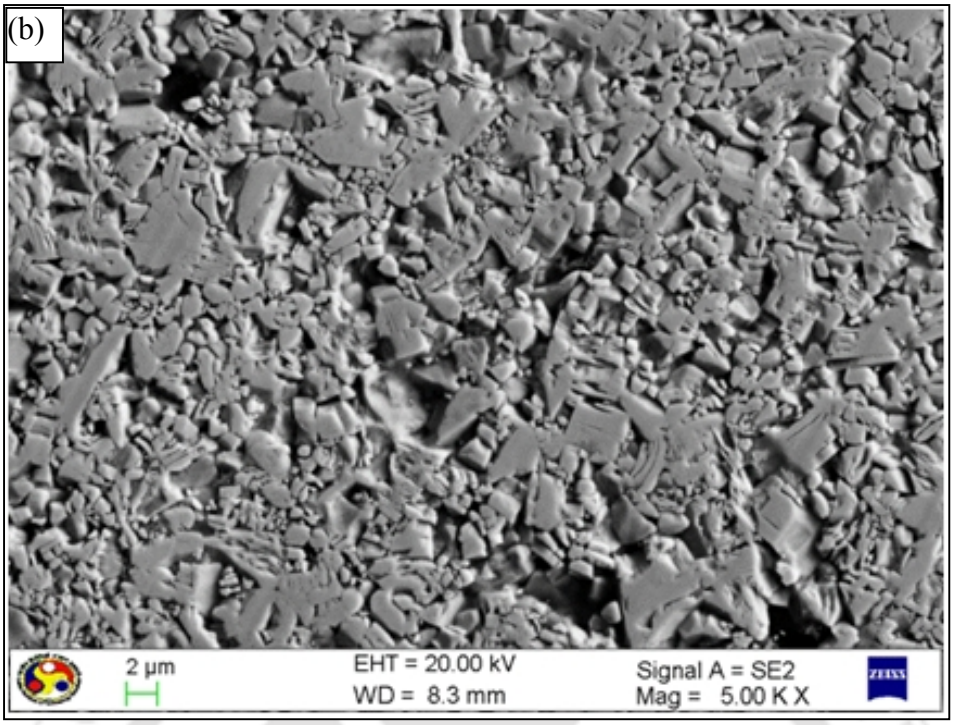


*Fig. 4. 8 (a) Worn out surface of the WC-Co- 5 wt. % $CaF_2$; and (b) Worn out surface of the WC-Co- 5 wt. % $CaF_2$, close up view.*

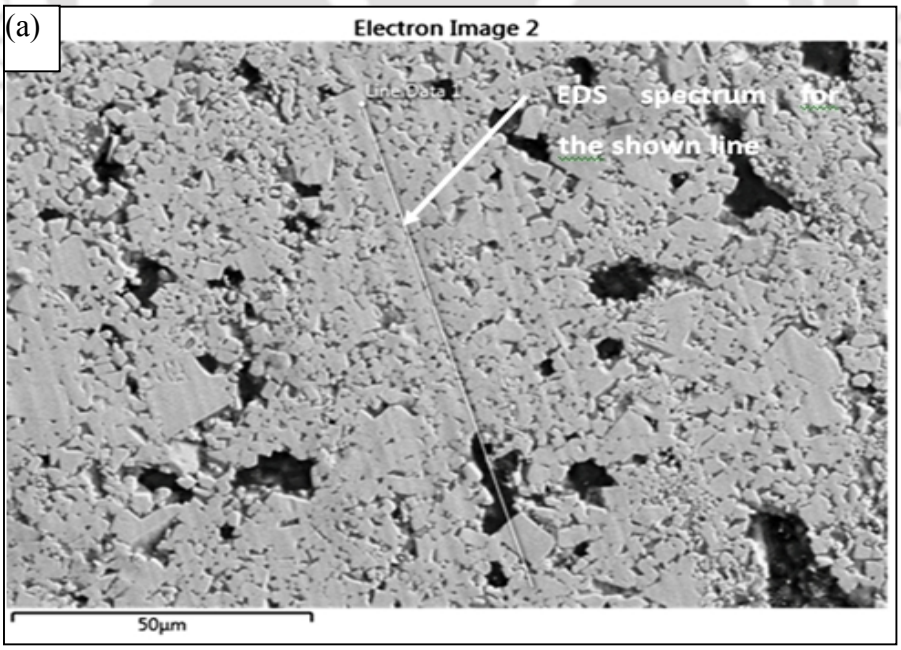


*Fig. 4. 9 (a) Considered worn out surface (b) EDS spectrum along the considered line of wornout surface*

Figures 4.10(a-f) confirmed the presence of tungsten, carbon, cobalt, calcium and fluoride on the test surface. The tungsten carbide throughout surface uniformly distributed and tungsten carbide gives strength and wear during wear test against commercial grade tungsten carbide disc material. The excess amount of calcium and fluorides were observed at the surface cavity (seen as a black spot).

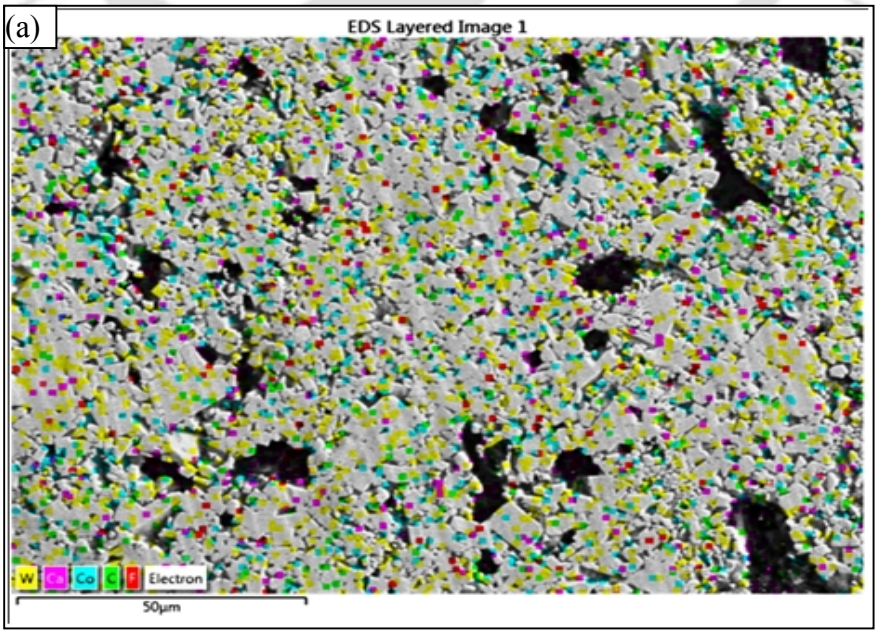

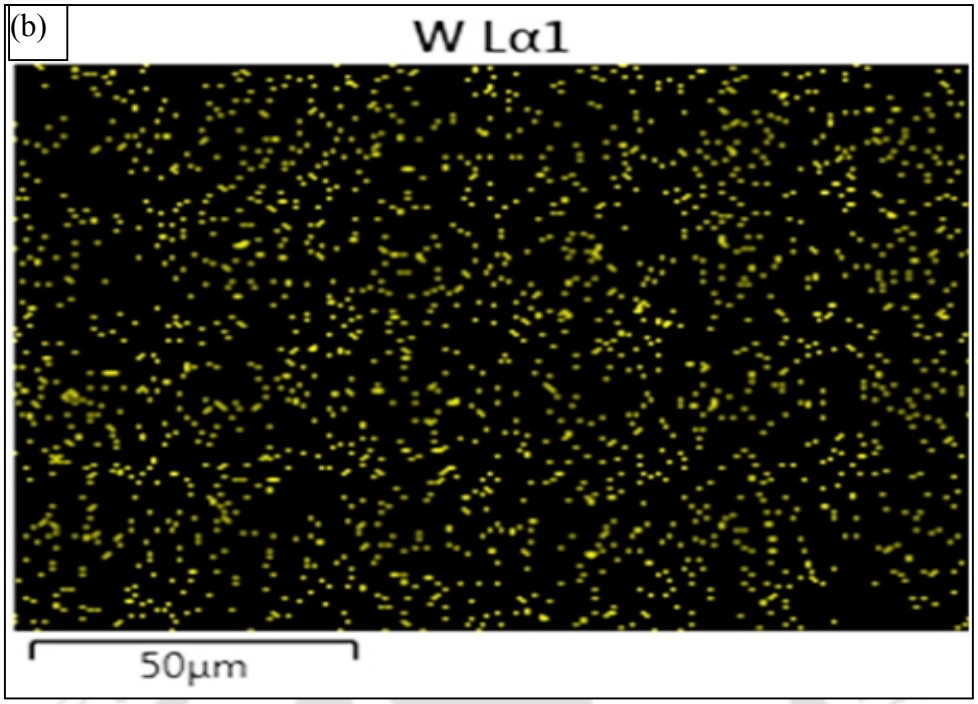


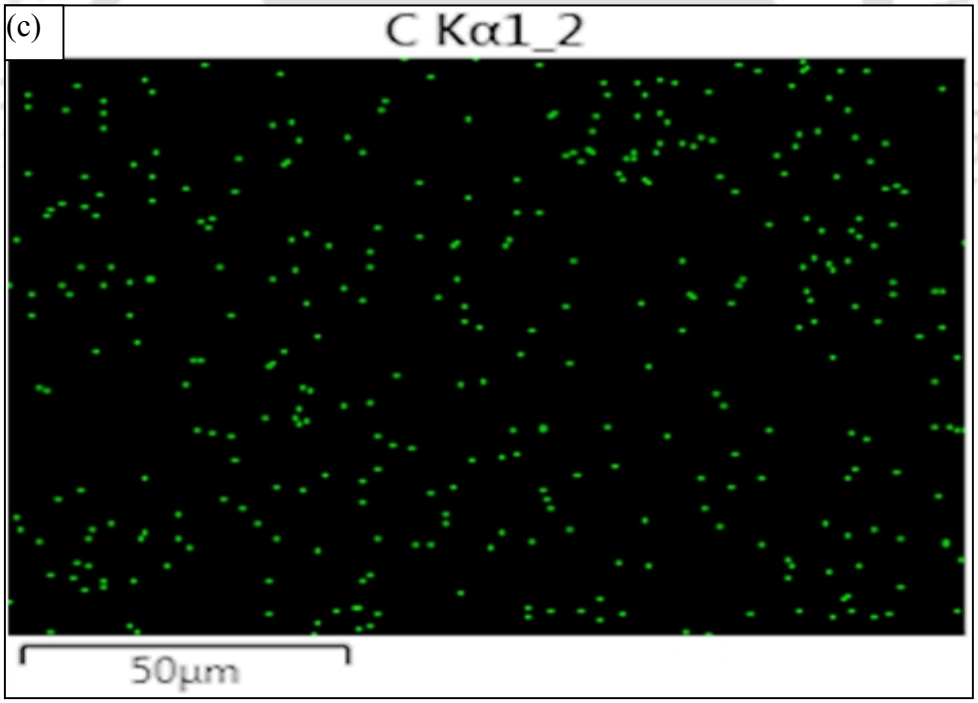

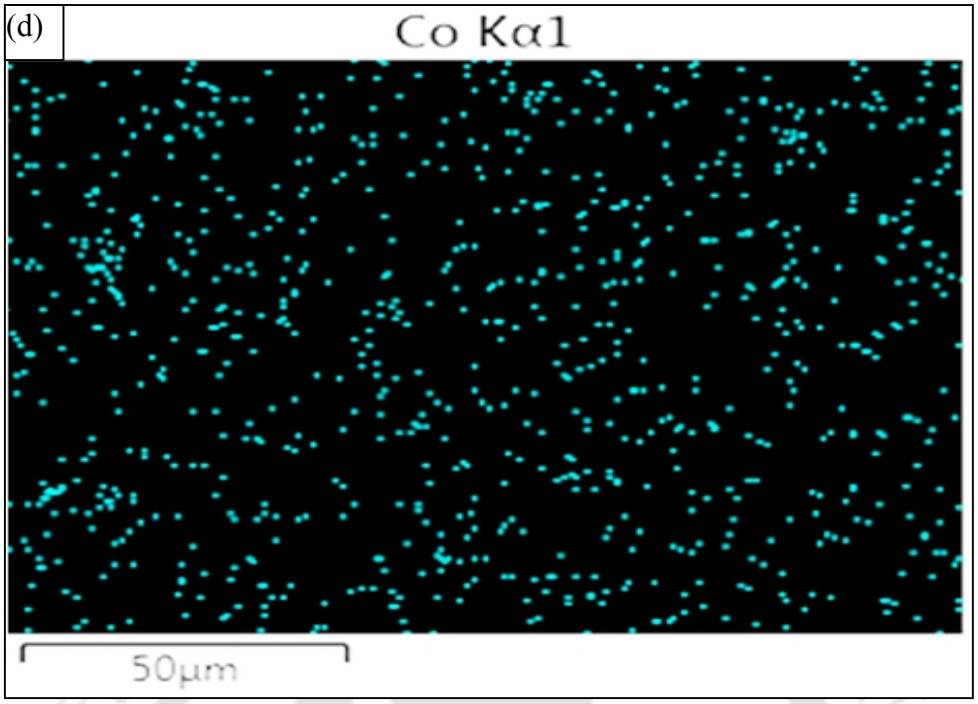


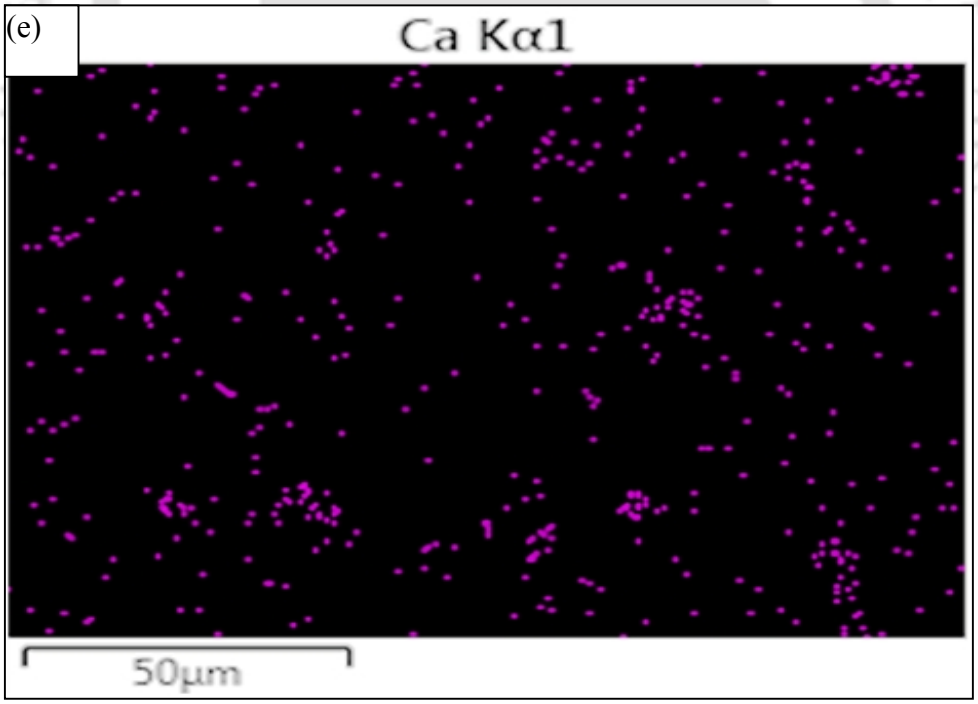

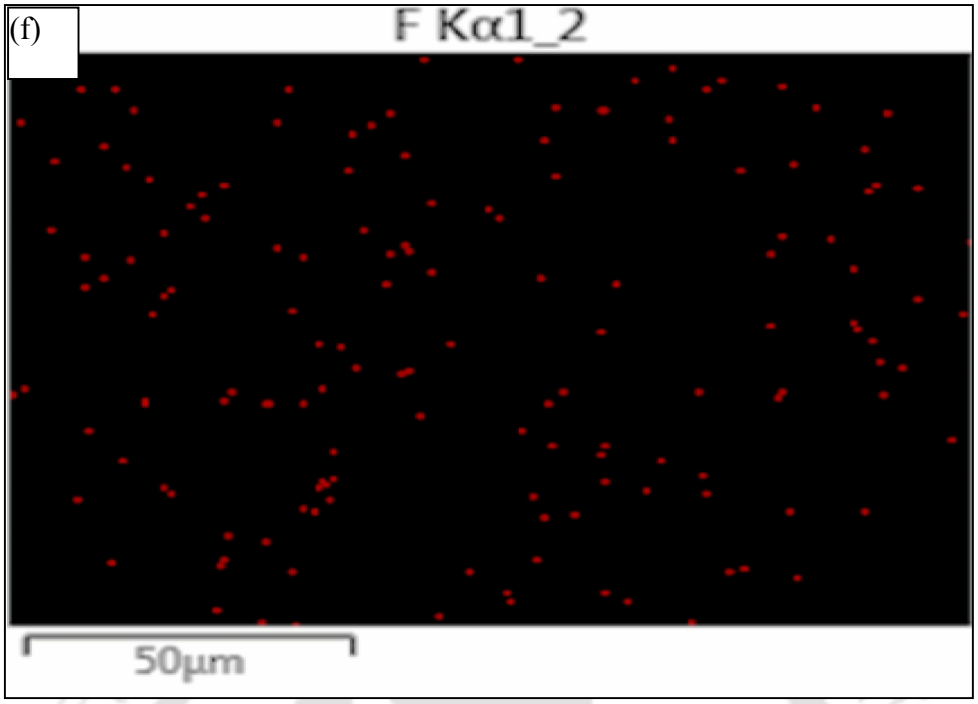


*Fig. 4.10 (a) Worn-out surface with elemental mapping (b) Tungsten mapping of the worn-out surface (c) Carbide mapping of the worn-out surface (d) Cobalt mapping of the worn-out surface (e) Calcium mapping of the worn-out surface and (f) Fluoride mapping of the worn-out surface.*

The presence of calcium fluoride on the worn surface gives information of lubrication during wear test. Surface roughness of the test material after test was measured by the contact stylus type roughness tester. Figures 4.11(a-c) shows the surface profile, where surface length of 0.03 in (X axis) is magnified 200 times and vertical deviation from the surface (Y axis) is magnified 10,000 times. Figures 4.11(a-c) shows the roughness profile of the surface after the adhesive wear test.

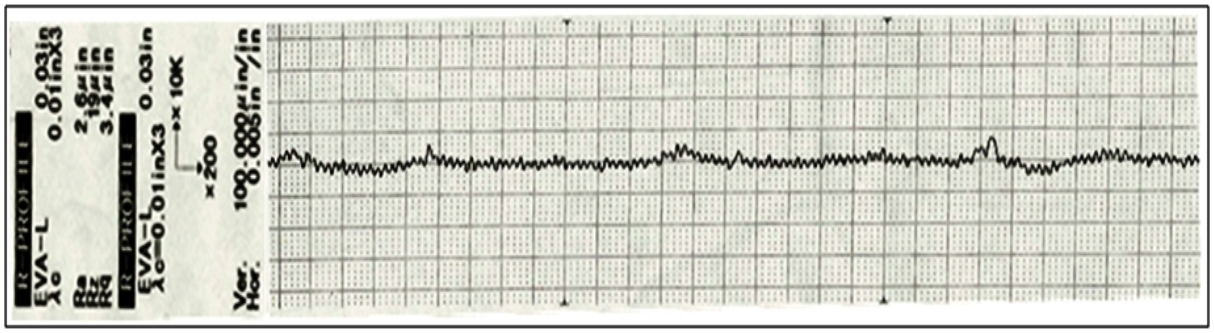

Fig. 4. 11 *(a) Surface of the test material before testing; (b) Surface of the test material after testing: straight WC–Co. (c) Surface of the test material after testing: WC–Co–5wt. % $CaF_2$.*

All the test materials were prepared to have the same roughness (Ra=0.07-0.12 μm) and the wear resistance of the test material is indicated by its final surface roughness. The final surface roughness of the WC-Co-5 wt.% $CaF_2$ (Ra 0.05-0.11μm) confirmed less frictional resistance and less wear. During the testing, the formation of $CaF_2$ film on the surface of counter disc helps to reduce its friction, wear and surface roughness. The final surface roughness of the straight WC-Co exhibited higher surface roughness (Ra 0.38 μm). This behavior is due to the absence of $CaF_2$ particles as well as less hardness when compared to other investigated materials.

### 4.3.4 Surface of the counter disc

Counter disc surface (commercial WC-6 % Co) was observed under non contact 3D profiler (figures 4.12 (a-b)) to understand the wear mechanism. Okonkwo *et al*. (2012) also reported the deposition of transferred material with profilometry. Mild carbon steel (AISI 108) steel

balls were made to slide against the counter disc (AISI D2) at various temperatures. Large amounts of materials were found to be deposited on the counter disc when the temperature increased from ambient to 50°C.

In this work, after every test counter disc surface was cleaned with acetone and dried to remove all the wear debris. Sliding direction was clearly visible on the counter disc (0.8 × 0.8 mm) surface. Among the test and counter disc material, counter disc material has superior strength and hardness. Hence the test materials worn out particles were transferred to the surface of the counter disc material due to the adhesive mechanism. Figure 4.12(a) shows the 3D image and the 2D surface profile of the counter disc before testing.

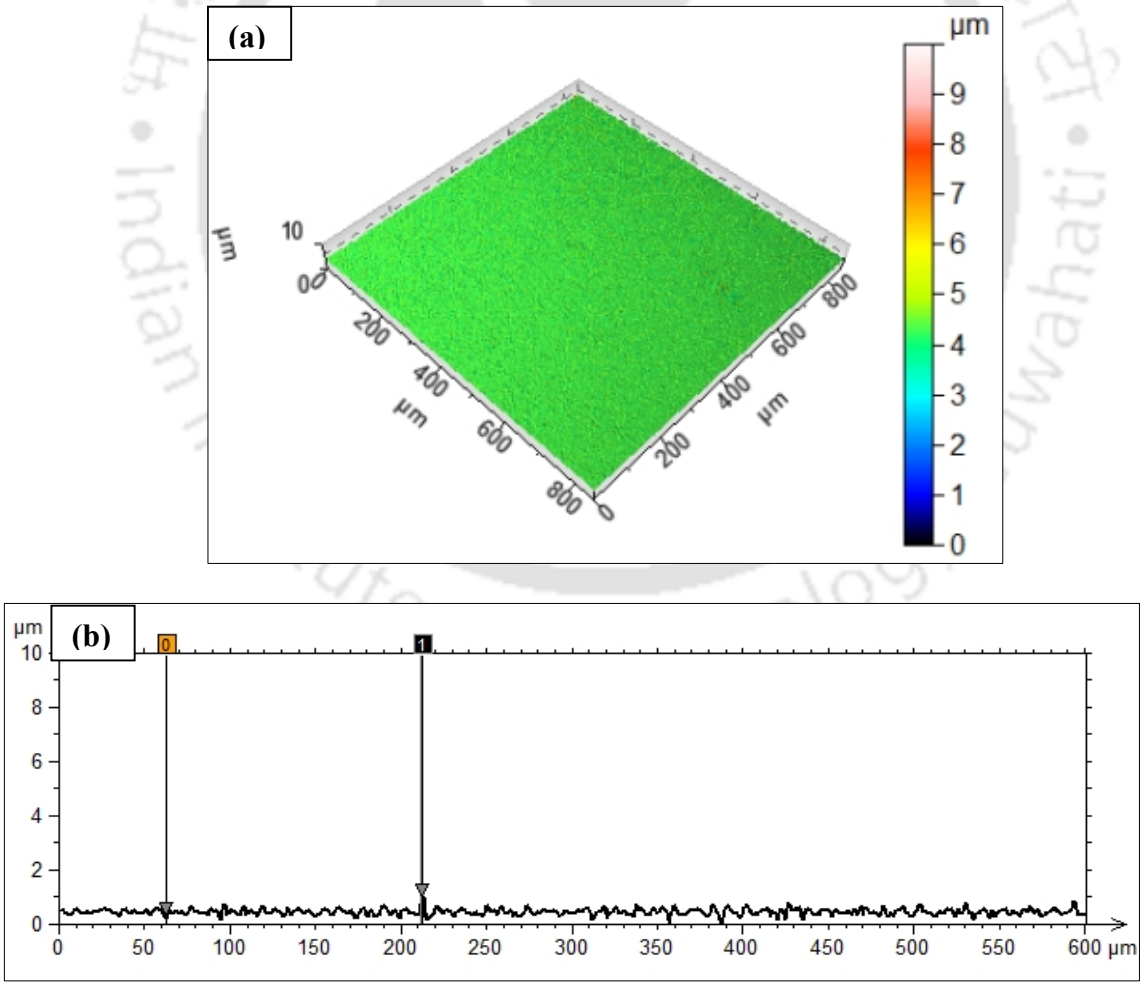

Fig. 4.12 *(a) Surface of the counter disc before testing; (b) waviness of counter disc surface before testing*

Figure 4.13(a-b) shows the counter disc after sliding against straight WC (19.62N, normal load, 0.5 ms-1 speed). Figure 4.14(a-b) shows the counter disc after sliding against WC-Co-5 wt.% $CaF_2$ material (19.62N, normal load, 0.5 $ms^{-1}$ speed). The counter disc surface before testing did not show any transfer film and the surface deviations were found to very minimal (figure 4.13 (a)). The counter disc surface after sliding against straight WC showed the existence of thin transfer film due to the extrusion of binder cobalt.

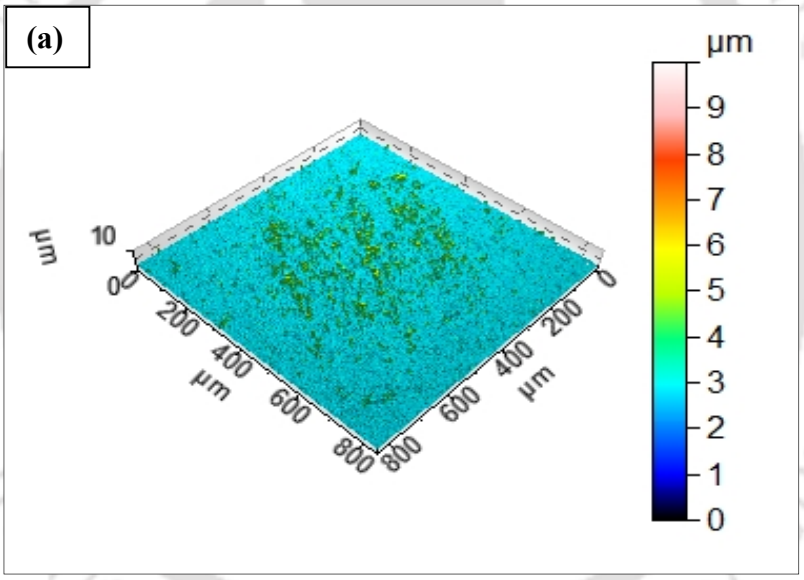


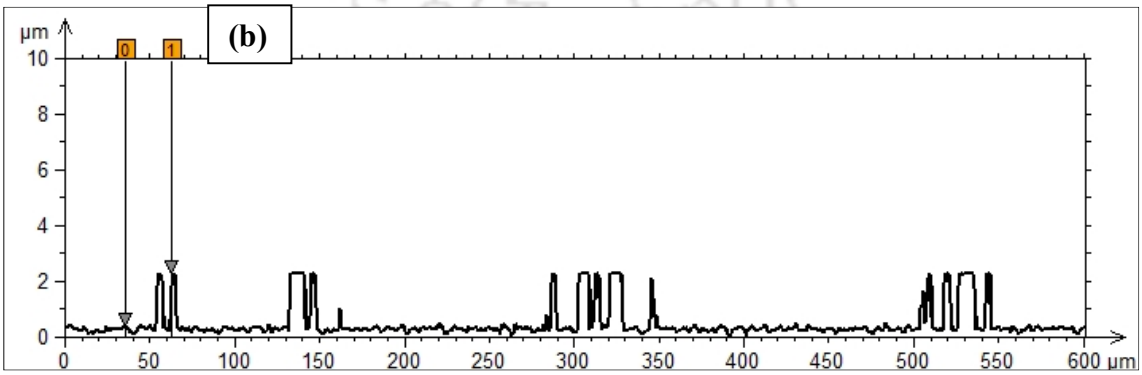

Fig. 4.13 *(a) Surface of the counter disc after testing against straight WC (19.62 N, normal load, 0.5 ms$^{-1}$, speed) (b) waviness of counter disc surface testing against straight WC after testing*

This soft phase cobalt formed a transfer film on the counter disc (figure 4.13(b)). Counter disc after sliding against WC with 5 wt.% $CaF_2$ exhibited very thick transfer films due to the extrusion of cobalt as well as soft phase solid lubricant $CaF_2$ (figure 4.14(a-b)). The amount of transfer material deposited on the disc when slid against WC-Co-5 wt.% $CaF_2$ is larger when compared to that of plain WC (figure 4.14(b)).

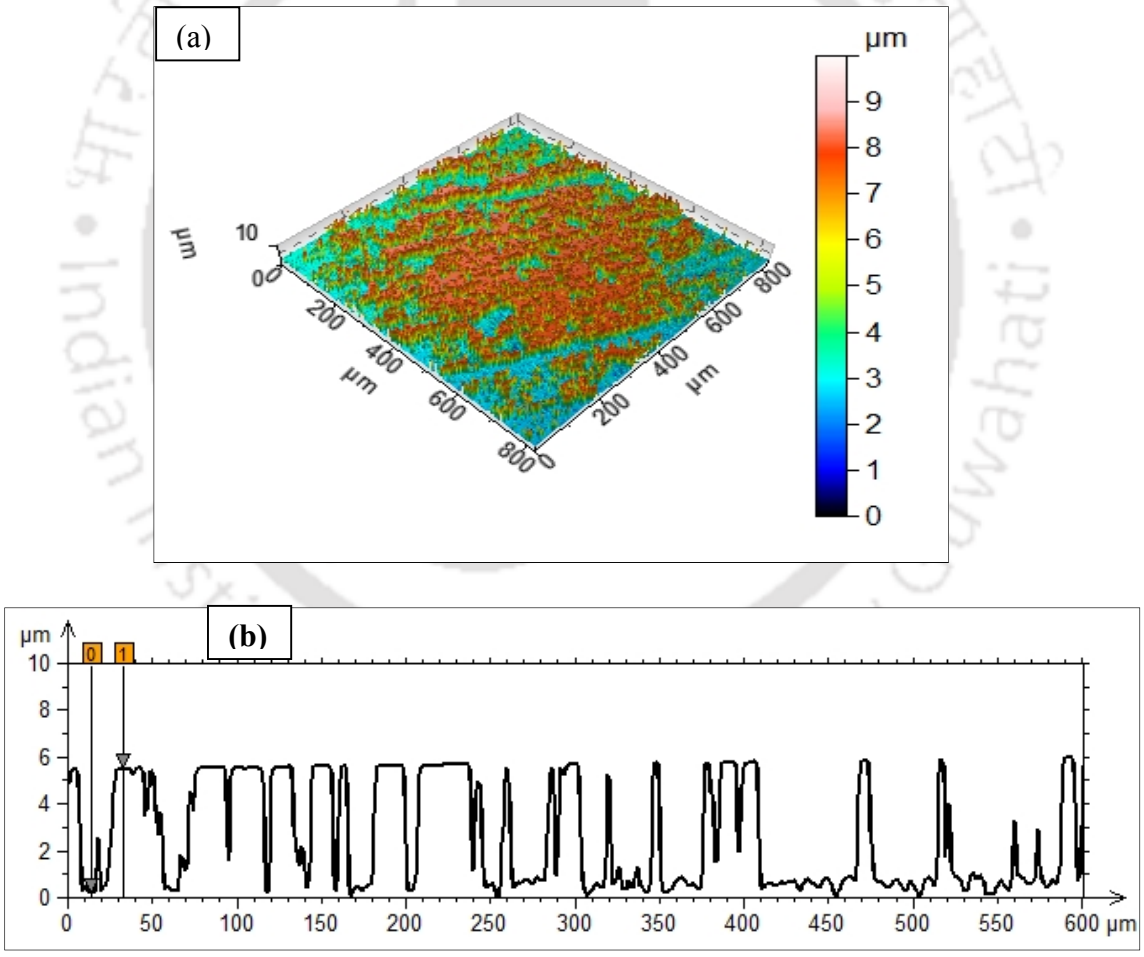


*Fig. 4.14 (a) Surface of the counter disc after testing against WC-5 wt. % $CaF_2$ (19.62 N normal load, 0.5 ms$^{-1}$ speed) (b) Waviness of counter disc surface testing against WC-5 wt. % $CaF_2$ after testing*

Similar tribo films were observed on the test surface and reported by other researchers (Klassen et al., (2010); Pirso et al., (2006); Engqvist et al., (2000)). Klaasen et al. (2010) observed tribofilms on the surface of carbide composites when slid against mild steel. Binder extrusion and adhesive interaction were identified for this film formation. Pirso et al., (2006) also observed the transfer films on the tungsten carbides when slid against the steel disk. Engqvist *et al*., (2000) also observed tribo films on the tungsten carbide when slide against the same material.

Surface roughness of the counter disc (before testing) and after testing against WC-Co-5 wt.% $CaF_2$ was also measured by the contact stylus type roughness tester to confirm adhesive behavior (figures 4.15(a-b)). The initial surface roughness of the disc was 0.06-0.11µm; the disc exhibited 0.13 µm after it was tested against WC-5 wt. % $CaF_2$

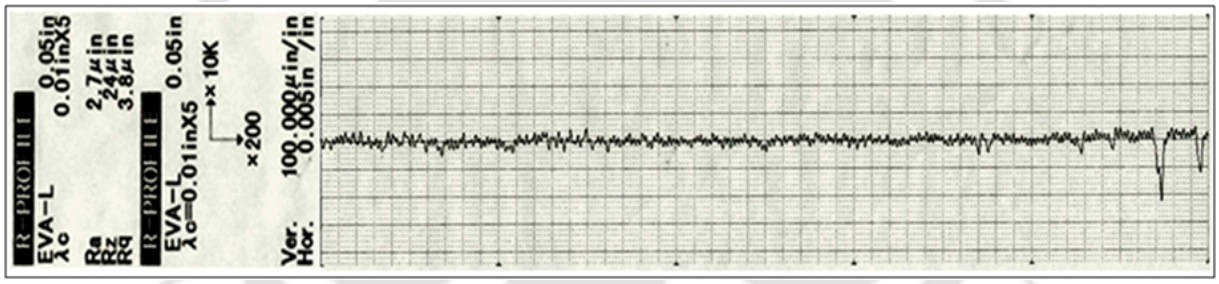

*Fig. 4.15 (a) Counter surface before testing*

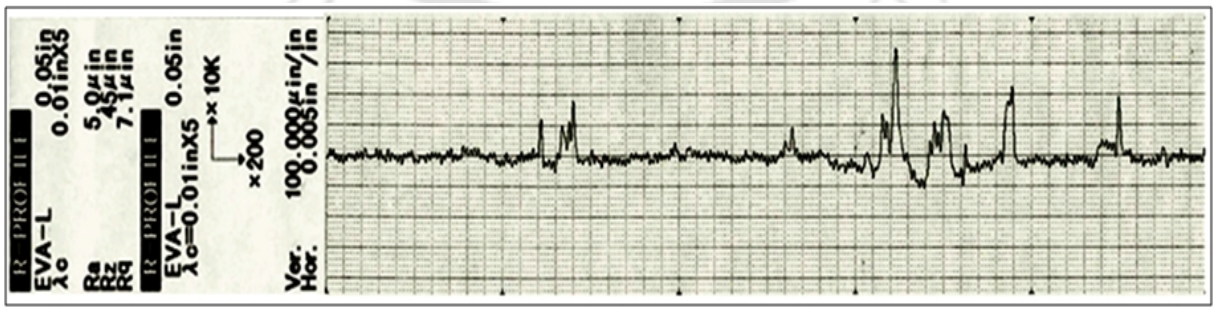

*Fig. 4.15 (b) Counter surface after testing against WC–Co–5wt.% $CaF_2$*

Presence of calcium fluoride helps to bind the carbide particles well and improve wear resistance. In-sufficient and excess amount of $CaF_2$ contribute to the poor bonding between carbide particles. The balling phenomenon and cracks around the carbide grains confirmed this poor bonding. The balling phenomenon of the test material and the presence of cracks around the carbide grains were reported in detail at the section 2. Thus among the test material, straight WC-Co material exhibits poor bonding amongst the carbide particles and WC-Co-5% $CaF_2$ material exhibits superior bonding among the carbide particles.

## 4.4 SUMMARY

Developed tungsten carbide based solid lubricant materials were evaluated for the adhesive wear performance in the pin on disc test configuration. In addition, the scratch resistance test was carried out on the plain WC-Co and WC-Co-5 wt.% $CaF_2$ materials. Following major conclusions were arrived from the above investigation

- Amongst the investigated material, WC-Co-5 wt.% $CaF_2$ exhibited least friction and superior wear resistance in the adhesive condition due to the formation of transfer film on the counter disc
- The surface temperature of WC-Co-5 wt.% $CaF_2$ material exhibited less surface temperature due to the less frictional resistance during sliding
- Non contact 3D profiler confirmed the strong transfer film formation on the counter disc when slid against WC-Co- 5 wt.% $CaF_2$ material.

# CHAPTER 5

# PERFORMANCE EVALUATION OF TUNGSTEN CARBIDE BASED SELF-LUBRICANT CUTTING TOOL

## 5.1 INTRODUCTION

In the recent years, manufacturing industries are shifting their focus towards green manufacturing (machining without coolants) to protect the environment from the harmful effect of coolants. However, dry machining generates more heat which in turn reduces cutting tool life and increases the production time. Research and developments are being carrying out to develop cutting tool to improve wear resistant by texturing, coating as well as with the addition of solid lubricants (Xing[1,2] *et al.*, 2014; Deng *et al*., 2005, 2006, 2009, 2013; Lie *et al*., 2009).

Xing[1] *et al.* (2014) developed textured $Al_2O_3$/TiC cutting tools and $MoS_2$ were burnished into the textures. The developed cutting tool with wavy micro scale textures on the rake face exhibited superior wear resistance when compared to the other investigated cutting tools. Xing[1] *et al.* (2014) coated $WS_2$/Zr on textured $Al_2O_3$/TiC ceramic cutting tools. A textured tool was found to be effective while machining hardened steel and it reduces the cutting force, cutting temperature, and friction between tool-chip interfaces. Deng *et al.* (2006) developed $Al_2O_3$/TiC with $CaF_2$ through milling, compacting and sintering route. Hardened steel and cast iron were machined with developed cutting tool materials. The friction coefficient between chip and $Al_2O_3$/TiC/$CaF_2$ ceramic cutting tools was lesser due to the formation of a self-lubricating film on the tool-chip interface. Deng *et al.* (2009) drilled micro-holes on the rake and flank surface of WC/Co tools and $MoS_2$ were filled inside the holes. The cutting forces and friction coefficient of the self-lubricated tools were significantly reduced. Micro holes at the rake surface exhibited less force than that of

cutting tool having holes at the flank surface. Deng *et al*. (2013) coated $WS_2$ by PVD technique on the textured WC/TiC/Co cutting tool. Textured and $WS_2$ coated cutting tool experienced less cutting forces when compared to that of conventional cutting tool and textured cutting tools. Both liquid and solid lubricants were found to be equally effective in reducing the contact length and coefficient of friction at the chip-tool interface.

From the literature survey, it is found that research works has been carried out to improve the wear resistance of cutting tool through texturing, coating as well with the addition of solid lubricants. From the above literature, it is inferred that commonly used cutting tool material tungsten carbide and thermally stable calcium fluoride were not considered for cutting tool material. This work attempt to understand the performance of tungsten carbide based calcium fluoride material as a cutting tool.

## 5.2 MATERIALS AND MACHINING CONDITIONS

Tungsten carbide with the various amount of calcium fluoride was considered; milling and compacting characteristics were carried out and evaluated for the transverse rupture strength (Chapter 2). Developed cutting tool materials with the various amount of calcium fluoride were evaluated for the friction and wear performance under abrasive and adhesive condition (Chapter 3 and 4). Developed cutting tool materials were cut in to 12 X 10 X 5 mm size and brazed on the tool shank (ISO 6 R2020 P30). Subsequently cutting tool was grounded to have the rake angle ($\gamma_o$) of 4° and the clearance angle ($\alpha_o$) of 15° and nose radius of 0.3 mm. Lei *et al.* (2009) utilised textured tungsten carbide cutting tool to machine the mild steel material, wherein similar cutting tool geometry (5° rake angle and 15°clearance angle) was considered.

Turning operation was considered to investigate the machining performance of the developed cutting tool. Cutting was performed with the three different cutting tools (a) In-house developed

WC-Co-5$CaF_2$ (b) In-house developed WC-Co and (c) Commercial tungsten carbide insert (Miranda Tools, WC-Co, 1250HV). Figure 5.1 shows the developed WC-Co-5 wt.% $CaF_2$ cutting tool. The prepared cutting tool material brazed with standard shank and followed by setting required cutting angles for mild steel machining using grinding machine and Tool maker microscope (figure 5.2). Machining experiments were carried out in the lathe (Chamundi, LB17) mounted with a four component, piezo-electric dynamometer (Kistler, 9272). During turning, all the three components of forces were measured and continuously acquired in a personal computer. In the present investigation, the average temperature of the cutting tool was measured with thermal imaging camera (Infratec, VarioCAM hr head 480SL).

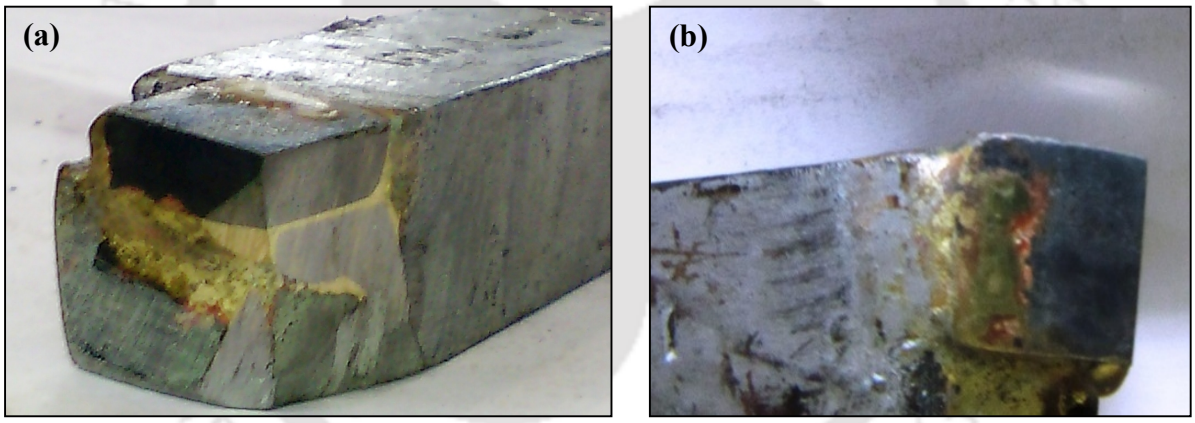


*Fig. 5.1 In-house developed WC-Co-5 wt.% $CaF_2$ cutting tool: (a) Isometric view (b) Top view*

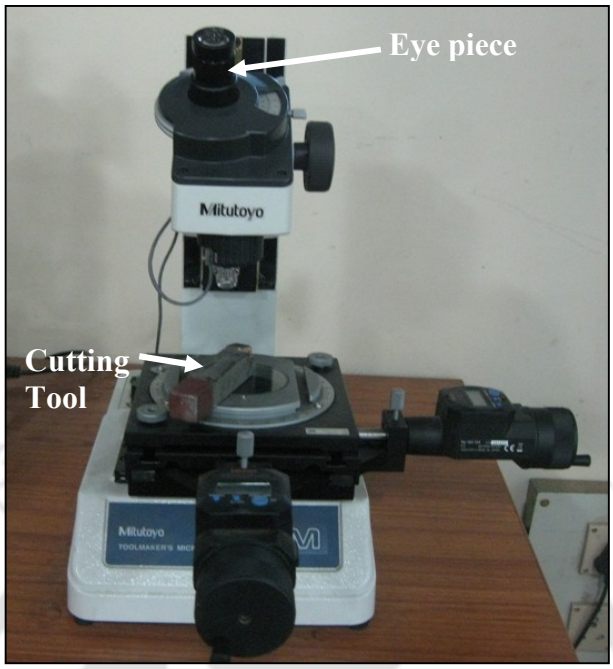


*Fig. 5.2 Tool makers' microscope used for measuring angles of cutting tool geometry*

The emissivity of the cutting tool was set at 0.85 and a small region was chosen to measure the temperature while machining. The table 5.1 reported the summary of evaluated mechanical and wear properties of the developed WC-Co-5 wt.% $CaF_2$ and WC-Co materials. The Steel (AISI 1020; C 0.18%, Si 0.5%, Mg 0.85% and S 0.05%, P 0.02%) of 62 mm initial diameter and 140 HB hardness was machined by three considered cutting tools. Work-piece was machined for 150 mm cutting length with 0.5 mm depth of cut, 0.3 mm/rev of feed and cutting speed (80-100 m/min) was selected to machine steel from the prior research work carried out by the following researchers so that reasonable surface finish can be achieved. Deng *et al.* (2009) drilled micro-holes on the rake and flank surface of WC/Co tools and $MoS_2$ were filled inside the holes. The cutting experiments were carried out on steel (35-40 HRC) at the cutting speed of 60-115 m/min. Lei *et al*. (2009) drilled micro holes on the rake surface of the tungsten carbide insert. Oil and tungsten disulfide were used to fill up these micro holes. Cutting experiments were carried out on

the cold rolled 1045 steel at cutting speed of 120 m/min. The same machining condition was repeated for three passes, (i.e. a total of 450 mm cutting length) and hence the total cutting period of 5 min was considered for the cutting tool life and tool wear investigation.

*Table. 5.1 Mechanical and tribological properties of a developed material*

| Developed cutting tool materials | Hardness (HRA) | Transverse rupture strength (MPa) | Coefficient of friction | | Wear rate ($mm^3$/Nm) | |
|---|---|---|---|---|---|---|
| | | | Adhesive | Abrasive | Adhesive ( X $10^{-9}$) | Abrasive (X $10^{-5}$) |
| WC-10Co | 82.34 ± 3 | 969 ± 48 | 0.39-0.41 | 0.40-0.44 | 7.37 ± 0.3 | 2.7 ± 0.3 |
| WC-10Co-5$CaF_2$ | 84.95 ± 2 | 1502 ± 75 | 0.23-0.24 | 0.25-0.28 | 1.68 ± 0.1 | 0.7 ± 0.2 |

Figure 5.3 shows the view of the work piece in a lathe with dynamometer and infra red camera. The rake surface of the cutting tools and machined chip morphology was examined under the scanning electron microscope (LEO, 1430 vp).

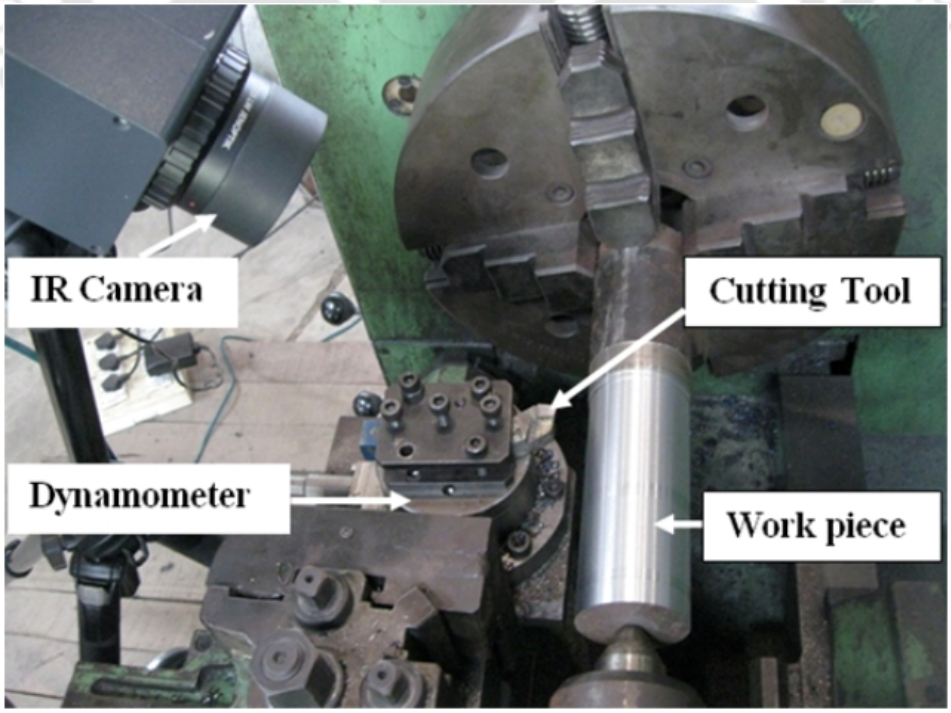


*Fig. 5.3 View of the machining in a lathe with dynamometer and infra red camera*

The initial and final surface roughness of work-piece was measured using contact type surface measurement device (Mitutoyo, Surftest SJ-400). Machined surfaces were also observed under non contact three dimensional profiler (Taylor Hobson CCI MP) to understand the mechanism of metal removal,

## 5.3 RESULT AND DISCUSSION

### 5.3.1 Cutting Forces

In machining, measurement of cutting forces helps to understand machinability of work-piece material and power consumption. In addition, the surface quality of the work-piece and cutting tool life can be understood with the cutting forces. The figure 5.4(a-c) shows the cutting, feed and radial forces generated by the in-house developed cutting tools and commercial cutting tool at 80 m/min. This measured cutting, feed and radial force are tangential, axial and radial components of the cutting respectively. It is observed that the all these forces increased gradually and then fluctuate around a mean value. The main cutting force generated by the considered cutting tools are shown in figure 5.4(a), WC-Co-5 wt.% $CaF_2$ cutting tool exhibited a 20 % reduction of cutting force. The presence of solid lubricants on the rake and flank surface of the cutting tool reduces the resistance, when interacting with the work-piece and generated chip. Figure 5.4(b) shows the feed force generated and figure 5.4(c) shows the radial force generated by considered cutting tools. All the component of cutting forces reduces, while machining with the solid lubricant cutting tool compared to the other investigated cutting tools. Thus reduction of resistance contributes for the reduction of cutting forces in all the three directions. The magnitude of cutting force is found to be more than that of feed and radial forces like in most machining conditions. The radial force is found to be least among the cutting and feed forces. The ratio of cutting force, feed force and the radial force varies with the approach angle, geometry of the cutting tool and feed rate (HMT,

1980) In turning, the magnitude of the cutting force, the feed force and the radial force are in the descending order (Xing[1] *et al,*. 2014; Deng *et al.,* 2013; Lie *et al*., 2009; Lian *et al*. 2013). All the force components exhibited the same trend; WC-Co-5 wt.% $CaF_2$ cutting tool exhibited least force when compared to that of developed WC-Co cutting tool and commercial WC-Co cutting tool. Commercial WC-Co cutting tool material exhibited slightly lesser force (in all three directions) when compared to that of developed WC-10Co cutting tool. To confirm the effect of solid lubricant, machining was carried out at another cutting speed, 100 m/min. The figure 5.4(d) summarises all three force components generated by the considered cutting tools at 100 m/min cutting speed. Similar to the cutting speed of 80 m/min, WC-Co-5 wt.% $CaF_2$ cutting tool generate the least force at all three directions.

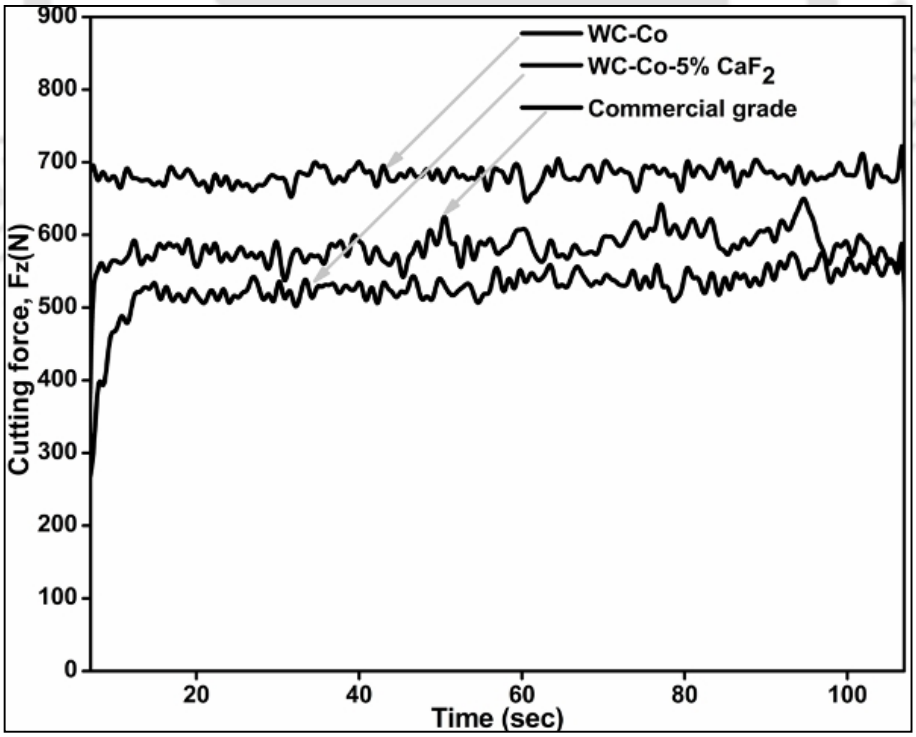


*Fig. 5.4 (a) Cutting force exhibited by considered cutting tools at 80 m/min*

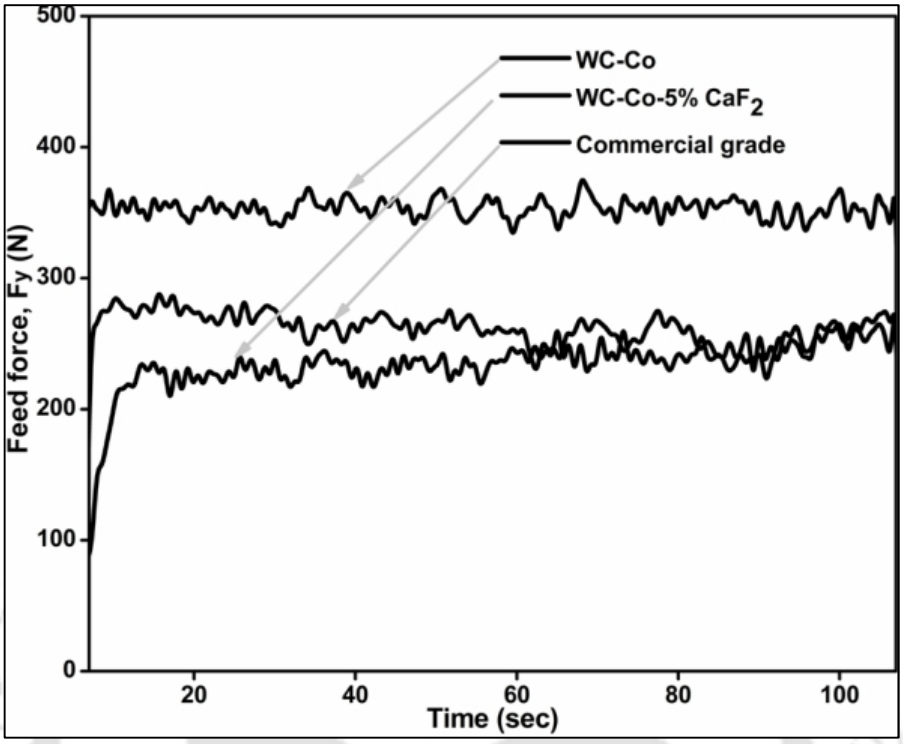


*Fig.5.4 (b) Feed forces exhibited by considered cutting tools at 80 m/min*

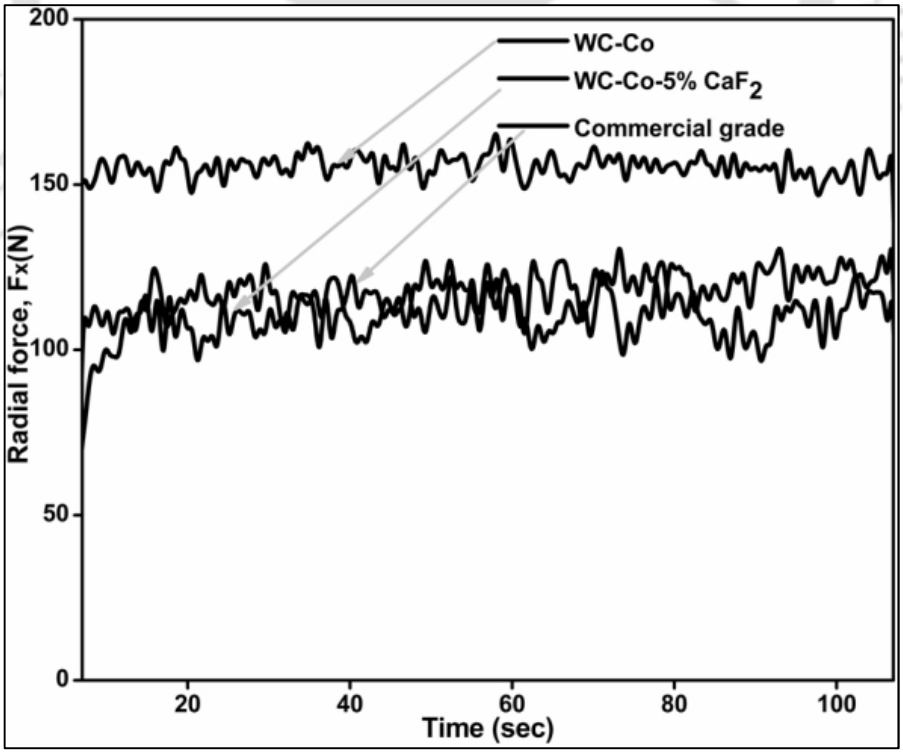


*Fig. 5.4(c) Radial force exhibited by considered cutting tools at 80 m/min*

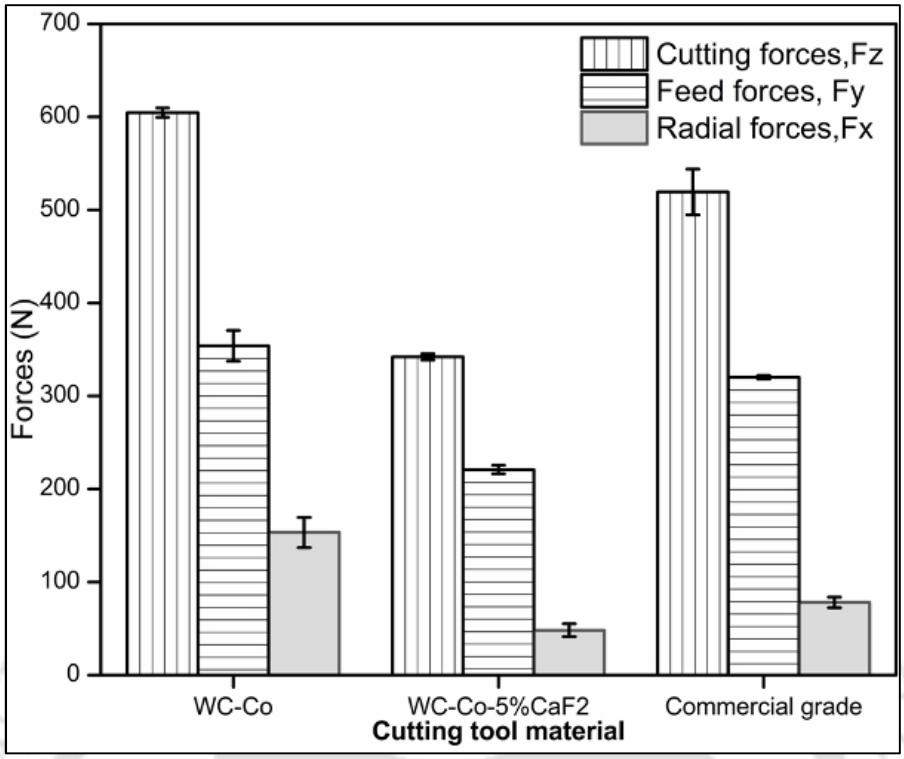


*Fig. 5.4(d) Forces generated by the considered cutting tools at 100 m/min*

Xing[1] *et al.* (2014) observed similar behaviour while machining with textured and solid lubricant $Al_2O_3$/TiC cutting tools. Textured and solid lubricant cutting tool exhibited less cutting, feed and radial forces when compared to that of a conventional cutting tool. Lian *et al.* (2013) also observed a similar trend when $WS_2$ was added to the ceramic cutting tool. Solid lubricant coated tools generated lower (10-20 %) cutting forces ($F_z$, $F_y$ and $F_x$) compared to that of uncoated tools. Friction coefficient of the coated tool was lower than that of an uncoated tool.

### 5.3.2 Co-efficient of Friction

The major amount of heat generated in metal cutting is due to the friction between cutting tool, work piece and generated chip. By reducing friction at cutting tool-chip, heat generated during metal cutting can be significantly reduced. It was found that WC-Co-5$CaF_2$ cutting tool material

exhibited less frictional resistance under abrasive and adhesive conditions. WC-Co-5 wt.% $CaF_2$ exhibited 30-32 % less coefficient of friction when compared to that WC-Co under abrasive condition (Section 3.3.1). Under adhesive condition, WC-Co-5 wt.% $CaF_2$ exhibited 38-44 % less coefficient of friction compared to that of WC-Co (Section 4.3.1). During cutting, a significant amount of heat is generated due to the material shearing and surface interaction with cutting tool and the major amount of heat is transferred to the work piece chip; hence work-piece chips slide over the cutting tool at elevated temperature. Thus in the cutting process, the movement of the chip over the cutting tool cannot be analogues to the simple sliding motion either under abrasive or adhesive conditions at laboratory room temperature condition. Many researchers (Xing[1] *et al.,* 2014; Deng *et al.,* 2005; Deng *et al.,*2006) utilized the radial and tangential component of cutting forces using the following relation (Cheng, 1992) to estimate the average friction coefficient at the tool-chip interface while machining.

$$\mu = \tan(\beta) = \tan(\upsilon_o + \arctan(F_y / F_Z) \qquad (5.1)$$

where β is the friction angle, $\nu_o$ is the rake angle, $F_y$ is the radial thrust force, and $F_z$ is the main cutting force. From the measured radial force, cutting force and rake angle of the cutting tool, the frictional coefficient between tool-chip was computed and plotted in figure 5.5**.** Friction coefficient at the tool-chip interface of cutting tools, WC-Co, WC-Co-5 wt.% $CaF_2$ and commercial WC-Co at 80 and 100 m/min are shown in figure 5.5. At 80 m/min, coefficient of friction between the chip and WC-Co cutting tool is 0.7-0.8. However, the coefficient of friction between the chip and WC-Co-5 wt.% $CaF_2$ is 0.4-0.5. Friction coefficient at the tool-chip interface reduced by 40-50 % with the addition of solid lubricant $CaF_2$ at 80 and 100 m/min. Deng *et al.* (2006) developed $Al_2O_3$/TiC with $CaF_2$ and used above equation 5.1 for estimating the coefficient of friction from the cutting experiment. $Al_2O_3$/TiC without $CaF_2$ exhibited 0.6-0.7

while machining (60-80 m/min cutting speed, depth of cut 0.4 mm, 0.1 mm/r feed) hardened steel. Addition of $CaF_2$ reduced coefficient of friction by 15-40 %. $Al_2O_3$/TiC with $CaF_2$ exhibited a 20 % reduction of friction coefficient when the cutting speed increased from 60 to 80 m/min. In the present investigation also, a maximum 20 % drop in coefficient of friction is observed when the cutting speed increased from 80 to 100 m/min.

Deng *et al.* (2005) developed $Al_2O_3$-$TiB_2$ and observed a reduction of 24-42 % of frictional coefficient when the $TiB_2$ increases from 10 to 40 %. A maximum 30 % drop in coefficient of friction was observed, when the cutting speed increases from 50 to 200 m/min. Deng *et al*. (2013) observed a 13-27 % reduction of frictional coefficient by the textured and $WS_2$ deposited cutting tool. When the cutting speed increased from 50 to 250 m/min, textured and $WS_2$ deposited coating tool exhibited about 27 % reduction of frictional coefficient.

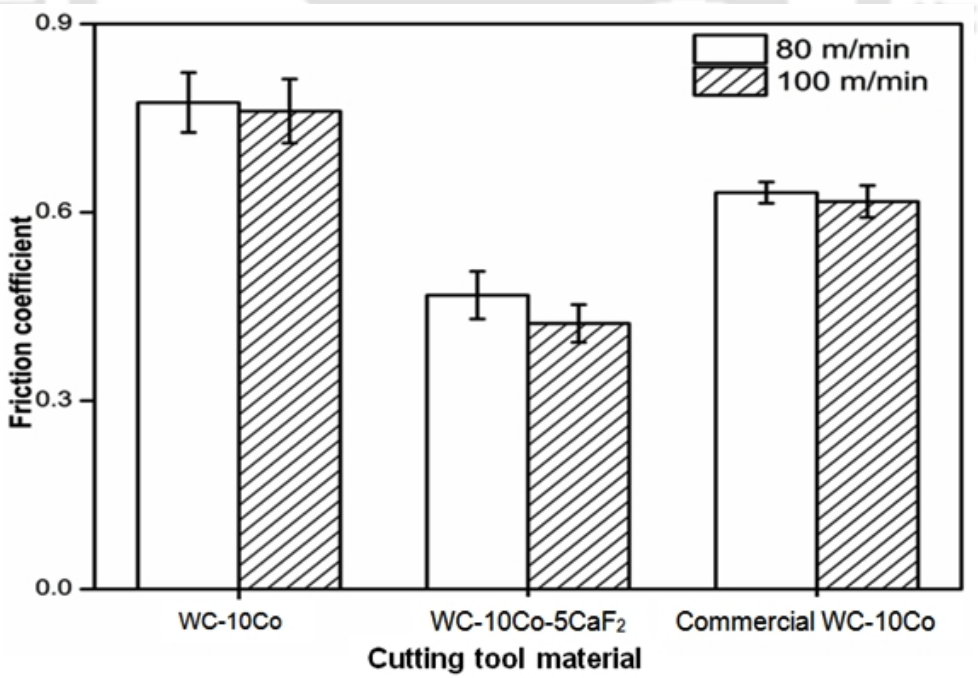


*Fig. 5.5 Predicted Frictional coefficient between tool and chip*

### 5.3.3 Average Cutting Tool Temperature

Heat generated due to cutting significantly affects the cutting tool life and its performance. Figure 5.6(a) shows the acquired thermal image while cutting steel at 80 m/min with WC-Co-5 wt.% $CaF_2$ cutting tool. It is to be noted, this temperature is not an actual temperature of the tool-chip interface, and this is only average temperature of the cutting tool near tool-chip interface. This temperature can provide relative amount of heat generation by the considered cutting tool. Figure 5.6(b) shows the average temperature of the cutting tool while machining steel at 80 m/min cutting speed. The mean cutting temperature gradually increased in the beginning and reached saturation for all the considered cutting tool materials. The mean cutting temperature of WC-10 Co commercial grade and developed WC-Co reached about 200°C and 270°C respectively. A reduction of 40-50 % was observed, when cutting was carried out with WC-Co-5 wt.% $CaF_2$ cutting tool at 80 m/min.

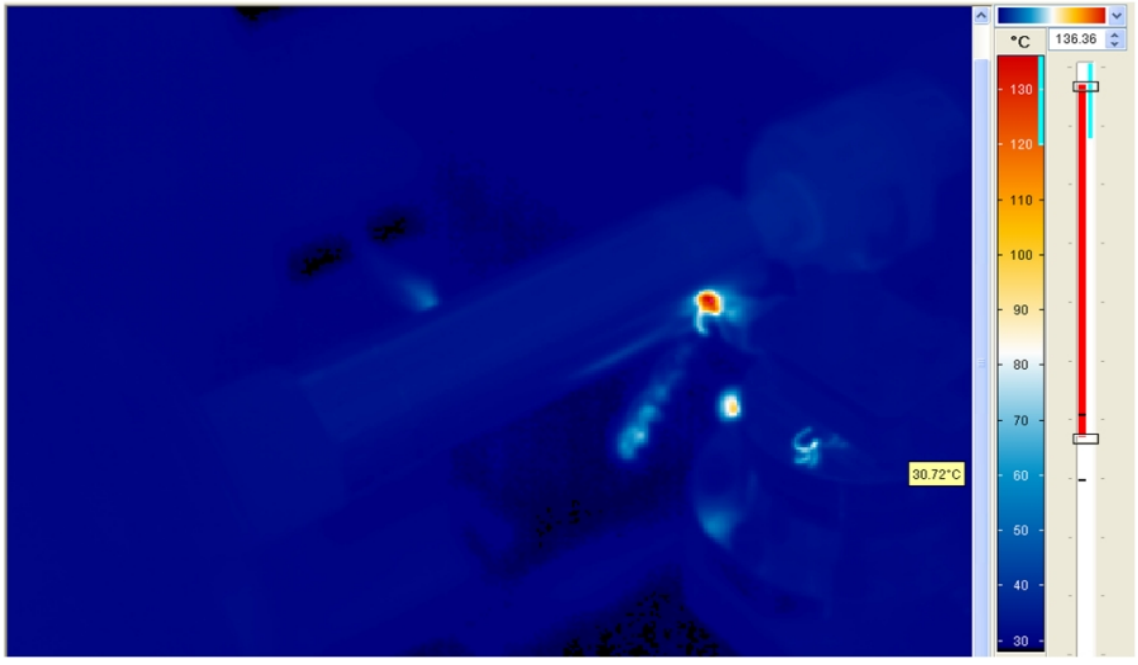


*Fig. 5.6(a) Thermal image acquired while machining*

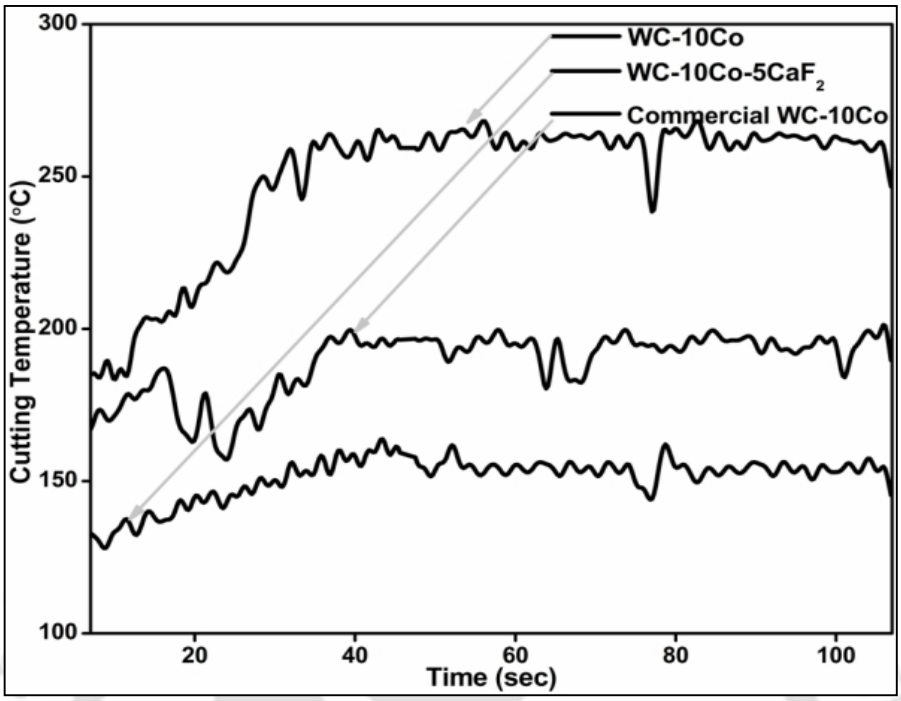


*Fig. 5. 6(b) Measured average temperature of the cutting tool at 80 m/min*

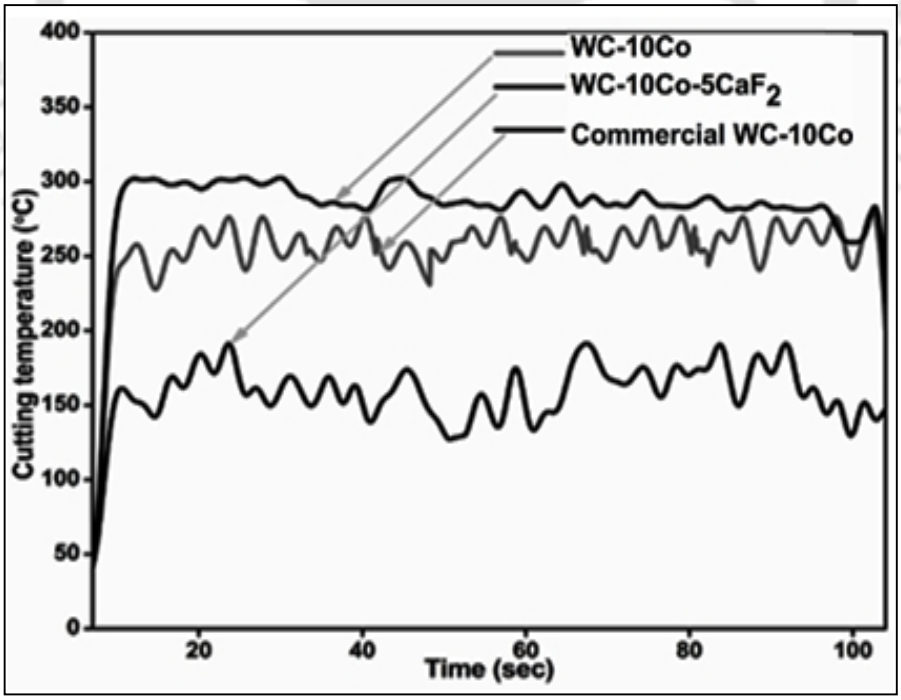


*Fig. 5.6(c) Measured average temperature of the cutting tool at 100 m/min*

The presence of solid lubricant $CaF_2$ in the cutting tool rake and the flank surface significantly reduces coefficient of friction at the tool-chip interface. The reduction of frictional coefficient reduces resistance offered, which in turn reduces heat generation in cutting. Measurement of temperature at 100 m/min cutting speed (Fig 5.6(c)) also confirmed the same fact. However, the amount of heat generated and hence the net surface temperature measured is slightly higher at 100 m/min. Deng *et al*. (2013) measured the temperature of tool-chip interface when machined with a commercial tool, textured tool and the textured tool filled with $WS_2$ at 50-250 m/min cutting speed. A reduction of 15 % temperature was observed at 100 m/min with the textured tool filled with $WS_2$. Xing[1] *et al.* (2014) observed a reduction of 10 % drop with textured and solid lubricant $Al_2O_3$/TiC cutting tools at 80 m/min cutting speed. While evaluating the adhesive wear performance of developed materials, WC-Co-5 wt.% $CaF_2$ cutting tool exhibited 25-35% drop in temperature (Section 4.3.2).

### 5.3.4 Cutting Tool Wear

The major problem associated with the dry machining is the excessive heat generation during cutting which results in shorter cutting tool life. Steel work-piece was machined at 80 m/min with three different considered cutting tools. The rake surface of the cutting tools was observed after 5 min of cutting life. Fig. 5.7(a) shows the rake surface of the developed WC-Co, which confirmed predominant abrasive wear marks in the direction of chip flow. Close up view of the rake surface (Fig 5.7(b)) confirmed deep ploughing marks. Fig. 5.8(a) shows the rake surface of the WC-Co-5 wt.% $CaF_2$ cutting tool. Close up view of the rake surface (Fig 5.8(b)) revealed ridges parallel to the direction of chip flow and dislodgment of carbide particles are also distinctly seen. Figure 5.9(a) shows the rake surface of the commercial WC-Co tool which revealed adhesive wear

marks. Close up view of the rake surface (Fig 5.9(b)) confirmed localised plastic shearing in the direction of chip flow.

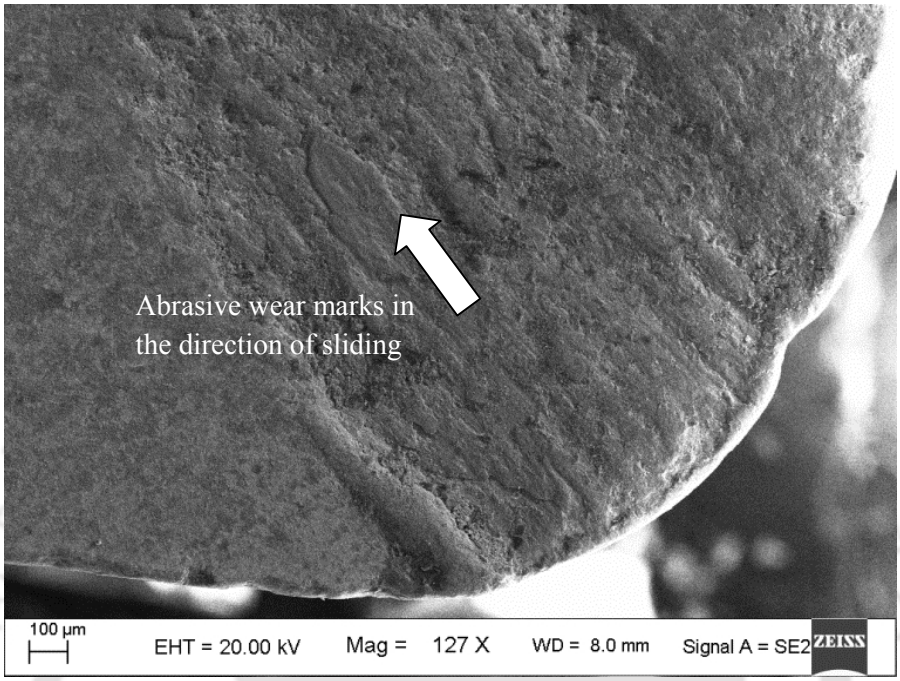


Fig. 5.7 (a) Rake surface of the cutting tool without $CaF_2$ showing severe wear

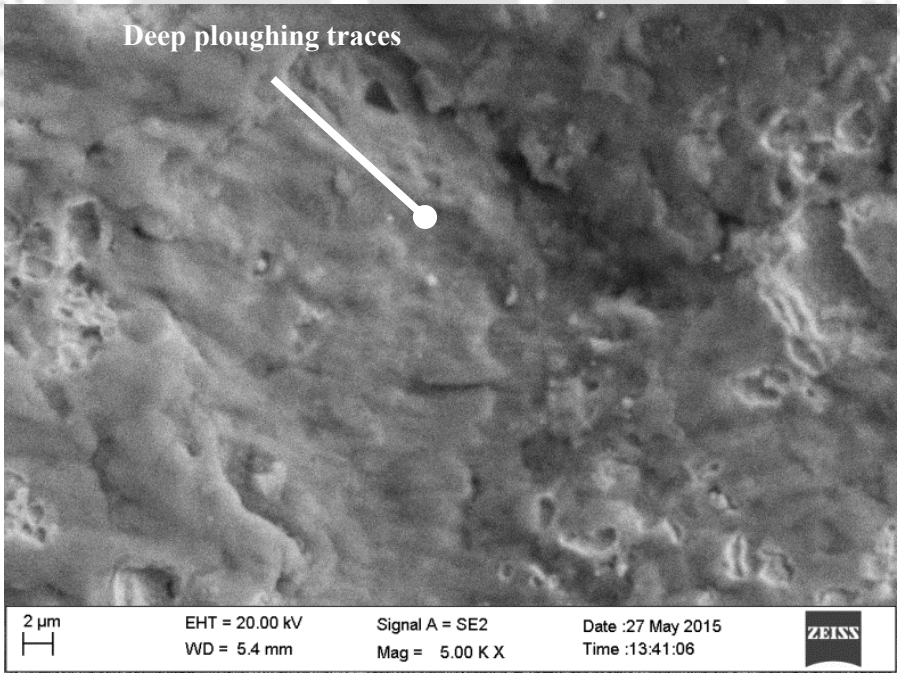


*Fig. 5.7 (b) Close up view of the rake surface of the cutting tool without $CaF_2$*

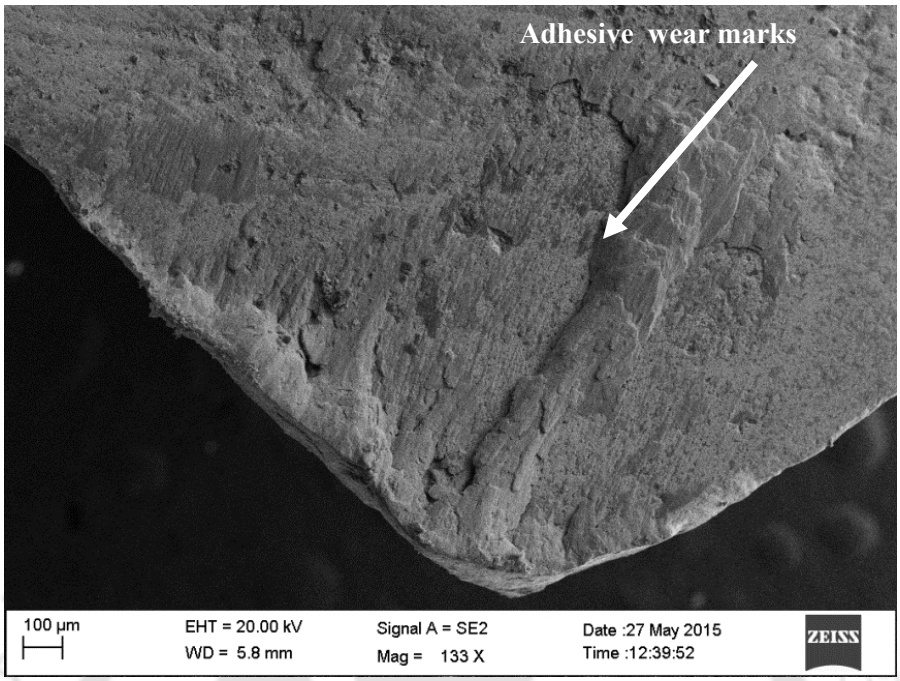


*Fig. 5.8 (a) Rake surface of the cutting tool with $CaF_2$ showing mild wear*

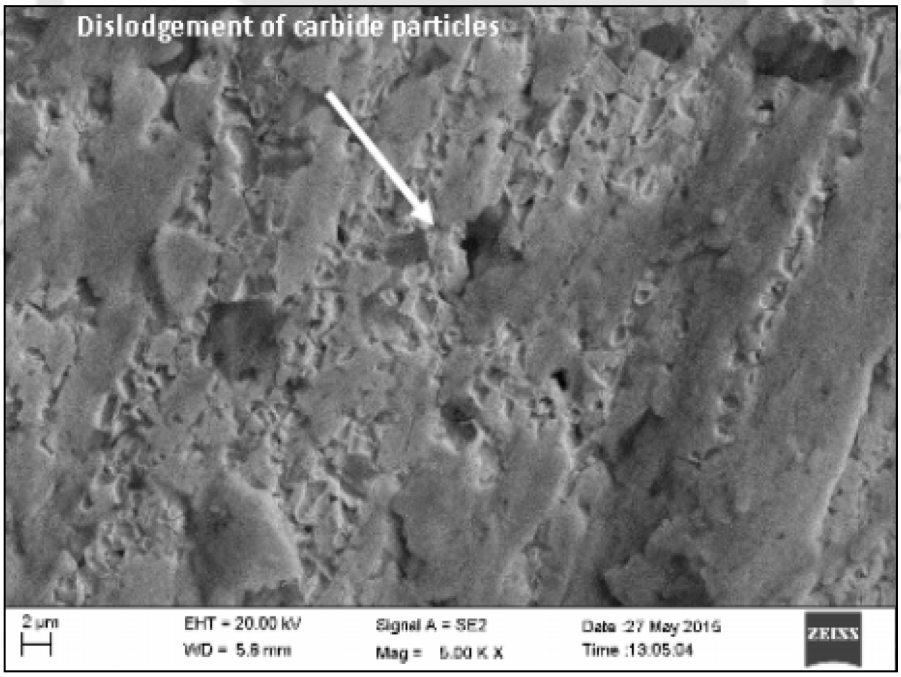


*Fig. 5.8 (b) Close up view of the rake surface of the cutting tool with $CaF_2$*

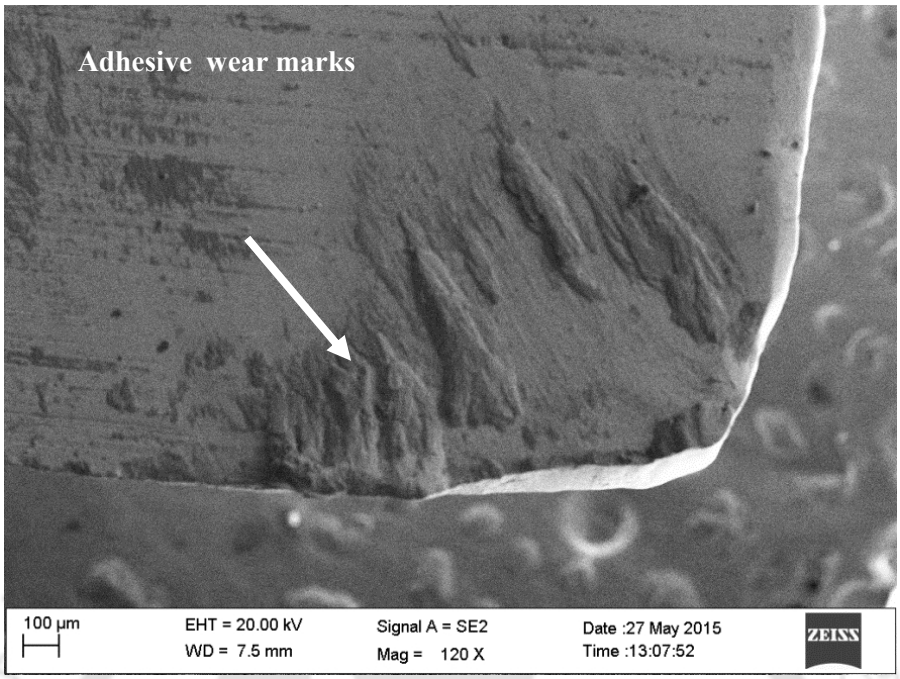


*Fig. 5.9 (a) Rake surface of the commercial cutting tool showing nominal wear*

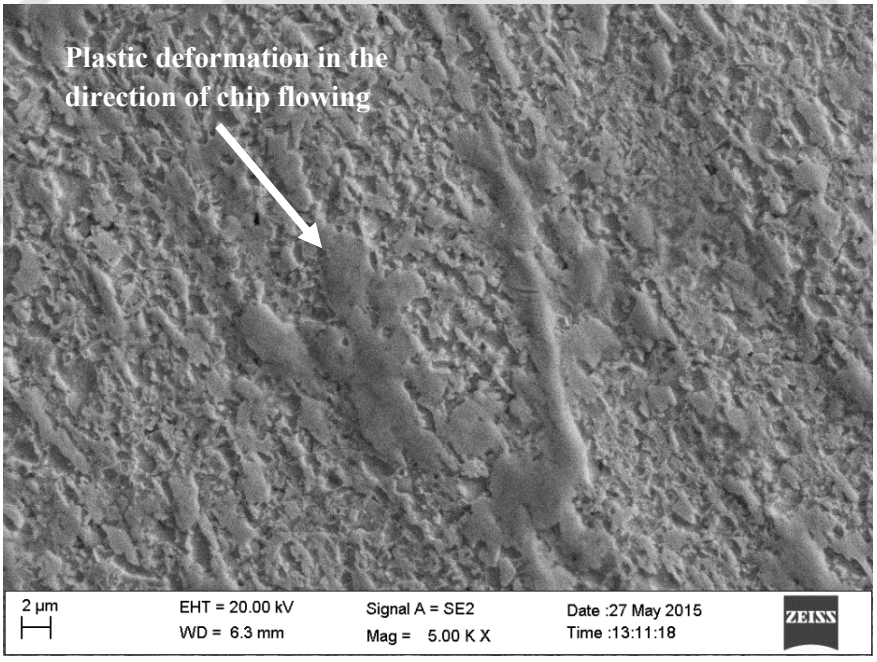


*Fig. 5.9 (b) Close up view of the rake surface of the commercial cutting tool*

The rake surface of the WC-Co-5 wt.% $CaF_2$ cutting tool was evaluated for the element distribution through EDS mapping (Fig. 5.10) confirmed the presence of W, C, Ca, Co, F and Fe.

The presence of the Fe element on the rake surface of the cutting tool confirmed the adhesion from the steel work piece due to the pressure and heat produced during cutting.

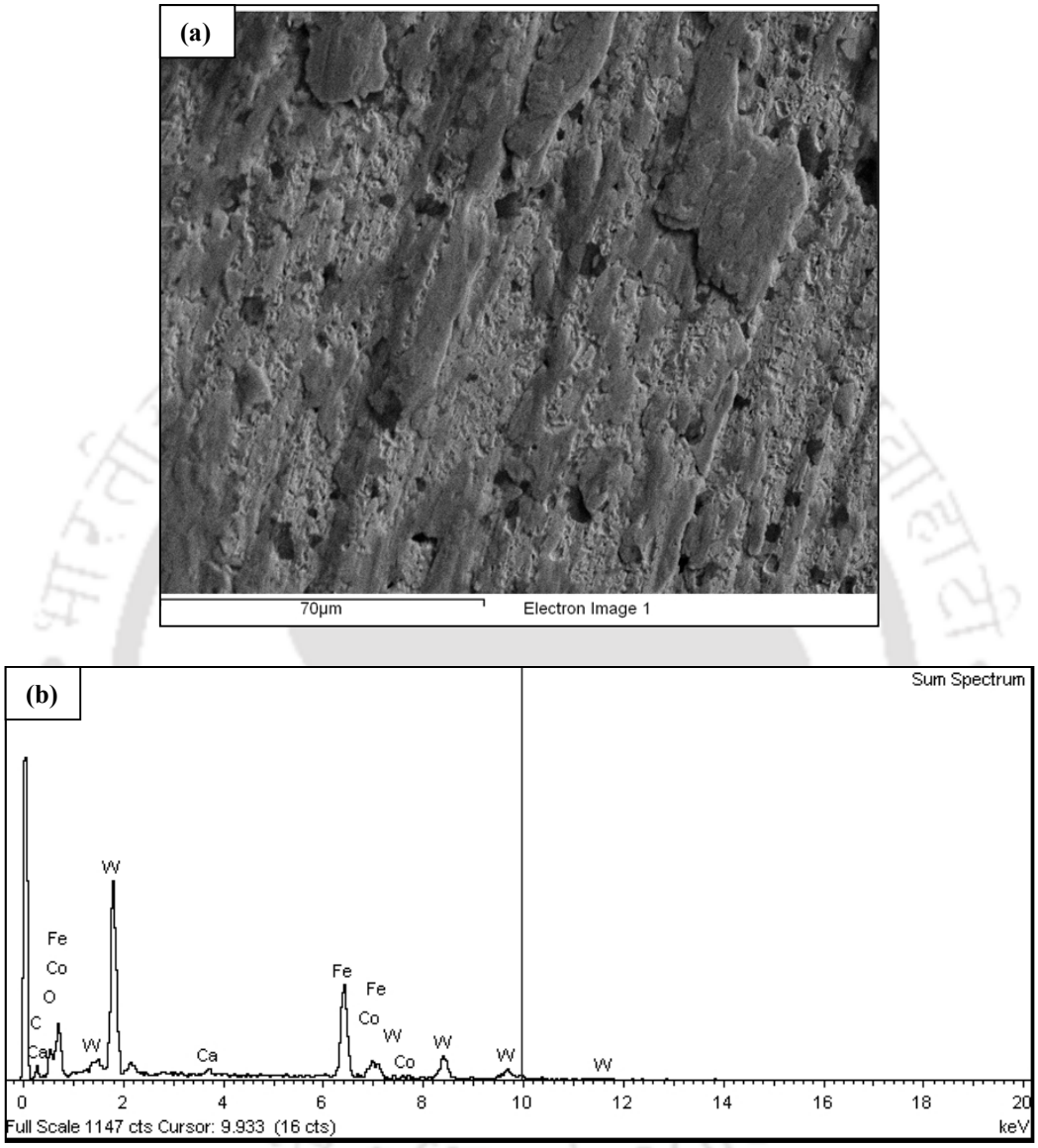


*Fig. 5.10 (a) Considered WC-Co-5 wt.% $CaF_2$ cutting tool surface for the elemental mapping (b) EDS spectrum of the of the considered cutting tool worn out surface*

Figure 5.11 shows the flank wear measurement of the cutting tool evaluated with the aid the tool maker's microscope after 5 min of cutting time. Measured flank wear of WC-Co-5 wt.% $CaF_2$ cutting tool at both 80 and 100 m/min cutting speed revealed 15-18 % reduction when compared

to that WC-Co. Xing[1] *et al.* (2014) investigated textured and solid lubricant $Al_2O_3$/TiC cutting tool performance. The crater wear at the flank surface of the textured and solid lubricant burnished cutting tool is found to the less when compared to the conventional cutting tool. The EDX surface of the solid lubricant cutting tool confirmed the presence of Mo and S. Xing[2] *et al*. (2014) developed coated and textured ceramic tools for machining hardened steel. Chipping and excessive abrasive marks were observed at the conventional cutting tool flank surface, whereas cutting tool coated with $WS_2$/Zr exhibited no chipping and EDX mapping identified Zr and the small amount of W and S.

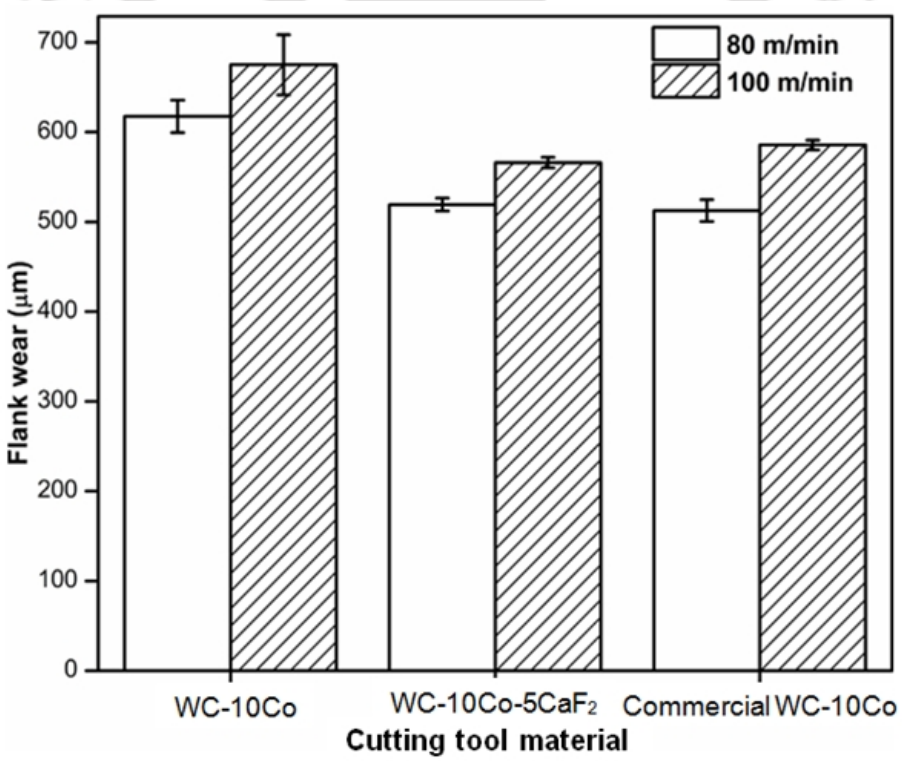


*Fig. 5.11 Measured flank wear of the considered cutting tool*

Achieving required surface roughness on the work piece is a major concern in all the machining process (figure 5.12(a-c)). Surface roughness of the initial workpiece was 2.8-3.2 μm. Final surface roughness of the workpiece machined by WC-10Co cutting tool was in the range of 4.1-

4.4 μm (Figure 5.12(a)). Final surface roughness of the workpiece machined by WC-Co-5 wt.% $CaF_2$ cutting tool was in the range of 3.4-3.8 μm (Figure 5.12(b)). Final surface roughness of the workpiece machined by commercial WC-Co cutting tool was in the range of 3.6-4.0 μm (Figure 5.12(c)).

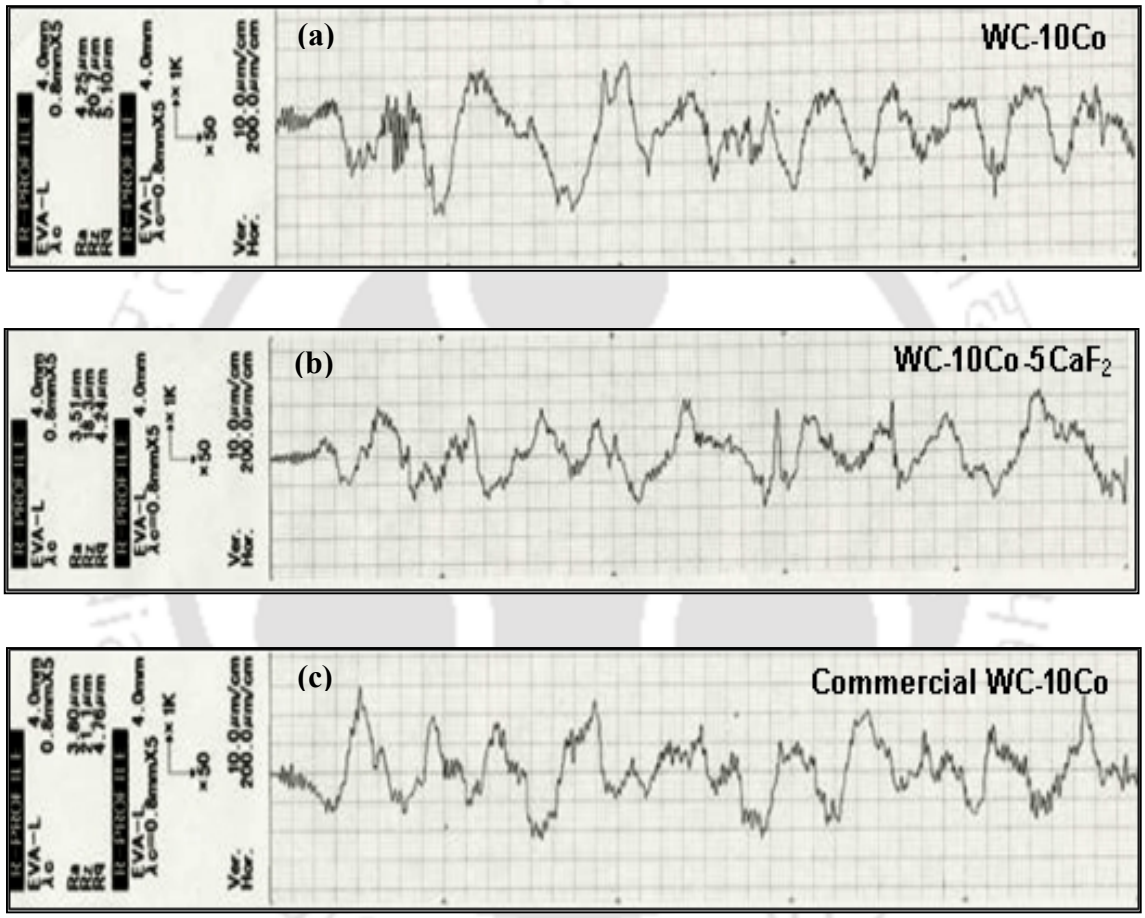


*Fig. 5.12 Surface roughness of the workpiece after machined with considered cutting tools (a) WC-Co (b) WC-Co-5 wt.% $CaF_2$ and (c) Commercial WC-Co (80 m/min)*

Presence of lubricant on the rake and flank surface of the cutting tool reduces friction between tool-chip and the machined surface which resulted in the decrease in surface roughness of the work piece. To understand the metal removal mechanism, machined surfaces were observed

optical microscope. Figure 5.13(a) shows the image of the machined surface of WC-Co-5 wt.% $CaF_2$, where feed marks were clearly revealed, however machined surface of all the considered cutting tool was almost same. Figure 5.13(b-c) shows the machined surfaces of WC-Co and WC-Co-5 wt.% $CaF_2$ observed under non contact three dimensional profilometer. Less resistance against the metal removal is exhibited by the workpiece while machining with WC-Co-5 wt.% $CaF_2$ cutting tool, measured cutting force confirmed this behaviour (Fig 5.4). Shear angle determines material removal mechanism. A larger shear angle is associated with low cutting force. Due to the less resistance, material was removed uniformly and feed marks edges are well defined.

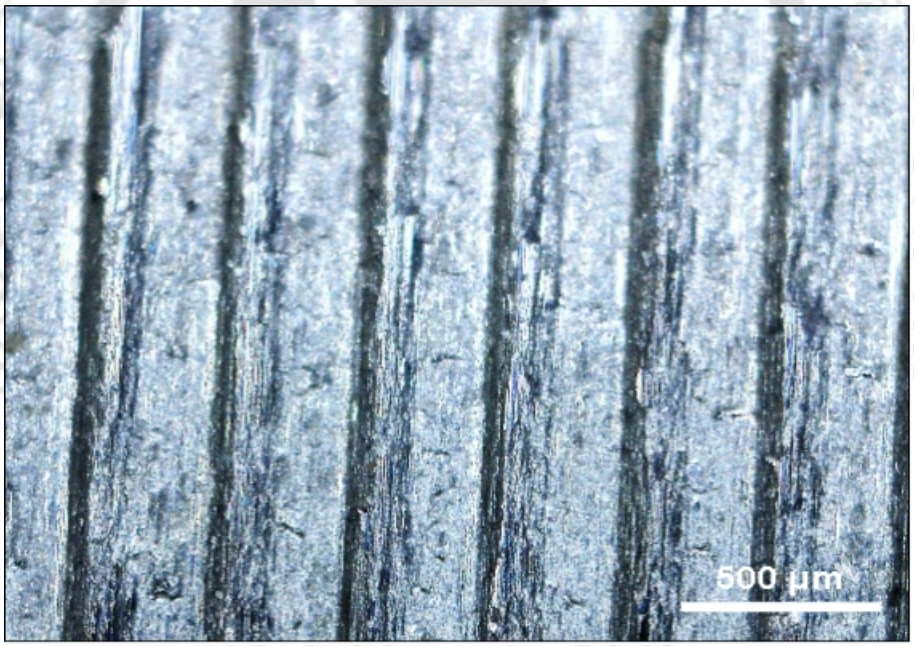


*Fig 5.13(a) Surface of the workpiece machined by developed material (WC-Co-5 wt.% $CaF_2$) under velocity of 80 m/min*

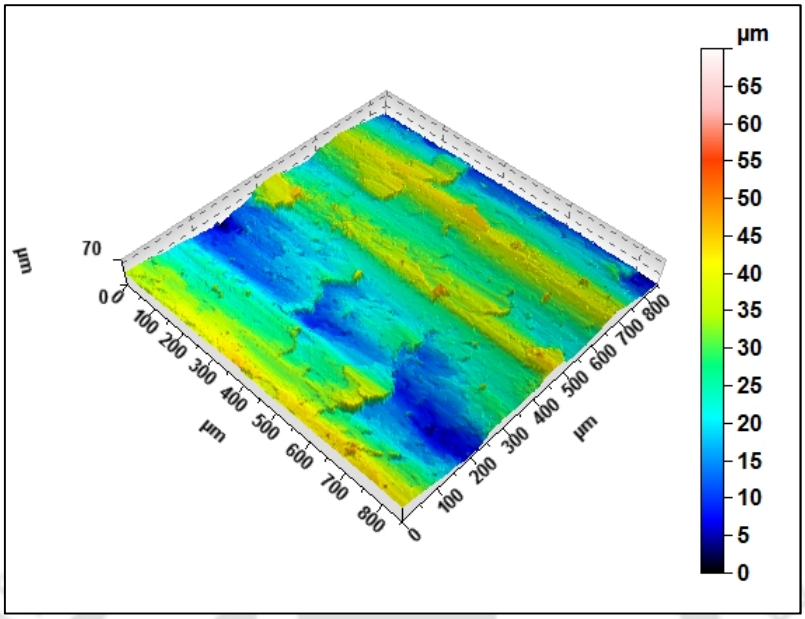


*Fig 5.13(b) Machined surface made by WC-Co (80 m/min) under non contact three dimensional profilometer*

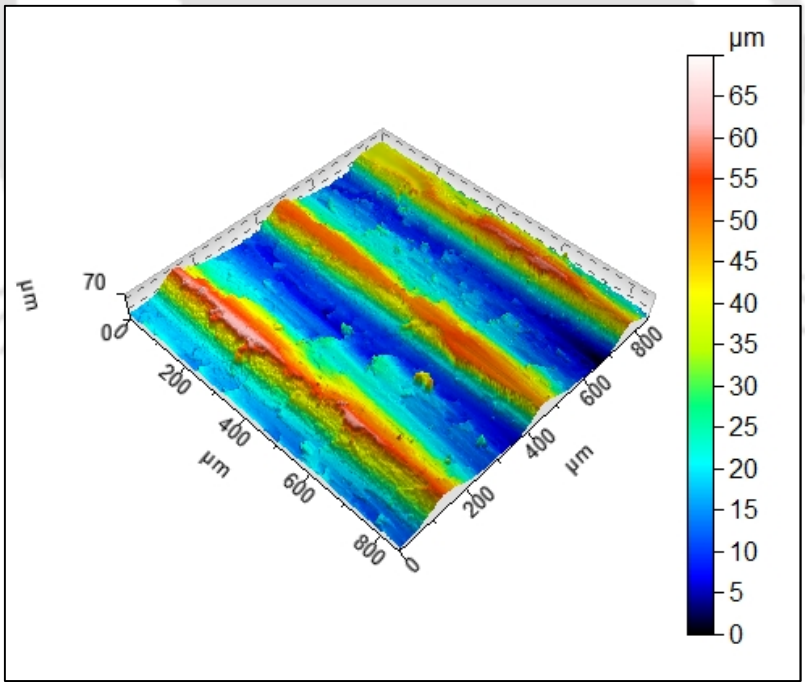


*Fig 5.13 (c) Machined surface made by WC-Co-5 wt.% $CaF_2$ (80 m/min) under non contact three dimensional profilometer*

Figure 5.13(b) shows the non-uniform material removal while machined with WC-Co. Figure 5.13(c) shows the uniform material removal while machined with WC-Co-5 wt.% $CaF_2$. Uniform material removal is confirmed by its surface roughness while machining with WC-Co-5 wt.% $CaF_2$ (Fig. 5.12).

### 5.3.5 Chip Morphology

The frictional characteristics at the tool-chip interface can be well understood by the morphology of machining chips. Low shear strength of $CaF_2$ contributed self lubricating behaviour. This inorganic solid material without lamellar structure is useful lubricant, particularly at high temperatures. Due to the strong adhesion and high lubricity at elevation temperature (Fedorchenko *et al*. 1970), $CaF_2$ formed thin film in between cutting tool and chip surface which prevented further tool wear by reducing friction. Less friction at tool-chip interface contributes to the less cutting temperature. Less cutting temperature, convert the chip into less ductile and promote chips curling. Thus curlier chips indicate less friction between the chip and the cutting tool (Trent and Wright, 2000). Figure 5.14 show the chip obtained from considered cutting tool material. Among the cutting tool, WC-Co-5 wt.% $CaF_2$ cutting tool generated chips with least radius. Figure 5.15(a-b) shows the back surfaces of the chip obtained while machining with the WC-Co and WC-Co-5 wt.% $CaF_2$ respectively. Chips produced by the WC-Co-5 wt.% $CaF_2$ cutting tool are curlier when compared to that of chips produced by the WC-Co cutting tool. Less friction (Fig. 5.5) and less temperature (Figure 5.6) generated by the WC-Co-5 wt.% $CaF_2$ cutting tool confirmed this fact. Biksa *et al.* (2010) also observed curlier chips while investigating the wear behaviour of the cemented carbide tool with nano multilayer coating. It was found that, multilayered AlTiN/MoN coated cutting tool generate less friction between the tool and chip, hence the chips becomes more curled when compared mono-layered AlTiN.

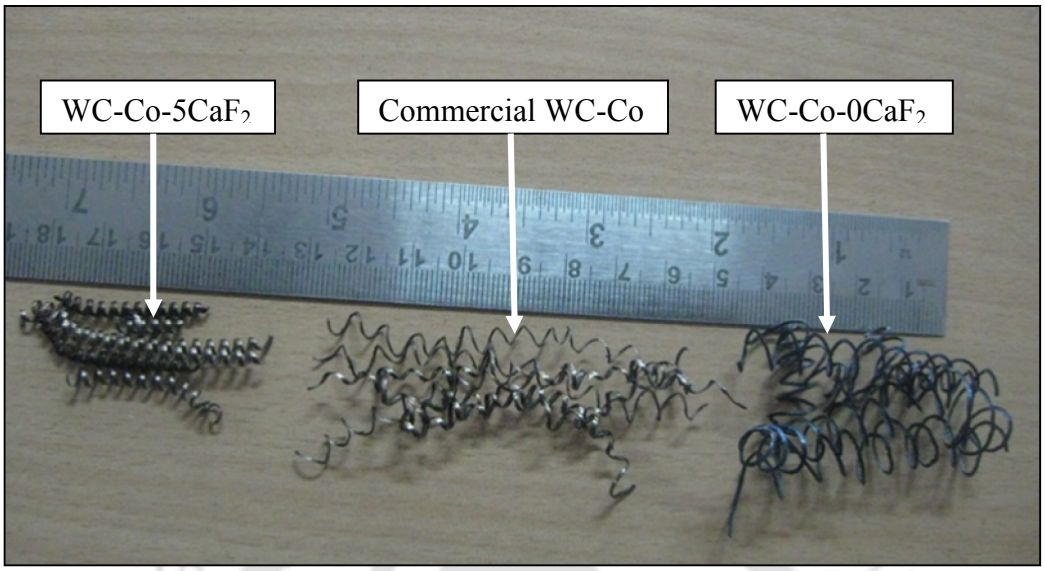


*Fig 5.14 Chips generated by the considered three cutting tools*

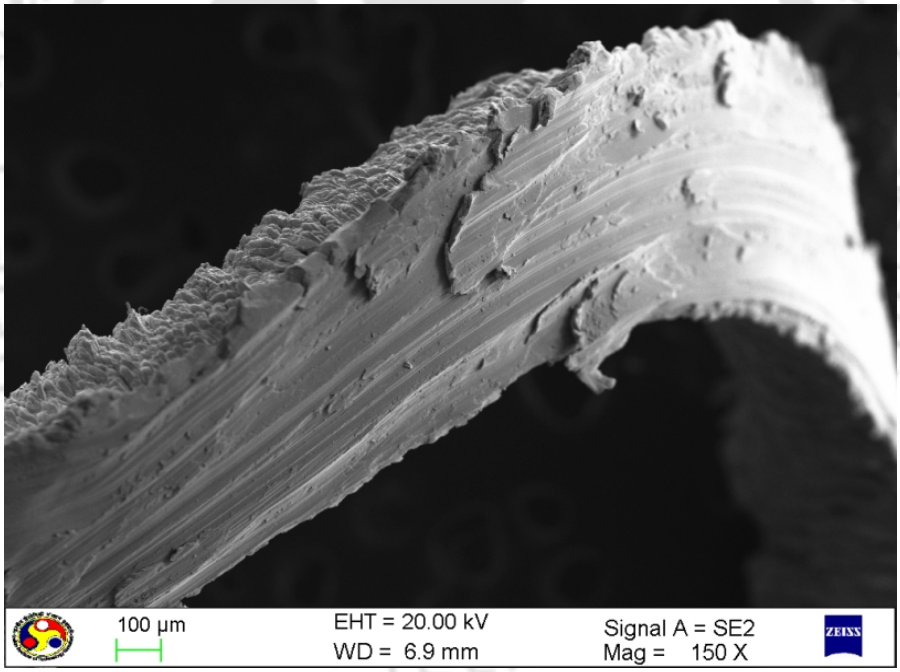


*Fig. 5.15 (a) Back surface of the chip produced by straight WC-Co cutting tool*

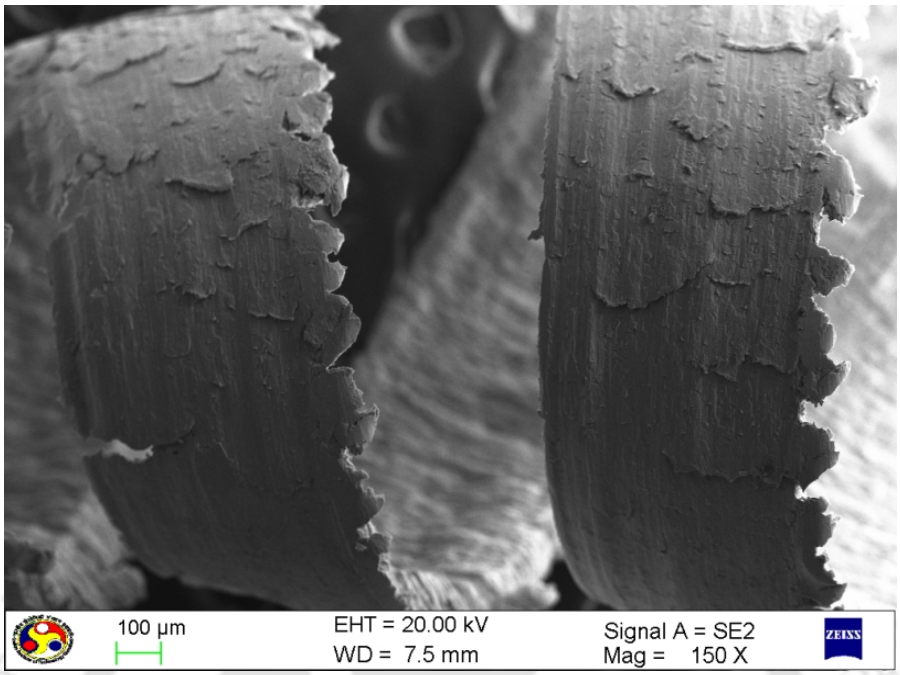


*Fig. 5.15 (b) Back surface of the chip produced by the WC-Co-5 wt.% $CaF_2$ cutting tool*

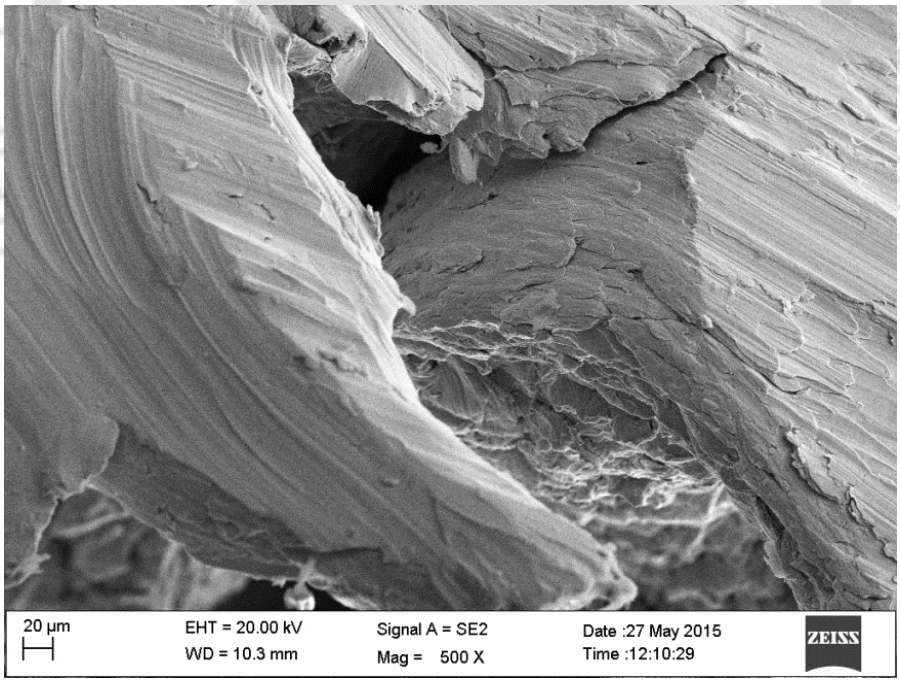


*Fig. 5. 16 (a) Serrated edge of the chip produced by straight WC-Co cutting tool*

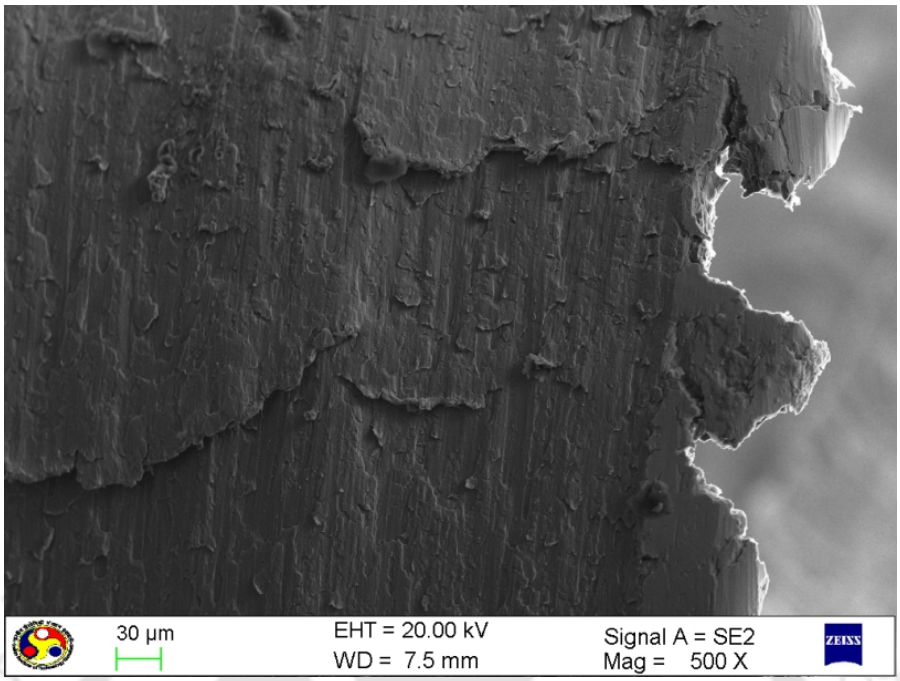


*Fig. 5.16 (b) Serrated edge of the chip produced by WC-Co-5 wt.% $CaF_2$ cutting tool*

Liang *et al.* (2011) investigated the effect of heat pipe cooling on chip morphology. Cutter with heat pipe produces chips having smaller helical radius when compared to the cutter without heat pipe.

In machining, the serrated chip flow is due to the breakage of steady chip flow. Serrated chip flow decreases the cutting tool life and deteriorates the work piece surface finish (G. Sutter, G. List, 2013). Figure 5.16 (a-b) shows the serration on the chip edge while machining with WC-Co and WC-Co-5 wt.% $CaF_2$ cutting tool respectively. WC-Co-5 wt.% $CaF_2$ cutting tool generated serrated chips having smaller size saw tooth when compared to that of WC-10Co cutting tool. This is also confirmed by the improved workpiece surface finish (less roughness) due to the WC-Co-5 wt.% $CaF_2$ cutting tool (Fig. 5.12). Bermingham *et al*. (2011) also observed small serrated chips while investigating with liquid nitrogen cooling. Guosheng *et al.* (2015) also observed minimum surface roughness at the beginning of the chip serration stage and maximum surface

roughness at the middle of the serration stage. Figure 5.17(a-b) shows the front/free surface of the chip produced by WC-Co and WC-Co-5 wt.% $CaF_2$ cutting tool respectively.

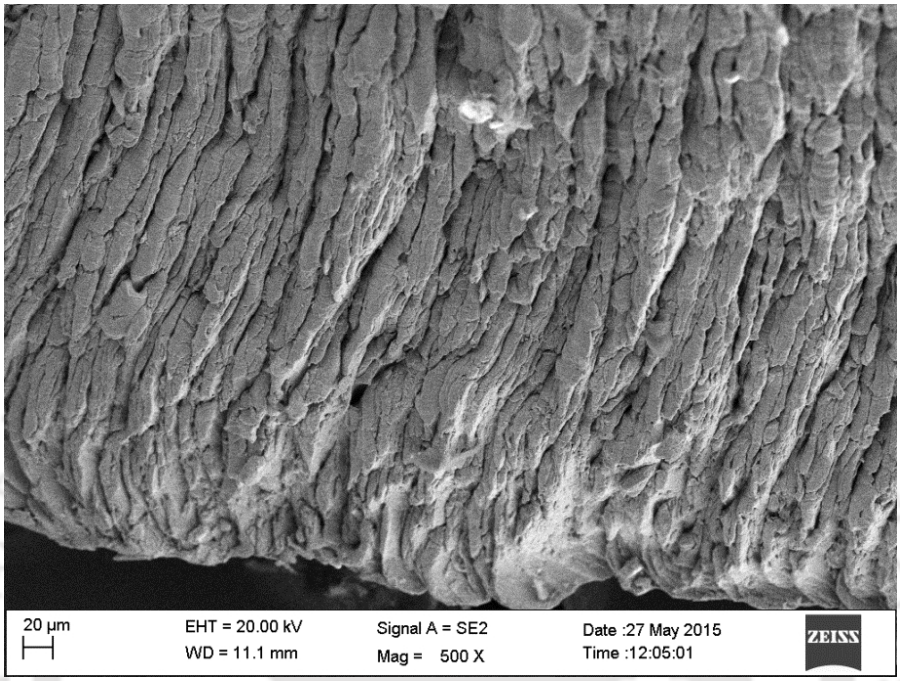


*Fig. 5.17(a) Front surface of the chip produced by WC-Co cutting tool*

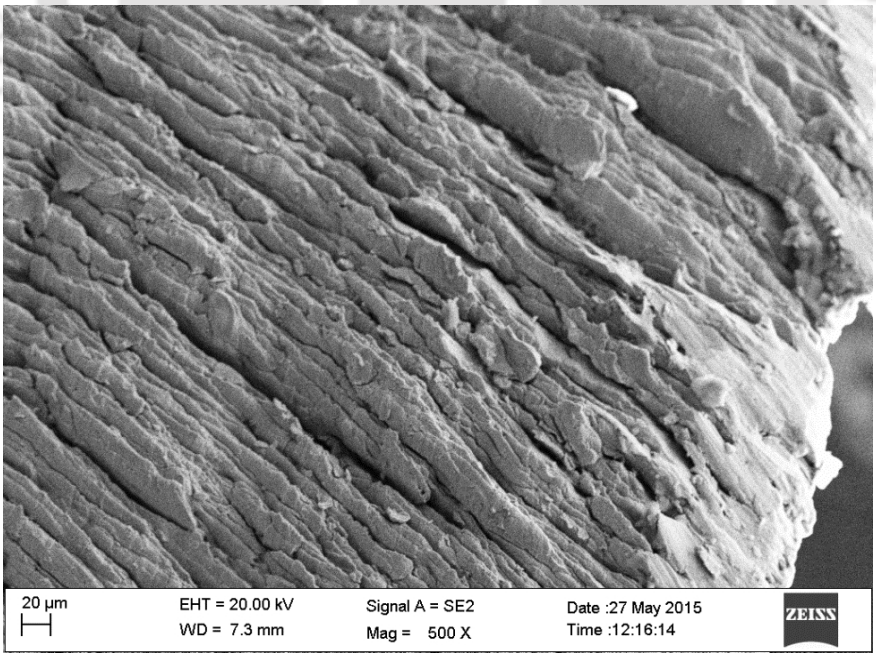


*Fig. 5.17 (b) Front surface of the chip produced by WC -Co-5 wt.% $CaF_2$ cutting tool*

The front surface revealed uniformly spaced lamella extends across the width of the chips and normal to the direction of chip flow. The presences of lamella structure on the free surface of the chips confirmed the dominance of shearing over ploughing and wear (Farid *et al*., 2011) by all the considered cutting tools. Figure 5.18 shows the EDS spectrum of the chip produced by the WC-Co-5 wt.% $CaF_2$ cutting tool, which confirmed the presence of the calcium and fluoride in the chip. During cutting due to the excessive pressure and temperature solid lubricant present in the cutting tool material transferred to the chip.

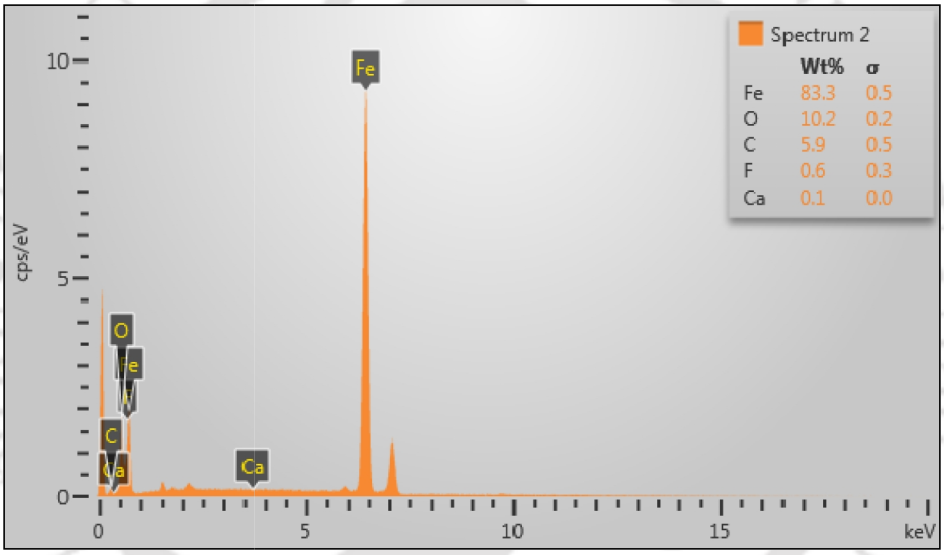


*Fig. 5.18 EDS spectrum of the of the considered chip produced by WC-Co-5 wt.% $CaF_2$*

## 5.4 SUMMARY

The present work reported the performance of the in-house developed tungsten carbide cutting tool with and without calcium fluoride. Machining was carried out in a lathe on steel at two different cutting speeds. Following major conclusions were arrived from the cutting experiments.

- In-house developed WC-Co-5 wt.% $CaF_2$ cutting tool exhibited lesser force (20-40 %) in all three components (tangential, axial and radial) due to the presence of sold lubricant on the rake and flank surfaces.
- The in-house developed WC-Co and commercial WC-Co cutting tool generated more cutting temperature (40-50 %) compared to that of developed WC-Co-5 wt.% $CaF_2$ cutiting tool.
- Machined surface morphology confirmed less resistance while machining with WC-Co-5$CaF_2$ cutting. Surface roughness of the generated surface confirmed the role of solid lubricant.
- Chip generated from the WC-Co-5 wt.% $CaF_2$ cutting tool exhibited more curling and smaller size of the saw tooth. The chip with smaller size saw tooth feature indicated the improved surface finish of the work piece and more chip curling indicated less temperature during cutting.
- Chip generated from the WC-C0-5 wt.% $CaF_2$ cutting tool revealed the traces of calcium and fluoride and confirmed lubrication effect during machining.

# CHAPTER 6

# CONCLUSION

In the present work, tungsten carbide, cobalt and calcium fluoride were used as basic cutting tool material, binder and solid lubricant respectively. Considered materials were milled in the planetary ball mill at various hours for the milling characterization with the aid of a scanning electron microscope, laser particle size analyser and an X-ray diffraction. Green compacted test specimens were compacted uniaxially at various pressure for compacting characteristics. To understand the effect of solid lubricant on transverse rupture strength, various weight percentages of solid lubricant was considered. Subsequently test specimens were sintered in a tube furnace under nitrogen atmosphere. Green as well as the sintered density of the sintered specimens was measured. Servo hydraulic dynamic testing machine is used to evaluate the transverse rupture strength of the developed material.

Developed solid lubricant materials were cut into specimens and tested against silicon carbide abrasive sheet and sintered disc (commercial WC-6 % Co) in the standard pin on disc configuration. Frictional resistance and wear and surface temperature of the test specimen was continuously measured during testing. The initial and final weight of the test specimen was used to measure the wear resistance .The initial and final roughness of the test specimen were measured by the portable surface roughness tester. Scanning electron microscope as well as non-contact surface profilometer was used to investigate the worn-out surface of the test specimens. In addition, the scratch resistance test was carried out on the straight WC-Co and WC-Co-5 wt.% $CaF_2$ materials.

Developed cutting tool materials were cut and brazed on the tool shank. Subsequently cutting tool was grounded to have the required rake angle and the clearance angle. Machining experiments were carried out in the lathe. During turning, all the three components of forces were measured and continuously acquired and the average temperature of the cutting tool was measured with thermal imaging. Machining was carried out in a lathe on steel at two different cutting speeds.

Following major conclusions were arrived from the present work

- 40 hours of milling period found to be most suitable for the chosen materials and milling condition to obtain superior density and hardness.
- The fractured surface of the WC-Co-5 wt.% $CaF_2$ material while evaluating transverse rupture strength revealed superior bonding between tungsten carbide particles among all other investigated materials under test condition. In sufficient and excess amount of $CaF_2$ reduces wetting and excess melting which results in sintering defect.
- Among the investigated test material, WC-Co-5 wt.% $CaF_2$ exhibited superior abrasive wear resistance and the lowest friction coefficient (0.25-0.28) due to its combination of superior hardness and lubricating behaviour at the test condition.
- WC-Co-5 wt.% $CaF_2$ exhibited wedge groove feature whereas, the straight WC-Co material exhibited brittle fracture with crater and hillocks features under abrasive condition
- The final surface roughness of the test material as well as 3D surface profile confirmed superior wear resistance when compared to all other considered materials.
- Among the investigated material, WC-Co-5 wt.% $CaF_2$ exhibited least friction and superior wear resistance in the adhesive condition also due to the formation of transfer film on the

counter disc. Non contact 3D profiler confirmed the strong transfer film formation on the counter disc when slid against WC-Co-5 wt.% $CaF_2$ material.

- The surface temperature of WC-Co-5 wt.% $CaF_2$ material exhibited less surface temperature due to the less frictional resistance during sliding.
- In-house developed WC-Co-5 wt.% $CaF_2$ cutting tool exhibited lesser force (20-40 %) due to the presence of sold lubricant on the rake and flank surfaces. The in-house developed WC-10Co and commercial WC-Co cutting tool generated more cutting temperature (40-50 %) compared to that of developed WC-Co-5 wt.% $CaF_2$ cutting tool.
- Machined surface morphology confirmed less resistance while machining with WC-Co-5 wt.% $CaF_2$ cutting. The chip generated exhibited more curling and smaller size of the saw with traces of calcium and fluoride to confirm the lubrication effect while machining.

## REFERENCES


1. Abdel, H., El-Hofy, G. Fundamentals of Machining Processes: Conventional and Nonconventional Processes (2nd Ed). *CRC Press, Taylor & Francis Group*, London, ISBN 978-1-4665-7703-9, 2014.
2. Ahmadian, M., Wexler, D., Chandra, T., and Calka, A. Abrasive wear of WC–FeAl–B and WC–Ni3Al–B composites. *International Journal of Refractory Metals and Hard Materials*, 2005, **23**, 155–159.
3. Astakhov, VP. Effects of the cutting feed, depth of cut, and workpiece (bore) diameter on the tool wear rate. *International Journal of Advanced Manufacturing Technology*, 2007, **34**, 631–640.
4. ASTM B925-08. Standard Practices for Production and Preparation of Powder Metallurgy (PM) Test Specimens. ASTM International, West Conshohocken, 2003.
5. ASTM B962-08. Standard Test Methods for Density of Compacted or Sintered Powder Metallurgy (PM) Products Using Archimedes' Principle. ASTM International, West Conshohocken, 2013.
6. ASTM B406-96. Standard Test Method for Transverse Rupture Strength of Cemented Carbides. ASTM International, West Conshohocken, 2013.
7. ASTM B331-95. Standard Test Method for Compressibility of Metal Powders in Uniaxial Compaction. ASTM International, West Conshohocken, 2011.
8. ASTM G99-05. Standard Test Method for Wear Testing with a Pin-on-Disk Apparatus. ASTM International, West Conshohocken, 2010.
9. Avettand, F.M.N., Taillard, R., Dhers, J., and Foct, J. Effect of ball milling parameters on the microstructure of W–Y powders and sintered samples. *International Journal of Refractory Metals and Hard Materials*, 2003, **21,** 205–213.
10. Babu, M., Lee, JH., Lee JK., Cho, KY., Suryanarayana, C., and Hong, SJ. Effects of atmosphere and milling time on the coarsening of copper powders during mechanical milling. *Powder Technology*, 2014, **256**, 251–256.
11. Bafrooei, HB., Ebadzadeh, T., and Majidian, H. Microwave synthesis and sintering of forsterite nanopowder produced by high energy ball milling. *Ceramics International*, 2014, **40**, 2869–2876.

12. Bermingham, MJ., Kirsch, J., Sun, S., Palanisamy, S., and Dargusch, MS. New observations on tool life, cutting forces and chip morphology in cryogenic machining Ti-6Al-4V. *International Journal of Machine Tools and Manufacture,* 2011, **51**, 500–511.
13. Bhushan, B. Introduction to Tribology. *John wiley & Sons, New York*, ISBN: 978-1-119-94453-9, 2002.
14. Biksa, A., Yamamoto, K., Dosbaevaa, G., Veldhuis, SC., Fox-Rabinovich, GS., Elfizy, A., Wagg, T., and Shuster, L.S. Wear behavior of adaptive nano-multilayered AlTiN/$Me_xN$ PVD coatings during machining of aerospace alloys. *Tribology International*, 2010, **43,** 1491–1499.
15. Blau, P.J. Friction, Lubrication and Wear Technology. *ASM Metals Handbook* **Vol.18**, ISBN: 978-0-87170-380-4. 1997.
16. Blombery, R.I., Perrot, C.M., and Robinson, P.M. Abrasive wear of tungsten carbide–cobalt composites. 1. Wear mechanism. *Materials Science and Engineering*, 1974, **13**, 93–100.
17. Bolton, J.D., and Gant, A.J. Fracture in ceramic-reinforced metal matrix composites based on high-speed steel. *Journal of Materials Science*, 1998, **33**, 939–953.
18. Bolton, J.D., and Gant, A.J. Liquid phase sintering of metal matrix composites containing solid lubricants. *Journal of Materials Processing Technology*, 1996, **56**, 136–147.
19. Bolton, J.D., and Gant, A.J. Phase reactions and chemical-stability of ceramic carbide and solid lubricant particulate additions within sintered high-speed steel matrix. *Powder Metallurgy*, 1993, **36**, 267–274.
20. Bonny, K., Baets, P.D., Perez, Y., Vleugels, J., and Lauwers, B. Friction and wear characteristics of WC–Co cemented carbides in dry reciprocating sliding contact. *Wear*, 2010, **268**, 1504–1517.
21. Borah, A., Robi, P.S., and Srinivasan, A. Synthesis of nano-crystalline RuAl by Mechanical Alloying. *Metals and Materials International*, 2007, **13**, 293–302.
22. Brant, G. Flank and crater wear mechanisms of alumina-based cutting tools when machining steel. *Wear*, 1986, **112**, 39–56.
23. Briscoe, B. J., and Rough, S. L. The effects of wall friction on the ejection of pressed ceramic parts. *Powder Technology*, 1998, **99**, 228–233.
24. Briscoe, B. Wear of polymers: an essay on fundamental aspects. *Tribology International*, 1981, **14**, 231–243

25. Canakci, A., Erdemir, F., Varol, T., and Patir, A. Determining the effect of process parameters on particle size in mechanical milling using the Taguchi method: Measurement and analysis. *Measurement,* 2013, **46**, 3532–3540.
26. Cha, S.I., Hong, S.H., Ha, G.H., and Kim, B.K. Microstructure and mechanical properties of nanocrystalline WC–10Co cemented carbides. *Scripta Materialia*, 2001, **44**, 1535–1539.
27. Cheng, RY. Principle of Metal Cutting (2nd Ed.). China Machine Press, Beijing, 1992.
28. Dabhade, V.V., Rama Mohan, TR., and Ramakrishnan, P., Nanocrystalline titanium powders by high energy attrition milling. *Powder Technology*, 2007, **171**, 177–183.
29. Deng, J., Yunsong, L., and Youqiang, X. Performance of femtosecond laser-textured cutting tools deposited with $WS_2$ solid lubricant coatings. *Surface and Coatings Technology,* 2013, **222**, 135–143.
30. Deng, J., Ze, W., Yunsong, L., Ting, G., and Jie, C. Performance of carbide tools with textured rake-face filled with solid lubricants in dry cutting processes. *International Journal of Refractory Metals and Hard Materials*, 2012, **30**, 164–172.
31. Deng, J., Song, W., Zhang, H., Yan, P., and Liu, A. Friction and wear behaviors of the carbide tools embedded with solid lubricants in sliding wear tests and in dry cutting processes. *Wear*, 2011, **270**, 666–674.
32. Deng, J., Song, W., and Zhang, H. Design, fabrication and properties of a self-lubricated tool in dry cutting. *International Journal of Machine Tools and Manufacture*, 2009, **49**, 66–72.
33. Deng, J., Li Y., and Song W. Diffusion wear in dry cutting of Ti–6Al–4V with WC/Co carbide tools. Wear, 2008, **265**, 1776–1783.
34. Deng, J., Liu, L., Yang, X., Liu, J., Sun, J., and Zhao, J. Self-lubrication of $Al_2O_3$/TiC/$CaF_2$ ceramic composites in sliding wear tests and in machining processes. *Materials and Design*, 2007, **28**, 757–764.
35. Deng, J., and Cao, T. Self-lubricating mechanisms via the in situ formed tribofilm of sintered ceramics with $CaF_2$ additions when sliding against hardened steel. *International Journal of Refractory Metals and Hard Materials*, 2007, **25**, 189–197.
36. Deng, J., Cao, T., Yang, X., and Liu, J. Self-lubrication of sintered ceramic tools with $CaF_2$ additions in dry cutting. *International Journal of Machine Tools and Manufacture,* 2006*,* **46,** 957–963.

37. Deng, J., Can, T., and Sun, J. Microstructure and mechanical properties of hot-pressed $Al_2O_3$/TiC ceramic composites with the additions of solid lubricants. *Ceramic International*, 2005, **31**, 249–256.
38. Deng, J., Cao, T., and Liu, L. Self-lubricating behaviors of $Al_2O_3/TiB_2$ ceramic tools in dry high-speed machining of hardened steel. *Journal of the European Ceramic Society*, 2005, **25**, 1073–1079.
39. Dhanasekaran, S., and Gnanamoorthy, R. Abrasive wear behavior of sintered steels prepared by $MoS_2$ addition. *Wear*, 2007, **262**, 617–623.
40. Dixit, US., Sarma, D.K., and Paulo, DJ. Environmentally Friendly Machining. *Springer Briefs in Applied Sciences and Technology*, Springer, London, ISBN 978-1-4614-2307-2, 2012.
41. Dobrzanski, LA., and Dolzanska, B. Hardness to toughness relationship on WC-Co tool gradient materials evaluated by Palmqvist method. *Archives of Materials Science and Engineering*, 2010, **43**, 87-93
42. Dong-hu, L., Yong, L, Da-peng, Z., Yan, W., Jing-hua, F., Yu-ren, W., and Zu-ming, L. Effect of ball milling time on microstructures and mechanical properties of mechanically-alloyed iron-based materials. *Transaction non ferrous metal society of china*, 2010, **20**, 831–838.
43. Duman, D., Gokce, H., and Cimenoglu, H. Synthesis, microstructure, and mechanical properties of WC–TiC–Co ceramic composites. *Journal of the European Ceramic Society*, 2012, **32**, 1427–1433.
44. Dvornik, MI., and Zaytsev, AV. Research of surfaces and interfaces increasing during planetary ball milling of nanostructured tungsten carbide/cobalt powder. *International Journal of Refractory Metals and Hard Materials,* 2013, **36**, 271–277.
45. Ederer, L. The effect of zinc stearate on the compaction and sintering characteristics of a Ti-6%Al-4%V hydride-dehydride powder. *ME Thesis*, Department of mining and metallurgical engineering, Mc Gill University, Canada, 1999.
46. Edwards, R., Cutting Tools. Institute of Materials. London, ISBN: 13-9780901716484, 1993.
47. Enayati, M.H., Aryanpour, G.R., and Ebnonnasir, A. Production of nanostructured WC–Co powder by ball milling. *International Journal of Refractory Metals and Hard Materials*, 2009, **27**, 159–163

48. Engqvist, H., Hogberg, H., Botton, G.A., Ederyd, S., and Axen, N. Tribofilm formation on cemented carbides in dry sliding conformal contact. *Wear*, 2000, **239**, 219–228.
49. Farid, A.A., Sharif, S., and Idris, M.H. Chip morphology study in high speed drilling of Al–Si alloy. *International Journal of Advanced Manufacturing Technology,* 2011, **57**, 555–564.
50. Fedorchenko, I.M., Zozulya, V.D., and Schevchuk, Yu. F. Test methods and properties of materials: Lubricating properties of Calcium Fluoride. *Soviet Powder Metallurgy and Metal Ceramics*, 1970, **9**, 818–820.
51. Gant, A.J., and Gee, M.G. A review of micro scale abrasion testing. *Journal of Physics D: Applied Physics*, 2011, **44**, 1–15.
52. Gant, A.J., and Gee, M.G., May, A.T. Micro abrasion of WC–Co hardmetals in corrosive media. *Wear*, 2004, **256**, 954–962.
53. Garg, P., Park, S.J., and German, R.M. Effect of die compaction pressure on densification behavior of molybdenum powders. *International Journal of Refractory Metals and Hard Materials,* 2007, **25**, 16–24.
54. German, R.M. Sintering theory and practice. John Wiley & Sons, incorporation, USA, 1996.
55. Gheisari, KH., Javadpoura, S., Oh, JT., and Ghaffari, M. The effect of milling speed on the structural properties of mechanically alloyed Fe 45%Ni powders. *Journal of Alloys and Compounds*, 2009, **472**, 416–420.
56. Gomari, S., and Sharafi, S. Microstructural characterization of nanocrystalline chromium carbides synthesized by high energy ball milling. *Journal of Alloys and Compounds*, 2010, **490**, 26–30.
57. Gordo, E., Gomez, B., Ruiz-Navas, E.M., and Torralba, J.M. Influence of milling parameters on the manufacturing of Fe–TiCN composite powders. *Journal of Materials Processing Technology*, 2005, **162–63**, 59–64.
58. Goudarzi, M., and Akhlaghi, F. Effect of nanosized SiC particles addition to CP Al and Al–Mg powders on their compaction behavior. *Powder Technology*, 2013, **245**, 126–133.
59. Grzesik, W., Zalisz, Z., and Krol, S., and Nieslony, P. Investigations on friction and wear mechanisms of the PVD-TiAlN coated carbide in dry sliding against steels and cast iron. *Wear*, 2006, **261**, 1191-1200.
60. Gu, D,. Zhang, G., Dai, D., Wang, H., and Shen, Y. Nanocrystalline tungsten nickel heavy alloy reinforced by in-situ tungsten carbide: Mechanical alloying preparation and

microstructural evolution. *International Journal of Refractory Metals and Hard Materials*, 2013, **37**, 45–51.

61. Gu, D., and Shen, Y. Balling phenomena during direct laser sintering of multi-component Cu-based metal powder. *Journal of Alloys and Compounds*, 2007, **432**, 163–166.
62. Guosheng, S., Zhanqiang, L., Liang, L., and Bing, W. Influences of chip serration on micro-topography of machined surface in high-speed cutting. *International Journal of Machine Tools and Manufacture,* 2015, **89**, 202–207.
63. Han, Y., Fan J., Liu T., Cheng, H., and Tian, T. The effect of trace nickel additive and ball milling treatment on the near-full densification behavior of ultrafine tungsten powder. *International Journal of Refractory Metals and Hard Materials*, 2012, **34**, 18–26.
64. Hedayati, M., Salehi, M., Bagheri, R., Panjepour, M., and Maghzian, A. Ball milling preparation and characterization of poly (ether ether ketone)/surface modified silica nanocomposite. *Powder Technology,* 2011, **207,** 296–303.
65. Hewitt, S.A., and Kibble, K.A. Effects of ball milling time on the synthesis and consolidation of nanostructured WC–Co composites. *International Journal of Refractory Metals and Hard Materials*, 2009, **27**, 937–948.
66. Hewitt, S.A., Laoui, T., and Kibble, K.K. Effect of milling temperature on the synthesis and consolidation of nanocomposite WC–10Co powders. *International Journal of Refractory Metals and Hard Materials*, 2009, **27**, 66–73.
67. HMT, Production Technology (1st Ed.). Tata McGraw Hill Publishing Company Limited, New Delhi, ISBN-13:978-0-07-096443-3, 1980.
68. Hua, Y., Peilei, Z., Yu, Z., Qinghua, L., Shanglei, Y., and Chonggui, L. Microstructure and tribological properties of laser-clad Ni–Cr/TiB2 composite coatings on copper with the addition of $CaF_2$. *Surface Coating Technology*, 2012, **206**, 4046–4053.
69. Huang, X. H., and Chang, J. Synthesis of nanocrystalline wollastonite powders by citrate-nitrate gel combustion method. *Materials Chemistry and Physics*, 2009,**115**, 1–4.
70. Jayashree, B., John, J.R., Jeyakumar, A., Ghosh, A., and Tewari, U.S. Influence of solid lubricants and fibre reinforcement on wear behaviour of polyethersulphone. *Tribology International*, 2000, **33**, 697–706.

71. Jia, K., Fischer, T.E., and Gallois, B. Microstructure, hardness and toughness of nanostructured and conventional WC–Co composites. *Nanostructured Materials*, 1998, **10**, 875–891.
72. Jian, L.L., and Dang, SX. Tribological properties of nickel-based self-lubricating composite at elevated temperature and counter face material selection. *Wear*, 2008, **265**, 533–539.
73. Kagnaya, T., Boher, C., Lambert, L., Lazard, M., and Cutard, T. Wear mechanisms of WC–Co cutting tools from high-speed tribological tests. *Wear*, 2009, **267**, 890–897.
74. Kato, H., Takama, M., Iwai, Y., Washida, K., and Sasaki, Y. Wear and mechanical properties of sintered copper–tin composites containing graphite or molybdenum disulfide. *Wear*, 2003, **255**, 573–578.
75. Khan, AS., Farrokh, ., and Takacs, L. Effect of grain refinement on mechanical properties of ball milled bulk aluminum, *Materials Science and Engineering A*, 2008, **489**, 77–84.
76. Klaasen, H., Kubarasepp, J., Roosaar, T., Viljus, M., and Traksmaa R. Adhesive wear performance of hardmetals and ceramets. *Wear*, 2010, **268**, 1122–1128.
77. Koley, S., Ghosh, A., Sahu, A. K., Tewari, R., and Suri, A. K. Correlation of compaction pressure , green density, pore size distribution and sintering temperature of a nano-crystalline 2Y-TZP-$Al_2O_3$ composite. *Ceramics International*, 2011, **37**, 731–739.
78. Lameck, N.N.S. Effects of Grinding Media Shapes on Ball Mill Performance. *M.S. Thesis*. University of the Witwatersrand, Johannesburg, 2005.
79. Langford, J.J., and Wilson, A.J.C. Scherrer after sixty years: a survey and some new results in the determination of crystallite size. *Journal of Applied Crystallography*, 1978, **11**, 102–113.
80. Lei, S., Devarajan, S., and Chang, Z. A study of micropool lubricated cutting tool in machining of mild steel. *Journal of Materials Processing Technology*, 2009, **209,** 1612-1620.
81. Li, A., Zhao, J., Wang, D., Gao, X., and Tang, H. Three-point bending fatigue behavior of WC–Co cemented carbides. *Materials and Design*, 2013, **45**, 271–278.
82. Li, R., Liu, J, Shi, Y., and Wang, L. Balling behavior of stainless steel and nickel powder during selective laser melting process. *International Journal of Advanced Manufacturing Technology*, 2012, **59**, 1025–1035.

83. Li, Y., Liu, N., Zhang, X. and Rong, C. Effect of Mo addition on the microstructure and mechanical properties of ultra-fine grade TiC-TiN-WC-$Mo_2C$-Co Cermets. *International Journal of Refractory Metals and Hard Materials*, 2008, **26**, 190–196.
84. Li, J.L., and Xiong, D.S. Tribological properties of nickel-based self-lubricating composite at elevated temperature and counterface material selection. *Wear*, 2008, **265**, 533–539.
85. Lian, Y., Deng, J., Guangyuan, Y., Hongwei, C., and Jun, Z. Preparation of tungsten disulfide ($WS_2$) soft-coated nano-textured self-lubricating tool and its cutting performance. *International Journal of Advanced Manufacturing Technology*, 2013, **68**, 2033–2042.
86. Liang, L., Yanming, Q., and Zhiyong, K. Investigation of tool-chip interface temperature in dry turning assisted by heat pipe cooling. *International Journal of Advanced Manufacturing Technology,* 2011, **54**, 35–43.
87. Lin, N., Wu, C.H., He, Y.H., and Zhang, D.F. Effect of Mo and Co additions on the microstructure and properties of WC-TiC-Ni Cemented carbides. *International Journal of Refractory Metals and Hard Materials*, 2012, **30**, 107–113.
88. Lin, H.M., Liao, Y.S., and Wei, C.C. Wear behavior in turning high hardness alloy steel by CBN tool. Wear, 2008, **264**, 679–684.
89. Liu, ZY., Xu, SJ., Xiao, BL., Xue, P., Wang, WG., and Ma, ZY. Effect of ball-milling time on mechanical properties of carbon nanotubes reinforced aluminum matrix composites. *Composites Part A: Applied Science and Manufacturing*, 2012, **43**, 2161–2168
90. Liu, N., Chao, S., and Huang X. Effects of TiC /TiN addition on the microstructure and mechanical properties of ultra-fine grade Ti (C,N)-Ni cermets. *Journal of the European Ceramic Society*, 2006, **26**, 3861–3870.
91. Liu, N., Xu, Y., Li, Z., Chen, M., Li, G. and Zhang, L. Influence of molybdenum addition on the microstructure and mechanical properties of TiC based cermets with nano-TiN modification. *Ceramics International*, 2003, **29**, 919–925.
92. Lu, J., Yang, S., Wang, J., and Xue, Q. Mechanical and tribological properties of Ni-based alloy/$CeF_3$/graphite high temperature self-lubricating composites. *Wear*, 2001, **249**, 1070–1076
93. Lu, L., Lai, M.O., and Froyen, L. Effect of mechanical milling on the properties of Mg–10.3% Ti and Mg–5% Al–10.3% Ti metal–metal composite. *Journal of Alloys and Compounds*, 2005, **387**, 260–264.

94. Mahmoodan, M., Aliakbarzadeh, H., and Gholamipour, R. Microstructural and mechanical characterization of high energy ball milled and sintered WC–10 wt%Co–xTaC nano powders. *International Journal of Refractory Metals and Hard Materials,* 2009, **27,** 801–805.

95. Mandel, K., Krüger, L., and Schimpf, C. Particle properties of submicron-sized WC-12Co processed by planetary ball milling. *International Journal of Refractory Metals and Hard Materials,* 2014, **42,** 200–204.

96. Martin, L.P., Hodge, A.H., and Campbell, GH. Compaction behavior of uniaxially cold-pressed Bi-Ta composites. *Scripta Materialia*, 2007, **57**, 229–232.

97. Matthews, A., Leyland, A., Holmberg, K., and Ronkainen, H. Design aspects for advanced tribological surface coatings. *Surface Coating Technology*, 1998, **l00–101**, 1–6.

98. Meng, H., Zhang, Z., Zhao, F., and Qiu, T. Preparation of WC nanoparticles by twice ball milling. *International Journal of Refractory Metals and Hard Materials,* 2013, **41,** 191–197.

99. Miyoshi, K. Solid Lubrication Fundamentals and Applications. *NASA Glenn Research Center, Cleveland*, Ohio, 2000.

100. Mohammad Sharifi, E., Karimzadeh, F., and Enayati, M.H. Fabrication and evaluation of mechanical and Tribological properties of boron Carbide reinforced aluminum matrix nano composites. *Materials and Design*, 2011, **32**, 3263–3271.

101. Momozawa, A., Koike, w., Nakamura, S., Kato, H. and Takagi, K. Effect of Mn content on the properties of TiC / $TiB_2$ base cermets. *Solid State Sciences*, 2012, **14**, 1729–1733.

102. Moon, I.H., and Choi, J.S. Dependence of green strength on contact area between powder particles for spherical copper powder compacts. *Powder Metallurgy*, 1985, **28**, 21-26.

103. Mosbah, A.Y., Wexler, D., and Calka, A. Abrasive wear of WC–FeAl composites. *Wear*, 2005, **258**, 1337–1341.

104. Nampi, PP., Kume, S., Hotta, Y., and Watari, K. The effect of polyvinyl alcohol as a binder and Stearic acid as an internal lubricant in the formation and subsequent sintering of Sprayed–dried alumina. *Ceramics International*, 2011, **37**, 3445–3450.

105. Nouri, A., Hodgson, PD., and Wen, C. Effect of ball-milling time on the structural characteristics of biomedical porous Ti Sn Nb alloy. *Materials Science and Engineering C*, 2011, **31**, 921–928.

106. Okonkwo, P.C., Kelly, G., Rolfe, B.F., and Pereira M.P. The effect of temperature on sliding wear of steel–tool steel pairs. *Wear*, 2012, **282-283**, 22–30.

107. Pazhanivel, B., Prem Kumar, T., and Sozhan, G. Machinability and scratch wear resistance of carbon-coated WC inserts. *Materials Science and Engineering B*, 2015, **193**,146–152.

108. Peng, Z., Shaolian, Z., Zhiguo, Z., and Wei, L. Microstructure and hardness of WC–Co particle reinforced iron matrix surface composite. *China Foundry Research Division*, 2013, **10**, 374–379.

109. Peng, F., Oladapo, E.O., Fang, Z.Z., and Sohn, H.Y. Effect of WC particle size on Co distribution in liquid-phase-sintered functionally graded WC–Co composite. *International Journal of Refractory Metals and Hard Materials*, 2008, **26**, 98–105.

110. Pirso, J., Letunovits, S., and Viljus, M. Friction and wear behavior of cemented carbides. *Wear*, 2004, **257**, 257–265.

111. Pirso, J., Viljus, M., and Letunovits, S. Friction and dry sliding wear behavior of cermets. *Wear*, 2006, **260**,815–824.

112. Poquillon, D., Lemaitre, J., Baco, C.V., Tailhades, P.H., and Lacaze, J. Cold compaction of iron powders-relations between powder morphology and mechanical properties. Part I: powder preparation and compaction. *Powder Technology*, 2002, **126**, 65–74.

113. Poussard, G.J.L., Milhet, X., Huvier, C, and Dinhut, J.F. Consolidation of iron powders through the influence of phosphate thin films. *Journal of Materials Processing Technology*, 2008, **205**, 151–159.

114. Qiao, Z., Cheng, J., Kong, L., Yang, J., Bi, Q., and Yang, J. Investigation of (WAl) C–Co ceramic composites with the additions of fluoride solid lubricants: preparation, mechanical properties and tribological behaviors. *International Journal of Refractory Metals and Hard Materials,* 2013, **41**, 322–328.

115. Raghu, T., Sundaresan, Ramakrishnan, P., and Rama Mohan, T.R. Synthesis of nanocrystalline copper–tungsten alloys by mechanical alloying. *Materials Science Engineering A*, 2001, **304–306**, 438–441.

116. Rajinikanth, V., and Venkateswarlu, K. An investigation of sliding wear behaviour of WC–Co coating. *Tribology International*, 2011, **44**, 1711–1719.

117. Rao, P.N. Manufacturing Technology: Metal Cutting and Machine Tools (Vol. 2, 23rd Ed.). *Tata McGraw Hill education (India) Private Limited, New Delhi,* ISBN: 13-978-1-25-902956-1, 2009.

118. Razavi-Tousi, S.S., Yazdani-Rad, R., and Manafi, S.A. Effect of volume fraction and particle size of alumina reinforcement on nano composites compaction and densification behavior of Al-$Al_2O_3$. *Materials Science and Engineering A*, 2011, **528**, 1105–1110.

119. Reid, C. B., Forrester, J. S., Goodshaw, H. J., Kisi, E. H. and Suaning, G. J. A study in the mechanical milling of alumina powder. *Ceramic International*, 2008, **34**, 1551–1556.

120. Saha, BP., Kumar, V., Joshi, S.V., Balakrishnan, A., and Martin, C.L. Investigation of compaction behavior of alumina nano powder. *Powder Technology*, 2012, **224**, 90–95.

121. Sarin, V.K. Cemented carbide cutting tools, in Chin, D.Y. (Ed.). *Advances in Powder Technology, ASM Material Science*, Louisville, KY, 1981, 253–287.

122. Scharf, T.W., and Prasad, S.V. Solid lubricants: A review. *Journal of Materials Science*. 2013, **48**, 511–531.

123. Schubert, W.D., Neumeister, H., Kinger, G., and Lux, B. Hardness to toughness relationship of fine grained WC–Co hardmetals. *International Journal of Refractory Metals and Hard Materials*, 1998, **16**, 133–142.

124. Senthilvelan, S., and Robi, P.S. Processing of self lubricating cutting tool material. *Proceedings of 17th International Symposium Processing and Fabrication of Advanced Materials. Indian Institute of Technology Delhi*, 2008, 193–201.

125. Shahdad, S.A, and Mccabe, J.F., Hardness measured with traditional Vickers and Martens hardness methods. *Dental Materials*, 2007, **23**, 1079–1085**.**

126. Shaji, S., and Radhakrishnan, V. An investigation on solid lubricant moulded grinding wheels. *International Journal of Machine Tools and Manufacture*, 2003, **43**, 965–972.

127. Shaji, S., and Radhakrishnan, V. A study on calcium fluoride as a solid lubricant in grinding. *International Journal of Environmentally conscious Design and Manufacturing*, 2003, **11**, 29–36.

128. Sharifi, E.M., Karimzadeh, F., and Enayati, M.H. Fabrication and evaluation of mechanical and tribological properties of boron carbide reinforced aluminum matrix nano composites. *Materials and Design*, 2011, **32**, 3263–3271.

129. Shatov, A.V., Ponomarev, S.S., and Firstov, S.A. Fracture of WC–Ni cemented carbides with different shape of WC crystals. *International Journal of Refractory Metals and Hard Materials*, 2008, **26**, 68–76.

130. Shetty, D. K., Wright, 1. G., Mincer, E N., and Clauer, A. H., Indentation fracture of WC-Co cermets. *Journal of Materials Science*, 1985, **20**, 1873–82.

131. Shiau, F., Fang, T., and Leu, T. Effect of milling and particle size distribution on the sintering behaviour and the evaluation of the microstructure in sintering powder compacts. *Materials Chemistry and Physics*, 1998, **57**, 33–40.

132. Shin, H., Lee, S., Jung, H.S., and Kim, JB. Effect of ball size and powder loading on the milling efficiency of a laboratory-scale wet ball mill. *Ceramics International*, 2013, **39**, 8963–8968.

133. Shipway, P.H., McCartney, D.G., and Sudaprasert, T. Sliding wear behaviour of conventional and nanostructured HVOF sprayed WC–Co coatings, *Wear*, 2005, **259**, 820-827.

134. Showaiter, N., and Youseffi, M. Compaction, sintering and mechanical properties of elemental 6061 Al powder with and without sintering aids. *Materials and Design*, 2008, **29**, 752–762.

135. Sliney, H.E. Solid Lubricants. *National Aeronautics and Space Administration, Lewis Research Center*, NASA Technical Memorandum 103803, N91-22396, 1991.

136. Sliney, H.E. Solid lubricant materials for high temperatures: a review. *Tribology International*, 1982, **15**, 303–315.

137. Sliney, H.E., Wide temperature spectrum self-lubricating coatings prepared by plasma spraying. *Thin Solid Films*, 1979, **64**, 211–217.

138. Sliney, H.E. Dynamics of Solid Lubrication as Observed by Optical Microscopy. *Tribology Transactions*, 1978, **21**,109–117.

139. Sliney, H.E., Strom, T.N., and Allen, G.P. Fluoride Solid Lubricants for Extreme Temperatures and Corrosive Environments. *ASLE Transactions*, 1965, **8**, 307–322.

140. Song, J., Huang, C., Lv, M., Zou, B., Wang, S., Wang, J., and An, J. Effects of TiC content and melt phase on microstructure and mechanical properties of ternary $TiB_2$- based ceramic cutting tool materials. *Materials Science and Engineering A*, 2014, **605**, 137–143.

141. Stojanovic, B.D., Skorokhod, V.V., and Nikolic, M. Advanced Science and Technology of Sintering. *Springer Science & Business Media*, ISBN 978-1-4419-8666-5, 1999.

142. Suresh Kumar Reddy, N., and Venkateswara Rao, P. Experimental investigation to study the effect of solid lubricants on cutting forces and surface quality in end milling. *International Journal of Machine Tools and Manufacture*, 2006, **46**, 189–198.

143. Suzuki, H., and Hayashi, K. The effect of the carbon content on the properties of WC-TiC-Co alloys. *Transactions of the Japan Institute of Metals*, 1966, **7**, 199–202.

144. Suryanarayana, C. Mechanical alloying and milling. *Progress in Materials Science*, 2001, **46**, 1–184.

145. Suryanarayana, C. Mechanical alloying and milling. *CRC Press, Technology and engineering*, ISBN-13: 978-0824741037, 2004.

146. Sutter, G., and List, G. Very high speed cutting of Ti–6Al–4V titanium alloy–change in morphology and mechanism of chip formation. *International Journal of Machine Tools and Manufacture,* 2013, **66**, 37–43.

147. Suzuki, H., and Hayashi, K. The effect of the carbon content on the properties of WC–TiC–Co alloys. *Transactions of the Japan Institute of Metals*, 1966, **7**, 199–203.

148. Taha, M., Palette, J., Jorand, Y., and Fantozzi, G., Samdi, A., Durand, B. Compaction and sintering behaviour of zirconia powders. *Journal of the European Ceramic Society*, 1995, **15,** 759–768.

149. Teer, D.G. New Solid lubricant coatings, *Wear*, 2001, **251**, 1068–1074.

150. Tousi, R.S.S., Rad, R.Y., and Manafi, S.A. Effect of volume fraction and particle size of alumina reinforcement on compaction and densification behaviour of Al-$Al_2O_3$ nano composites. *Materials Science and Engineering A*, 2011, **528**, 1105–1110

151. Trent, E.M., and Wright, PK. Metal Cutting (4th Ed.). *Butterworth-Heinemann Ltd, Boston*, ISBN: 0-7506-1068-9, 2000.

152. Trent, E.M. Metal Cutting (2nd Ed.). *Butterworths & Co (Publishers) Ltd, Boston*, ISBN: 0-408-05031-4, 1984.

153. Uhrenius, B., Carlsson, B., and Franzén, T. A study of the Co-W-C system at liquidus temperatures. *Scandinavian Journal of Metallurgy*, 1976, **5**, 49–56.

154. Upadhyaya, A., and Upadhyaya, G.S. Powder Metallurgy Science Technology and Materials. *University Press, India*, ISBN: 9781439857465, 2011.

155. Upadhyaya, G.S. Cemented Tungsten Carbides: Production Properties and Testing, *Noyes Publications, Fairfield, New Jersy, USA*, ISBN: 0-8155-1417-4, 1998.

156. Upadhyaya, G.S., and Bhaumik, S.K. Sintering of submicron WC–10wt. % Co hard metals containing nickel and iron. *Materials Science and Engineering A*, 1988, **105–06**, 249-256.

157. Vamsi Krishna, P., Srikant, R.R., and Rao, DN. Solid lubricants in machining. *Proceedings of Institute of Mechanical Engineers, part-J: Journal of Engineering Tribology*, 2011, **225**, 213–227.

158. Vamsi Krishna, P., and Nageswara Rao, D. The influence of solid lubricant particle size on machining parameters in Turning, *International Journal of Machine Tools and Manufacture*, 2008, **48**,107–111.

159. Wang, B., and Liu, Z. Cutting performance of solid ceramic end milling tools in machining hardened AISI H13 steel. *International Journal of Refractory Metals and Hard Materials*, 2016, **55**, 24–32.

160. Wang, X., Xiaoxiang, HE., and Hailian, G. Influence of Mo on the microstructure and mechanical properties of TiC-based cermets. *Rare Metals*, 2010, **29**, 346–350.

161. Wang, WF. Effect of Powder Type and Compaction Pressure on the Density, Hardness and Oxidation Resistance of Sintered and Steam-treated Steels. *Journal of Materials Engineering and Performance*, 2007, **16**, 533–538.

162. Wang, H.M, Yu, Y.L., and Li, S.Q. Microstructure and tribological properties of laser clad $CaF_2/Al_2O_3$ self-lubrication wear-resistant ceramic matrix composite coatings. *Scripta Materialia*, 2002, **47**, 57–61.

163. Wang, G.M., and Campbell, S.J. Synthesis and structural evolution of tungsten carbide prepared by ball milling. *Journal of materials science*, 1997, **32**, 1461–1467.

164. Wu, Z., Deng, J., Zhang, H., Lian, Y., and Zhao, J. Tribological behaviour of textured cemented carbide filled with solid lubricants in dry sliding with titanium alloy. *Wear*, 2012, **292–293**, 135–143.

165. Xing, Y., Deng, J., Jun, Z., Guodong, Z., and Kedong, Z. Cutting performance and wear mechanism of nanoscale and microscale textured $Al_2O_3$/TiC ceramic tools in dry cutting of hardened steel. *International Journal of Refractory Metals and Hard Materials*, 2014, **43**, 46–58.

166. Xing, Y., Deng, J., Shipeng, L., Hongzhi, Y., Rong, M., and Peng, G. Cutting performance and wear characteristics of $Al_2O_3$/TiC ceramic cutting tools with $WS_2$/Zr soft-coatings and nano-textures in dry cutting. *Wear*, 2014, **318**, 12–26.
167. Yamagunchi, K., Takakura, N., and Imatani, S. Compaction and Sintering Characteristics of Composite Metal powders. *Journal of Material Processing Technology*, 1997, **63**, 364-369.
168. Yang, L.J. Wear coefficient of tungsten carbide against hot-work tool steel disc with two different pin settings. Wear, 2004, **257**, 481–495.
169. Yigit, R., Celik, E., Findik, F., and Koksal, S. Effect of cutting speed on the performance of coated and uncoated cutting tools in turning nodular cast iron. *Journal of Materials Processing Technology*, 2008, **204**, 80–88.
170. Yih, S.W.H., and Wang, C.T. Tungsten Sources, Metallurgy, Properties, and Applications. *Plenum Press, Newyork and London*, 1979.
171. Yuan, J., Zhu, Y., Ji, H., Zheng, X., Ruan, Q., Niu, Y., Liu, Z., and Zeng, Y. Microstructures and tribological properties of plasma sprayed WC–Co–Cu–$BaF_2$/$CaF_2$ self-lubricating wear resistant coatings. *Applied Surface Science*, 2010, **256**, 4938–4944.
172. Zhang, F. L., Zhu, M., and Wang, C.Y. Parameters optimization in the planetary ball milling of nanostructured tungsten carbide/cobalt powder. *International Journal of Refractory Metals and Hard Materials,* 2008, **26,** 329–333.
173. Zhang, L., Wang, Y., Yu, X., Chen, S., and Xiong, X. Crack propagation characteristic and toughness of functionally graded WC–Co cemented carbide. *International Journal of Refractory Metals and Hard Materials*, 2008, **26**, 295–300.
174. Zhang, H., Lu, Q., Zhang, L., and Fang, Z. Z. Dependence of microcrack number density on microstructural parameters during plastic deformation of WC-Co composite. *International Journal of Refractory Metals and Hard Materials,* 2010, **28**, 434–440.
175. Zhang, Y.F., Lu, L., and Yap, S.M. Prediction of the amount of PCA for mechanical milling. *Journal of Materials Processing Technology*, 1999, **89–90**, 260–265.